EXPERIMENTAL ANALYSIS INTO THE INFLUENCE OF VARIOUS VOLTAGE PULSE WAVEFORMS ON THE PERFORMANCE CHARACTERISTICS OF ELECTROCHEMICAL MICROMACHINING (EMM)

THESIS SUBMITTED BY

HIMADRI SEKHAR PANDA

DOCTOR OF PHILOSOPHY (ENGINEERING)

DEPARTMENT OF PRODUCTION ENGINEERING

FACULTY COUNCIL OF ENGINEERING & TECHNOLOGY

JADAVPUR UNIVERSITY

KOLKATA-700 032

INDIA

2024

JADAVPUR UNIVERSITY
KOLKATA-700 032

Index No. 288/21/E
Registration No. 1012116002

TITLE OF THE Ph.D. (Engg.) THESIS:

EXPERIMENTAL ANALYSIS INTO THE INFLUENCE OF VARIOUS VOLTAGE PULSE WAVEFORMS ON THE PERFORMANCE CHARACTERISTICS OF ELECTROCHEMICAL MICRO-MACHINING (EMM)

NAME, DESIGNATION & INSTITUTION OF THE SUPERVISORS:

Dr. BIJOY BHATTACHARYYA

Professor, Department of Production Engineering,
Jadavpur University,
Kolkata –700032, India.

List of publications

1. **Journals**

(a) International journals

(i) Himadri Sekhar Panda, Koushik Mishra, and B. Bhattacharyya. "Anodic polarization study of step pulse waveform for machining accuracy in electrochemical micromachining." *Journal of The Electrochemical Society* 169.5 (2022): 053504.

(ii) Himadri Sekhar Panda, and B. Bhattacharyya. "Improvement of surface finish and accuracy utilising multi-step pulse waveforms in electrochemical micromachining." *Sādhanā* 48.3 (2023): 134.

(iii) Himadri Sekhar Panda, and B. Bhattacharyya. "Performance improvement of electrochemical micromachining employing pulse width modulation." *Journal of Manufacturing Processes* 112 (2024): 187-201.

(iv) Himadri Sekhar Panda, and B. Bhattacharyya. "Multi-frequency modulation in electrochemical micromachining for fabrication of precision microchannel." *Journal of Machining Science and Technology* (Under review).

(b) National journals

(i) Himadri Sekhar Panda, and B. Bhattacharyya. "Effect of step pulse waveform in electrochemical micromachining for dimension control." *Manufacturing Technology Today* 22.5 (2023): 13-17.

2. **Book Chapters**

(i) Himadri Sekhar Panda, and B Bhattacharyya. "Influence of voltage pulse on machining accuracy in electrochemical micromachining." *Advances in Micro and Nano Manufacturing and Surface Engineering: Proceedings of AIMTDR 2021*. Singapore: Springer Nature Singapore, 2022. 53-65.

3. **List of paper presented in International conferences**

(i) Himadri Sekhar Panda & B. Bhattacharyya, "Influence of voltage pulse on machining accuracy in electrochemical micromachining", 8th International & 29th All India Manufacturing Technology, Design and Research Conference (AIMTDR 2021), 9th–12th Dec., 2021, PSG college of Technology and Applied Research, Coimbatore, India. AIMTDR 2021.

(ii) Himadri Sekhar Panda & B. Bhattacharyya, “Effect of step pulse waveform in electrochemical micromachining for dimension control”, 12th International Conference on Precision, Meso, Micro and Nano Engineering (COPEN 2022), 9th-11th Dec., 2022, IIT Kanpur, Uttar Pradesh, India.

(iii) Himadri Sekhar Panda & B. Bhattacharyya, “Improvement of electrochemical micromachining by pulse amplitude modulation of step pulse waveform”, 9th International & 30th All India Manufacturing Technology, Design and Research Conference (AIMTDR 2023), 8th–10th Dec., 2023, PSG IIT-BHU, Varanasi, India.

Patents: Nil

Awards: Nil

PROFORMA – 1

"Statement of Originality"

I Himadri Sekhar Panda registered on 30th July 2021 do hereby declare that this thesis entitled "EXPERIMENTAL ANALYSIS INTO THE INFLUENCE OF VARIOUS VOLTAGE PULSE WAVEFORMS ON THE PERFORMANCE CHARACTERISTICS OF ELECTROCHEMICAL MICRO-MACHINING (EMM)" contains literature survey and original research work done by the undersigned candidate as part of Doctoral studies.

All information in this thesis have been obtained and presented in accordance with existing academic rules and ethical conduct. I declare that, as required by these rules and conduct, I have fully cited and referred all materials and results that are not original to this work.

I also declare that I have checked this thesis as per the "Policy on Anti Plagiarism, Jadavpur University, 2019", and the level of similarity as checked by iThenticate software is 6 %.

Signature of Candidate: Himadri Sekhar Panda
Date: 08/04/2024

Certified by Supervisor(s):
(Signature with date, seal)

1. 08/04/2024

Professor
Production Engineering Department
Jadavpur University
Kolkata - 700 032

JADAVPUR UNIVERSITY

FACULTY OF ENGINEERING & TECHNOLOGY

DEPARTMENT OF PRODUCTION ENGINEERING

CERTIFICATE FROM THE SUPERVISOR

This is to certify that the thesis entitled **"EXPERIMENTAL ANALYSIS INTO THE INFLUENCE OF VARIOUS VOLTAGE PULSE WAVEFORMS ON THE PERFORMANCE CHARACTERISTICS OF ELECTROCHEMICAL MICRO-MACHINING (EMM)"** submitted by **Mr. HIMADRI SEKHAR PANDA**, who got his name registered on 30th July 2021 for the award of Ph.D. (Engg.) degree of Jadavpur University, is absolutely based upon his own work under the supervision of **PROF. BIJOY BHATTACHARYYA** and that neither his thesis nor any part of the thesis has been submitted for any degree/diploma or any other academic award anywhere before.

B. Bhattacharyya 08/04/2024

Signature of the Supervisor

With

Date and Office Seal

Professor
Production Engineering Department
Jadavpur University
Kolkata - 700 032

ACKNOWLEDGEMENT

The insight presented in this thesis is undoubtedly a result of the contributions made by numerous outstanding individuals. The author expresses sincere gratitude to the Ph.D. (Engg.) thesis supervisor, Dr. Bijoy Bhattacharyya, Professor in the Production Engineering Department at Jadavpur University, Kolkata. The author acknowledges Dr. Bhattacharyya for his unwavering guidance, helpful suggestions, continuous association, support, encouragement, and valuable advice throughout every stage of this research work. The author recognizes that without Dr. Bhattacharyya's constructive and timely advice, the thesis would not have progressed as smoothly as it did.

The author also extends appreciation for the cooperation and encouragement received from Dr. Biplab Ranjan Sarkar, Dr. Biswanath Doloi, Dr. Shankar Chakrabarty, and the Head of the Department, Dr. Bijan Sarkar, and all the faculty members of the Production Engineering Department at Jadavpur University during the research work. Special thanks go to Mr. Biswanath Das, Mr. Ravishankar Pramanik, Mr. Bishwajit Pathak, Mr. P. Bari, and Mr. Subir Sanyal for their consistent support during the developmental and experimentation stages.

The author expresses gratitude to fellow colleagues, Mr. Naresh Besekar, Mr. Santosh Kumar, Mr. Sudip Santra, Mr. Mohit Pandey, existing research scholars of NTM-1 & 2 Lab, Arimdam Maity PG students of NTM-2 Lab, and ex-PG students for their constant cooperation, useful assistance, and support during the research work. Special thanks are extended to the FET office and Research section for their cordial assistance and administrative support. The author acknowledges the All India Council for Technical Education, New Delhi, for introducing the QIP (Engg.) scheme.

Lastly, the author expresses gratitude to parents, Mr. Hrisikesh Panda and Mrs. Minati Panda, for their belief in education and unwavering support, as well as to younger brother and all family members for their constant encouragement and support. The author acknowledges the understanding and sacrifice of his wife and beloved little son, without whom completing this work would have been much more challenging. Finally, the author sincerely thanks all those who directly or indirectly contributed to this research work, making it a success.

Himadri Sekhar Panda.

(Himadri Sekhar Panda)

PREFACE

Due to the advancement of technology in the micro-engineering industry, the fabrication of precise micro-components is essential. Miniaturization of components and systems has established their significance in all fields of application, such as biomedical, electronics, aviation, micro-mechanics, and so on. Micromachining techniques are used to produce micro-electromechanical systems (MEMS). For example, in electronic devices, after introducing integrated circuits (IC) in the form of very large scale integration (VLSI), it becomes more compact and small in size, i.e., micro/nano-scale e.g. processors of cell phones, laptops, cameras, electronics micro-surgery instruments, etc. In aerospace industries, light weight and hard materials are the major requirements for shaping and surface structuring with high accuracy. In meeting the expectations of next-generation components design, electrochemical machining (ECM) providing higher accuracy and superior surface finishes. When ECM is specifically applied in micro-manufacturing for precision shaping, it is referred to as electrochemical micromachining (EMM). EMM boasts several advantages, including no tool wear, absence of thermal and stress effects, higher metal removal rate, and the localized anodic dissolution for achieving better surface finish, etc.

However, in EMM, the removing of oxide layers, gas films, bubbles, and sludge are challenging. Previous research has indicated that researchers have explored various methods, including tool vibration; electrolyte flushing, electrolyte jet, and mixed gas jet, to remove oxide layers, gas films, bubbles, and sludge for enhancing anodic dissolution in electrochemical micromachining (EMM). Conversely, these techniques can cause issues such as unwanted vibrations of micro-tools and workpieces, reduced accuracy, and disruption of proper electrolyte flow to the target machining zone. Moreover, there are significant gaps in the investigation of EMM performance which is closely linked to the characteristics of voltage pulse waveforms. Understanding how these waveforms affect to enhance the performance of EMM and advance micro-manufacturing capabilities. This knowledge gap underscores the importance of systematic experimental analysis to elucidate the complex relationships between waveform parameters of power supply and the improvement of EMM performance. Hence, a new DC pulse waveform has been designed to enhance the performance of EMM. Keeping in view, the existing research gap in the EMM process, the following research objectives have been considered.

(i) To develop an Electrochemical Micro-Machining (EMM) setup using various sub-systems, such as a mechanical machining unit, pulse D.C power supply, controller unit, and machining chamber for performing experiments.

(ii) To design and develop new voltage pulse patterns that introduces bunch of short pulses to improve machining performance. To study other important factors such as variation of pulse on time, frequency and duty cycle of pulse waveform during EMM operation.

(iii) To develop mathematical models for volumetric material removal (VMR), power transmission, transient response of double-layer capacitor, and root mean square (R.M.S) voltage for pulse-on time to gain understanding into the performance of the new voltage pulse pattern techniques and analyze the inter-electrode electric field properties, such as current density, energy density, electric field strength, and power loss, by utilizing simulation processes.

(iv) To minimize stray current effects, current density, short-circuit effects, and monitor the current-voltage characteristics by employing workpiece and tool insulation methods and discontinuous tool feed rate control technique under new pulse pattern techniques.

(v) To improve machining accuracy and surface quality by developing voltage pulse width modulation and pulse amplitude modulation techniques for achieving better performance characteristics of EMM.

(vi) To further investigate machine performance with the help of new pulse patterns accompanied by multi-frequencies for improving accuracy in terms of overcut, shape of the machined profile, tapering effect, and surface finish, etc.

The thesis has been structured in line with abovementioned objectives and all research work and results as obtained have been described in a well-organized manner into eight chapters in details here under:

Chapter 1 deals with the introductory part i.e. history and progress of EMM process considering its working principle, process parameters and other influencing factors, process capabilities, limitations, importance and applications in miniaturization. Literature review of previous work done includes fundamentals of EMM, role of various process parameters on the machining performance, and recent advancement on voltage pulse waveform for finding out the existing knowledge gap to outline the research objectives.

Chapter 2 focuses on development of EMM setup and effect of operational features for the fabrication of microfeatures of different geometries and the detailed experimental procedure for the enhancement of machining performance. The components include procured ones, the specification, and capability of which have been selected according to setup configurations requirements, machining conditions and needs; while others have been developed indigenously in house for fulfilling the experimental requirements. The modifications and improvements on the base setup have been conducted repeatedly based on the research needs and to facilitate performance enhancement in machining process. Influence of power supply in EMM, such as importance of DC pulse waveform in EMM, influence of different types of DC pulse waveform in EMM, effect of pulse voltage, effect of pulse frequency, effect of duty cycle are discussed in-depth. Additionally, other process parameter i.e., electrolytes and flushing process, effect of micro-tool feed rate, and initial inter electrode gap with their role in EMM process are discussed in this chapter.

In **Chapter 3,** highlighted the present research focused on the improvement of machining accuracy by modifying the traditional rectangular pulse waveform into a novel step pulse waveform, which is designed indigenously with a series of short rectangular pulses with different amplitudes. Comparative experiments have been conducted between rectangular and step pulse waveforms to investigate the behaviour of waveforms, the characteristics of anode polarization at different applied voltages, the transition from active to passive dissolution and the influence of applied voltage on overcut and tapering effects of microholes, machining on stainless steel (SS 304).

Chapter 4 emphasises the further improvement of machining accuracy by insulation technique and discontinuous microtool feed control technique under the application of step pulse waveform. In EMM, as the tool-tip area is very small compared to the workpiece, the stray current plays a significant role in pitting effects and irregular machining. To reduce the stray current effects, a new technique of workpiece and tool insulation is introduced, and its effectiveness is verified through the machining of microholes. The effects of insulation technique on electrolyte potential and current density are investigated through simulation process and overcut and precise shape of microhole machining for different voltages is investigated experimentally. In the present study, overcut, shape of the machined microhole, stray current effect, short circuits, and current-voltage characteristics during machining have been investigated under the application of new discontinuous microtool feed control technique. The main objective of

this research work is that by employing microtool feed rate control, short circuits eliminates, improves regular machining and uniformity of profile shape.

In **Chapter 5**, the difficulties of EMM in stagnant electrolyte solutions have been highlighted. These include challenges such as improving mass transport and enhancing the conductivity of electrolytes, which are particularly challenging tasks due to the presence of bubbles and sludge that increase the shielding effects. Keeping in view, multi-step pulse waveform (MSPW) has been designed indigenously, where different peak voltages with short duration times are incorporated in each pulse on time. The effect of the multi-step pulse waveform (MSPW) on the improvement of EMM's performance has been investigated and compared with conventional rectangular pulse waveform (RPW). For better understanding, the power transmissions of both pulse waveforms at different applied voltages have been theoretical estimated and compared between the two waveforms. To understand the current density and electric potential distribution, simulation processes have been carried out. Experimentally current density analysed for various machining times at different frequencies. Finally, depth, diameter, etch factor, surface roughness, microsparks affected zone, and pitting effects of microdimples have been investigated under the best parametric condition of MSPW. Additionally, microholes have also been fabricated at the same parametric condition to justify the better utility of MSPW.

Chapter 6 provides an overview of another new pulse width modulation (PWM) technique of step pulse waveform. This technique has been developed to further control the potential transmission into the electrolyte, thereby enabling significant control of moderate amount of anodic dissolution. To verify the feasibility of PWM technique, machining accuracy is investigated in the influence of different applied voltages, regulated duty cycles, frequencies, and lateral tool feed rates. The machining accuracy has been investigated in terms of overcut of microgroove width, depth, taper angle, and surface roughness of microgrooves. In EMM, appropriate voltage choice is crucial for the improvement of material dissolution localization and the control of stray current. Higher voltage increases overcut, taper angle, and surface roughness. Lower voltage minimizes overcut, but it affects the shape of features due to irregular machining. To address these drawbacks, a new pulse amplitude modulation (PAM) technique of step pulse waveform has been designed indigenously. To verify the feasibility of the PAM technique, machining performance in terms of overcut, taper angle and surface roughness of microgrooves have been investigated at different lateral tool feed rates and frequencies.

Chapter 7 delves into the major contributions of the present research. A novel multi frequency modulation (MFM) technique of the step pulse waveform has been designed indigenously by a function generator and utilized as an inexpensive technique to improve electrochemical micromachining performance. To determine the best parametric combination of MFM for enhancing machining performance, experiments have been conducted at different lower and higher frequencies, pulse cycle times, applied voltages, and lateral tool feed rates. The influence of these process parameters has been investigated on overcut, depth, tapering effects, homogeneity, uniformity, irregularity, profile shape, and surface finish. By utilizing the best parametric combination of multi-frequency modulation (MFM) of the step pulse waveform, precision L-shaped microchannels on SS304 have been successfully fabricated. To identify the best technique, microchannels have been fabricated under the application of pulse width modulation (PWM), pulse amplitude modulation (PAM), and multi-frequency modulation (MFM). To assess the effectiveness of the new step pulse waveform with multi-frequency (MFM) modulation technique, a comparison is made with results obtained by other past research employing tool vibration techniques during the machining of titanium by EMM. Lastly, **Chapter 8** consolidates the outcomes of the present research work, along with the future scope of research in the area of EMM during micromachining of SS304 and difficult-to-cut titanium materials, aim to improve machining performance for advanced industrial and biomedical applications.

The aim of this research work is determined to be the invention of a simple methodology for improving the flushing efficiency and confining the current distribution within the machining gap. In order to achieve this, a novel DC step pulse waveform has been designed indigenously by a function generator and utilized as an inexpensive technique to improve the electrochemical micromachining (EMM) performance. To get an idea about the performance of the step pulse waveform, volumetric material removal and power transmission for pulse on time have been theoretically estimated and compared with conventional rectangular pulse waveform. For better understanding, the operational mechanism of the step pulse waveform has also been investigated through simulation processes. This new step pulse waveform with various techniques, i.e., tool and workpiece insulation, microtool feed rate control, multi-step pulse, automatic pulse width modulation, automatic pulse amplitude modulation, multi-frequency modulation, has been employed innovatively in stagnant electrolyte to flush out the gas bubbles and sludge from the machining area. The most salient and unique research finding that has

been observed in the present research includes the development of an electrochemical machining experimental system setup for fabricating various microfeatures on SS304 and also has tried to justify the uniqueness and originality of the present work by incorporating various novel methodologies and investigations. In the context of enhancing electrochemical micromachining performance, the machining criteria, i.e., overcut, depth, tapering effects, homogeneity, uniformity, irregularity, profile shape, and surface finish, have been investigated. The analysis of fabricated microfeatures based on a critical examination of various SEM micrographs to determine the influence of significant EMM parameters on machining accuracy and surface roughness during micromachining. One of the major contributions of the present research is that by utilizing the best parametric combination of multi-frequency modulation of the step pulse waveform, which enables the successful fabrication of precise microholes on titanium material without the need for complex electrolyte flushing and tool vibration arrangements, which are most difficult to machining by EMM. The investigation in the new field of electrochemical micromachining can be of enormous support to the present manufacturing industries because of its expected superiority of machining characteristics with respect to other machining processes. Hence, the extensive research will help to bridge the existing gap in research and knowledge by contributing to a cost-effective machining system for fabricating intricate microfeatures on challenging to machine titanium materials for advanced microengineering applications. It will also provide an appropriate platform for the commercialization of this emerging anodic dissolution process.

VITA

The author, Mr. Himadri Sekhar Panda, the son of Mr. Hrisikesh Panda and Mrs. Minati Panda, was born on December 26th, 1984, in Contai, West Bengal, India. He successfully completed his Higher Secondary Certificate examination under the West Bengal Board of Secondary Education in 2002 with first-class honors. Furthermore, he earned his Bachelor's degree in Electronics and Communication Engineering from Kalyani Govt. Engineering College, Nadia, under the West Bengal University of Technology (WBUT), graduating with first-class honors in 2008. The author pursued Master's degree in Mechatronics Engineering from the National Institute of Technical Teachers' Training & Research (NITTTR), Kolkata, in 2011, under the West Bengal University of Technology (WBUT). Subsequently, from 2011 to 2018, the author served as an Assistant Professor in the Electronics and Communication Engineering Department at IMPS College of Engineering & Technology, Malda, West Bengal. From 2018 onwards, the author has been an Assistant Professor in the Electronics and Communication Engineering Department at Ramgarh Engineering College (established by the Government of Jharkhand and operated by Techno India under PPP).

In March 2021, the author joined the Production Engineering Department at Jadavpur University, Kolkata, as a Research Scholar under the Quality Improvement Programme (Engg.) scheme of the All India Council of Technical Education (AICTE). Since then, the author has been actively engaged in research work in the field of Electrochemical Micromachining. Notably, the author has already published three research papers in international journals and presented several research papers at various international conferences.

Dedicated to my parents, teachers, life partner, son and well-wishers for their endless support and love...

TABLE OF CONTENTS

CHAPTER 3

CHAPTER 4

CHAPTER 5

CHAPTER 6

CHAPTER 7

CHAPTER 8

LIST OF FIGURES

LIST OF TABLES

Chapter 1: Introduction

1.1 Introduction

Due to the advancement of technology in the micro-engineering industry, the fabrication of precise micro-components is essential. Miniaturization of components and systems has established their significance in all fields of application, such as biomedical, electronics, aviation, micro-mechanics, and so on. Micromachining techniques are used to produce micro-electromechanical systems (MEMS). For example, in electronic devices, after introducing integrated circuits (IC) in the form of very large scale integration (VLSI), it becomes more compact and small in size, i.e., micro/nano-scale e.g. processors of cell phones, laptops, cameras, electronics micro-surgery instruments, etc. In aerospace industries, light weight and hard materials are the major requirements for shaping and surface structuring with high accuracy. In meeting the expectations of next-generation components design, electrochemical machining (ECM) providing higher accuracy and superior surface finishes. When ECM is specifically applied in micro-manufacturing for precision shaping, it is referred to as electrochemical micromachining (EMM). EMM boasts several advantages, including no tool wear, absence of thermal and stress effects, higher metal removal rate, and the localized anodic dissolution for achieving better surface finish, etc.

However, in EMM, the removing of oxide layers, gas films, bubbles, and sludge are challenging. Researchers have explored various methods to address these, including tool vibration, electrolyte flushing, electrolyte jet, and mixed gas jet, etc. Extensive research has focused on optimizing process parameters to improve localization effects and reduce unwanted excessive dissolution. However, electrolyte flushing in EMM can lead to issues such as unwanted vibrations of micro-tools and workpieces, reduced accuracy, and disruption of proper electrolyte flow to the target machining zone. The voltage pulse waveforms play a crucial role in improving the performance of EMM. Therefore, investigating these waveforms is essential for understanding the reasons behind the performance improvements. This knowledge gap emphasizes the importance of a systematic experimental analysis to clarify the complicated relationships between waveform parameters of power supply and performance improvement of EMM. The meticulous effects on crucial performance improvement are required to be investigated through the design of pulse waveforms with various parameters, including amplitude, frequency, duty cycle, and waveform shape, etc.

1.2 Electrochemical Micromachining: An overview

1.2.1 Basic principle

Electrochemical machining is an old technique developed by Russian scientist W. Gusseff in 1929. The process of material dissolution in EMM follows Michael Faraday's law of electrolysis. EMM involves an anodic dissolution process where the workpiece acts as the anode, and a microtool serves as the cathode when a low-voltage DC pulse is applied between the electrodes. According to Faraday's law of electrolysis, the workpiece material dissolves into metallic ions through electrochemical reactions, as illustrated in Figure 1.1. The shape, size, machining accuracy, and surface finish of the machined micro-feature depend on various machining conditions. The rate of material dissolution is influenced by the machining current, machining time, atomic weight of the workpiece, and the valency of the ion produced. The hardness or other mechanical properties of the material do not impact the material's dissolution. During machining, the shape of the microtool remains unchanged, allowing it to be used multiple times for the fabrication of microfeatures.

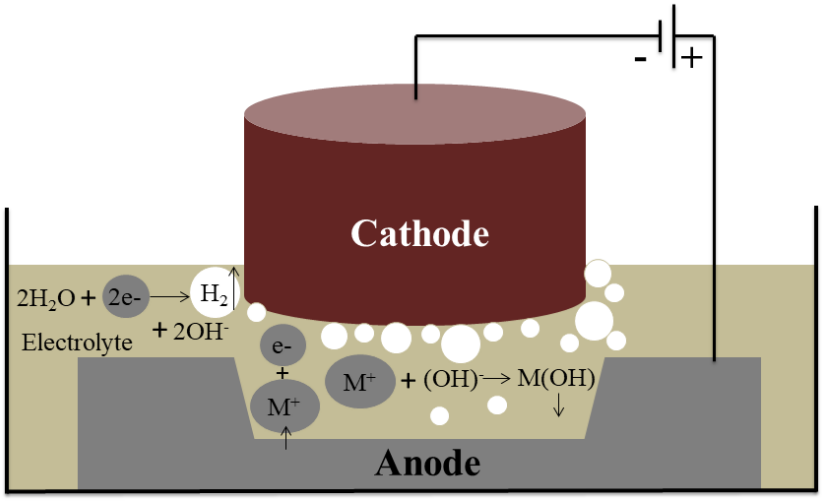

Figure 1.1 Schematic diagram of the electrochemical micromachining process

Faraday's law of electrolysis can be summarized as follows:

(i) The quantity of chemical change produced by an electric current, such as the dissolution or deposition of a material is directly proportional to the amount of electricity passed.

(ii) The amounts of different substances dissolved or deposited by the same quantity of electricity are proportional to their respective chemical equivalent weights.

In the quantitative form, Faraday's two laws state that

$$m \propto It\varepsilon \tag{1.1}$$

Where, m is weight of material dissolved or deposited, I is current passes through the electrodes for time t, and Ɛ is equivalent weight of the material.

Introducing the constant of proportionality F commonly called Faraday constant (96,500 C/mol). From equation (1.1), the rate of mass removal can be calculated as

$$m = \frac{It}{F} \cdot \frac{M}{z} \tag{1.2}$$

Where, M is molar mass of the substance, and z is the valance number of ions of the substance (electrons transferred per ion). Note that M/z is the same as the equivalent weight of the material. If the density of the anode material is ρ_m, the volumetric removal rate is given by

$$V_M = \frac{MI}{\rho_m zF} \tag{1.3}$$

Ohm's law mathematically expresses for a constant inter-electrode gap (IEG) as

$$I = \frac{V}{R_{electrolyte}} \tag{1.4}$$

Where, V is the applied voltage between two electrodes, and $R_{electrolyte}$ is resistance of electrolytes between the inter-electrode gap. The resistance of specific electrolytes between IEG can be given as

$$R_{electrolyte} = \frac{\rho_e h}{A} \tag{1.5}$$

Where, ρ_e is the specific resistance or resistivity of the electrolyte, h is inter-electrode gap, and A is the area of the electrode.

The volume of material removed can be written by combination of Faraday's two laws and Ohm's law as follows:

$$V_M = \frac{MVAt}{\rho_m \rho_s zFh} \tag{1.6}$$

Where, density of material is ρ_m. From the above equation (1.6), it can be observed that anodic dissolution depends on the atomic weight, the valency of the ions produced, and the current passing through the electrodes over a unit of time. Alternatively, it can be stated that the material dissolution rate is not influenced by the hardness of the material. The shape of the cathode remains unchanged, indicating no tool wear, which proves highly beneficial for machining hard materials to fabricate complex micro-features. The material removal rate (MRR) basically depends on the following factors which are

discussed below [1].

(a) Anodic reaction,

(b) Mass transport and current density, and

(c) Current distribution and shape control.

1.2.2 Anode and cathode reaction

When potential is applied across the workpiece (anode) and the microtool (cathode), both submerged in an electrolyte with a specific inter-electrode gap, electrons transfer between ions and electrodes to complete the electric circuit. The electric current is sustained by removing electrons from the atomic structure of the workpiece, i.e., the current is carried by the ions. Thus, metal dissolves atom by atom from the anode surface, entering the electrolyte as positive ions. Positively charged ions migrate through the electrolyte toward the cathode, while negatively charged ions move towards the anode, as illustrated in Figure 1.1. This ion movement is accompanied by electron flow in the opposite direction outside the cell, both actions resulting from the applied potential difference. The electrochemical reactions occurring at the anode and cathode during machining are as follows:

(a) Anode reactions

The anodic reactions occur at a moderate current density under various machining conditions. Two possible reactions can take place at the anode, which are discussed below:

(i) Evolution of oxygen or hydrogen gas

$$2H_2O \rightarrow O_2 \uparrow +2H^+ + 2e^- \quad \text{(In acidic electrolyte)} \tag{1.7}$$

$$4(OH)^- \rightarrow 2H_2O + O_2 \uparrow +2H^+ + 4e^- \quad \text{(In alkaline electrolyte)} \tag{1.8}$$

(ii) Dissolution of metal ions

The metal (M) dissolution takes place as

$$M \rightarrow M^+ + e^- \tag{1.9}$$

$$M^+ + (OH)^- \rightarrow M(OH) \downarrow \text{(Sludge)} \tag{1.10}$$

(b) Cathode reactions

Similarly, two possible reactions also occur at the cathode:

(i) Evolution of hydrogen gas

$$2H^+ + 2e^- \rightarrow H_2 \uparrow \quad \text{(In acidic electrolyte)} \tag{1.11}$$

$$2H_2O + 2e^- \rightarrow H_2 \uparrow \quad \text{(In alkaline electrolyte)} \tag{1.12}$$

(ii) Neutralization of positive metal ions

When a metal ion reaches the cathode, it seeks to neutralize.

$$M^+ + e^- \rightarrow M \tag{1.13}$$

The above reactions at the anode and cathode illuminate that material dissolution takes place at the anode in the form of ionic species, while the electrolyte serves as the carrier of current.

1.2.3 Mass transport and control of anodic dissolution

Mass transport plays a crucial role in the distribution of current between two electrodes, influencing the shaping and surface finish. The effectiveness of mass transport is attributed to a combination of the salt film mechanism and the acceptor mechanism in anodic dissolution. The rate of transport of dissolution products from the anode surface is governed by the salt film mechanism, occurring at the anode surface. Simultaneously, the rate of transport of negative ions from the cathode to the anode is known as the acceptor mechanism. In this process, complex ions react with dissolved metal ions and transform into hydrated complex ions. The efficiency of this mass movement is influenced by the following factors:

(a) Migration: The movement of charge body under the influence of an electric field.

(b) Diffusion: The movement of species under the influence of the gradient of chemical concentration.

(c) Convection: It is a hydrodynamic transport, where the electrolyte is flowing (laminar, turbulent) by the force of conviction.

In Electrochemical Micromachining (EMM), current density plays a crucial role in improving surface finish and accuracy. Higher current density may lead to negatively impacting surface finish and accuracy. Conversely, lower current density results in minimal anodic dissolution, leading to irregular machining and improved surface roughness. Therefore, for better surface finish and accuracy, maintaining a limited current density is essential, allowing control through convective mass transport.

1.2.4 Current distribution and shape control

In Electrochemical Micromachining (EMM), current distribution plays a crucial role in shaping and generating features. Three different scales are considered for EMM: workpiece scale, pattern scale, and feature scale. At the workpiece scale, the geometry of both the workpiece and the tool can influence current distribution. Mass transport controls

current density at the pattern scale, while at the feature scale; current distribution depends on the spacing and geometry of the features. For effective shape control management, the current density at the anode is influenced by geometry, anodic reaction, electrolyte conductivity, and hydrodynamic conditions [2-5]. Workpiece shape can be generated using two techniques: by employing a predesigned tool or by controlling the movement of the micro-tool. Predesigned tools are suitable for fabricating larger micro shapes due to their simplicity, whereas utilizing tool movement can reduce machining costs and the complexity of fabricating critical tool shapes. In the tool movement process, the tool initially moves downward to the required depth and then horizontally along a predesigned path for shape fabrication. This approach contrasts with predesigned tools that move solely along the vertical axis, providing an alternative method for achieving the same shape.

1.3 Equilibrium electrode potential

1.3.1 Behavior of electrical double layer

When an electrode is immersed in an electrolyte solution, a potential difference is established between the electrode and the solution. Equilibrium is reached when the positive charges in the solution and the negative charges in the metal are equal. At this condition, metal ions are unable to cross the energy barrier until the applied voltage exceeds the activation potential [6]. At the electrode-electrolyte interface, these opposite charges form a double layer, behaving similarly to a two-plate capacitor. The inner layer, consisting of solvated ions and located close to the electrodes, is known as the compact Helmholtz plane (HP). On the solution side, where mobile ions are more diffused and more ohmic drops occur, it is known as the Gouy-Chapman layer, as shown in Figure 1.2(a). Figure 1.2(b) illustrates an equivalent electrical circuit (EEC) model of electrochemical micromachining (EMM), based on the Randles circuit model. For the anode, two parallel resistances, the charge transfer resistance (R_{Act}) and the double layer resistance (X_c), are connected in series with the electrolyte resistance ($R_{electrolyte}$).

The double-layer capacitance can be written as:

$$C_{dlayer} = C_{dl}.A \tag{1.14}$$

Where, A is tool tip area, C_{dl} is specific double-layer capacitance of Gouy–Chapman–Stern model [7].

Let, the double layer capacitive resistance, X_c.

$$X_c = 1/2\pi f C_{dlayer} \tag{1.15}$$

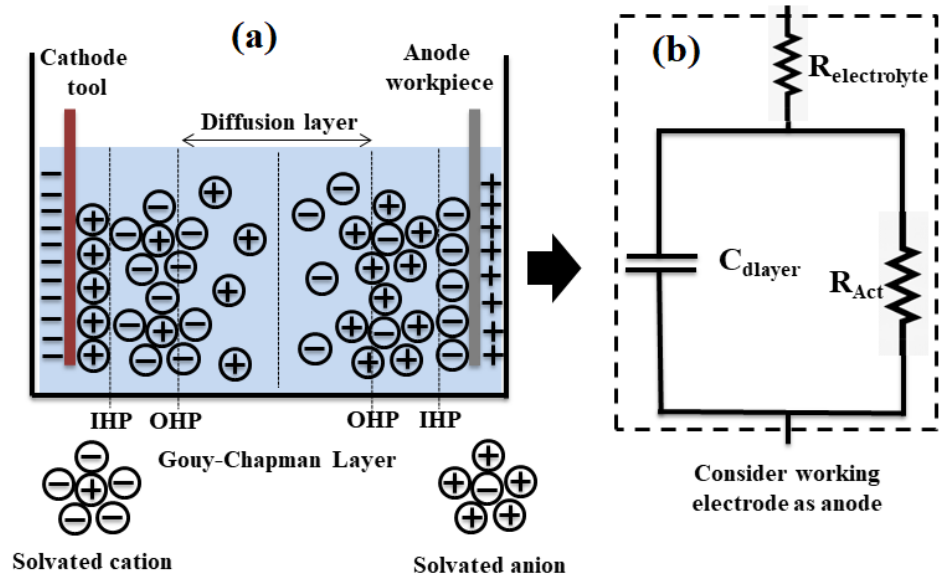

Fig. 1.2 Equivalent electrical circuit model of EMM

Where, f is the frequency of voltage pulse waveform.

From Butler–Volmer equation, charge transfer resistance can be calculated as shown below.

$$R_{Act} = \frac{R_{gas} T n_e}{F i_0} \tag{1.16}$$

Assuming number of electrons transferred n_e to be 1 i.e., 100%, universal gas constant R_{gas} (8.314 J/K mol), temperature T (K), exchanged current density i_0 which depends on specific electrolyte concentration.

1.3.2 Irreversible electrode reactions

In EMM, current flow is occurred due to applied external voltage between two electrodes, resulting in anodic dissolution takes place. The current flow can be increased when the difference potential rises between equilibrium and working potential. This condition of electrode reaction is said to be irreversible and the difference between the equilibrium and working values of the potentials is known as overpotential. It is commonly accepted that, in most electrochemical reactions, there are three specific types of overpotential such as activation, concentration, and resistance.

Polarization

When atoms leave the cathode in the form of ions and move towards the electrode to regain their atomic state, no current flows between the two electrodes. This process continues until equilibrium is reached, resulting in the development of a potential difference between the electrode and electrolyte interfaces, known as electrode potential.

This potential acts as a barrier that obstructs further reactions. When external energy, i.e., voltage, is applied between the two electrodes, ions are discharged at the required rate to facilitate the flow of current through the barrier. Therefore, polarization refers to the deviation of the equilibrium potential caused by the excess flow of current at the anode or cathode. The extent of this polarization can be measured by estimating the overpotential.

The electrode polarization (ΔE) can be written as:

$$\Delta E \equiv E_i - E_0 \tag{1.17}$$

Where, E_i and E_0 are the potential at current flow and zero current condition. At nonzero current flow condition, the total current i in a cell can be written as

$$i = i_A \pm i_C$$

(1.18)

Where, i_A is anode current for forward reaction (oxidation), and i_C is cathode current for reverse reaction (reduction). In the case of equilibrium, the oxidation rate is equal with reduction rate. Therefore, the total current becomes zero at equilibrium state.

Now, condition 1:

When oxidation rate is greater than reduction rate, then anode current is higher than cathode current i.e., $i_A > i_C$. This condition is known as anodic polarization which can be represented as:

$$E_A - E_0 \equiv \Delta E \qquad \text{(+ ve potential)} \tag{1.19}$$

Condition 2:

When reduction rate is larger than oxidation rate, cathode current rises more than anode current i.e., $i_C > i_A$. This condition is known as cathode polarization which can be represented as:

$$E_C - E_0 \equiv \Delta E \qquad \text{(- ve potential)} \tag{1.20}$$

A polarization curve can be generated by plotting anodic potential against current density. This curve provides insights into the relationship between anodic potential and current density in the process of anodic dissolution. The polarization curve serves as a fundamental experimental tool in electrochemistry and finds applications in the development of various processes such as electroplating, electro-polishing, and other electrolysis process.

1.4 Major process parameters in EMM

The anodic dissolution is the basic fundamental process in EMM, where material can remove from the surface of workpiece as ionic label. Effective precision machining can

be achieved by carefully controlling the process variables in the EMM system [8-9]. Major machining criteria, including material removal rate, profile accuracy, and surface finish, can be enhanced by controlling various process parameters [10]. These parameters are applied voltage, frequency, duty cycle, electrolyte type, electrolyte concentration, initial inter-electrode gap; tool feed rate, electrolyte flushing, and etc. Some of predominant process parameters, which improve the performance of EMM [11], are listed as follows:

(a) Type of Power supply,
(b) Role of different electrolyte,
(c) Flow rate of electrolyte, and concentration,
(d) IEG (Gap between microtool and workpiece), and
(e) Micro tool feed rate, etc.

The details classification of process parameters and their important role in process performance are discussed in subsequent chapters.

1.5 Electrochemical Micromachining: Present Need

Electrochemical micromachining (EMM) has some unique advantages over other competing micro-fabrication process technologies. Consequently, EMM has been engaged to meet the demanding requirements of various micro-engineering fields. It has been used in automated large scale micro-manufacturing for better shaping and surface finishing. However, it has certain limitations from an application perspective.

1.5.1 Advantages

The advantages of EMM can be categorized into material and product benefits, machine advantages, usability of microtools and their development, and economic gains.

(a) Material and products advantages

In EMM, material is removed from the workpiece through an electrochemical dissolution process. The material removal rate depends on the material's atomic weight, the valency of ions produced, and the current passed through the electrolyte over a specific time. Notably, hardness, toughness, and thermal resistance of the material do not influence the material removal rate. Chemically inert materials and those with poor electrical conductivity can also be effectively machined using the EMM system. EMM is a non-contact process, meaning the microtool does not touch the workpiece during machining. Consequently, thermal effects, physical stress, and mechanical strain do not occur on the microproducts. Additionally, there is no upper layer deformation observed on microproducts, such as heat-affected zones, white layers, and micro-cracks. The

formation of burrs on microproducts is also prevented through this process.

(b) Machine advantages

(i) The initial investment in designing the EMM system is not high, and the recurring cost of system operation is very low.

(ii) During anodic dissolution, the shape of the microtool remains unchanged because only hydrogen gas is evolved, and the material of the microtool does not dissolve.

(iii) The EMM process exhibits high repeatability and scalability.

(iv) The EMM process requires low energy consumption.

(c) Usability of microtool and its development

(i) No tool wear occurs during the EMM process, allowing the same tool to be used for repeated machining.

(ii) A simple cylindrical microtool rod can be employed for fabricating various complex micro-features.

(iii) Various micro-tool shapes can be employed to improve machining accuracy.

(iv) Microtools can be easily fabricated using both conventional and nonconventional processes.

(v) The EMM process allows the fabrication of microtools as per requirements, minimizing setup errors and costs.

(vii) Insulating the side wall of the microtool enhances its longevity and stability in the EMM process.

(d) Economic advantages

(i) Productivity in EMM can be enhanced by using multiple micro-tools as cathodes to generate the same feature in a single run.

(ii) Compared to other tool-based micromachining processes, the initial setup as well as running cost of EMM is significantly lower.

(iii) EMM is an eco-friendly and comparatively less polluting process, leading to reduced costs associated with protective and preventive subsystems.

1.5.2 Applications

The major advantage of EMM lies in the removal of material in the form of ions from the workpiece, enabling the precise fabrication of accurate micro-features. These advantages are particularly effective not only in the micro-range but also in the nano-range. In the micro-range, the applications of EMM can be categorized into three domains: machining, finishing, and surface structuring applications. To enhance comprehension, the chronological improvement of EMM in accuracy and micro-scaling is presented in

Figure.1.3.

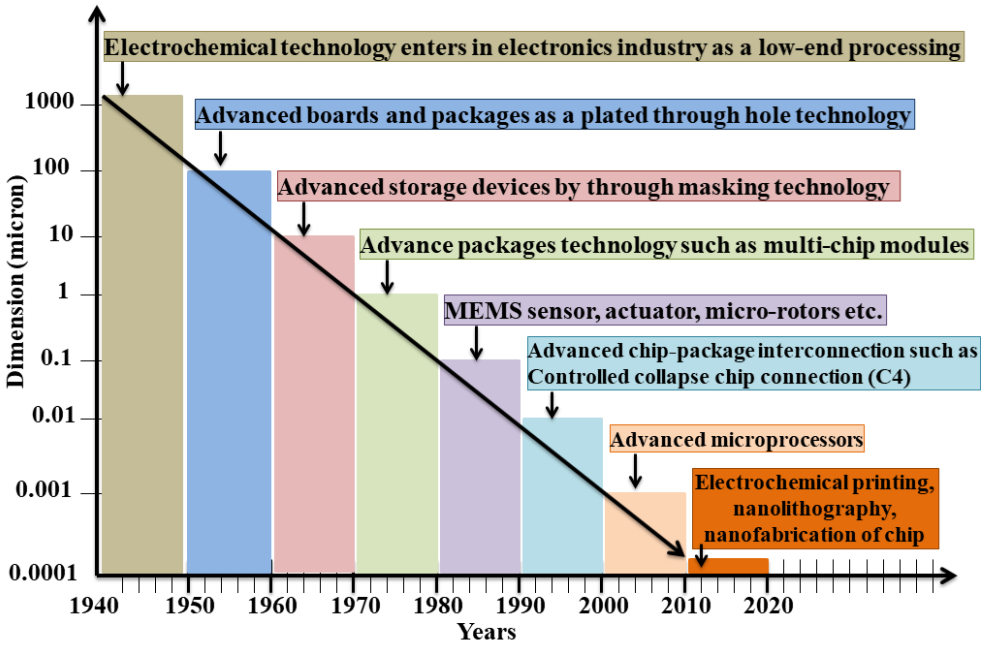

Fig. 1.3 Chronological progression of EMM towards advanced Micro-to-Nanofabrication

(a) Machining applications

The machining of micro-components becomes a crucial concern in modern technology through the EMM process. While several techniques exist for fabricating three-dimensional (3D) micro-features, EMM stands out as one of the best techniques for machining various micro-features with higher accuracy and quality. Some examples of machining applications include micro-nozzles, nozzle plates for inkjet printer heads, micro-slitting by electrochemical saw, microholes, microslots, microchannels, chip interconnection, multichip module packages, etc.

(b) Finishing applications

Due to size limitations, improving the finishing of micro-components is a challenging task. When micro-components are fabricated using different methods, certain micro-features, such as uneven and irregular edges, microburrs, and rough surfaces, occur and need correction. EMM is an alternative technique through which these micro-features can be effectively minimized for both soft and hard materials, including copper, aluminum, steel, nickel, titanium, and their alloys.

1.5.3 Limitations

While EMM offers numerous advantages, it also has a few limitations from an application perspective. These limitations are discussed on a case-by-case basis.

(a) Oxide layer formation

When the anodic dissolution process occurs, oxygen evolution takes place near the anode surface. This oxygen leads to the formation of an oxide layer on the anode surface. The thickness of the oxide layer depends on the combination of material and electrolyte. This oxide layer creates a barrier between the two electrodes, disrupting the proper flow of current through this barrier. As a result, the continuous anodic dissolution process is obstructed, leading to irregular machining with poor surface finish. However, by selecting the optimal combination of EMM process parameters; this passive oxide layer can be minimized.

(b) Metal deposition on micro tool

To enhance machining accuracy, the initial interelectrode gap (IEG) is maintained as narrow as possible, typically in the range of 10–20 μm. In this narrow gap, sludge cannot remove completely, resulting in some metal ions are deposited on the microtool surface. This phenomenon is particularly noticeable at higher frequencies. At higher frequencies, the small pulse period time prevents the metal ions from being adequately removed from the machining zone. The deposited material on the microtool reduces the IEG and creates a short circuit during machining; resulting in the generation of microsparks, which keeps a negative impact on surface finish and accuracy.

(c) Stray current effects

The control of stray current is a primary challenge in EMM. During anodic dissolution, current flux flows from the machining area of workpiece to the tool tip area. However, some undesired current flux also flows from the nearest machining area, which is not part of the desired requirement. This unwanted current is known as stray current, and it can remove material across the machining area. As a result, overcut may increase, and surface finish can become poor. By insulating the peripheral circumference of the microtool, reducing gap between tool and workpiece, and using an insulated mask, the effect of stray current can be effectively minimized.

(d) Machining time

Compared to other machining processes, the machining time of EMM is higher. This is because small amount of material is removed for each pulse, leading to an increase in total machining time. However, the use of multiple micro tools can help to minimize the overall machining time.

(e) Microtool handling

Microtool handling is a significant challenge in EMM. During the preparation and mounting of microtools, there is a high probability of damaging the microtool.

Additionally, there is a risk of damage during machining if a short circuit occurs. Achieving precision movement of the microtool in EMM is a challenging task, and alignment errors can result in poor profile accuracy.

1.6 Review of past research

Since the 19th century, electrochemical micromachining (EMM) has been employed for machining micro features on advanced engineering materials. Due to its various advantages over other machining processes, significant research has been conducted on EMM at various research centres, technological universities, and industries. EMM has emerged as a preferred technique to meet the demands of manufacturing compact devices, such as sensors, connectors, actuators, and smaller consumer electronics. However, there are numerous complexities and intricacies in the process, especially when dealing with hard alloy materials. To enhance the performance of EMM, researchers have explored and applied a greater number of process parameters and various techniques. For an overall perspective on EMM, some significant publications are presented chronologically in Figure 1.4 [12-30].

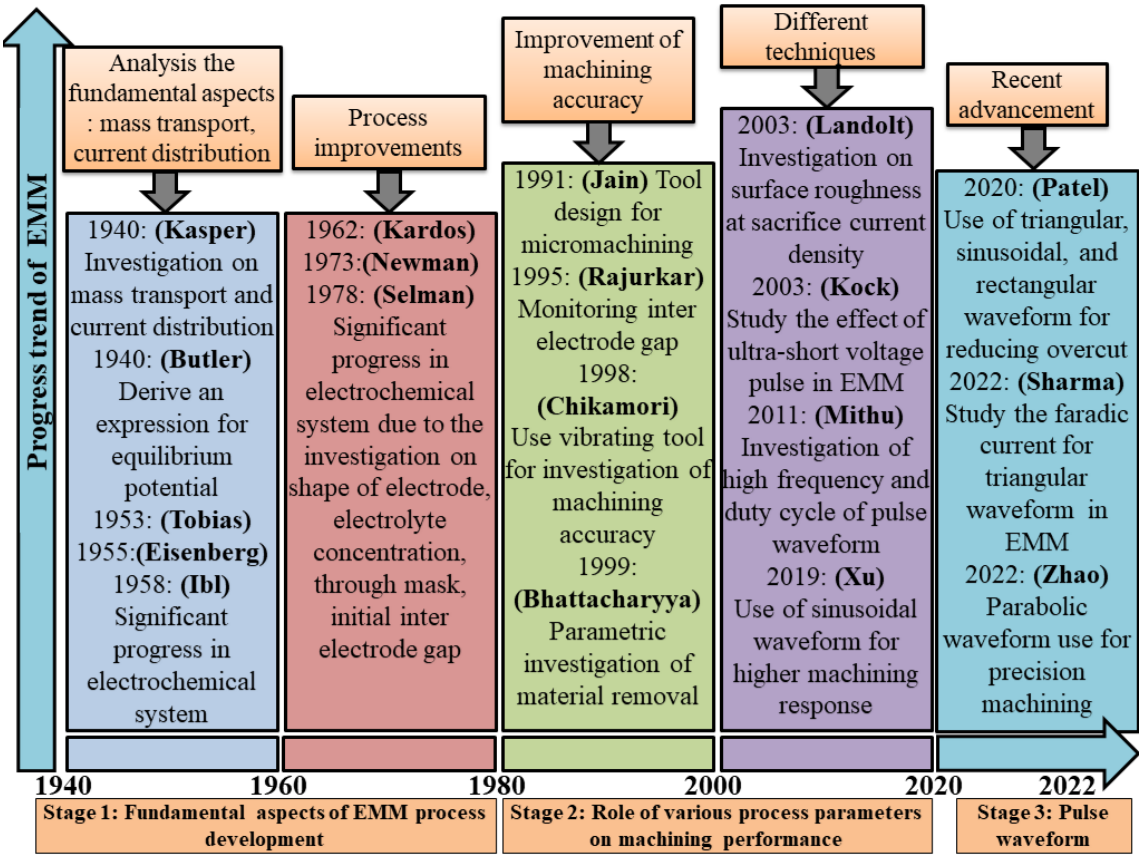

Fig. 1.4. A short chronological review of EMM progress

The details literature reviews are categorized as follows:

(i) Fundamental aspects of EMM process development,

(ii) Role of various process parameters on the machining performance, and

(iii) Recent advancement on electrical pulse waveform.

(i) Fundamental aspects of EMM process development

Many attempts have been made to create a functioning setup in this novel field of micromachining. The goal is to understand the different aspects of machining and explore its capabilities. In this context, managing the output efficiently is essential for controlling and achieving the desired results. Furthermore, the results are dependent on the accurate machining conditions, which might again add flexibility in meeting specific output requirements. In order to understand the fundamental concepts of the electrochemical micromachining (EMM) process, i.e., basic principles, machining characteristics, and EMM setup development, a detailed review of various research articles is presented in the following discussion.

Datta et al. [27] demonstrated that electrochemical micromachining (EMM) plays a promising role in the fabrication of microcomponents in the modern electronics industry. The authors investigated the maskless EMM technique, revealing that by varying pulsating current parameters such as pulse on time, pulse off time, and current density, the desired machining rate can be achieved. The authors also explored a maskless electrochemical micromachining technique and investigated instances of electrochemical capillary drilling, focusing on micro holes ranging from 0.25 to 0.4mm in diameter. The authors highlighted that EMM shows great promise as a future micromachining technique across various application areas due to several advantages, including higher machining rates, improved precision and control, and the ability to work with a wider range of materials. However, authors also highlighted the importance of fully understanding the high-rate anodic dissolution process for EMM to become an efficient micro-manufacturing technique.

Datta and Harris [28] illustrated the benefits of the electrochemical micromachining (EMM) process over the wet chemical etching process. Comparative experiments between wet chemical etching and EMM for molybdenum mask fabrication were conducted. EMM in a salt solution at ambient temperature was compared with conventional chemical etching processes using a ferricyanide solution at 55°C. Performance criteria such as machining rate, surface finish, aspect ratio, and simplicity of operation were investigated. The rate of metal removal in EMM is governed by the machining current, which can reach significant levels under appropriate hydrodynamic conditions within the electrochemical cell. Metal removal rates in EMM have been

observed to be orders of magnitude greater than those in chemical etching. In EMM, specific current density is effective for achieving smooth surfaces and uniform patterning. The authors promoted EMM as an environmentally friendly processing technology, considering operator safety, waste disposal and electrolyte monitoring and control.

Rajurkar et al. [29] highlighted the use of ECM concepts for electrochemical etching of microparts in the electronics industry. The authors also discussed a comprehensive review of current research, development, and industrial practices in ECM. It covers the fundamental principles of ECM and recent efforts to enhance ECM tool design. Additionally, the authors introduce the concept of pulse ECM along with its associated technological advancements. The author also discussed the modeling and simulation of numerically controlled (NC) ECM processes. Furthermore, the review addresses the applications of ECM in microfabrication and surface finishing, as well as concerns related to environmental impact. It explores the basic principles of hybrid machining, which involves integrating ECM with both traditional and nontraditional machining processes. The benefits and various applications of hybrid machining are also discussed. The authors stressed that EMM offers better control and flexibility for micro-fabrication, requiring minimal monitoring and raising fewer environmental concerns. To improve the process for silicon fabrication and LIGA, technical issues were addressed, including stray metal removal, tool structure, electrolyte flow, and machining gap. For the application of self-acting fluid film bearings, micro-features, i.e., micro-groove, were fabricated through EMM, and it was emphasised that this process is very helpful.

Masuzawa T. [30] described the principle of electrochemical dissolution for micromachining, emphasizing the importance of tools for 3D micromachining through electrochemical etching. In this research work, the author provides a summary of the fundamental concepts and applications of major micromachining methods. The basic characteristics of each method group are examined, drawing upon various machining phenomena. The advantages of EMM were highlighted, such as almost zero machining force and machined surface is free from damage, stress, or heat effects. The authors also emphasized that the mechanical properties of the workpiece do not influence the material removal mechanism. The concluding part of this research work aims to delineate the scope of "micro" within micromachining. Literally, "micro" in micromachining denotes 'micrometer' and encompasses the range from 1 μm to 999 μm. However, "micro" also conveys the notion of "very small." In the domain of machining, the fabrication of very small products poses considerable challenges. Thus, "micro" should also signify

dimensions that are too small to be easily machined. Indeed, the definition of "micro" varies depending on factors such as individual perspective, machining techniques, types of products, or materials involved.

Datta et al. [31] reviewed electrodepositing and dissolution processes, discussing the crucial role of mass transport and current distribution. The authors illustrated the shape evolution through resist mask, cavity etching, and foil etching, stressing anisotropic anodic etching of metals through masks for the dissolution process. EMM represents a relatively recent technique employed for the precise shaping and surface structuring of metallic materials. The authors also discussed that electro polishing, applied to copper, nickel, and stainless steels metals; serve various purposes in micro fabrication and other industrial sectors. Additionally, chemical-mechanical polishing (CMP) plays a vital role in multilevel chip manufacturing, garnering significant attention in the electronics industry for ongoing enhancements. The authors highlighted EMM as a fast-growing technology in the electronics and microsystems industries. Additionally, addressing issues related to nanoscale structuring, fabricating high aspect ratio structures, exploring new functional alloys, developing multidimensional interconnects, and implementing automated large-scale processes, including additive control and electrolyte recycling, are crucial.

Schuster et al. [32] utilized ultra-short voltage pulses in electrochemical micromachining, discovering ultra-short pulse’s effectiveness in localizing the dissolution process and improving machining precision. The authors proposed the versatility of electrochemical processes for the nanometer range, offering new prospects for modern micromachining technologies. The authors also introduced a method for localizing electrochemical reactions on conducting materials with sub-micrometer precision. This involves creating a tool electrode directly on the workpiece, achieved through local etching of material. Control over the tool electrode's position in three dimensions enables precise 3D micromachining with sharp resolution. This precision is facilitated by applying ultra-short voltage pulses lasting only nanoseconds. These pulses exploit the short time constant for charging the double layers (DL) on the electrodes i.e., a product of electrolyte resistance and DL capacity. Consequently, significant charging occurs only at electrode separations within the nano to micrometer range. As electrochemical reaction rates are exponentially linked to the potential drop in the DL, reactions are highly localized to these polarized electrode regions in very close proximity.

Bhattacharyya et al. [33] presented an EMM setup including components such as

a mechanical machining unit, a power supply unit, and an electrolyte flow system. The authors successfully demonstrated the control of the inter-electrode gap using microprocessor-based controller systems. The authors explored the possibilities of electrochemical machining for micro manufacturing applications aims to establish its widespread utilization within the electronic and precision manufacturing industries. The authors also discussed various types of electrolytes and their pH values, suggesting the use of a neutral (pH=7) electrolyte solution to dissolve impurities. By decreasing the electrolyte concentration and machining voltage authors investigated the gap reduction between tool and workpiece. Authors highlighted the characteristics of tool materials for utilization in EMM. Where, tool materials must have good thermal and electrical conductivity, corrosion resistance, high machinability, etc. The diameter of tool should be in order of 150-200μm, which gives a high current density. Finally, the authors have effectively utilized the developed EMM setup to explore the potential for employing electrochemical material removal mechanisms in micro machining.

Kirchner et al. [34] introduced the use of mixed electrolytes, specifically concentrated hydrofluoric and hydrochloric acid, in the EMM process. Ultra-short (nanosecond) voltage pulses were employed to control electrochemical reactions for sub-micrometer precision machining. The authors showed that the formation of a passive layer on stainless steel could be prevented by choosing an appropriate mixture of electrolyte. The formation of a passive layer on stainless steel was effectively hindered by selecting the right combination of HF and HCl. A thorough investigation was conducted to analyze the impact of pulse duration and amplitude on machining precision. Through the use of appropriately designed tool electrodes, it became feasible to directly carve freestanding cantilevers or microstructures into metal sheets. The material was delicately removed, unveiling its grain structure without resorting to any chemical or mechanical alterations. This was evidenced by the vibration frequency measurement of the cantilever, which closely aligned with values obtained from the bulk material properties.

Kozak et al. [35] established a mathematical model and verified experimentally by using a developed ECMM system. The authors studied the effect of voltage and tool feed rate on process performance. Employing microsecond pulse durations and maintaining a small interelectrode gap through precise, numerically controlled tool electrode movement ensures the attainment of desired outcomes. The authors also explored the influence of voltage and feed rate on process efficacy while machining intricate cavities, ranging from 160μm to 180μm in slot width with straight edges. The experimental results reveal that

ECMM as a promising method for crafting complex micro cavities. However, the authors underscored the need for additional research into incorporating planetary motion into the tool electrode, integrating micro EDM and micro ECM, and fabricating 3-D micro cavities. The critical factors influencing ECMM process performance include voltage, feed rate, frequency, and duty factor. The model's high R2 value (95.76%) from ANOVA results validates its accuracy. The theoretical hypothesis of utilizing high-frequency pulses to achieve smaller gaps has been confirmed through experimentation. Results at higher frequencies (1 MHz) demonstrated smaller side and frontal gaps with sharper edges compared to those at 250 KHz. The authors concluded that ECMM is a promising machining method for fabricating complex microcavities.

Forster et al. [36] fabricated 3D microstructures using the die-sinking EMM process under tool electrode vibration. The authors observed that when the tool electrode moves toward the workpiece with vibration assistance, the electrolyte pressure in the gap increases, resulting in high electrical conductivity and low resistance of the electrolyte. Conversely, when the tool electrode moves back, the inter-electrode gap increases, improving electrolyte flushing and shape accuracy. Die-sinking ECM with a vibrating tool-electrode facilitates the production of microstructured parts in a range of highly stressed metals, even with high aspect ratios. It enables the creation of 3D geometries featuring intricate shapes and smooth surfaces. Ongoing research focuses on refining techniques for microstructuring various metals and exploring diverse applications. The development of a new generation of controlled three-axis ECM machines is essential to further advance this field. Experimental findings indicate a reduced occurrence of short-circuits and enhanced processing stability. Material removal rates achieved through ECM-milling are comparable to those of ECM-die-sinking. For example, stainless steel ECM-milling yields a rate of 0.049g/min, while ECM-die-sinking achieves 0.051g/min. This emphasizes the necessity for controlled ECM machines with three or more axes to accommodate the ECM-milling process. The authors concluded that tool-electrode vibration is effective for fabricating microstructures of highly stressed metals with high aspect ratios.

Cagnon et al. [37] generated 3D micro-features on stainless steel using mixed electrolytes and ultra-short voltage pulses, specifically HCL and HF. This technique presents an opportunity to merge the adaptability of 'top-down' approaches with the precision of 'bottom-up' methods for crafting three-dimensional electrochemical microstructures. By directly controlling electrochemical reaction rates on the workpiece

surface, it leverages local polarization of the double layer. This method utilizes the finite time constant associated with the polarization of the double layer (DL) upon application of a voltage pulse. This time constant is determined by the product of electrolyte resistance along the current path and the double layer capacitance, thus linearly correlating with the separation between the electrodes. The machining of the 200μm deep structure followed procedures akin to conventional milling. Throughout the process, the tool-to-workpiece contacts were monitored in real-time, adjusting the tool's feed accordingly to prevent such occurrences. The authors examined the oxide flitters formed during the fabrication of microholes on a stainless steel surface. The authors also observed that these electrochemically formed oxide flitters transformed into thick oxide films through progressing oxidation. These thick oxide flitters insulated the machining area, obstructing further electrochemical machining. The authors suggested that employing more aggressive electrolytes could prevent the formation of thick oxide layers.

Kozak et al. [38] investigated anodic dissolution under ultra-short voltage pulses. Additionally, the authors put forth a mathematical model designed to forecast the shape of the workpiece based on specific machining conditions. This model operates on the assumption of a coordinate system affixed to the workpiece during machining, with a moving boundary simulation employed for shape prediction. Validation of the mathematical model was achieved through comparison with experimental findings. The authors concluded that pulse voltage and feed rate exert a substantial influence on the machining performance of EMM. The findings from both theoretical and experimental inquiries into the correlation between characteristic shape dimensions imparted onto the anode-workpiece surface by micro-features of the cathode-tool electrode under specific machining conditions are elucidated. This investigation encompasses the electrochemical replication of slots, mini-holes, grooves, and insulating groove features. Moreover, the study delves into the limiting factors of micro-ECM concerning replication and micro-shaping with non-profiled tool electrodes. The authors concluded that the machining performance of EMM can be improved with ultra-short voltage pulses.

Rajurkar et al. [39] presented technical developments in electro-physical and chemical micromachining processes in a review article. The authors discussed process principles, mechanisms, characteristics, capabilities, and models of these processes, highlighting applications in various micro-engineering fields. The applications of electro-physical and chemical processes for machining were explored extensively, encompassing a wide array of components such as spinning nozzles, blanking dies, gears, optical parts,

blanking punches, drawing dies, coining dies, fluidic devices, molds for optical devices, texturing tools, medical parts, and medical tools. Researchers advocated for further advancements in instrumentation and control systems, as well as the integration of CAD/CAM systems for nano-machining. Scaling up processes for parallel processing during the machining of 3D micro features was also recommended. Addressing research issues such as the theoretical understanding of electro-physical and chemical processes at nanoscopic scales, the influence of materials, the effect of residual stresses, and environmental control were identified as crucial areas for future exploration. The authors also addressed research issues at nanoscopic scales, material influences, residual stresses, environmental control, and supporting technologies like standardization, metrology, and equipment design, along with non-technological issues like environmental effects and education.

Kock et al. [40] demonstrated the application of ultra-short voltage pulses in electrochemical machining, improving precision down to the lower nanometer range for fabricating three-dimensional structures. The authors explained that local charging of the double layer (DL) enabled control of the local electrochemical dissolution rate, leading to the successful fabrication of spirals on Ni sheet. The gap width between the tool and the workpiece was successfully reduced to approximately 600nm, with walls of comparable thickness exhibiting surface roughness and radii of curvature less than 100nm. The precision achieved in the machining process, as demonstrated in this study for structuring Ni, aligns favorably with high-performance lithographic methods. While high-resolution electron beam lithography can attain structure sizes on the order of 10-30nm, it is typically constrained to thin, essentially two-dimensional structures. The authors emphasized the critical significance of employing nanosecond voltage pulses for effectively localizing electrochemical reactions.The authors concluded that nanosecond voltage pulses play a crucial role in strongly localizing electrochemical reactions.

Shi Hyoung Ryu [41] developed an eco-friendly micro-ECM system using non-toxic electrolytes. The authors generated microholes and micro-cavities on the SS304 plate, investigating machining characteristics such as citric acid concentration, tool electrode baseline potential, pulse amplitude, pulse duration time, and pulse frequency. By applying pulses of a few hundred nanoseconds duration between tungsten SPM tip and SS304 work material, the electrochemical dissolution region is confined very near the tool tip end. The optimal conditions for micro drilling entail pulse amplitude of 7–8V, pulse duration of 300–350ns, a tool electrode baseline potential of -1.5 to -2V, and a pulse

frequency lower than 1MHz to ensure sufficient pulse off-time. A desirable concentration of citric acid is found to be 0.3M for electrochemical micromachining. Under the specified electric and chemical conditions, micro holes of 60µm and 90µm in diameter with depths of 50µm and 100µm, respectively, are drilled on SS304. Additionally, micro circular and square cavities with central islands are manufactured using the electrochemical milling process. Experimental results confirm the feasibility of micro electrochemical machining using citric acid electrolyte. The authors concluded that employing citric acid electrolyte for micro electrochemical machining is feasible and has the potential to be an environmentally friendly technique for commercial and industrial applications.

Bhattacharyya et al. [42] designed an independent EMM setup to effectively control the electrochemical machining process parameters for meeting micromachining requirements. The developed EMM setup includes various sub-components and systems, including a mechanical machining unit, a microtooling system, an electrical power and regulating system, and a regulated electrolyte flow system. The mechanical machining unit of the EMM system consists of components such as the machine body, feeding mechanism for microtools, machining chamber, and work mounting mechanism. A precise primary feed screw enables the microtool to travel 5 to 20µm. For the created EMM setup, the authors employed a DC pulsed power supply module with a voltage range of 0 to 15V and a current rating of up to 5A. Centrifugal pumps were utilized to propel medium-velocity electrolyte across the machining gap. The authors integrated all these system components in a way to conduct basic and fundamental research in the field of EMM.

Zhao et al. [43] developed micro-ECM setup to fabricate a deep micro-hole with a diameter of approximately 100µm on stainless steel, which had a thickness of 750µm. The study focused on investigating the viability of micro-ECM at the micro to meso-scale. The authors created high-frequency short-pulse micro-energy power supplies, incorporating a detection system for monitoring the machining operation's state. This system provided data on machining voltage and machining current, potentially aiding in automating the machining process. The authors emphasized the need for more comprehensive research, particularly on micro-ECM machine tools, electrolyte and process parameter optimization, and system control of the machining process. Such efforts are deemed essential for achieving improved machining performance, including accuracy, smaller machining size, and the production of high-quality three-dimensional

micro parts.

Yong et al. [44] developed an experimental EMM setup for electrochemical micromachining, consisting of a computer, a pulsed power supply, and functionalities for gap management and machining process detection. The authors conducted successful micromachining experiments on microhole drilling and micro electrochemical deposition using the developed setup. Building upon the fundamental experimental behavior of electrochemical machining current with gap variance, a micro gap control strategy was introduced. This strategy involves monitoring the current jump-up to constrain the machining gap within 10 and 20μm. Machining experiments encompassed microhole drilling, layer-by-layer scanning machining, and micro electrochemical deposition. Preliminary results demonstrated the feasibility of localized electrochemical micromachining. To enhance machining accuracy and achieve smaller sizes, further research is necessary on electrolyte optimization, electrode insulation, and systematic control of the machining process. Additionally, authors proposed a micro gap control strategy based on the fundamental experimental behavior of electrochemical machining current with gap variance.

Kurita et al. [45] conducted electrochemical machining experiments to validate the effectiveness of the EMM setup. The electrochemical micromachining (ECMM) setup included a machining gap control system, with a current sensor positioned between the electrodes and interfaced to the mechanical system's actuators. In addition to validating the setup's effectiveness, the authors successfully performed 3D shape micromachining using a developed prismatic electrode. The authors produced a prismatic electrode with a base shape of 200 μm square. A machining system was developed to achieve three-dimensional shape electrochemical micromachining. The machining speed is observed to increase with the rise in machining voltage. However, beyond a predetermined threshold, the speed decreases due to the formation of bubbles from the electrode surface. To enable high-speed and small side-gap machining, the optimal machining pulse-on time and piezo-oscillation amplitude in this system were explored. Additionally, the machining speed and side gap were found to increase with electrolyte concentration. Furthermore, a constant current machining power supply and current controlling program suitable for electrochemical micromachining were developed to facilitate the process.

Zhang et al. [46] developed an innovative nanosecond pulse power supply for micro-ECM, utilizing the smallest pulse on time, i.e., 50ns. Two complementary MOSFETs, namely the IRF510 and IRF9510, were utilized to create a chopper circuit. The P-type

IRF9510 and N-type IRF510 MOSFETs can be independently driven by opposing voltage signals. Additionally, the authors devised a rapid protection circuit to safeguard against tool and workpiece damage resulting from short circuits. To prevent waveform distortion, especially at higher pulse frequencies, the authors created a complementary chopper circuit. Additionally, the authors developed a rapid protection circuit to prevent damage to tools and workpieces from short circuits effect. The power supply was utilized for several ECM experiments, and the results indicate that using a high-frequency power supply with a short pulse width leads to the creation of a higher quality surface finish and increased machining precision.

Huaiqian et al. [47] proposed the use of pure water electrochemical micromachining (PW-ECM) for aerospace applications. The authors highlighted the benefits of using pure water in electrochemical machining (ECM) to prevent corrosion of machined parts and minimize environmental contamination. The authors also developed a setup for pure water ECM (PW-ECM) incorporating a cation exchange membrane to enhance the potential gradient between the anode and cathode, thereby achieving higher material removal rates. Micro machining experiments were conducted, and the effects of damages to the workpiece surface resulting from short circuits and sparks were analyzed. To mitigate workpiece surface degradation, the authors combined micro-ECM with ultrasonic vibration. This, in turn, enhanced the localization and quality of the machined surface. Additionally, pressure waves generated during ultrasonic vibration-assisted PW-ECM were found to disrupt the formation of passive layers on the workpiece surface and effectively remove electrolytic slime, thereby improving the localization and quality of the machined surface.

Zhang et al. [48] conducted an investigation into the mechanism of electrochemical micromachining (EMM) with ultra-short voltage pulses and developed a theoretical model for the process. The authors examined the impacts of electrode gap and pulse parameters on the outcomes of EMM. The authors developed an experimental EMM system comprising an X–Y dimensional stage equipped with a motor driver, stepping motor, harmonic gear decelerator, ball screw, and motion parts. The data processing and movement control were centralized around a PC810 professional computer and a PCI-7344 multi-function control card from NI Corp. The feed distance per step in X–Y–Z directions was set at 0.08μm. Additionally, a hall current sensor was employed to detect the machining current signal. This sensor transformed the current signal from milliampere scale into a 0~5V voltage signal, which was then relayed to the analog input channel of

the PCI-7344 control card for real-time monitoring of the machining status. The authors successfully achieved the fabrication of troughs with a width of 20μm through the application of ultra-short voltage pulses, utilizing a tool electrode with a diameter of 10μm. The study's findings suggest that a decrease in voltage amplitude and pulse on-time duration may lead to an improved precision of microstructure shape.

Zhangz et al. [49] established an electrochemical micromachining system based on the principle of electrochemical material dissolution to produce microtools and microfeatures on a workpiece. The experimental setup included mechanical movement equipment, an ultra-short pulse power supply, an electrolyte circulation system, and a hall current sensor for detecting the machining status. With this machining system, the fabrication of probe shapes and fine surfaces of microelectrodes has been efficiently achieved online. Additionally, a finely shaped cross micro-groove has been machined subsequently using the electrochemical dissolution method. Integrating the machining of micro-tools and micro-workpieces into the same micro-ECM system has resolved critical issues related to the fabrication and assembly of micro-tools. Utilizing a fabricated tungsten microtool and ultra-short voltage pulses, the authors effectively created precise microgrooves with sharp edges on a nickel sheet through the process of electrochemical micromachining.

Mithu et al. [50] designed an electrochemical micromachining (ECM) work cell based on waveforms generated system to mitigate the negative effects associated with electrochemical micromachining operations. The authors employed a function generator to create pulses with various characteristics, used a digital storage oscilloscope to record the pulses, and implemented a computer-controlled guidance system to feed the tool and the workpiece. Pre-fabricated tungsten microtools were utilized by the authors to drill microholes in nickel, employing the pulse waveform monitoring approach as a predictive tool. The pulse waveforms generated during machining were analyzed in correlation with material removal rate, machining time, and the dimensions of the machined micro holes. Based on the experimental results, the authors concluded that the waveform generated during machining contains valuable information regarding material removal rate, machining time, and the dimensions of fabricated micro holes.

Thanigaivelan et al. [51] developed a constant gap control system for electrochemical micromachining (EMM). The setup maintained the initial set gap constant during milling by sending suitable command signals to the stepper motor through the microcontroller unit. The tool electrode feed mechanism, boasting a resolution of 2μm along the Z axis, is

meticulously crafted with a stepper motor and 8051 microcontroller. This setup meticulously maintains the initial set gap consistently throughout the machining process by issuing appropriate command signals to the stepper motor via the microcontroller unit. Continuous monitoring of the gap current in a closed-loop system is facilitated by a current sensor, which provides feedback to the microcontroller unit. For the fabrication of the work holding fixture, electrically nonconductive perspex material is utilized and securely mounted within the machining chamber. The electrolyte supply and cleaning system comprises a pump and filter. The authors conducted experiments on stainless steel (304) workpiece, employing tool electrode tips of various shapes, such as flat, conical with rounded and truncated cone.

Munda et al. [52] developed an EMM system, which contains multiple sub-components, including a mechanical machining unit, a microtool vibrating unit, an electrical power and controlling system, and a controlled electrolyte flow system, among others. The established EMM configuration demonstrates the ability to sustain the necessary IEG throughout the EMM procedure. The authors utilized a piezoelectric transducer (PZT) to provide vibration to the microtools, enhancing the circulation of electrolyte in the machining zone and leading to a reduction or elimination of microsparks generation. The authors endeavored to develop a comprehensive mathematical model that captures the interdependent and higher-order effects of various machining parameters such as machining voltage pulse on/off ratio, machining voltage, electrolyte concentration, voltage frequency, and tool vibration frequency on the primary micromachining criteria: material removal rate and radial overcut. To achieve this, they utilized response surface methodology (RSM) and incorporated relevant experimental data obtained through experimentation.

Zhu et al. [53] developed an experimental system to implement a hybrid process that combines grinding and electrochemical removal for machining precision small holes in hard materials. The experimental configuration involved a tool rotation and movement apparatus, a workpiece holder, an electrolyte cell, an electrolyte supply and filter, a power supply, a motion control system, and a data acquisition system. The experiments considered crucial parameters, namely machining voltage, tool rotational speed, and tool feed rate, to achieve a balance between material removal rate through electrochemical dissolving and abrasive mechanical grinding. By carefully controlling parameters such as machining voltage, tool rotation speed, and feed rate, the process achieves a balance between material removals via grinding and electrochemical machining. Consequently,

precision holes with sharp edges and no burrs are obtained. Moreover, the proposed process effectively removes the recast layer, enhancing the overall machining quality.

Spieser et al. [54] presented and discussed the problematic areas of electrochemical micromachining (μECM). The authors provided a comprehensive overview of the challenges faced by μECM technology developers and highlighted the latest innovative solutions. The authors introduced a comprehensive methodology for establishing the inter-electrode gap, where a minor voltage is administered to the electrochemical cell. Subsequently, the tool is advanced towards the workpiece until the identification of a short circuit. The tool is then gradually withdrawn at a slow pace until the electrical connection becomes imperceptible, facilitating the determination of the location of the workpiece's surface. The authors proposed that significant work is needed to consistently regulate the inter-electrode gap, suggesting the integration of fuzzy logic and neural networks knowledge into the μECM system for a more efficient and accurate machining process, particularly in modern control systems.

(ii) Role of various EMM process parameters on machining performance

The process parameters of the EMM system are crucial in achieving precise and effective machining at submicron levels. The electrochemical micromachining process is affected by several process parameters, including the applied voltage, machining current, type of electrolyte and concentration, inter-electrode gap (IEG), and micro tool feed rate. These parameters have a significant impact on the key machining criteria, such as metal removal rate, surface finish, and profile accuracy. This section of the literature review provides an analysis of the findings of different researchers regarding the impact of EMM process parameters on the enhancement of precision in the fabrication of micro features through EMM. These research initiatives are described below.

Bhattacharyya et al. [55] examined the impact of key process parameters, namely machining voltage and electrolyte concentration, on the material removal rate (MRR) and overcut in the micromachining of micro holes on a 0.4mm thick copper sheet. The authors noted an upward trend in the material removal rate (MRR) and radial overcut of micro holes with an increase in the machining voltage and electrolyte concentrations under specific parametric conditions. Based on the experimental outcomes, the authors determined a parametric combination of machining voltage and electrolyte concentration that can be utilized to achieve higher rates and accuracy in the machining of a micro hole on a very thin copper plate.

Bhattacharyya et al. [56], conducted a study to investigate the impact of different

electrochemical micromachining parameters, including machining voltage, electrolyte concentration, pulse period, and frequency, on the material removal rate, accuracy, and surface finish of micro holes fabricated on a 0.15 mm thick copper workpiece. The researchers explored the effects of various process parameters on unit removal (UR) and side gap, as well as precision and surface integrity, particularly in relation to the stray current affected area under specific parametric conditions. The experimental findings revealed that the UR exhibits an increase in response to both voltage and frequency across all parametric combinations.

Li et al. [57] conducted experiments through EMM to examine the effects of several important process parameters, including pulse frequency, tool feed rate, machining voltage, and electrolyte concentration, on the precision of micro-hole machining on stainless steel using a micro tool made of platinum wire. The authors noted that an increase in pulse frequency results in a decrease in the diameter of machined micro-holes, improving shape accuracy. Additionally, an increase in micro tool feed rate leads to a reduction in the side gap of the micro-hole. The authors observed that the diameter of a machined micro-hole increases with the voltage at a specific parametric combination. The authors identified effective process parameters for achieving higher machining accuracy of micro holes.

Lee et al. [58] conducted research on the characteristics of EMM, exploring various parameters such as voltages, currents, interelectrode gap size, electrolyte concentrations, machining time, and duty factor through simulations and experiments. The authors documented this information in their study and successfully created a tungsten carbide microprobe with a diameter of up to 10 μm through EMM fabrication techniques. Emphasizing the significance of controlling machining accuracy in relation to current density and inter-electrode gap, the authors observed a significant increase in the material removal rate (MRR) with respect to pulse-on time and applied pulse voltages. Furthermore, authors found that the hole size increased proportionally with pulse-on time and applied voltage.

Bhattacharyya et al. [59] aimed to examine the impact of key electrochemical process parameters, including machining voltage, electrolyte concentration, pulse on time, and frequency of pulsed power supply, on the material removal rate (MRR) and precision of electrochemical machining systems for micromachining. The authors proposed that maintaining a minimal inter-electrode gap of approximately 20 μm may enhance the precision of the machine's shape. Based on experimental findings, the authors

concluded that maintaining a lower electrolyte concentration, coupled with higher machining voltage and a moderate pulse-on time, results in a more precise shape with reduced overcut at a moderate material removal rate.

Yong et al. [60] explored the fabrication of complex grooves on a Nickel plate with a thickness of 100 µm. The investigation delved into various electrochemical process parameters, including electrical parameters, feed rate, electrode geometry features, and electrolyte composition, to assess their impact on machining quality. The authors specifically examined how pulse on time influences shape precision and the working end shape of the electrode on the machined surface quality. This study revealed that increased pulse frequency actually led to a decrease in machining accuracy. The authors attributed this to maintaining a constant pulse rate while reducing the pulse interval duration over the course of a pulse cycle, resulting in longer machining duration and, consequently, reduced accuracy.

Yong et al. [61] introduced a micro gap control method designed to regulate the distance between the cathode and anode in electrochemical micromachining. This approach involves the synthetic use of side-insulated electrodes with pulsed current, a widely adopted technique for various machining applications including micro-hole drilling, layer-by-layer scanning machining, and micro electrochemical deposition. The precise management of the electrode gap, typically within a range of a few 10 µm, is achieved by leveraging the sudden current variance signal during experimentation. The authors proposed for further exploration in areas such as electrolyte properties, electrode insulation, and systematic control of the machining process to enhance the understanding and capabilities of this micro gap control approach.

Zhang et al. [62] conducted a study to explore the impact of pulse parameters on the production of microgrooves through electrochemical micromachining (EMM). The research utilized a tungsten microtool with a diameter of 10µm that was fabricated in-situ. The authors reported that the width of the machining gap exhibited a linear variation in relation to both the pulse on-time and voltage. The study revealed that a reduction in pulse duration led to a corresponding decrease in the gap between the wall of the groove and the tool edge. The findings from the study suggest that decreasing voltage amplitude and shortening pulse on-time can contribute to achieving a more precise microstructure shape.

Jo et al. [63] achieved successful micromachining of features using a micro disk-shaped electrode with an insulating layer. Pulse on-time control was utilized to create a

reverse taper, barrel-shaped micro hole. The authors also successfully machined spherical cavities by manipulating the machining gap, achieved through adjusting not only the pulse duration but also the dissolution time. Proficiency in machining microgrooves within the microhole's wall was demonstrated through a technique involving the displacement of the tool electrode towards the centre of the hole, followed by an eccentric rotation of the tool electrode. The process incrementally increased the distance between the axis of rotation and the axis of the hole to gradually remove the surface layer in a layer-by-layer manner.

Malapati et al. [64] conducted an investigation to examine the impact of different process parameters in electrochemical micromachining (EMM), such as machining voltage, electrolyte concentration, frequency pulse period, and duty factor, on the achievement of micromachining requirements in terms of material removal rate and machining accuracy. The authors conducted experiments on copper sheet to determine the optimal zone that would improve machining accuracy and a significant amount of material removal rate. According to the experimental findings, it was observed that conducting machining with low voltage and short pulse periods resulted in a decrease in the dissolution rate and reaction products. Furthermore, these reaction products could be efficiently eliminated during the pulse off-time due to the lower amount of dissolved reaction products and the longer duration of the pulse off-time compared to the pulse on-time. This study revealed that the reduction in side gap leads to improved accuracy and surface integrity.

Jain et al. [65] studied the impact of process parameters, including voltage, electrolyte concentration, pulse duty cycle, and feed rate, on the machined hole diameter. The authors have formulated a mathematical model to establish a quadratic relationship between the diameter of the microhole and the parameters of the machining process. Based on the experimental observations and mathematical analysis, the authors concluded that an increase in voltage results in an increase in microhole diameter. Conversely, an increase in feed rate leads to a decrease in microhole diameter due to the reduced time available for machining. The relationship between duty cycle and microhole diameter is such that an increase in duty cycle results in a corresponding increase in pulse on time. This increase in pulse on time leads to a greater availability of electric charge for material removal, which, in turn, causes an increase in microhole diameter.

Kim et al [66] studied the impact of various EMM process parameters on the micromachining of 3D micro features on stainless. The authors noted that the machining

gap, which refers to the radial difference between the diameter of micro holes and that of micro tools, exhibits an upward trend with an increase in electrolyte concentration. The authors have identified that the unstable machining is caused by the prevention of uniform dissolution due to the depletion of ions in low concentration. The authors have indicated that there is a positive correlation between the size of micro holes and the magnitude of the applied voltage and pulse duration. The authors of this study have suggested that in order to attain a high level of machining resolution, it is advisable to utilize low voltage in conjunction with a short pulse on time. The disc type micro tool has been developed by the authors as a means to achieve taper-free micro features through a layer-by-layer micromilling approach.

Ghoshal et al. [67] performed an experimental investigation on various process parameters, including the pulse frequency of applied voltage, micro tool feed rate, and electrolyte concentration, with the aim of reducing the impact of taper angle, overcut, and corner deviation in micro features. The authors have confirmed from the experimental findings that the machining process is governed by the charging time constant of the double layer at higher pulse frequencies. Consequently, the machining resolution is significantly reduced, leading to a decrease in overcut. The authors have also observed that there is a reduction in overcut as the feed rate is increased. The authors have identified that as the Z-depth of the micro tool increases during operation, the surface area in contact with the workpiece also increases, resulting in equal current density on both the top and bottom sides of the workpiece. Therefore, the rate of dissolution is equated and the micro features are observed without any tapering. An increase in tool feed rate has been found to result in a higher taper, which can be attributed to insufficient dissolution time. It is noteworthy that the maximum current density is located in the bottom side zone of the anode in close proximity to the micro tool. The authors demonstrated the production of taperless micro features utilizing a forward taper micro tool through fabrication.

Ozkeskin et al. [68] developed a high frequency closed-loop EMM system. The present system involves the assessment of signals obtained from an ammeter and a laser displacement sensor, which serve as feedbacks for current and position, respectively. These signals are processed on a controlling computer. Serial communication is facilitated via a serial instrument controller interface board. Subsequently, the output signal underwent manipulation in accordance with input assessments and has been subsequently transmitted to actuators in order to execute the necessary operation. The

dynamic feedback control system was employed by authors to examine the impact of EMM process parameters, specifically pulse frequency, on micro microhole overcut and MRR. The study's authors reached the conclusion that the utilization of high frequency pulsed input resulted in a reduction in feature size and material removal rate, while simultaneously enhancing feature quality. The implementation of closed-loop inter electrode gap control has been found to result in expedited machining time and increased material removal rate.

Ahn et al. [69] investigated the impact of pulse off time on machining accuracy through the use of EMM to drill micro holes on stainless steel. The authors explicated the functions of the pulse off-time in terms of the potential charge that is discharged from the double layer capacitance during pulse off time. Subsequently, the thermal energy generated by the electric current, known as Joule heat, is dissipated, thereby preventing the electrolyte from reaching its boiling point. In turn, the ions that have undergone depletion during the operational period are restored through the processes of convection and diffusion of the electrolyte. In cases where the pulse off-time is insufficient for the elimination of charged ions, the diameter of the hole undergoes a continuous increase, similar to the machining properties observed with direct current voltage. The formation of bubbles caused by a comparatively short off-time interval induces surface roughness during machining and elevates the electrolyte's local resistance, ultimately leading to the creation of a taper.

Sen et al. [70] illustrated a comprehensive review of macro to micro hole drilling by electrochemical methods. Different electrochemical hole drilling techniques, including electrochemical micro hole drilling, shaped tube electrolytic machining (STEM), capillary drilling (CD), electro stream drilling (ESD), jet electrolyte drilling (JED), and laser-jet ECJM, have been discussed by the authors. The author’s highlighted important elements in micro- and macro-hole drilling, such as oversize or overcut, electrolyte properties' effects, tool insulation's effects, applied voltage's effects, tool feed rates' effects, aspect ratio's effects, shape's effects, and surface finish's effects. The authors emphasized that electrochemical hole drilling procedures are a superior option than all other unconventional hole drilling techniques for drilling cross-holes and simultaneously drilling numerous holes of various shapes. The lacks of residual tensions and superior surface polish have been the distinguishing characteristics of ECM drilling methods.

Mithu et al. [71] investigated the effects of applied frequency and duty cycle in electrochemical micro drilling. The researchers conducted experiments utilizing microtools of varying lengths and compared the resulting material removal rate (MRR) and machining duration. The authors noted that an increase in applied frequency resulted in a decrease in material removal rate (MRR) for short and long microtools, as well as an increase in machining time. The MRR and machining time exhibited a positive and negative correlation, respectively, with an increase in duty cycles. The authors have deduced from their experimental findings that a significant correlation exists between the dimensions and configuration of the microhole produced and the frequency and duty cycle employed during the micro drilling process. The results indicate that the MRR is significantly greater for a short tool as compared to a long tool. The findings of the authors indicate a positive correlation between the frequency of application and the incidence of short circuits. The observed reduction in entrance and exit diameters can be attributed to a lower degree of side erosion.

Fan et al. [72] employed an innovative rotational mechanism to create a micro hole on stainless steel plate. The authors have noted that the utilization of cathode tool rotation has demonstrated efficacy in the retrieval of insoluble sludge from a deep hole, as well as in mitigating the challenges associated with filling deep hole with electrolyte. In addition to the utilization of a rotational tool cathode, a pulsed power generator has been used to facilitate intermittent machining, thereby enhancing the accuracy of the resultant workpiece. The influence of working parameters, including pulsed on-times, applied voltages, electrolyte concentrations, pulsed frequencies, tool feeding rates, tool diameters, tool rotational rates, and hole depth, on the hole overcut during electrochemical micro-drilling has been examined by the authors.

Tsui et al. [73] conducted electrochemical microdrilling (ECMD) using a micro helical tool. According to the authors, the utilization of the microhelical tool in machining operations is expected to facilitate the infusion of fresh electrolyte into the machining zone and its subsequent flow into the bottom of the electrode through the inter-electrode gap, owing to the tool's shape and rotational movement. The aforementioned mechanism facilitates the renewal of the electrolyte by squeezing the reaction products through the electrode's helical groove, thereby removing them from the machining zone. The present research presents a cost-effective and straightforward approach to enhance the precision of the side gap, inlet diameter, and outlet diameter of the micro hole in the

electrochemical micromachining (ECMD) procedure. The authors conducted an analysis of the flow field status in order to gain an understanding of the flow field within the inter-electrode gap, utilizing computational fluid dynamics (CFD) application software.

Yang et al. [74] employed a semi-cylindrical micro tool electrode with the aim of addressing the challenge of electrolyte diffusion during electrochemical drilling. Furthermore, the authors implemented ultrasonic vibrations on the electrolyte to enhance its flow within the confined machining gap during the process of small hole machining. The authors placed emphasis on the utilization of a semi-cylindrical tool during machining, as it allowed for greater flow space for the electrolyte. This, in turn, facilitated the drilling of a hole to a depth of 300μm. For achieving this goal using a cylindrical tool without the presence of ultrasonic oscillations poses a challenge. The efficacy of machining has been shown to be higher when employing the semi-cylindrical tool in conjunction with ultrasonic vibrations, as evidenced by the authors. The application of ultrasonic vibrations resulted in enhanced electrolyte diffusion and convection, along with effective elimination of bubbles. This led to significant reduction in machining time. The reduction in machining time resulted in the inhibition of dissolution at the entrance of the hole, leading to an enhancement in machining accuracy.

Koyano et al. [75] conducted micro hole machining on stainless steel utilizing the electrostatic induction feeding method through the EMM system. The present technique involves the coupling of pulse voltage to the tool electrode through capacitance. The duration of the electrolytic current pulse is determined by the rise and fall time of the voltage pulse. The short duration of the voltage pulse leads to a considerably reduced gap width. The researchers noted that the reduction of pulse duration and pulse voltage, coupled with an increase in feed speed, can result in the attainment of micro holes with narrow gap widths. The protective oxide layer formed on the surface of the tungsten tool electrode resulted in minimal wear. The authors have devised and exhibited a servo feed system that relies on the assessment of gap voltage. This system has been utilized to machine micro-holes that possess a sharp edge and straight wall.

Park et al. [76] demonstrated a successful machining of deep micro holes with insulated tool electrodes in their investigation. The impact of tool electrode size on micro ECM has been studied, revealing that an increase in tool electrode size corresponds to an increase in the actual rising time of the double layer potential, while the cell impedance decreases. Hence, it is imperative to ensure a minimum pulse on-time to achieve an efficient potential for the prosperous machining process, considering the size of the tool

electrode. To employ the effective potential, an extended pulse on-time is necessary; however, this leads to an enlargement of the machining gap. The authors have assumed that the side insulation of the tool electrode is an efficient technique for mitigating the real-time increase of the double layer potential and for reducing the impact of size when the machining depth is substantial.

Thanigaivelan et al. [77] fabricated micro-holes in copper sheet by utilizing a developed EMM setup. The authors investigated the impact of process parameters on the material removal rate (MRR) and overcut, such as electrolyte concentration, machining voltage, frequency, and duty cycle. To determine the key factor influencing the EMM process, authors used Taguchi's quality design concept. Identifying optimal process parameters for minimizing overcut and maximizing material removal rate (MRR) is succeeded by confirmation tests to validate the predictions. Process parameters such as electrolyte concentration, voltage, duty cycle, and frequency were systematically altered using an L_{18} orthogonal array design. The optimal settings for minimizing overcut were identified as electrolyte concentration of 25g/l, machining voltage of 9V, frequency of 40Hz, and duty cycle of 34%. Conversely, to maximize material removal rate (MRR), the ideal parameters were found to be electrolyte concentration of 20g/l, machining voltage of 7V, frequency of 50Hz, and duty cycle of 65%. Through analysis of the F value (ANOVA), it was determined that the most influential factors affecting overcut and MRR were electrolyte concentration and frequency, respectively. Confirmation tests confirmed substantial enhancements in overcut and MRR, showing improvements of approximately 19% and 20.78% from the initial machining parameters to the optimized ones.

Ryu [78] employed electrochemical micromachining (EMM) with multiple electrodes to fabricate an array of micro holes. Simultaneously, three micro holes have been machined on a stainless steel plate. The authors maintained a feed rate that was half of the feed rate used in the machining process employing a single electrode. The use of multiple electrodes in machining, results in a reduction of the current for each hole, necessitating an increase in machining time. However, the duration of machining, concerning the number of electrodes employed, does not exhibit a proportional increase due to the influence of ion diffusion on the dissolution rate, in addition to the impact of current. The utilization of multiple electrodes has been proposed by the authors as a beneficial approach to enhance the efficiency of the EMM procedure. As a precaution to prevent excessive dissolution, the authors have developed a disk-type electrode, which has the capability to machine microstructures with a high aspect ratio while exhibiting

minimal taper.

Das et al. [79] fabricated circular micro holes on stainless steel by using a rotating cylindrical tool that was mounted on the machine spindle and rotated during the EMM operation. The authors successfully managed to achieve a less taper micro hole while maintaining satisfactory circularity. Nonetheless, the authors have not taken into account the radial overcut phenomenon as a result of the potential eccentric rotation of the micro tool. Therefore, the authors recommend exercising caution when mounting the tool onto the machine spindle in order to minimize eccentric rotation. The significance of achieving a minimal taper angle has been emphasized by the authors that highlighted the criticality of the flushing condition within the inter-electrode gap.

Malapati et al. [80] developed an EMM setup to create microchannels on a copper sheet. The researchers examined the impact of various factors, including pulse frequency, machining voltage, duty ratio, electrolyte concentration, and micro-tool feed-rate, on key outcomes such as material removal rate (MRR) and machining precision, as measured by width-over-cut (WOC), length-over-cut (LOC), and the linearity of the micro-channel. Authors developed mathematical models using response surface methodology (RSM). The machining of micro channels has been achieved through the implementation of a scanning type strategy, which involves the utilization of a micro-tool for the purpose of machining micro-channels. The authors have devised a multi-optimal combination of process parameters to attain the highest Material Removal Rate (MRR) while enhancing accuracy, specifically the width overcut (WOC) and linearity of the microchannel.

Ghoshal et al. [81] utilized sinking and milling techniques as a novel approach for the fabrication of micro channel. The present methodology involves the vertical movement of a micro tool to attain the final or requisite depth of the machined feature, which is subsequently followed by milling along the path of the micro features. The authors have devised a simulation model for the sinking and milling method, which demonstrates the distribution of equipotential curves in the cross-sectional gap between the micro tool and workpiece. The results of this research suggest that the sinking and milling technique for microchannel generation is more effective over the scanning method in terms of minimizing taper angle.

Rathod et al. [82] employed advanced EMM systems to fabricate blind micro grooves on stainless steel. The study conducted by the authors aimed to examine the impact of various EMM parameters, such as applied voltage, pulse frequency, duty ratio;

tool feed rate, and electrolyte concentration, on the precision of machining. Specifically, the authors investigated the width overcut, depth overcut, and material removal rate during the creation of microgrooves in stainless steel. In order to enhance the precision of microgrooves, the authors suggest utilizing a lower machining voltage, decreasing the electrolyte concentration, increasing the pulse frequency, reducing the duty ratio, and elevating the tool feed rate.

Rathod et al. [83] successfully fabricated 'C'-shaped microgrooves and multiple microgrooves suitable for micro thermal devices by employing optimal parametric settings during machining. The stability of the machining process has been investigated by the authors through the measurement of microgroove widths at various positions along the length of the microgroove. The authors investigated the impact of several process parameters in electrochemical micromachining (EMM) on machining accuracy. Specifically, the effects of applied voltage, pulse frequency, duty ratio, electrolyte concentration, and microtool scanning speed have been investigated to evaluate the accuracy of microgroove machining. The authors observed that the application of higher voltage results in an increase in the radius of curvature at the base of the microgroove, as well as in the microgroove width, depth, and taper angle along its sides. This phenomenon can be attributed to the heightened current density that occurs with increased voltage. The authors emphasized the importance of utilizing machining techniques with higher pulse frequency, scanning speed, lower applied voltage, duty ratio, and electrolyte concentrations to achieve precise microgrooves with better process control.

Liu et al. [84] introduced a layer by layer micro electrochemical milling technique. According to a mathematical model, the authors have identified that the milling layer thickness must be larger than the cylindrical electrode diameter to ensure adequate form accuracy. To address the challenge of breakage during the clamping process of micron-scale electrodes, authors proposed the use of an in situ fabricated cylindrical electrode. The micro cylindrical electrode, with a diameter of 10μm, has been successfully fabricated in situ. The authors investigated the mechanism and develop a mathematical model for the machining process involved in this innovative approach. Authors performed micro electrochemical milling experiments on nickel-base super alloy (GH3030) plate for illustrating the effects of machining parameters on the side gap, which has been taken into consideration for the assessment of machining localization. To achieve high machining quality, various suggested values for key machining parameters have been put forward. The successful fabrication of complex microstructures

underscores the potential of micro electrochemical milling as a promising micromachining technique for producing intricate MEMS (Micro-Electro-Mechanical Systems) components. Future research aims to fabricate even more complex structures with free surfaces using micro electrochemical milling technology, thereby advancing the capabilities of MEMS fabrication.

Yuan et al. [85] presented electrochemical micromachining under a mechanical motion mode. The authors proposed a method for aligning tools based on the feedback of tunnel current. Researchers investigated the effects of motion mode, rate, and the distance between the tool and workpiece on micromachining quality. The ultra-short voltage pulse technique (USVP) was utilized under the mechanical motion mode to exhibit multiscale ECMM on a copper (Cu) workpiece. The authors observed that an increase in the moving rate of the tool results in a decrease in groove width. Simultaneously, the uniformity of the groove improves with an increase in the rate of movement. Enhancing the rate of movement facilitates the extraction of machined products from the machining zone, thereby improving mass transfer.

Ghoshal et al. [86] investigated the optimal scanning speed for layer-by-layer micromachining of microchannels in EMM. The authors formulated an equation for calculating theoretical scanning speed, which was subsequently validated through experimental verification. The authors highlighted that the theoretical scan feed rates closely matched the experimental ones. Optimal feed rates were determined for different electrolyte concentrations under a consistent average applied voltage of 3V and a duty ratio of 34%. Research findings indicated that the EMM process exhibits instability when the concentration level is reduced to 0.05M. The authors also investigated the impact of microtool vibration on the microchannel generation process during scanning. Surface finish quality is achieved through the vibration of a microtool, exhibiting amplitude of 0.3μm and operating at a frequency of 80Hz. The study concluded that using a scanning technique for micro profile generation in EMM has the potential to enhance surface quality by providing fresh electrolyte at the machining zone, influenced by the scanning speed of the microtool.

(iii) Recent advancement on electrical pulse waveform

In the presence of oxide layer and gas bubbles, improvement of anodic dissolution is a challenging tusk for EMM. To reach the proper localization of anodic dissolution for precision machining, the control of potential transmission and current density are very essential. As the tool-tip area is very small as compared to the workpiece, stray current

plays a significant role in shape control management of machined products. Under different process parameter combination, localization effects can improve and reduce the extra dissolution from the target area. But, recently, several new electrical pulse waveforms such as rectangular, sinusoidal, parabolic, triangular, etc. have been used as an alternative technique to improve the material dissolution. The various research initiatives regarding different pulse pattern techniques, the rationale behind their usage, and the potential impact of these strategies on outcomes have been stated as follows:

Xu et al. [87] achieved the fabrication of micro-structures with excellent machining resolution by employing sinusoidal voltage pulses as an alternative to expensive ultra-short voltage pulses. Pulsed electrochemical micromachining utilizes the capacitive properties of the double layer to enhance machining profile precision when brief voltage pulses are applied. Metal dissolution during these pulses is primarily confined to the electrode regions where the gap between the tool and workpiece is minimal. The study also estimates the loading time of the double layer and introduces a method to quantify the precision of metal removal by comparing the calculated results with an ideal removal profile. Additionally, the research explores the impact of pulse characteristics on the dissolution process, revealing that a strongly non-linear polarization, when combined with nanosecond pulses and a small gap size, increases the precision and confinement of the metal removal process.

Xu et al. [88] have discovered that the machining resolution for microstructuring can be improved by establishing a positive feedback loop between two electrodes. The study investigates two fundamental methods aimed at enhancing machining resolution in pulse electrochemical micromachining. The first method involves a common approach: the reduction of pulse duration. The second, less frequently utilized technique, focuses on increasing the time constant within the circuit. The experimental investigation introduces an innovative approach for augmenting the time constant to further refine machining resolution. This novel technique introduces a positive feedback loop into the equivalent circuit of electrochemical micromachining, allowing the adjustment of the time constant through feedback gain control. As a result, feedback gain emerges as an effective control parameter for improving machining resolution. Experimental results reveal that an increase in feedback gain leads to a significant enhancement in resolution.

Patel et al. [89] found that under the application of a triangular pulse waveform overcut can be significantly reduced compared to sinusoidal and rectangular pulse waveforms. The authors attempted to reduce pulse energy by adjusting the duty cycle and increasing

the pulse frequency, such as heightened voltage requirements and increased idle time during machining. A theoretical model is first developed to quantify the input energy per pulse for voltage pulses of different shapes, including rectangular, sinusoidal, and triangular forms. Three numerical models for sinusoidal, rectangular, and triangular voltage pulses are created to predict the current density. Simulation results reveal that triangular voltage pulses result in the smallest diameter of micro-dimples compared to sinusoidal and rectangular pulses, respectively. The model's findings are validated using experimental observations, showing a reasonable correlation between the two. This emphasizes the efficacy of adjusting voltage pulse waveforms to optimize energy input and, consequently, machining outcomes in ECMM processes.

Xu et al. [90] suggested that by combining additional differential circuits with the rectangular pulse waveform, a real pulse signal can be generated, and using this signal, the machining gap can be reduced 11 times as compared to the rectangular pulse waveform. The resolution of pulse electrochemical micromachining technology can be significantly enhanced by reducing pulse duration and altering the voltage signal waveform. The machining accuracy and energy per pulse as functions of the differential times of the differential circuits have been calculated, in contrast to simulated and experimental results. In comparison to the use of rectangular pulses, this waveform approach can reduce the energy per pulse by approximately six times and can enhance the machining gap by a factor of approximately eleven. Employing this method, microstructures were successfully fabricated and achieved nanometer-level machining accuracy, demonstrating the feasibility and effectiveness of the proposed micromachining technique.

Sharma et al. [91] conducted an experimental investigation into faradic current using an electrochemical impedance spectroscopy system. The study revealed that optimizing the shape of the triangular pulse waveform, specifically achieving less pulse rising time and maximum falling time for each pulse on time, improves the localization of anodic dissolution. The findings indicate that rectangular pulse waveforms yield better machining efficiency. This research introduces a method for differentiating between capacitive and Faradaic currents in an electrochemical system under various pulsed potential waveforms. Ultimately, the authors concluded that the trends of Faradaic current obtained from the simulation closely align with the experimental results, highlighting the effectiveness of this approach.

Zhao et al. [92] discovered that by reducing the energy of the parabolic voltage signal, the

machining gap can be minimized by ten times more compared to the rectangular voltage signal. This study introduces a novel approach to electrochemical micromachining using a parabolic voltage signal. The method is presented by developing a mathematical model for the equivalent circuit that underlies this approach. In contrast to the use of rectangular pulses, employing the parabolic waveform notably reduces the energy delivered per pulse to approximately one-eighth of the original amount. This method has proven successful in practical applications, enabling the processing of microstructures with exceptional machining accuracy at the nanometer level. An important advantage of this proposed technique is that it obviates the requirement for costly ultra-short pulse power supplies, making it a more accessible and cost-effective solution for industrial applications in the field of micromachining.

1.7 Existing knowledge gap to outline the research objectives

The increasing demand for miniaturization across various industries has prompted scientists and engineers to explore different micromachining processes for advance materials, aiming to provide innovative solutions for microengineering applications. While stainless steel is commonly used for manufacturing microcomponents, because it exhibits a confluence of mechanical robustness, resistance to corrosion, and adjustable optical characteristics, while also has conductivity, affordability in terms of production expenses, and flexibility. Advanced engineering materials offer superior properties, such as enhanced strength, durability, corrosion resistance, and tailored characteristics that make them more suitable for specific microengineering applications compared to stainless steel. However, a low-cost, quicker, and more accurate micro-fabrication process is required for the micromachining of simple microfeatures as well as 3D geometries with complex shapes and smooth surfaces in order to microfabricate structures. Thus, the material qualities of stainless steel fall greater of those of advanced engineering materials in various applications, including microsurgery, biotechnology, life science, microfluidics, high-temperature settings, and mechanical applications. Microfeatures including microholes, microgrooves, and 3D microfeatures have been fabricated on metallic surfaces using a variety of micromachining processes, including photolithographic machining, chemical etching, electro-discharge machining, ultrasonic micromachining and laser machining, etc. When used in real-world situations, these strategies have some significant drawbacks. For example, when photolithographic machining for high aspect ratio, masks are difficult to use, and starting costs are high, it all makes machining less precise. The most common challenges in micro-EDM are

microtool wear and imperfections created at the machined surfaces. Compared to other methods, laser micromachining is quicker and more precise, although heat-affected zones surrounding the machined surfaces are inevitable. Additionally, as depth increases, the microstructure tapers as a result of the laser's lower penetrating energy.

However, the electrochemical micromachining (EMM) technique has a remarkable ability to fabricate crack-free, stress-free, and heat-effect-free smooth surfaces on metallic materials, regardless of their hardness. As a non-contact machining method, EMM eliminates tool wear, thereby enhancing its suitability for large-scale production. Extensive literature surveys reveal that high-precision microgrooves are preferable in applications such as micro thermal devices, reactors, biomedical diagnostics, aviation, and cooling channels due to their ability to achieve better surface finishes. Similarly, precise microholes and microchannels are widely used in electronics circuits, automobiles, microsurgery tools, and so on.

In the presence of oxide layers, gas films, bubbles, and sludge in narrow inter-electrode gaps, improving anodic dissolution is a challenging task for EMM. Researchers have used various arrangements to remove sludge and gas bubbles from the machining zone, such as tool vibration, electrolyte flushing, electrolyte jets, mixed gas jets, etc. Extensive research has been carried out under different process parameter combinations to improve the accuracy of EMM. In EMM, electrolyte flushing creates several problems, such as generating unwanted vibrations of the micro-tool and workpiece, hampering accuracy, and disturbing the proper supply of electrolyte at the target machining zone.

However, there are significant gaps in the investigation regarding the improvement of proper localization of anodic dissolution and the control of potential transmission and current density for precision machining, without employing the electrolyte flushing arrangements, expensive ultra-high-frequency pulse power supplies, and other mechanical applications. Recently, various popular pulse pattern waveforms, such as sinusoidal, triangular, and parabolic, have been employed to enhance the accuracy of EMM, assisted with electrolyte flushing or tool vibration. Therefore, to enhance EMM performance, further investigation has to be carried out to develop various new innovative pulse waveform techniques aimed at flushing out gas films, bubbles, and sludge from the narrow inter-electrode gap under stagnant electrolyte conditions. To verify the feasibility of these new techniques, attempts have to be made to fabricate various micro-features, including microholes, microdimples, microgrooves, complex microgrooves, etc., on advanced engineering materials.

1.8 Objectives of the Present Research

Previous research has indicated that researchers have explored various methods, including tool vibration; electrolyte flushing, electrolyte jet, and mixed gas jet, to remove oxide layers, gas films, bubbles, and sludge for enhancing anodic dissolution in electrochemical micromachining (EMM). However, these techniques can cause issues such as unwanted vibrations of micro-tools and workpieces, reduced accuracy, and disruption of proper electrolyte flow to the target machining zone. Moreover, there are significant gaps in the investigation of EMM performance which is closely linked to the characteristics of voltage pulse waveforms. Understanding how these waveforms affect to enhance the performance of EMM and advance micro-manufacturing capabilities. This knowledge gap underscores the importance of systematic experimental analysis to elucidate the complex relationships between waveform parameters of power supply and the improvement of EMM performance. Hence, a new DC pulse waveform has been designed to enhance the performance of EMM. Keeping in view, the existing research gap in the EMM process, the following research objectives have been considered.

(i) To develop an Electrochemical Micro-Machining (EMM) setup using various sub-systems, such as a mechanical machining unit, pulse D.C power supply, controller unit, and machining chamber for performing experiments.

(ii) To design and develop new voltage pulse patterns that introduces bunch of short pulses to improve machining performance. To study other important factors such as variation of pulse on time, frequency and duty cycle of pulse waveform during EMM operation.

(iii) To develop mathematical models for volumetric material removal (VMR), power transmission, transient response of double-layer capacitor, and root mean square (R.M.S) voltage for pulse-on time to gain understanding into the performance of the new voltage pulse pattern techniques and analyze the inter-electrode electric field properties, such as current density, energy density, electric field strength, and power loss, by utilizing simulation processes.

(iv) To minimize stray current effects, current density, short-circuit effects, and monitor the current-voltage characteristics by employing workpiece and tool insulation methods and discontinuous tool feed rate control technique under new pulse pattern techniques.

(v) To improve machining accuracy and surface quality by developing voltage pulse

width modulation and pulse amplitude modulation techniques for achieving better performance characteristics of EMM.

(vi) To further investigate machine performance with the help of new pulse patterns accompanied by multi-frequencies for improving accuracy in terms of overcut, shape of the machined profile, tapering effect, and surface finish, etc.

As mentioned earlier, the developed experimental EMM setup will play a helpful role to justify the uniqueness and originality of the present research work by incorporating various novel methodologies i.e. various pulse pattern techniques and exploring the possibilities of micromachining of various microfeatures on stainless steel SS304 material. The investigation of different influencing parameters of new developed pulse waveforms during EMM will help to understand the dissolution behaviour. The analysis of fabricated microfeatures based on critical examination of various SEM micrographs to determine the influence of significant pulse waveforms parameters on machining accuracy and surface roughness during micromachining may be another significant outcome. Moreover, the extensive research will help to bridge the existing gap in research and knowledge by contributing to a cost-effective machining system for fabricating intricate microfeatures on challenging to machine titanium materials for advanced microengineering applications. It will also provide an appropriate platform for the commercialization of this emerging anodic dissolution process.

Chapter 2: Development of setup and role of operational features of EMM

2.1 Introduction

The fundamental mechanism driving metal removal in electrochemical machining (EMM) revolves around anodic dissolution, wherein metals are removed from the workpiece surface atom by atom. Achieving effective and highly precise machining at submicron levels requires optimal control of the process variables within the EMM system. Several process factors significantly influence key machining criteria in electrochemical machining. These include precise microtool movement, maintaining narrow and uniformly regulated IEG (Inter electrode gap) throughout machining, ensuring the arrangement and rigidity of mechanical structures, fulfilling power supply requirements, implementing in-process monitoring, and organizing microtool and workpiece holding arrangements. Each of these variables plays a crucial role in determining important machining outcomes such as metal removal rate, surface finish, and profile accuracy, etc.

In order to delve into enhancing the EMM process, it's crucial to understanding the key factors that impact EMM criteria. Examining the factors that influence the EMM process can lead to the development of strategies that optimize control, enhancing precision and efficiency in metal removal operations. Despite advancements, there are still limited micromachining systems developed by research institutes, academic universities, and commercial companies. Some of these systems are multipurpose, serving both EMM and micro electro-discharge machining needs. Numerous research papers detail EMM's capabilities in fabricating microtools, machining microholes, and forming microstructures. However, as of today, there has a notable absence of a commercially available, ready-to-use EMM machining setup for micromachining applications. This gap persists due to the varying electrochemical micromachining parameters, dependent on electrode-electrolyte combinations and the desired shape and size of micro features, alongside the required machining accuracy. Consequently, achieving specific micro features with the desired machining accuracy necessitates a customized electrode-electrolyte combination and often requires distinct machining strategies.

The design of the EMM system configuration has been established considering following points of the above mentioned demands and with the subsequent research objectives:

(i) Establishment of a micromachining system with a rigid mechanical structure that allows for X, Y, and Z motions,

(ii) High-resolution microtool feeding setup,

(iii) Appropriate pulse voltage supply between tool and workpiece,

(iv) Electrolyte tank installation with a work holding fixture, and

(v) Fabrication of microtools with microtool holder, etc.

To construct different microfeatures on stainless steel (SS304) while achieving controlled anodic dissolution, an EMM setup has been effectively established in the current investigation through the implementation of systematic planning.

2.2 Details of EMM setup

The schematic representation depicted in Figure 2.1 illustrates a fundamental module of an EMM system configuration. This module comprises several subsystems, including mechanical machining unit, controller unit, direct current (DC) pulse power supply, and machining chamber equipped with work holding arrangement.

The fundamental operations of the distinct subsystems are outlined as follows:

2.2.1 Mechanical machining unit

The key objective of the mechanical machine unit is to give accurate motions to the microtool or workpiece, as well as support for the tool holder, the machining chamber, and other components as necessary. The primary machine structure, the machine controller unit, and a desktop computer with graphical user interface software are some of the components that make up the mechanical machining unit of the designed EMM system configuration.

(a) Main machine structure

The mechanical machining unit is able to configure into a gantry-type, construction depending on the manner in which the axes are placed, as illustrated in Figure 2.1. More workspace is offered in the gantry-type construction. Only one axis, the X-axis, is used to mount the work table, the machining chamber, and the system for holding the workpiece, leading to a stage with higher weight carrying capability. In order to minimize the initial cost of the machine, the other two axes, Y and Z, can be chosen to have a lower load-carrying capacity since these axes are relatively free. The gantry bridge consists of three units of long travel linear stages, which are operated by stepper motors, in a mutually perpendicular direction. The resolution of each stage is linear and measures 0.3125μm per incremental step of the stepper motor. The total travel length for the X and Y axes stage is 200mm, while the Z axis stage has a total travel length of 100mm. The platform's upper section is affixed with a base plate which includes an array of tapped holes for the

installation of various machining chamber units. The primary platform serves as the foundation for the machine structure, encompassing all stages and the base plate, and is supported by four adjustable mounts.

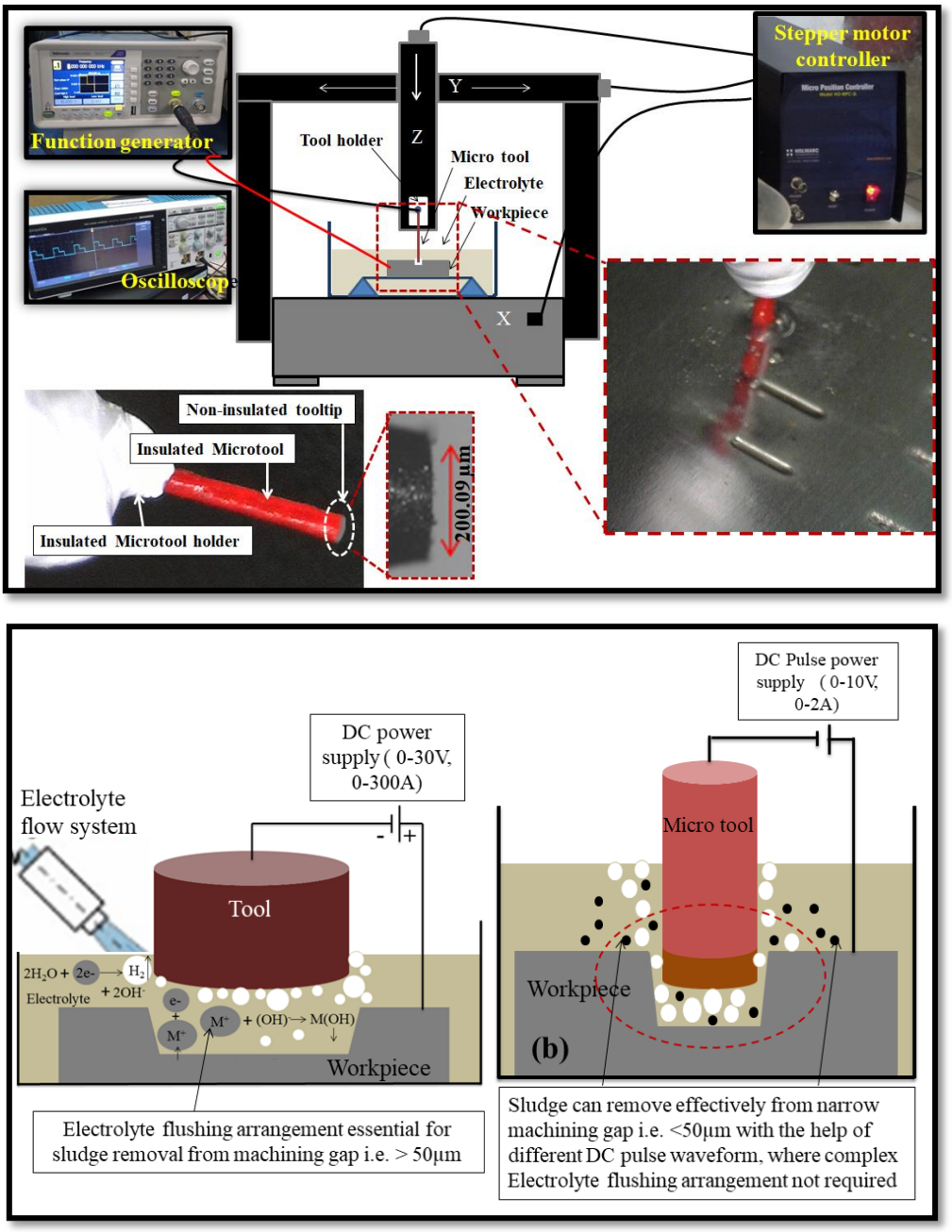

Fig.2.1 Schematic view of EMM system and advancement of the EMM technique in comparison to a simpler ECM process

(b) Machine controller unit

The stepper motors of all the long journey linear stages are synchronized and controlled by the machine controller unit, which also follows the user-specified route that is programmed into the machine. It connects the desktop computer, through serial port

RS232C, to the mechanical machine configuration. The position controller software on the desktop computer controls the motion of all the stepper motors which are connected to the machine controller unit.

(c) Position controller software

The user-friendly graphical interface of the position controller software makes it simple to operate the positioning system. There are two ways the user may interact with the system, or mechanical machining unit: manually and automatically using a computer programme. Each stage may be run at a unique speed and motion profile, with delays between motions, external devices or circuits actuated, and the stage itself triggered, all depending on the needs of the application. User-defined orders for stage motion may be entered into the software and carried out in a predetermined order.

2.2.2 Power supply unit

There are two types of applied power supply: full wave rectified direct current (D.C.) and pulse DC. The EMM process necessitates a significant current density of approximately 100 A/cm^2 to ensure optimal functionality. The possible outcome of this process is the generation of a substantial quantity of reaction byproducts, which may be only partially removed by the electrolyte, particularly in narrow inter electrode gap. The increase of contamination may result in the creation of deposits on the microtool, thereby obstructing the uniform dissolution of the workpiece material. Moreover, changes in the electrolyte composition and an increase in temperature can induce modifications in electrical resistivity, thereby deteriorating the accuracy of machining. The aforementioned issues may be effectively mitigated through the utilization of pulsed direct current voltage with suitable power parameters, compared to a continuous voltage source [21].

The technique of pulsed power supply micromachining involves periodic electrolyte change to achieve a higher instant current density during the pulse on-time. This approach leads to significant enhancements in machining accuracy and surface finish. The utilization of pulsed current enables the recovery of the proper gap during the pulse off time, thereby leading to controlled dissolution and enhanced accuracy compared to the deployment of continuous current. The use of pulsating current is particularly advantageous for achieving high-precision micromachining of delicate workpieces. In such cases, the flow rate of electrolyte may induce vibration and disturbance in the interelectrode gap (IEG). Due to it, in micromachining domain, electrolyte flushing is unsuitable. The process of anodic electrochemical dissolution takes place within a short

duration of pulse on-time. By reducing the pulse on-time to microseconds and increasing the current density, the precision and localization of anodic dissolution are enhanced. The removal of dissolution products from the IEG can be facilitated by the flow of electrolyte during the pulse off-times.

The power supply unit constitutes an essential component for EMM process. The power supply (DOSF-20V-60A, MATSUSADA, Japan) has been employed in this research work, as shown in Figure 2.2. The power supply has ability to provide a high current at a high frequency, while maintaining a predetermined value of various DC pulse waveforms. In the context of EMM processes, function generators and power supplies are commonly utilised. The power supply utilised in this EMM configuration has the capacity to produce an output voltage within the range of 0.1-20V, with increments of 0.1V. Additionally, it can generate pulse frequencies ranging from 1Hz-200kHz, with duty factor ranges spanning from 10-90%. Power supply is equipped with an integrated function generator capable of generating rectangular, square, triangular, and sine waveforms. Power supply has the capability to function in both constant voltage (CV) and constant current (CC) modes. Power supply has a maximum output current rating of 60A and equipped with supplementary features that enable over current protection (OCP) and over voltage protection (OVP) to ensure that the current and voltage levels remain within safe limits.

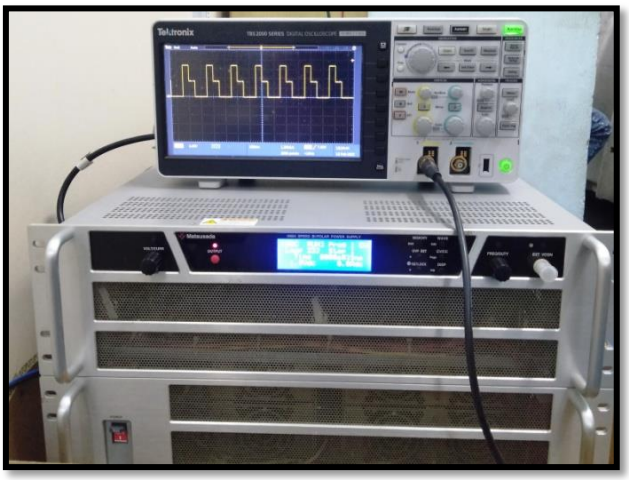

Fig. 2.2 DC pulse programmable power supply

(a) **Function generator**

A new DC pulse waveform has been designed indigenously by a function generator (AFG1022, Tektronix, US). With the help of arbitrary waveform design option of function generator, new pulse waveform can be designed through programming. Herein,

function generator can be employed as a power source instead of an expensive ultra-high-frequency DC pulse power supply. This function generator can supply maximum pulse voltage of 10 Vp-p, pulse frequency of up to 50MHz, and has the capacity to alter the duty ratio. The manipulation of pulse parameters, including pulse period, pulse amplitude, duty ratio (i.e. pulse 'on-time' and 'off-time'), pulse rise/fall times, and positive or negative bias, can yield varied outputs for a given frequency. These parameters are adjustable within a range from minimum to maximum values.

2.2.3 Data acquisition system

To facilitate the acquisition of data during the execution of the EMM process, various equipment such as digital storage oscilloscopes and digital multimeters have been utilised to monitor and record input and output voltage, frequency, waveform characteristics, and machining current, among other parameters.

(a) Digital storage oscilloscope

The digital storage oscilloscope (DSO) is employed for the purpose of observing and tracking the pulse waveform in the duration of micromachining operation. The digital storage oscilloscope (TBS2000) manufactured by Tektronix, with a bandwidth of 60MHz and a sampling rate of 1GS/s, has been utilized in the established configuration. The oscilloscope deals a visual representation of the pulse waveform, as well as accompanying information during machining. The utilisation of digital storage oscilloscope has been employed for the purpose of monitoring the machining conditions within a confined machining zone. Additionally, it has been utilised to identify the presence of any short circuit between electrodes by analysing the characteristics of the supplied pulse waveform. The digital storage oscilloscope has the capability to establish a connection with a desktop computer to enable real-time monitoring. The schematic view and oscilloscopic image of rectangular pulse waveform (RPW) and multi-step pulse waveform (MSPW) have been shown in Figure 2.3. Additionally, external storage devices can be utilised to directly store pulse parameters, which can then be subjected to subsequent analysis.

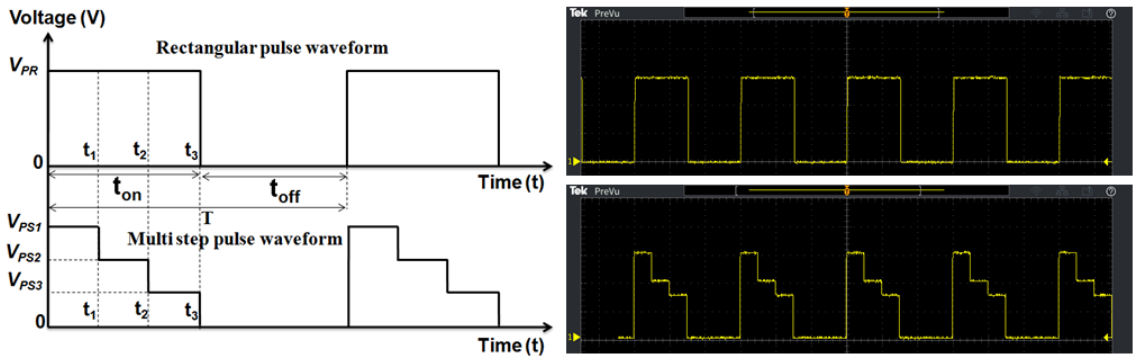

Fig.2.3 Schematic view and oscilloscopic image of rectangular pulse waveform (RPW) and multi-step pulse waveform (MSPW)

(b) Multimeter

In the experimental setup, a multimeter (U1252A, Agilent, United States) has been used to measure applied voltage, machining current, resistance, pulse frequency and capacitance, etc. A multimeter linked in series is required to measure the current flowing through the circuit during machining. It has also safety features mechanism for short circuit phenomena and over load circumstances to provide a delicate protection circuit to the machining system.

2.2.4 Machining chamber

(a) Electrolyte tank

In the EMM, stagnant electrolyte is preferable over flowing electrolyte in order to prevent unwanted microtool displacement. Therefore, an electrolyte chamber is used for electrolyte that has remained stationary. Workpiece i.e., anode and microtool i.e., cathode are immersed in an electrolyte with a very narrow IEG in an electrolyte chamber. A fixture for holding the workpiece is attached at the base of the electrolyte tank. Electrolyte tank construction materials are non-conductive, non-corrosive, light weight, transparent, and machinable to the desired size. In light of these specifications, Perspex material has been chosen for structuring of the electrolyte tank. Perspex is available in sheet form in a variety of sizes with a thickness ranging from 5mm to 100mm. For the manufacturing of different items with the necessary dimensions, sheets with a thickness of 12 mm and 25 mm have been employed. After that, it has been connected using stainless steel screws, and sealed with chloroform to make them leak-proof. Figure 2.4 illustrates a developed electrolyte chamber with a drain cock situated at the base of the tank on the front side to drain the tank's utilised electrolyte.

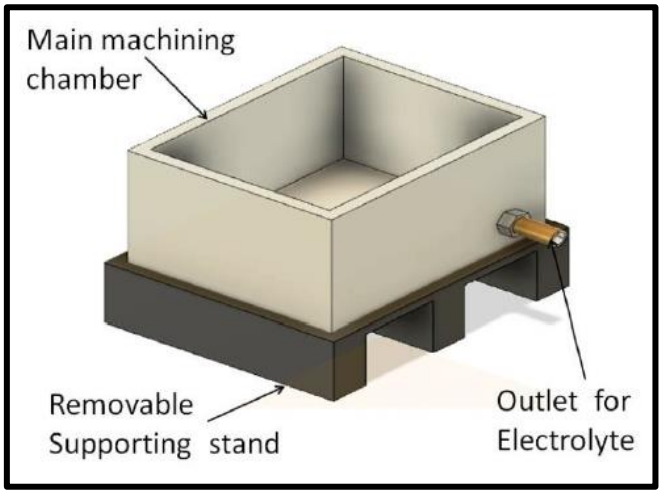

Fig. 2.4 3D schematic of main machining chamber

(b) Workpiece holding arrangement

A perspex workpiece holding structure is situated at the bottom of the electrolyte tank. The three-dimensional solid model of the work holding fixture, together with the workpiece and clamping nut-bolts, is shown in Figure 2.5. The M6 threaded breadboard, which is attached to the worktable with screws and nuts, is used to anchor the chamber and limit movement. The shape and size of the fixture have been designed to accommodate workpieces of various sizes and shapes. The workpiece can be securely clamped using a set of stainless steel clamping nut-bolts.

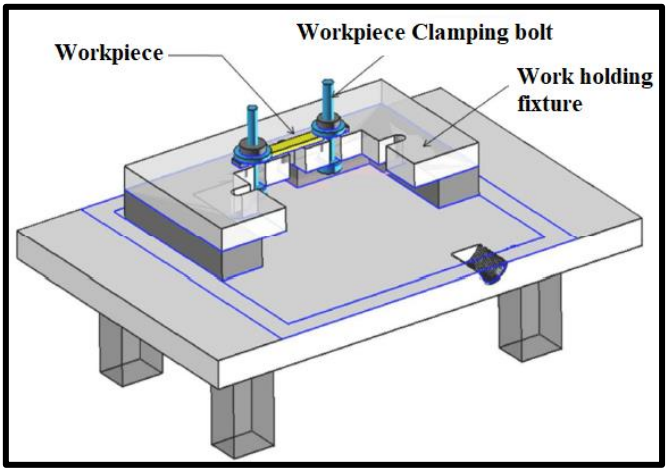

Fig. 2.5 3D schematic of workpiece holding arrangement

2.2.5 Specifications of the Developed EMM setup

The different EMM system components combined into a comprehensive configuration for precise control over the electrochemical dissolution process are shown in Figure 2.6. All the parts of the EMM system are visible in this photographic view.

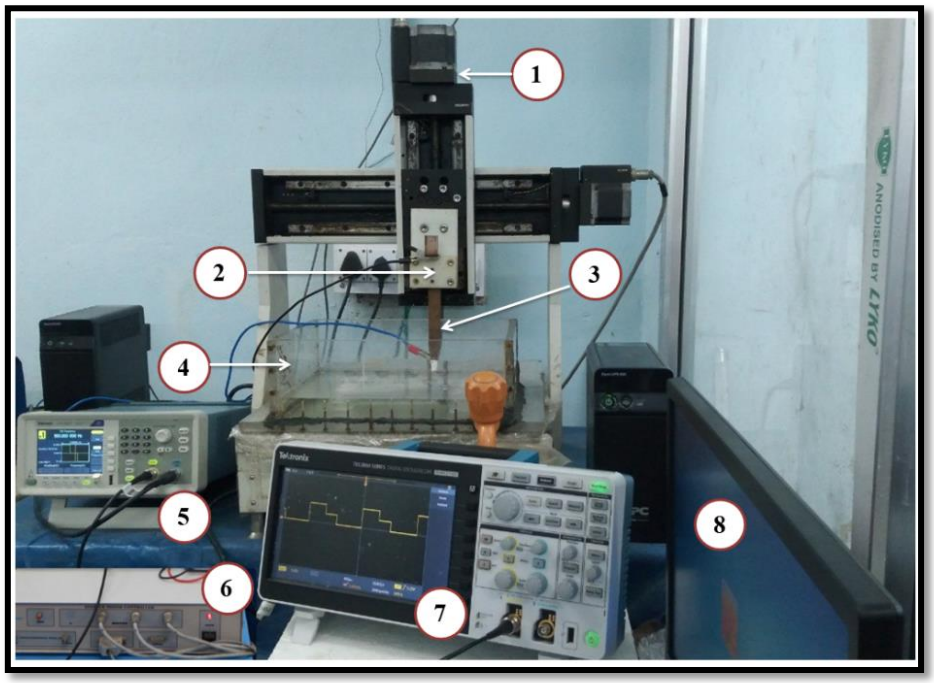

Fig. 2.6 Actual photograph of developed EMM setup consist with: Gantry x-y-z stage (1), Microtool holder fixture with z axis (2), Microtool holder (3), Machining chamber (4), Function generator (5), Stepper motors controller unit (6), Digital storage oscilloscope, and (7), Desktop computer (8)

Table 2.1 Specifications of the various units used in development of EMM setup

S.No.	Equipment	Specifications
1	**Mechanical Machining Unit (**Gantry Type**)**	
	Max. Travel of X/Y/Z-axis	200x200x100 mm
	Max. Speed of X/Y/Z	Axis 4 mm/sec
	Resolution of X/Y/Z axis	0.3125 µm
	Connector.	Three-8 pin for XYZ-axes each One RS 232 port for personal computer
	Power Supply	230 V AC / 50 Hz
	Software	Position controller software
2	**Microtool Holder**	Microtool holder 8mm x 125mm x 1mm thick copper sheet
	Tool Holding Fixture	60mm x100 mm x 8 mm Teflon-flat
3	**Power Supply Unit (MATSUSADA, Japan)**	
	Model	DOSF 20-60
	Output current	0.1-60A

	Output voltage	0.1-20 V
	Waveform and Frequency	Sine, Square, Triangle, Any arbitrary waveform 1Hz-200KHz
	Duty ratio	10-90%
	Input power	230 V AC / 50 Hz
4	**Function Generator (Tektronix- AFG 1022)**	
	Bandwidth	25MHz
	Signal Generator Modulation	AM, FM, FSK, PM
	Waveform	Sine, Square, Triangle, Any arbitrary waveform
5	**Digital Storage Oscilloscope** (Tektronix – TBS 2000)	
	No. of channels	2
	Bandwidth	60MHz, Sampling rate 1GS/s
6	**Digital Multimeter** (Agilent U1252A, USA)	
	Power supply	9 V Ni-MH rechargeable battery,
	Dimensions	94.4 × 203.5 × 59 mm
	Voltage (DC)	50mV-1000V, Resolution:0.001mV to 0.1V
	Resistance	500Ω to 500MΩ, Resolution:0.01Ω to .01MΩ
	Current (DC)	500µA to10A, Resolution:0.01µA to 0.001 A
	Capacitance	10nF to100mF, Resolution: 0.001nF to .01mF
	Duty cycle	DC Coupling 0.01% to 99.99%
7	**Machining Chamber**	
	Electrolyte Tank size	264 x 180 x 50mm
	Thickness of sheet	12mm
	Total height from base	102 mm
8	**Observation Microscope**	For on-line monitoring: DINOLITE 40X digital microscope, For off-line monitoring and imaging Leica DM-2500 optical microscope of magnification 5X, 20X ,50X and 100X and For SEM Micrograph: Scanning Electron Microscope (Zeiss EVO40)

2.3 Role of major operational features in process control of EMM

The precision of machined products and the stability of the EMM process depend on how the process parameters are selected, maintained, and controlled within the narrow

interelectrode gap (IEG). Applied voltage, machining current, electrolyte type and concentration, flow rate, inter-electrode gap (IEG), and other process variables for electrochemical machining have an significant impact on the machining criteria, such as metal removal rate, surface quality, profile accuracy, etc. The process parameters of EMM, which are factors that impact the machining accuracy of the workpiece, have been illustrated in the cause-and-effect diagram in Figure 2.7. To achieve effective and high-precision micromachining, the levels of control for the following primary process variables in the EMM system will need to be optimized.

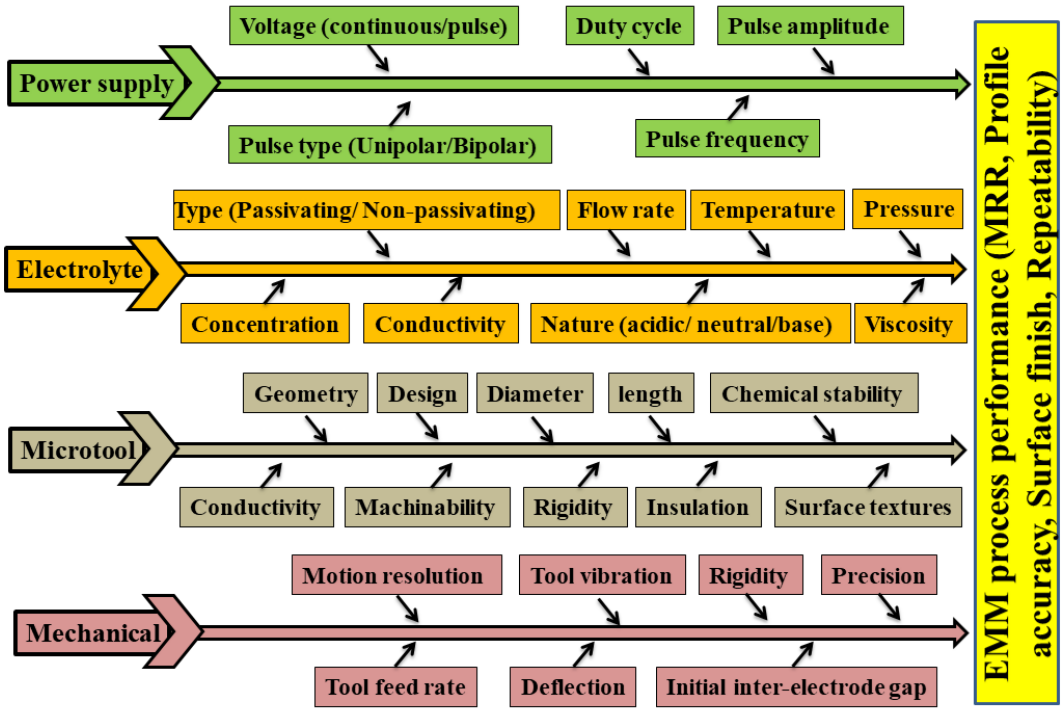

Fig. 2.7 Schematic diagram showing the influencing factors in EMM

2.3.1 Influence of power supply

2.3.1.1 Importance of DC pulse waveform in EMM

Over decades, the traditional rectangular pulse waveform has been used to the improvement of EMM accuracy. In narrow interelectrode gap (IEG), anode potential, overpotential, ohmic (IR) drop, and electrolyte resistance are more prominent and have much more impact on anodic dissolution. In the case of DC power supply for narrow IEG, an adequate amount of sludge is deposited on the tool surface, which acts as an electrical insulator that interrupts the anodic dissolution and creates the short-circuit effect. Due to this, the anodic dissolution cannot be continued uniformly during micromachining. However, by applying pulsed DC instead of a DC power supply, the maximum amount of sludge can be removed from the machine zone during the pulse off-

time. During pulse off time, machining is interrupted because, at that time, the applied voltage is zero. Thus, at that time, the new sludge formation possibility is very less than pulse on time. Therefore, after continuous machining when it stopped suddenly during pulse off time, a disturbance is created which produces pressure waves in the machining zone in turn helps to remove sludge. When pulse on-time is less than pulse off-time, the sludge can be completely removed from the machine zone without the involvement of any external mechanical force. The material removal in the ECM process is governed by Faraday's law of electrolysis. But in the case of EMM, the inter-electrode gap is very small, generally kept below 50 μm. In the electrolytic cell, when two metal electrodes are placed into an electrolyte solution, an equilibrium potential difference can be established between the metal and the solution. In this condition, the positive charge ions or cations are attached to the tool surface and the negative charge ions or anions are attached to the workpiece surface. Due to it, an electrical double layer (EDL) is generated. The behaviour of the EDL is analogous to a capacitor. When pulse voltage is applied between the two electrodes, the electrode potential cannot reach the peak voltage instantly. Thus, during pulse on time, initially, the peak voltage is reached through the EDL capacitor charging. When the EDL capacitor is fully charged, i.e., after the non-faradic time, a high rate of anodic dissolution can take place. Hence, metal ions and gas bubble occurrence can continue during the pulse on-time of the rectangular pulse waveform. Thus, during the pulse-on time, metal ions and gas bubble generation have not been controlled properly, and excessive sludge is deposited on the tool surface. Alternatively, when these gas bubbles break down at a higher anodic potential, micro-sparks can occur during machining, this increases the overcut and can reduce the machining accuracy. From the literature review, it has been noticed that triangular and sinusoidal waveforms have been used in place of rectangular waveforms for machining accuracy.

2.3.1.2 Influence of different types of DC pulse waveform in EMM

In EMM, process parameters are selected for the improvement of three basic factors such as machining efficiency, accuracy and quality. For the investigation of side gap in EMM, different type of pulse waveforms have been used as an alternative of direct current (DC) supply [93]. When pulse DC is used for EMM, anodic dissolution is taken place for each pulse on time, but during off time, this dissolution process remains stop. As a result, larger amount of material dissolution can be controlled; additionally pulse off time is effective for better sludge removal from the machining zone. During machining, sludge

obstructs the further current flow in-between two electrodes. Thus, by utilizing pulse DC, current flow also improved which is very effective for better localization. The improvement of machining accuracy depends on different pulse parameters such as duration of pulse on time and off time, voltage, frequency, and duty cycle, etc. Recently, several new electrical pulse waveforms such as sinusoidal, parabolic, triangular, etc. have been used as an alternative technique to improve the proper localization, and reduce the extra dissolution from the target area. The comparison study between conventional rectangular, sinusoidal and triangular pulse waveforms are presented in Figure 2.8. The total pulse on time is broken in 6 parts for three different signals such as rectangular, sinusoidal, and triangular waveforms, which is shown in a schematic diagram in Figure 2.8(a). From this investigation, it has been found that at t_3 time, the pulse voltage is same i.e., 10V for all waveforms, but at t_2 and t_4, time this voltage is different for waveforms such as for rectangular 10V, sinusoidal 8.65V, and triangular 6.66V. For better understanding simulation has been carried out through COMSOL software and it can be noticed that the current density is 1.47x 10^6A/m^2 for rectangular waveform, 1.31x 10^5 A/m^2 for sinusoidal and 2.88x 10^4 A/m^2 for triangular waveform. Thus, it can be observed that the current density is lower for triangular waveform and larger for rectangular waveform, and for sinusoidal waveform it is medium.

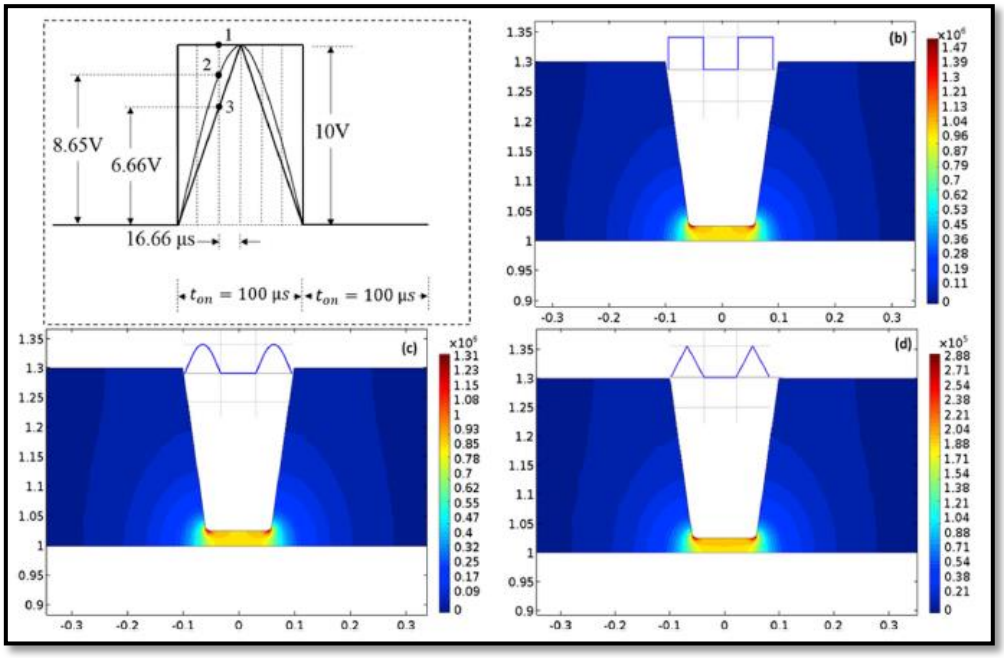

Fig. 2.8 Schematic diagram of pulse on time for rectangular sinusoidal, triangular waveforms (a), simulation results of current density of three waveforms (b, c, d) [89]

The reason of this fact is that during t_0 to t_2 and t_4 to t_6, the amplitude of rectangular waveform is higher than triangular and sinusoidal waveform. Only at the time of t_3, the amplitude of three waveforms is same. The root mean square (R.M.S) voltage for each pulse over time exhibits a higher value in the case of a rectangular pulse waveform, a moderate level for a sinusoidal waveform, and a lower value for a triangular waveform. Another important phenomenon is that the peak voltage duration time is longer for rectangular waveform, where sinusoidal and triangular waveforms have very short peak voltage duration time. Thus, rectangular waveform can removes larger amount of material from target area as compared to sinusoidal and triangular waveforms.

2.3.1.3 Effect of pulse voltage

The effect of pulse voltage in electrochemical micromachining (EMM) is a critical factor that determines the precision, material removal rate, and surface quality in the micromachining process. EMM is a non-traditional machining technique that employs an electrolyte and a high-frequency pulsating DC voltage to dissolve and remove material from the workpiece. Herein, the effects of pulse voltage in EMM are as follows:

(a) Material Removal Rate (MRR): The pulse voltage affects the current density at the inter-electrode gap. Higher voltages lead to higher current densities, which, in turn, influence the material removal rate and the shape and depth of the machined features. This is because a greater voltage difference between the workpiece and the tool electrode results in a more aggressive dissolution of material. However, there is an upper limit to this relationship because excessively high voltages can lead to excessive hydrogen evolution and thermal damage to the workpiece.

(b) Precision and Accuracy: Lower pulse voltages are often preferred when high precision and accuracy are essential. The use of lower voltages can produce finer and more controlled machining, which is essential in the application of complex microfeature's fabrication. High-voltage pulses can lead to a larger amount of material removal process, making them less suitable for precision machining.

(c) Surface Finish: The choice of pulse voltage also influences the surface finish of the machined part. Lower voltages tend to result in smoother surfaces, while higher voltages may lead to rougher surfaces due to increased material dissolution rates. Achieving the desired surface finish often involves a trade-off between voltage, material removal rate, and precision.

In experiment, selecting the appropriate pulse voltage in EMM involves an adjustment among these factors as mentioned above. Engineers and researchers must consider the specific requirements of the machining conditions, such as the desired material removal rate, surface finish, and dimensional accuracy, to determine the optimal voltage parameters. Additionally, the choice of electrolyte and tool material, as well as the design of the tool electrode, can also impact the effectiveness of the pulse voltage in EMM. Experimentation and process optimization are also necessary to achieve the desired results in electrochemical micromachining.

2.3.1.4 Effect of pulse frequency

The cycle period is relatively short when the frequency is very high. Once again, the charging of the double layer is necessary during each pulse on-time, which is occurred before the material dissolution. As a result, the amount of time in each cycle keeping for material dissolution is very limited. Double layer capacitance is constant for a given concentration of electrolyte-specific resistivity, and the double layer's charging time constant. As the double layer capacitance does not dependent on inter-electrode gap (IEG), EMM is possible to perform at extremely tiny IEG under the application of very high-frequency pulse. Thus, higher frequency with a lower IEG may lead to further improvement of machining accuracy. At high frequency, the cycle duration is much shorter, and anodic dissolution can occur during the pulse on-time. This leads to a decrease in the material removal rate, making it a more appropriate condition for electrochemical micromachining. When pulse on-time will go below the double layer charging time constant at much higher frequencies, there have no chance for machining. Hence, selection of pulse on time during higher frequency is most vital for controlled machining.

2.3.1.5 Effect of duty cycle

According to Faraday's law, a longer pulse period increases the pulse on-time, which raises dissolution and ultimately tends to raise unit removal [64]. Consequently, unit removal rises as duty cycle increases. The duty factor or duty ratio is used to represent the pulse-on and off time. The electrochemical dissolution of the anode occurs during on-time, and during off-time, these dissolved reaction products are entirely drained away from the machining zone, keeping it ready for the subsequent phase of dissolution. The

pulse off-time performs two tasks at once; first, because no machining is done during this time, reaction products are not produced; second, it helps in the removal of the dissolution products by flushing the electrolyte. In general, the on-time must be smaller than the off-time in order to maintain the IEG prepared for the next half-cycle (on-time) and entirely eliminate reaction products that have developed during the previous half-cycle (on-time) during off-time. When sludge removes properly from the machining zone, material removal rate increases. Lowering the pulse on-time also impacts the average machining current, which in turn decreases the current density, resulting in decreases material dissolution rate.

2.3.2 Influence of electrolyte and flushing process

Electrolytes are solutions that possess the ability to conduct current by generating ions. The electrolyte serves a dual purpose of enabling the electrical connection between the tool and the workpiece, as well as facilitating the desired machining responses. Typically, water in its pure form does not possess the ability to conduct electricity. However, the addition of any solvated ionic species to water results in its achievement of electrical conductivity. The electrical conductivity of an electrolytic solution is directly correlated with the concentration of ions present, which is influenced by the concentration level of the electrolyte, whether it is concentrated or dilute. Electrochemical reactions take place at the interface between an electrode and an electrolyte solution, typically a solution in bulk. The utilisation of electrode potential is employed to cause the dissolution of workpiece materials within an electrochemical cell. The dissolution process occurring within an electrochemical cell is dependent upon the hydrodynamic conditions of a given metal-electrolyte combination. The process of EMM involves a crucial responsibility of selecting an appropriate electrolyte for a given application. In general, the formation of oxide films on the surface of a workpiece facilitates anodic smoothing. However, in some cases, this process may result in short circuiting during EMM due to a narrower interelectrode gap (IEG). While the precipitate itself may not directly impact the process, its presence can increase the possibility of micro-tool damage resulting from a short circuit. Therefore, it is recommended to utilise a new and uncontaminated electrolyte for micromachining rather than employing a recirculation system.

Type of electrolytes

Electrolytes are characterised by the presence of unbound ionic species that provide electrical conductivity to the solution. The classification of electrolytes utilised in EMM can be based on their pH, which can be divided into three categories: acidic, neutral, and basic solutions, as illustrated in Figure 2.9. Electrolytes in the EMM process are chosen according to the specific workpiece material and process demands. The classification of electrolytes is primarily divided into two categories: passivating electrolytes that consist of oxidising anions, such as sodium nitrate and sodium chlorate, and non-passivating electrolytes that contain more aggressive anions, such as sodium chloride. Passivating electrolytes have been reported to provide superior machining accuracy, making it possible the machining of micro features with reduced side erosions. This phenomenon can be attributed to the development of oxide films and the occurrence of oxygen evolution within the stray current region.

The utilisation of acidic electrolytes in EMM offers benefits due to the production of soluble reaction products that can be easily removed from the narrow inter-electrode gap without causing any damage to the micro features of the microtool. The degree of dissociation of an electrolyte refers to the proportion of solute that undergoes dissociation into ions that possess the ability to conduct electric current, at a specific concentration. Electrolytes can be categorized as either strong or weak electrolytes, depending on the extent of solute dissociation. Strong electrolytes exhibit a significant degree of dissociation across a wide range of concentrations, whereas weak electrolytes tend to approach complete dissociation only at extremely low concentrations and exhibit a decrease in dissociation as concentration increases.

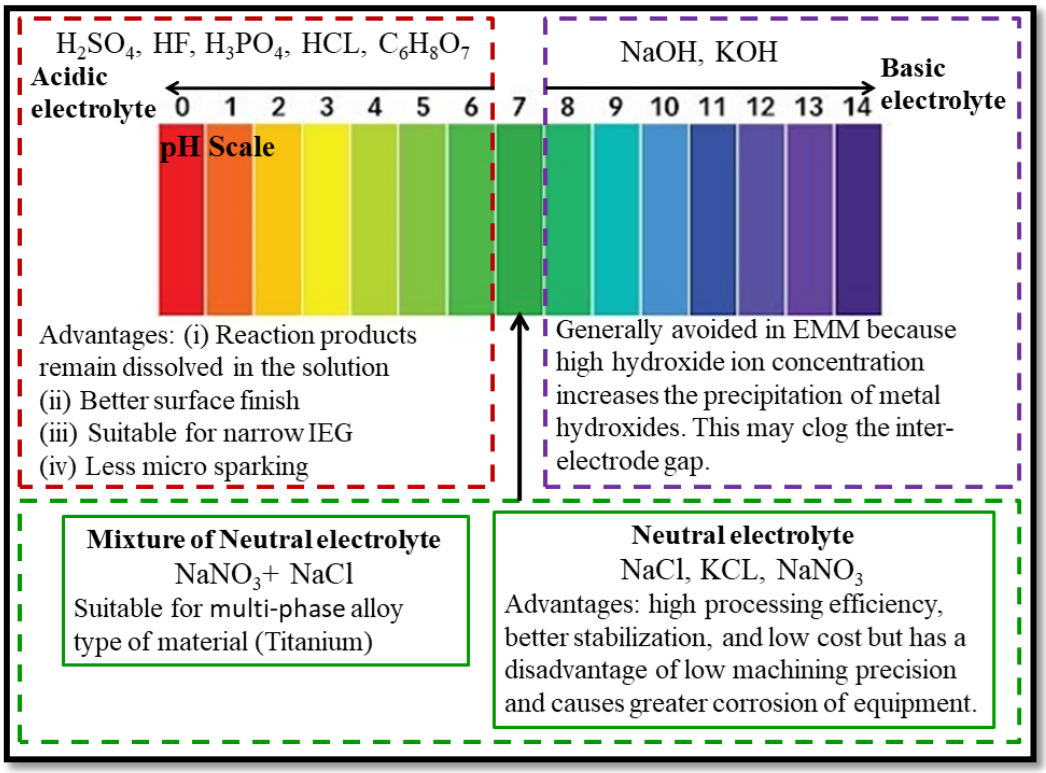

Fig. 2.9 Classification of the types of electrolytes used in EMM [94]

2.3.3 Effect of Microtool

Cylindrical rod of smaller size can be chosen as material for microtool. The ends of the microtool needs to be ground and polished to remove the end defects, and cleaned with acetone. To ensure the absence of flaws or cracks, inspection of all microtools should be observed by optical microscope (Leica DM 2500, Germany) before being soldered to the microtool holder. The finished microtool can be soldered to the front end of the tool holder. It is challenging to develop microtool for micromachining. It includes creating the microtool for proper machining, (i) selecting an acceptable material for the microtool, (ii) determining the exact shape of the microtool, and (iii) selecting tools, which also significantly impacts the cost and efficiency of the whole operation. The following are some of the most crucial details to understand about the microtool:

(a) Microtool material

In EMM, the micron-sized tools are used under hazardous working situations such as severely corrosive environments and increased temperatures owing to the Joules effect. As a result, microtool materials should have high electrical and thermal conductivity, strong wear, higher corrosion resistance, and better mechanical strength i.e. stiffness to handle electrolyte pressure. The microtool is often manufactured of chemically inert materials. The materials used include tungsten, copper, platinum, titanium, gold, nickel,

silver, molybdenum, and steel, which are employed as electrode in specialized applications. In order to get an appropriate microtool tip shape, the cut ends need to be ground and cleaned.

(b) Microtool shape, size, and surface finish

Microtool that are cylindrical, produced in diverse ways, and have flat, conical, reverse conical, spherical, or disc-shaped ends can be used in EMM. The size of the microtool is another crucial factor to increase machining performance. Increasing useful surface area in higher-diameter microtool improves the machining current and tool polarisation region. Surface defects on microtool have a direct impact on the quality of machined microfeatures. This phenomenon is seen on surfaces machined with a microtool that does not have a smooth surface. The existence of surface defects such as nicks, notches, scratches, lines, burrs, or similar types will be mirrored on the work surface. Hence, it is crucial to ensure a smooth surface for the microtool. Mechanical or chemical polishing can be used for microtool surface finishing.

(c) Microtool insulation

In EMM, stray current effects play a crucial role in increment of tapering effect and poor surface quality. Longer tool lengths during machining lead to slower machining speeds due to the increased stray current, resulting in greater overcut and pitting effects. Insulating the sidewalls of microtools is necessary to reduce stray current effects and prevent taper formation on the vertical walls of microfeatures. Utilizing sidewall insulation reduces the flow of current across the lateral surface of the microtool, thereby decreasing the rate of workpiece material dissolution along the sidewalls. The insulation thickness is few microns.

2.3.4 Influence of initial inter-electrode gap

The initial interelectrode gap (IEG), or the distance between the anode (workpiece) and cathode (microtool), is a crucial parameter for maintaining consistent metal removal during the process of EMM. A narrow initial interelectrode gap is considered for EMM, i.e., less than 30 μm to achieve the required level of accuracy. When the IEG is extremely narrow, on the other hand, it is essential to have a constant supply of new electrolyte and to remove all of the process by-products, such as sludge, heat, and gas bubbles that occur in the narrow machining zones. The initial inter-electrode gap in EMM can be reduced to micro-meter scale by decreasing the machining voltage and electrolyte concentration.

2.3.5 Influence of tool feed rate

In EMM, the time it takes to machine also affects how much the material dissolves. During machining of micro features, the tool feed rate controls how long the microtool stays in a certain place. Because of this, the microtool feed rate is one of the most important process parameters in EMM. To avoid short circuits during machining, the micro tool feed rate should always be less than the rate of material removal. This is because a short circuit can badly damage both the micro tool and the surface of the workpiece. Depending on the other EMM process factors, the right microtool feed rate can be selected. The estimation of the maximum feed rate of microtool under specific machining conditions can be accomplished by observing the incidence of sparks or short-circuits that arise between the microtool and the workpiece during the machining process.

Chapter 3: Experimental investigation of anodic polarization for improvement of machining accuracy under step pulse waveform

3.1. Introduction

The mechanism of EMM involves applying an electrical voltage pulse waveform between anode and cathode in the presence of an electrolyte solution, leading to anodic dissolution in the form of ions. This anodic dissolution rate depends on mass transport, current distribution, gas bubble generation, and behavior of the oxide film, among other factors. However, electrolyte flushing in EMM creates several problems such as generating unwanted vibrations of micro-tools and workpieces, hampering accuracy, and disturbing the proper addressing of electrolyte at the target machining zone. Hence, in the presence of oxide layers and gas bubbles, improving anodic dissolution poses a challenging task for EMM. To achieve proper localization of anodic dissolution for precision machining, controlling potential transmission and current density are essential. As the tool-tip area is very small as compared to the workpiece, stray current plays a significant role in shape control management of machined products. Localization effects can be improved under different process parameter combinations, resulting in reduction of extra dissolution from the target area. Recently, several new electrical pulse waveforms such as rectangular, sinusoidal, parabolic, triangular, etc., have been used as alternative techniques to improve material dissolution. Hence, meaningful investigations into polarization are essential for a better understanding of the impact of various pulse waveforms on electrochemical micromachining characteristics.

Due to industrial interest, the EMM process has been researched on different aspects such as machining accuracy, high MRR, smooth surface finish, stress-free surfaces, and machining ability of complex shapes, etc. However, previous research indicates insufficient emphasis on experimentally investigating anodic polarization to enhance machining accuracy with different pulse waveforms. Thus, the present research focuses on improving machining accuracy by modifying the traditional rectangular pulse waveform into a step pulse waveform, which is designed indigenously with a series of short rectangular pulses with different amplitudes. In the step pulse waveform, the partial discharging effect of the double-layer capacitor (DL-capacitor) is incorporated during the faradic time, allowing the pulse voltage to decrease from the maximum peak voltage to the second peak voltage during pulse on-time, thereby controlling anodic dissolution. To understand the transient response and total charging time of the DL-capacitor for different

waveforms, a mathematical model is established. Another mathematical model for volumetric material removal is developed to determine the minimal amount of material removed for each pulse on-time among various waveforms. Mathematically, the root mean square (R.M.S) voltage is calculated for each pulse on-time of different waveforms to find the least average voltage. Meticulous research and experiments have been carried out utilising the EMM setup. Comparative experiments have been conducted between rectangular and step pulse waveforms to investigate the behavior of waveforms, the influence of applied voltage on overcut and tapering effects, the characteristics of anode polarization at different applied voltages, and the transition from active to passive dissolution.

3.2 Transient response and total charging time of DL-capacitor for different waveforms

When a metal is placed in an electrolyte solution a potential difference is established between the metal and the solution and it becomes equilibrium when the positive charges in solution and negative charges in the metal are equal. At this condition, the metal ions are unable to cross the energy barrier until the applied voltage exceeds the activation potential. At the electrode-electrolyte interface, these opposite charges are represented as a double-layer, behaving similarly to a two-plate capacitor [6,95]. Figure 3.1(a) exhibits an equivalent electrical circuit (EEC) model of EMM, based on the Randles circuit model [96]. In anode, the two parallel resistances, such as the charge transfer resistance of R_{Act} and the double layer resistance of X_c, are connected with a series of electrolyte resistance $R_{electrolyte}$, as shown in Figure 3.1(b), which is discussed in chapter 1. Herein, the total equivalent resistance of EEC for the anode is considered as R_{eq}. Now, the EEC has been modified into a simple circuit, where an equivalent resistance i.e., R_{eq} is connected with double layer capacitor as shown in Figure 3.1(c). The capacitance of the double layer is represented as C_{dlayer}. When the total applied voltage of V_{in} is dropped across R_{eq} and C_{dlayer}, the current of I is generated in the closed circuit.

All resistances can be replaced by a single equivalent resistance which can be written as:

$$R_{eq} = R_{electrolyte} + \left(\frac{X_c \times R_{Act}}{X_c + R_{Act}} \right) \tag{3.1}$$

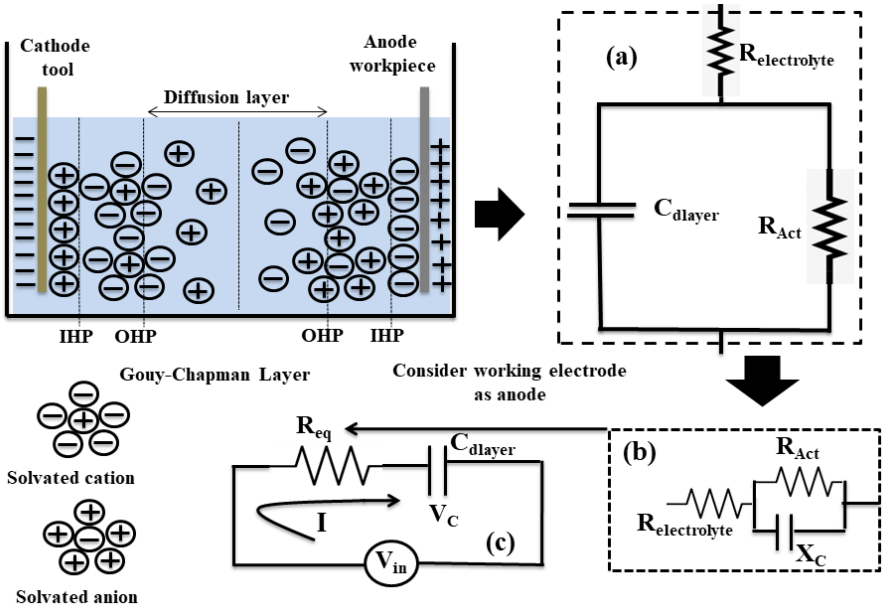

Fig. 3.1 Equivalent Electrical Circuit model of EMM

Applying Kirchhoff's voltage law in the RC circuit as shown in Figure 3.1(c), the total applied voltage of V_{in} can be calculated as

$$V_{in} = V_C + IR_{eq} \tag{3.2}$$

Where, I is close circuit current and V_C is voltage across DL-capacitor.

$$I = C_{dlayer}\frac{dV_C}{dt} \tag{3.3}$$

Since equation (3.2) can be written as

$$V_{in} = V_C + C_{dlayer}R_{eq}\frac{dV_C}{dt} \tag{3.4}$$

For DL-capacitor charging, the above equation can be written as

$$V_C = V_{in}[1 - e^{-t/R_{eq}C_{dlayer}}] \tag{3.5}$$

With the help of equation (3.5), voltage variation or transient response of DL-capacitor during charging time can be estimated.

Let's consider the time constant is τ for DL-capacitor.

$$\tau = C_{dlayer} \times R_{eq} \tag{3.6}$$

The fully charged DL-capacitor becomes discharged during the pulse-off time because the pulse voltage drops from maximum peak to zero. Thus, at the pulse-off time, the pulse voltage is zero.

Therefore, during discharging time, the voltage across DL-capacitor V_D can be calculated from equation (3.2) as:

$$0 = V_D + C_{dlayer} R_{eq} \frac{dV_D}{dt} \tag{3.7}$$

$$\frac{dV_D}{V_D} = -\frac{dt}{C_{dlayer} R_{eq}} \tag{3.8}$$

Let's integrate both sides of the equation (3.8), and can be expressed as:

$$\int \frac{dV_D}{V_D} = -\frac{1}{C_{dlayer} R_{eq}} \int dt \tag{3.9}$$

$$\log_e V_D = -\frac{t}{C_{dlayer} R_{eq}} + K \tag{3.10}$$

Where, K is constant. At the initial discharging time of the DL-capacitor i.e., t = 0, the DL-capacitor voltage is the maximum peak voltage i.e., $V_D = V_{in}$. Hence, applying these conditions, the value of K can be calculated as:

$$\log_e V_{in} = K \tag{3.11}$$

Now, applying the value of K in equation (3.10), V_D can be estimated as:

$$V_D = V_{in} e^{-t/\tau} \tag{3.12}$$

Utilising equations (3.12), the transient response of the DL-capacitor for discharging time can be estimated. By utilising equation (3.5), voltage variation across the DL-capacitor for charging time is estimated, when the input voltage is 1V and pulse on time is 5ms, as shown in Figure 3.2. From the figure 3.2, it has been noticed that when the DL-capacitor voltage reaches 0.632V or 63% of the maximum peak voltage, i.e., 1V, this time can be defined as the time constant of DL-capacitor. Thus, after 5-time constants, the DL-capacitor can be charged 99%, which is considered a transient period. Thus, the total charging time of the DL-capacitor or the non-faradic time of t_c can be estimated from figure 3.2 as

$$t_c = 5\tau \tag{3.13}$$

In the estimation of faradic time or machining time, this total time of non-faradic is helpful, as discussed later.

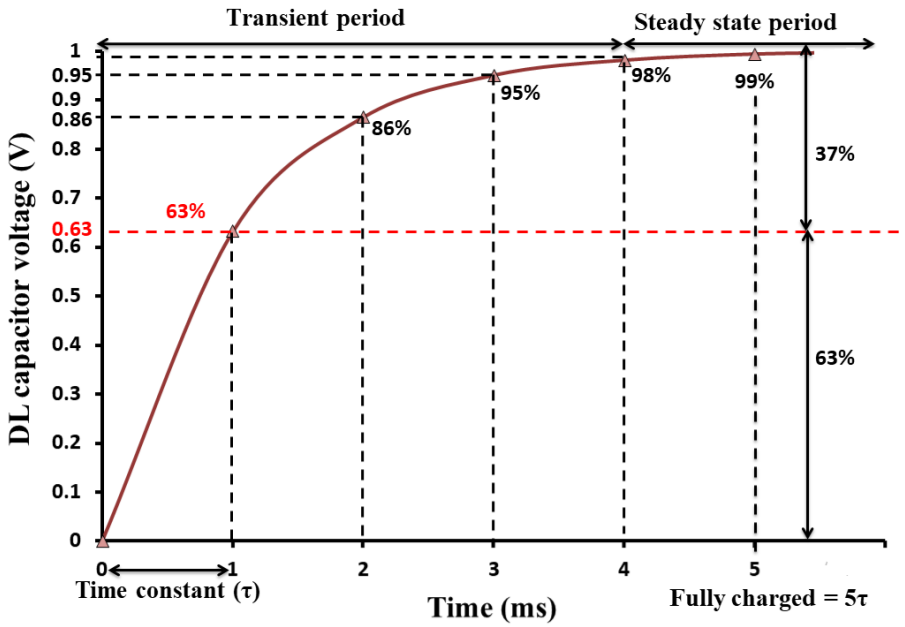

Fig.3.2 Transient response of DL-capacitor during pulse on time

When voltage is applied between anode and cathode in the presence of an electrolyte, the current is generated in the EMM cell and engaged for charging the DL-capacitor. The voltage across the DL-capacitor cannot reach the peak voltage until the DL-capacitor becomes fully charged. During this charging time, anodic dissolution is negligible, which is known as non-faradic time. Next, when the voltage across the DL-capacitor reaches the maximum peak voltage, anodic dissolution can take place properly because the maximum current is engaged for electrochemical reactions, which is known as faradic time. Similarly, from the equation (3.12), the transient response of the DL-capacitor can be analysed for discharging time. During this discharging time of the DL-capacitor, the rate of anodic dissolution decreases because at this time the voltage across the DL-capacitor drops exponentially from peak voltage. In order to better understand, this charging and discharging phenomenon are analysed by simulation process, which is discussed later in depth.

3.3 Design strategy of step pulse waveform

The design strategy of the step pulse waveform aims to control anodic dissolution during the faradic time. Thus, the partial discharging effect of the DL-capacitor is incorporated in the pulse-on time to regulate potential transmission in the electrolyte during each pulse-on time, as illustrated in Figure 3.3 (step pulse waveform). The critical aspect here is that the DL-capacitor does not discharge completely, as depicted in the GH region. To generate this partial discharging effect, two different peak voltages, V_{PS1} and V_{PS2}, are

incorporated during the pulse-on time, corresponding to the time intervals 0 to t_1 and t_1 to t_2, respectively. The first peak voltage of V_{PS1} is responsible for a higher rate of anodic dissolution, while the second peak voltage of V_{PS2} is utilized for lower anodic dissolution. As the voltage steps down from V_{PS1} to V_{PS2}, the discharging effect of the DL-capacitor occurs, leading to an exponential decrease in voltage. Consequently, anodic dissolution can be controlled for each pulse-on time.

For better understanding, the step pulse waveform is compared with the conventional rectangular pulse waveform. The charging and discharging effects are presented in a schematic diagram as shown in Figure 3.3. The non-faradic time or charging time of DL-capacitor i.e., t_C, is very important for micromachining because after this time proper anodic dissolution can take place. During charging time, the voltage variation across the DL-capacitor is the same for all types of DC pulse patterns because the time constant depends on the product of equivalent resistance of electrolyte and capacitance of the DL-capacitor, as illustrated in equation (3.6).

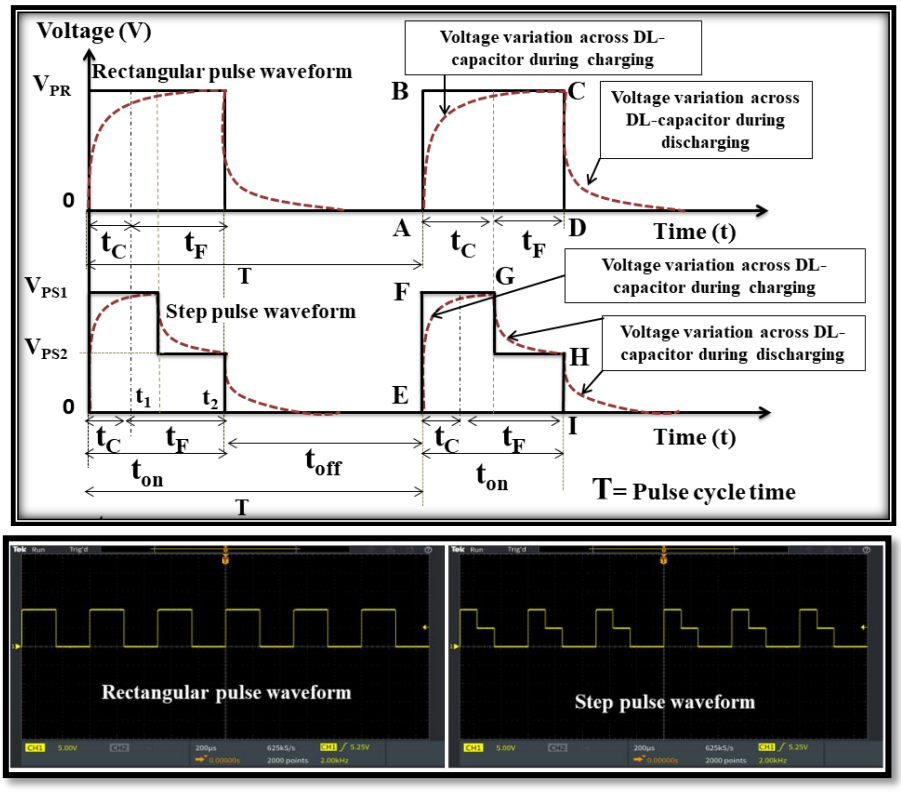

Fig.3.3 Schematic diagram of charging and discharging effects of DL-capacitor for rectangular and step pulse waveform

After charging time or non-faradic time (5τ), the DL-capacitor becomes fully charged and pulse voltage reaches the maximum peak voltage i.e., applied voltage, which is known as

faradic time t_F. At this condition, anodic dissolution takes place rapidly. As the pulse on time is the same for both rectangular and step pulse waveforms, the faradic time is also equal. During this faradic time, peak voltage remains constant for rectangular pulse waveform. Due to it, higher rate of anodic dissolution can take place, which removes unwanted extra material from the target area. However, in step pulse waveform, during the same faradic time, the peak voltage is divided into two different peak voltages with smaller duration and one partial discharging effect is also incorporated. As a result, a higher rate of anodic dissolution can be controlled significantly.

3.4 Mathematical modelling of volumetric material removal for different waveforms

In order to understand the material removal for each pulse on time of different waveforms, the estimation of volumetric material removal (VMR) is essential in EMM.

From Faraday's law and Ohm's law, the VMR can be determined as:

$$V_M = \frac{MAV_{in}t}{zFh\rho_m\rho_e} \tag{3.14}$$

Where, input voltage V_{in} (volt), molecular mass M, time t(s), electrode area A, valency of anodic metal z, Faraday const. F (96485 Coulomb/mol), initial inter-electrode gap h, specific electrolyte resistivity ρ_e, and density of material ρ_m. From equation (3.14) the volume of material removed can be estimated for each pulse on time of rectangular pulse waveform as

$$V_{M\_RPW} = \int_{t_1}^{t_2} \frac{MAV_{PR}}{zFh\rho_m\rho_e} dt \tag{3.15}$$

$$V_{M\_RPW} = \frac{MAV_{PR}}{zFh\rho_m\rho_e}(t_2 - t_1) \tag{3.16}$$

Where, time period from 0 to t_1 is non-faradic time and it can be estimated from the equation (3.13). Rest of non-faradic time is t_2 which is known as faradic time, as shown in Figure 3.3.

Similarly, for step pulse waveform, the volume of material removed can be calculated as:

$$V_{M\_SPW} = \int_{t_1}^{t_2} \frac{MAV_{PS1}}{zFh\rho_m\rho_e} dt + \int_{t_2}^{t_3} \frac{MAV_{PS2}}{zFh\rho_m\rho_e} dt \tag{3.17}$$

$$V_{M\_SPW} = \frac{MA}{zFh\rho_m\rho_e}[V_{PS1}(t_2 - t_1) + V_{PS2}(t_3 - t_2)] \tag{3.18}$$

From equations (3.16) & (3.18), the VMR can be estimated for rectangular waveform and step pulse waveform, respectively. To get an idea about the performance of step pulse waveform, VMR is calculated and compared with rectangular pulse waveform, as shown in Figure 3.4. Herein, the range of applied voltage is considered as 12V to 15V. The necessary different conditions considered for estimation are listed in Table 3.1. From the figure 3.4, it can be noticed that VMR increases with the increment of voltage. Compared to the rectangular pulse waveform, it can be observed that employing the step pulse waveform significantly minimizes VMR. Therefore, it is evident that under the same machining conditions and duration of pulse-on time, the step pulse waveform removes a lesser amount of material compared to the rectangular pulse waveform. Consequently, during machining, the step pulse waveform helps minimize the extra material dissolution from the target area.

Table 3.1: Parameters considered for the estimation of VMR

M (SS-304) (g/mol)	$C_{Adlayer}$ ($0.1MH_2SO_4$) ($\mu F/cm^2$)	F (C/mol)	Z	ρ_m (g/cm^3)	ρ_e ($0.1MH_2SO_4$) (Ωcm)	h (μm)	τ (ms)	R_{eq} (Ω)
55.36	10	96,485	2	8.03	50	20	1.59	159.28

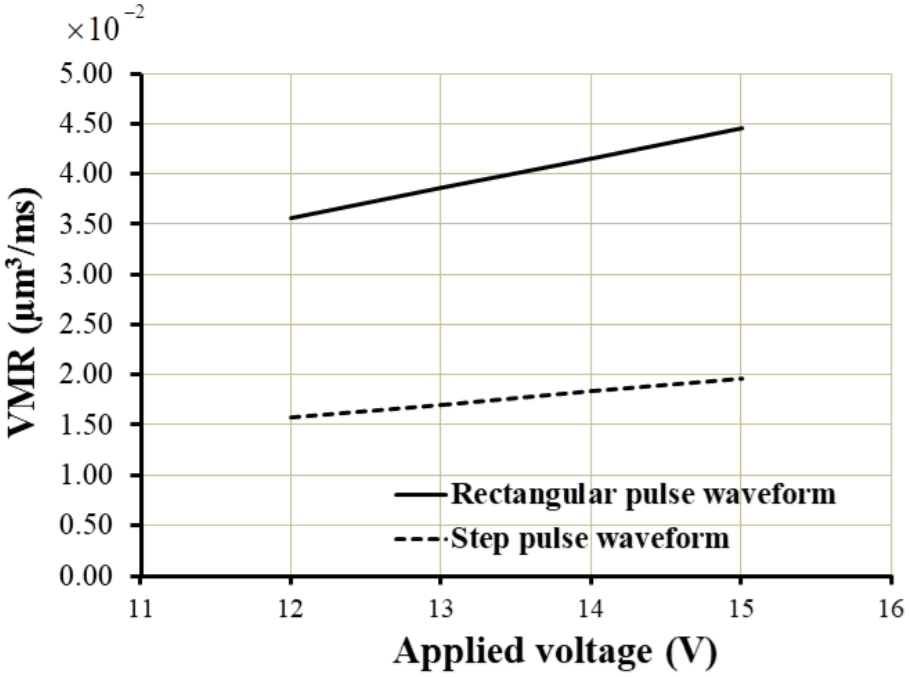

Fig.3.4 Volumetric material removal for each pulse on time

3.5 Mathematical estimation of root means square (R.M.S) voltage of pulse on time

It is notable that electrical DC pulse waveforms are in different patterns such as rectangular, sinusoidal, triangular, parabolic, etc. Thus, it is essential to calculate the average voltage of pulse on time when the applied voltage is the same. To determine the actual average voltage, calculation of the root mean square (RMS) value is essential. In this context, the performance of the step pulse waveform is compared with the conventional rectangular pulse waveform. Hence, the RMS voltage is estimated for both rectangular and step pulse waveforms, as shown in Figure 3.5.

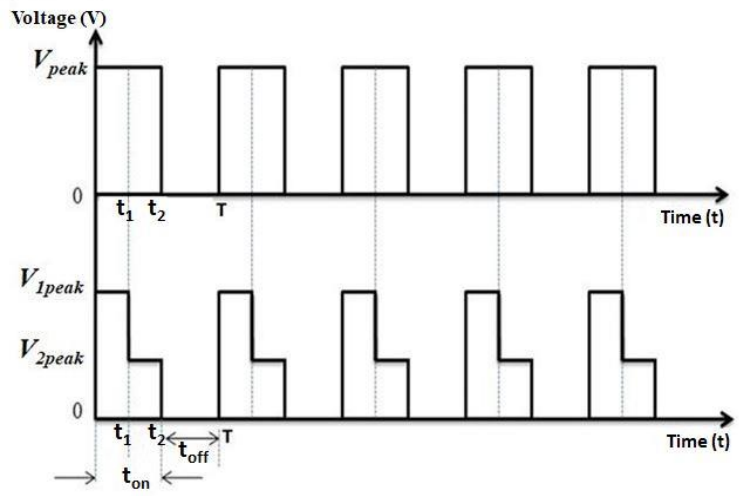

Fig.3.5. Estimation RMS voltage for rectangular and step pulse waveforms

The RMS value of rectangular pulse can be obtained as follows:

Let the function of the rectangular pulse waveform is f(t), peak voltage is V_{peak}, and pulse cycle time is T.

$$f(t) = V_{peak} \qquad 0 \le t \le t_2 \tag{3.19}$$

The RMS value defined as

$$f_{rms}^2 = \frac{1}{T}\int_0^{t_2} V_{peak}^2 .dt \tag{3.20}$$

Total RMS value of rectangular pulse

$$f_{rms\_square} = V_{peak}\sqrt{\frac{t_2}{T}} \tag{3.21}$$

$$D = \frac{t_2}{T} \tag{3.22}$$

Where, D is duty cycle of rectangular pulse.

Therefore, from equation (3.21) the RMS value of rectangular pulse

$$f_{rms\_square} = V_{peak}\sqrt{D} \tag{3.23}$$

The RMS value of step pulse can be obtained as follows:

Let the function of two section of the step pulse waveform is

$$f_1(t) = V_{1\_peak} \qquad 0 \le t \le t_1 \tag{3.24}$$

$$f_2(t) = V_{2\_peak} \qquad t_1 \le t \le t_2 \tag{3.25}$$

The RMS value defined as

$$f_{1\_rms}^2 = \frac{1}{T}\int_0^{t_1} V_{1\_peak}^2 .dt \tag{3.26}$$

$$f_{2\_rms}^2 = \frac{1}{T}\int_0^{t_2} V_{2\_peak}^2 .dt \tag{3.27}$$

Therefore, total RMS value of step pulse for one pulse cycle defined as

$$f_{rms\_step} = \sqrt{f_{1\_rms}^2 + f_{2\_rms}^2} \tag{3.28}$$

From equations (3.21) and (3.28), the RMS value of the rectangular and step pulse waveforms can be calculated, respectively. Energy differs among various pulse waveform patterns, such as sinusoidal, rectangular, triangular, and step. Although the peak voltage remains constant across these waveforms, the RMS value varies depending on the waveform's pattern. Consequently, the performance of EMM varies with different waveforms under the same applied voltage. Thus, it is essential to compare the RMS values while applied voltage is same for rectangular and step pulse waveforms. The energy transfer capacity of a pulse waveform is determined by its RMS value, which is proportional to the square root of the signal power. Therefore, the total energy transfer capacity of the step pulse waveform is lower than that of the rectangular pulse waveform during machining.

3.6 Simulation of transient response and total charging time of DL-capacitor under different waveforms

The simulations are conducted with an estimated equivalent resistance and capacitance of double layer for 0.1M H_2SO_4 solution, as mentioned in Table 3.1. By utilising equations (3.5) and (3.12) voltage variation across DL capacitor has been simulated through MATLAB software under programming module. To enhance comprehension, smaller

values are considered for the pulse on time and applied voltage, i.e., 0.5 ms and 1 V, respectively. From figure 3.6(a), it is evident that the time constant increases with an increase in the equivalent resistance Req or capacitance of the DL-capacitor.

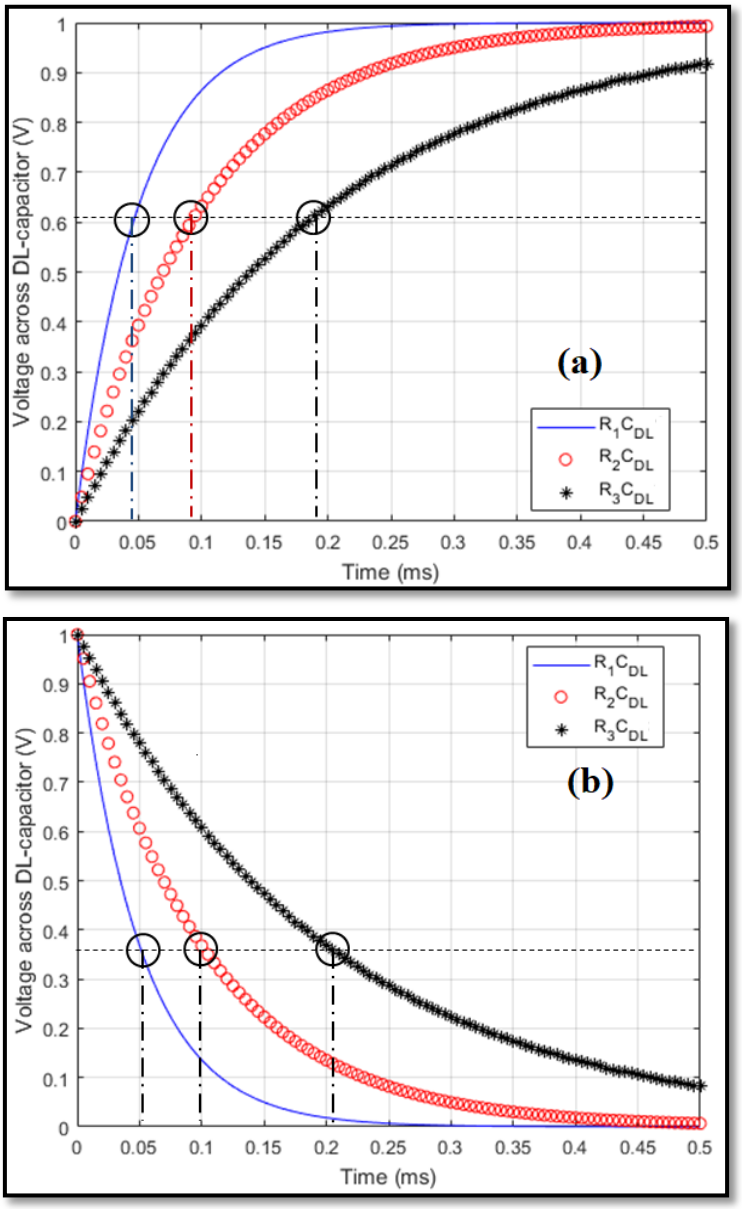

Fig.3.6. Simulation results of transient response of DL-capacitor for (a) charging (b) discharging

The simulation results reveal that the voltage across the DL-capacitor increases exponentially during the charging time. The time constant (τ) is the duration when the voltage across the DL-capacitor reaches 0.63V or when the DL-capacitor is charged to 63% of its capacity. Analyzing the graph, Fig.3.6 (a), it can be noticed that, at the same applied voltage and frequency, the time constant increases with an increase in the resistance of the electrolyte, while the capacitance of the DL-capacitor remains constant.

This indicates that, at specific electrolyte concentrations, the total charging time of the DL-capacitor remains constant for all pulse patterns.

Similarly, the transient response of the DL-capacitor during the discharging time is analyzed, as shown in Figure 3.6(b). During discharging, the time constant represents the time taken for the DL-capacitor when voltage drops to 0.37V. This discharging phase is responsible for decreasing in the rate of anodic dissolution, as the voltage drops exponentially from the peak or fully charged voltage of the DL-capacitor. Utilizing this discharging effect of the DL-capacitor, anodic dissolution can be controlled effectively. Hence, the partial discharging effect is intentionally incorporated during the faradic time of step pulse waveform.

To assess the voltage variation across the DL-capacitor during the pulse on time for different applied voltages, simulations are conducted with an estimated equivalent resistance and capacitance of double layer for 0.1M H_2SO_4 solution, as mentioned in Table 3.1. The results show that in the rectangular pulse waveform, the peak voltage remains constant during the faradic time, and the voltage across the DL-capacitor drops from the peak to 0V after the pulse on time, as illustrated in Figure 3.7(a). This leads to a higher rate of anodic dissolution and the removal of unwanted material from the target area. However, in the step pulse waveform, the voltage drops exponentially two times during the same faradic time, as illustrated in Figure 3.7(b). Consequently, anodic dissolution can be effectively controlled for each pulse on time.

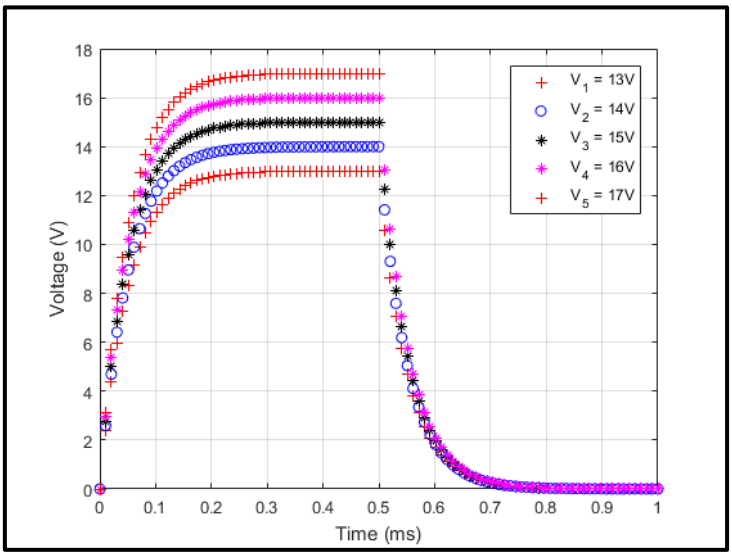

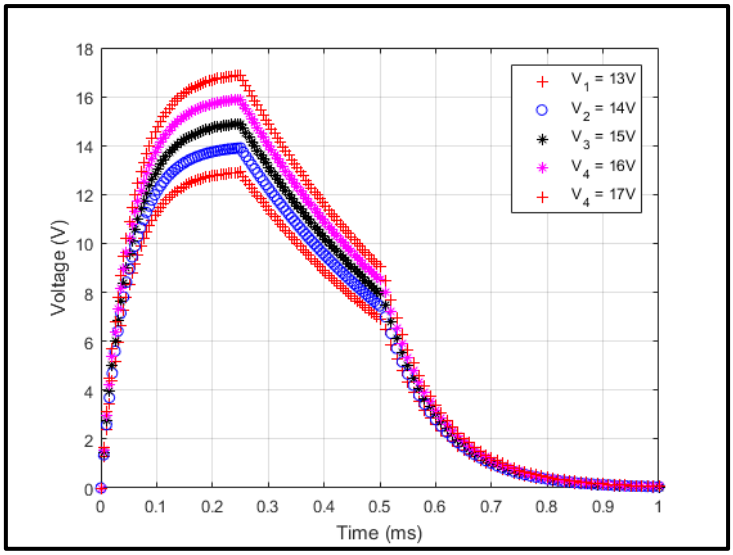

Fig.3.7 Voltage variation during pulse on time for (a) rectangular pulse waveform and (b) step pulse waveform

3.7 Effectiveness of step pulse waveform in EMM for stagnant electrolyte

The main objective of pulse pattern design is to decrease the energy of the step pulse waveform relative to the rectangular pulse waveform at the same applied voltage, while inducing a discharging effect of double layer capacitor during the faradic time. This design facilitates the development of anode potential oscillation during machining, leading to a moderate variation in current density. Consequently, the anodic dissolution rate decreases during the active state, and the transpassive state appear with a higher anodic potential. Moreover, the incorporation of two different peak voltages during the pulse on time and the shorter duration of peak voltage help in faster removal of bubbles from narrow inter-electrode area. As different peak voltages with short duration times are incorporated in each pulse on time, voltage drops from maximum peak to minimum peak during every pulse on time. As result, potential fluctuations occurring during machining. Based on the double layer theory of EMM, it has been identified that during pulse fall time, the bubbles' detachment rate increases effectively [96, 97]. Consequently, sludge effectively flushing out from the machining zone and removing obstacles to current flow. But, in a rectangular pulse waveform, the peak voltage remains constant throughout the pulse on time, potentially leading to a higher sustained current density. This could result in a higher rate of anodic dissolution during the active state, and lengthy passive state appears. Consequently, more current is engaged to increase the local temperatures of the oxide layer, leading to a sudden decrease in the anodic dissolution rate during the passive state, resulting in increments of the tapering effect [95]. Additionally, longer peak

voltages are the reason for the excessive evolution of bubbles in narrow inter-electrode gaps, which accumulate and break rapidly. Due to this, micro-sparks are generated, resulting in uncontrolled metal removal and irregular machining. Hence, when researchers used rectangular pulse waveform, various techniques, such as tool vibration, ultra-short pulse, bipolar pulse, higher frequency, mixed gas flushing etc., are employed in EMM to protect the evolution of larger gas bubble and their negative effects. However, the application of novel step pulse waveforms offers numerous advantages, including controlled material removal rates, improved flushing effects without costly external arrangements, minimized micro-spark effects, uniform current flow, and prevention of thick oxide layer formation.

3.8 Planning for experimental investigation

Utilizing rectangular and step pulse waveforms, microholes have been fabricated and analyzed for performance aspects of machining characteristics such as overcut, tapering effect, nature of waveform, anodic polarization, and transpassive mode during machining. A microtool made of a tungsten (W) rod with a diameter of 0.2 mm has been selected for EMM. Synthetic enamel has been coated on the sidewalls of the micro tools to minimize the stray current effect. Maskless stainless steel (SS304) with size, i.e., 15mm × 15mm × 0.1mm, has been chosen as workpiece. For better machining, 0.1 M H_2SO_4 solution has been chosen as electrolyte. The main reason behind the selection of this electrolyte is that it can almost dissolve the sludge and improve surface quality during micromachining. Machining accuracy has been investigated under the application of both rectangular and step pulse waveforms at applied voltage of 13V to 17V with a fixed duty ratio, pulse duration time, and pulse frequency. Under conditions without electrolyte flushing, the pulse off time should be longer for proper sludge removal. Keeping this in mind, duty cycle of 50% has been selected for the experiments. When high frequency is used, large peak voltage is required to reduce the DL-capacitor charging time. Due to this, the energy of the short pulse wave during machining is increased. To avoid this, lower pulse frequency of 500Hz has been chosen for micromachining. The initial inter-electrode gap has been selected as 20µm for all experiments. These machining conditions have been selected from previous research investigations when rectangular pulse waveform is used. All machining conditions are listed in Table 3.2. Utilising a programmable bi-polar 20V–100A pulse DC power supply (Matsusada, Japan) with a frequency range of 0 to 300 kHz, machining current and anode potential at various applied voltages has been measured. A

digital storage oscilloscope TBS2000 (Tektronix, USA) has been used for observing the characteristics of pulse waves and micro-sparks during micromachining. Measurement of the radial overcut of the machined micro-hole, and tool diameter has been taken by a microscope STM6 (Olympus, Japan) with 50X magnification.

Table 3.2 Machining conditions

Condition	Value
Micro tool (W)	Φ 0.2 mm
Workpiece (SS304)	15 x 15 x 0.1mm
Electrolyte (H_2SO_4)	0.1 mol/l
Applied voltage	13, 14, 15, 16, 17 volt
Pulse on time	50 ms
Pulse frequency	500 Hz
Duty ratio (%)	50%
Feed rate of micro tool	0.5 µm/sec
Initial interelectrode gap	20 µm

3.9 Results and Discussion

3.9.1 Influence of rectangular pulse waveform on machining characteristics

Mostly, researchers have been used conventional rectangular pulse waveform for electrochemical micromachining. Under the application of rectangular pulse waveform, various arrangements have also been applied to flush out the electrolysis products from the machining zone. It is essential to investigate the effect of rectangular pulse waveform on machining accuracy in stagnant electrolyte. Thus, an experimental setup has been designed, as described in chapter 2, and is being employed in the experimental study to investigate the influence of the rectangular pulse waveform on machining accuracy. In the experimental study, machining characteristics, i.e., anode polarization, transition behaviour from the active to the passive state, anode potential, and stray current effect, have also been observed. Machining accuracy has been measured in terms of the overcut and tapering effect.

3.9.1.1 Behaviour of rectangular pulse waveform during machining

Experiments have been conducted to observe anode potential and anode polarization under the application of the rectangular pulse waveform. The outcomes of the experiments have been plotted on graph and analysed. It can be observed that the peak voltage of the rectangular pulse waveform is 13V but the RMS voltage is 9.2V. The RMS voltage has been calculated with the help of equation 3.21. At the applied voltages of 14V, 15V, 16V, and 17V, the RMS voltages are 9.9V, 10.6V, 11.3V, and 12.1V,

respectively. For 13V to 17V, the voltage difference between peak and RMS is 3.8V, 4.1V, 4.4V, 4.7V, and 4.9V, respectively.

3.9.1.2 Characteristics of anode polarization on the different applied voltages

In order to better understanding, the characteristics of anodic polarization have been investigated at different applied voltage, as shown in Figure 3.8. It has been observed that at the applied voltage of 13V, the active state transits to the passive state when the anode potential reaches at 6V. During this active region, the metal surface becomes etched. When the anode potential is increased by more than 6V, oxide layer is formed on the anode, which reduces the dissolution rate. During the passive state, the current density reaches its maximum value of 47.6A/cm^2 and sustains throughout machining. Due to the longer duration of the passive state accompanied by high current density, the fast formation of a thick oxide layer is developed. In this condition, more gas bubbles are evolved in the machining zone, and more current is used for this purpose. At higher anodic potential, these gas bubbles are broken, resulting in occurrence of micro-sparks. Due to it, unwanted material removal increases. For other applied voltages, i.e., 14V, 15V, 16V, and 17V, it can be observed that the active state is larger than the lower voltage. In this region, the current density increases more, which leads to increment of metal dissolution rate. In between the anode potentials of 6V and 7V, the maximum current density can be obtained 63.49A/cm^2, which sustains almost throughout machining. As a result, passivation still occurs. As the high current density stands throughout the passivation region, excessive gas bubbles accumulate on the anode surface, which interrupts the continuous current flow. Due to it, irregular machining takes place and pitting effects appear across the machining zone. Additionally, greater power dissipation takes place through the oxide layer. As a result, the effective resistance of this layer increases and heat is generated simultaneously. Therefore, stresses are developed in this layer, which also creates a rupture in the layer. When the local temperature is increased by a higher current density, the excessive hydroxyl ions evolve with higher concentrations at the anode surface. Due to it, oxygen gas is also formed at a high rate and the oxidation process is continued during the total passive state which interrupted the further current flow. Hence, when the applied voltage rises, the dissolution rate also increases during the active state, but, in the passive state, it decreases significantly. Therefore, at higher applied voltage, the high current density is developed, which poses a negative effect on machining accuracy.

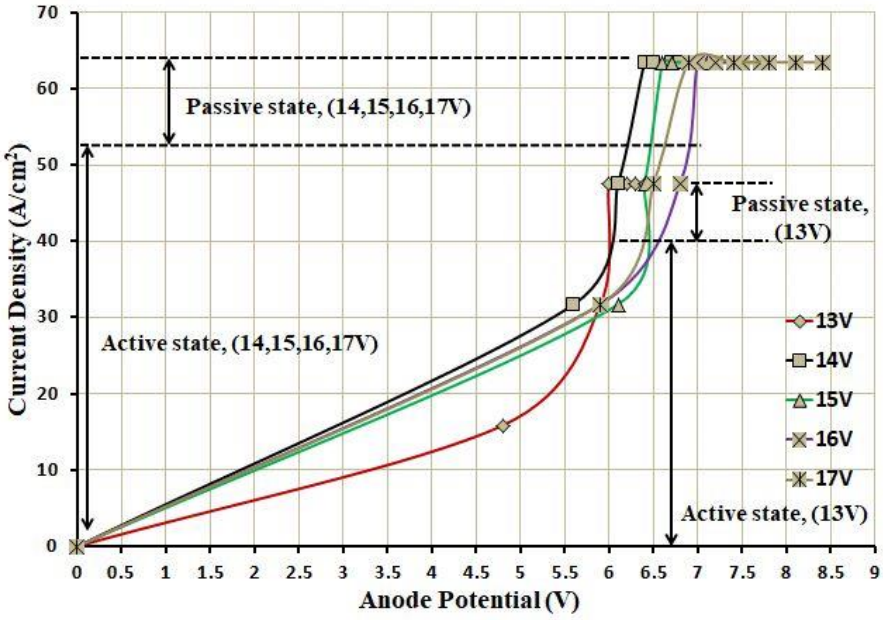

Fig. 3.8 Polarization curve at different applied voltages under rectangular pulse waveform

3.9.1.3 Transition from active to passive dissolution during machining

At different applied voltages, the behaviour of the active to passive dissolution during machining is shown in Figure 3.9. When the oxide layer is rapidly formed on an anode surface, this passive state appears. During the passive state, a solid oxide layer is formed and attached firmly to an anode surface, which reduces the dissolution rate initially. A greater amount of current density is generated when the thickness of this layer is increased as well as the gap between electrodes reduces. At that time more current is used to evolve the gas bubbles. When bubbles are broken inside of the machining zone, micro-sparks are generated. As a result, the uncontrolled material dissolution increases during machining. These phenomena are more prominent at higher applied voltages. It can also been observed that when the applied voltage increases, the transition period of the active to passive state becomes shorter and the duration of the active state is longer. It is also noticeable that after the active state, the anode potential is almost constant at the lower applied voltage of 13V to 14V. However, under the influence of higher applied voltages, the anode potential and its oscillation are enhanced more, which increases the current density. As a result, the oxide layer thicken which generates the local temperature. Due to this local heating, the hydroxyl ions evolve more and excessive gas bubbles are generated. These gas bubbles are broken due to higher anodic potential, by which micro-sparks are generated randomly. Thus, under the application of rectangular pulse

waveform, the generation of micro-sparks cannot be controlled properly and more irregular machining and unwanted material removes from the target area.

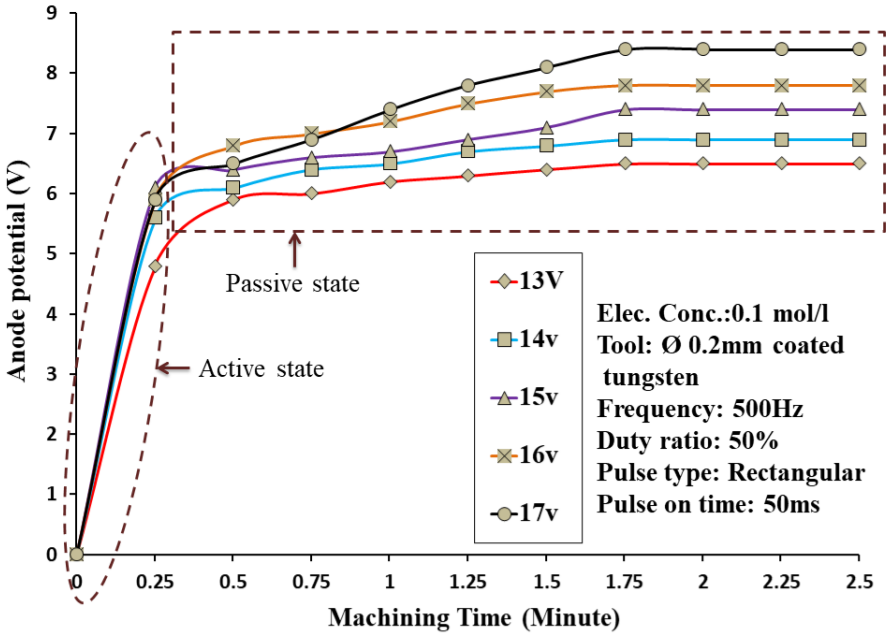

Fig. 3.9 Transition behaviour from active to the passive state under rectangular pulse waveform

3.9.1.4 Influence of applied voltages on overcut and tapering effect

The effect of rectangular pulse waveform on entry and exit overcuts for different applied voltages has been shown in Figure 3.10. From the graph (Fig. 3.10), it can be observed that as compared to the lower voltage region, i.e., 13V to 15V, the overcut increases more rapidly when the voltage is increased from 16V to 17V. At the higher voltage, excessive metal ions and gas bubbles are generated during the machining. When these gas bubbles are broken, micro-sparks generate. Another phenomena is that metal dissolution takes place with a higher rate when greater current density is developed. As a result, uncontrolled material is removed from the workpiece, and larger overcut is generated. It can be observed that at 13V, the difference between the entry and exit overcut of a microhole is 12.77µm. But at 15V, this difference is 18.58µm. At higher applied voltage, the current flow rate increases rapidly; as a consequence, a high rate of anode dissolution takes place from the entry area of the workpiece. The peak voltage of the rectangular pulse waveform is constant during the pulse on time. Hence, it has been observed that in a very small inter-electrode gap, the current density increases abruptly in the active state and is sustained consistently at its maximum value, i.e., 63.49A/cm^2 during machining, as illustrated earlier in Figure 3.8. Due to this, the fast formation of the oxide layer becomes

firmly attached to the metal and forms a barrier between the metal and the solution, which reduces the anodic dissolution rate after the active state. It has been observed from the graph that the shape of machined microholes is more tapered at higher applied voltages. It can be noticed that 12V is not applicable for the fabrication of microhole because there have a possibility of inadequate ionic dissolution. Thus, to avoid it, experiments have been conducted at 13V and above.

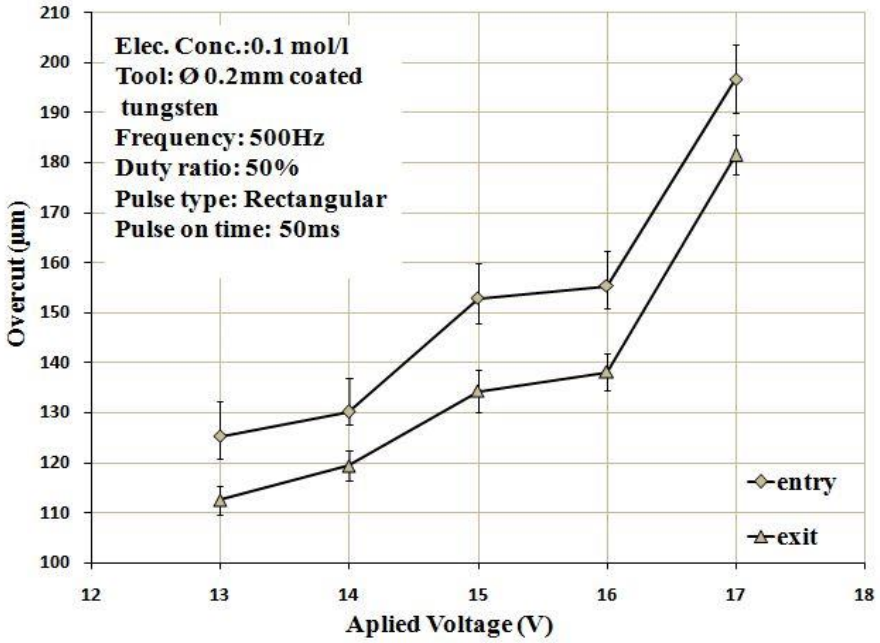

Fig. 3.10 Effect of rectangular pulse waveform on overcut and tapering

At the machine conditions, such as the voltage of 13V, electrolyte concentration of 0.1 mol/l, frequency of 500Hz, duty ratio of 50%, and 50ms of pulse on time, the overcut and tapering effects are obtained at 125.29µm and 12.77µm, respectively, as presented in Figure 3.11. Utilising the rectangular pulse waveform, microholes have been fabricated, whose entry side, exit side, and the cross-section area are shown in Figure 3.11 (a, b, and c). Small non-uniformity in the shape of a machined microhole can be noticed, which is caused by the stray machining effect. It can also been observed that a large stray current effect appears across the machined microhole. This phenomenon is occurred due to higher current density during the active state.

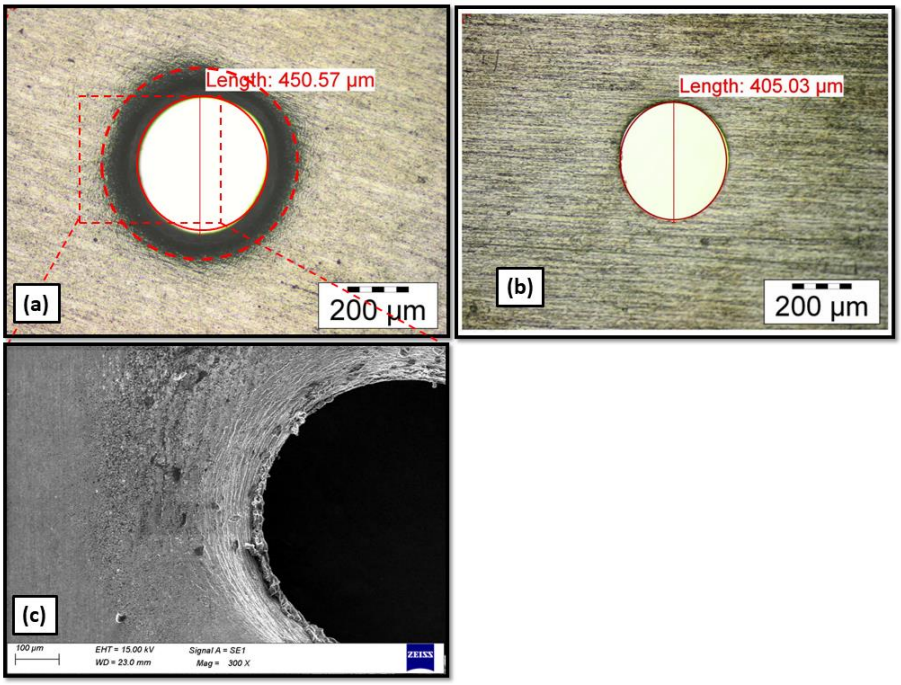

Fig.3.11. Micrograph of a machined microhole under rectangular pulse at 13V, (a) entry side, (b) exit side (c) cross-section area of microhole

3.9.2 Influence of step pulse waveform on machining characteristics

The step pulse waveform is designed as an alternative pulse pattern technique because at the same applied voltage and the duration of pulse on time, the average voltage of each pulse is lower than rectangular pulse waveform. Due to discharging effect of DL-capacitor during the faradic time of step pulse waveform, maximum peak voltage decreases exponentially to the half of maximum peak voltage. Due to it, oscillation of anode potential can develop during machining; resulting in the current density varies in a moderate range. As a result, the anodic dissolution rate reduces during the active state, and the transpassive state may appear with a higher anodic potential. Another advantage is that as the peak voltage duration time is shorter and two different peak voltages are incorporated in pulse on time, bubble evolution is faster which helps to flush out the sludge from machining zone effectively. As a consequence, the obstacles of current flow can be removed. Machining accuracy has been compared with a traditional rectangular pulse. In order to investigate the effect of step pulse waveform on machining characteristics such as anode polarization, transpassive state, anode potential, and stray current effect have also been observed and compared with the rectangular pulse waveform.

3.9.2.1 Behaviour of step pulse waveform during machining

It has been observed that a step pulse is nothing but a modified form of a conventional rectangular pulse waveform, as shown earlier in Figure 3.3. Pulse on time is split into two parts. The first part of the pulse on time is designed with the maximum peak voltage, and the second part is half of it. Thus, during pulse on-time, two different peak voltages are generated. Hence, RMS voltage calculations are necessary for this waveform. The maximum peak value of the step pulse waveform is considered for explanations due to its having two different peaks during pulse on time. From the waveform, it has been observed that the peak voltage of the step pulse is 13V but the RMS voltage is 7.3V. Similarly, at the applied voltages of 14V, 15V, 16V, and 17V, the RMS voltage is 7.8V, 8.4V, 8.9V, and 9.5V, respectively. It has been observed that the RMS voltages of the step pulse waveform are smaller than the rectangular pulse waveform, but the maximum peak voltages of both pulse waveforms are equal. The energy transfer capacity of the pulse waveform depends on the RMS value because it is equal to the root of the power of the signal. Due to this, the total energy transfer capacity of the designed step pulse waveform is less than the rectangular pulse waveform during machining.

3.9.2.2 Characteristics of anode polarization on the different applied voltages

The nature of anodic polarization under the application of step pulse waveform has been shown in Figure 3.12 to 3.16. Herein, the step pulse waveform has been employed to investigate the anodic polarization at different applied voltages. Thus, anodic polarization has been analysed separately for the applied voltage of 13V to 17V. At the applied voltage of 13V, it has been noticed that the duration of the active state is small compared to the rectangular pulse waveform (Fig.3.8) and its transit to the passive state when the anode potential rises more than 4V, which is smaller than the rectangular pulse waveform, as shown in Figure 3.12. As the current density varies in a moderate range, i.e., 0 to 33A/cm^2 during the active state point B in figure 3.12, the proper rate of anodic dissolution can take place, which is clearly understood from the polarization graph. Utilizing step pulse waveform, a moderate range of current density has been achieved because RMS voltage of step pulse waveform is 20.65% lower than the conventional rectangular pulse waveform. After the active stage, the passive state develops and sustains almost constant for a short duration, which has been shown in the graph by the CD line. At that state, the current density is almost constant. Whenever potential is increased over 5.2V, the transpassive state appears accompanied by polishing action, and this region is

represented on the graph as DE. It can also be noticed that transpassive dissolution is occurred when current density rises abruptly. From the appearance of the transpassive state, it can be understood that the oxide layer becomes thin and compact. At the transpassive state, more current can penetrate the oxide layer. Thus, excessive gas bubble evolution has been minimized, which is not observed in the case of the rectangular pulse waveform. Therefore, by utilizing the step pulse waveform, micro-sparks can be minimized significantly. When the applied voltage is 14V, the nature of anodic polarization is slightly different from the lower applied voltage, which is presented in Figure 3.13. From the graph, it has been noticed that the passive state is sustained more as compared to 13V. Due to the large passive state, more gas bubbles evolved during machining. As a result, at 14V, more micro-sparks can occur due to these gas bubbles, which is broken at a higher anodic potential. Hence, unwanted material removes from the target area. From the anodic polarization curve, as shown in Figure 3.14, it has been observed that at 15V, the passive state is very small compared to 14V and the transpassive state appears quickly. Additionally, it can also be noticed that the current density reaches at 47.62A/cm^2, which is higher than the lower applied voltage. As a result, the thickness of the oxide layer decreases rapidly and becomes a conductor, which allows for passing the maximum current. As a consequence, more anodic dissolution can take place during the transpassive state. Similarly, at higher applied voltages, these behaviors can also be observed. From figure 3.15, it can be observed that when anode potential increases more than 5.4V, the active state transits to the passive state. As compared to the lower applied voltage, the current density of the active state is much higher, i.e., 63.49A/cm^2. Due to higher current density, the anodic dissolution rate is greater than the lower applied voltage. Similarly, at an applied voltage of 17V, the current density of the passive state and its duration are greater than the lower applied voltage, as shown in Figure 3.16.

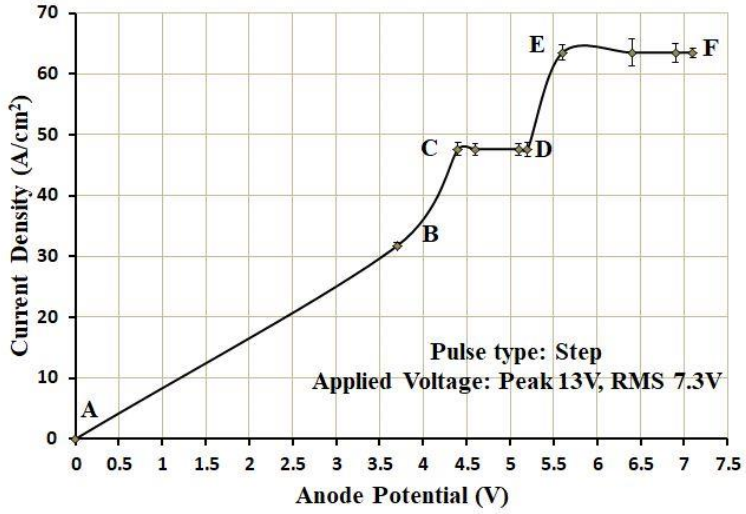

Fig.3.12. Polarization curve at an applied voltage of 13V

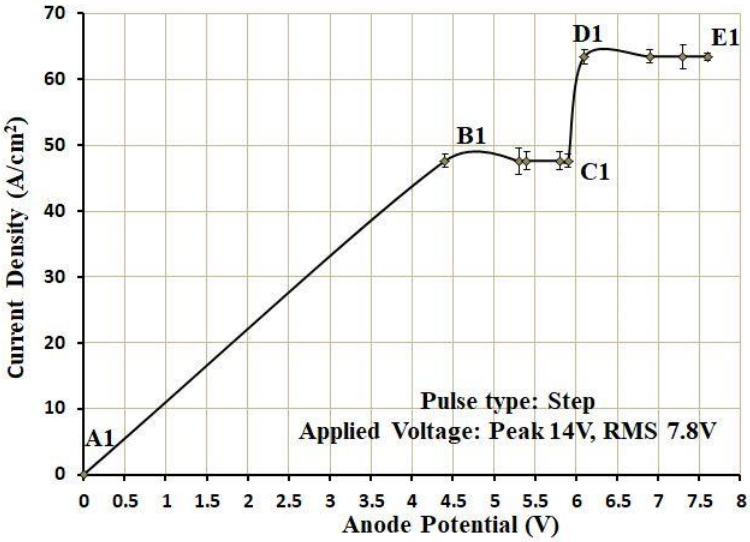

Fig.3.13. Polarization curve at an applied voltage of 14V

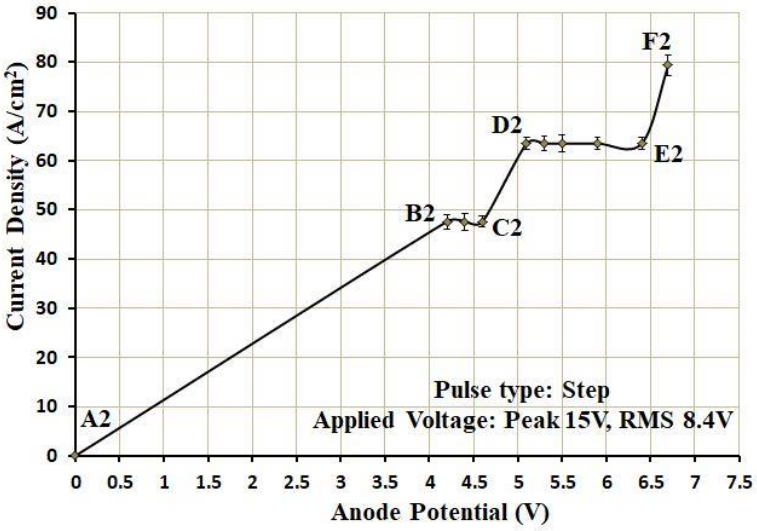

Fig.3.14. Polarization curve at an applied voltage of 15V

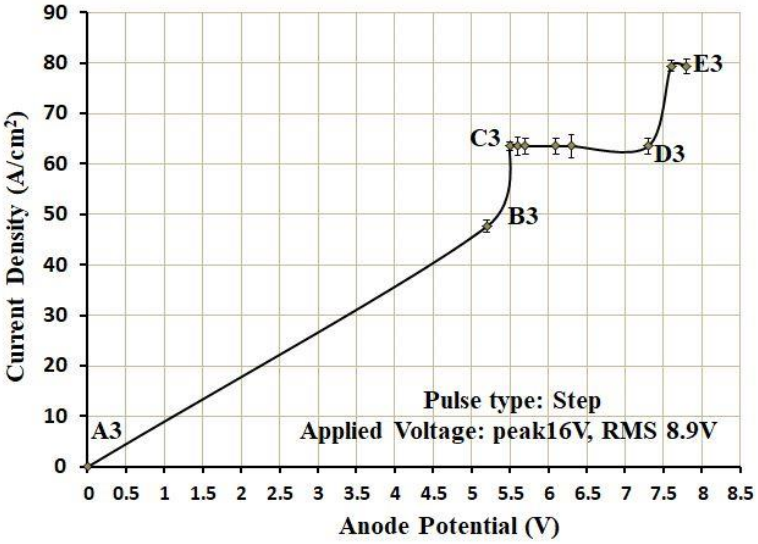

Fig.3.15. Polarization curve at an applied voltage of 16V

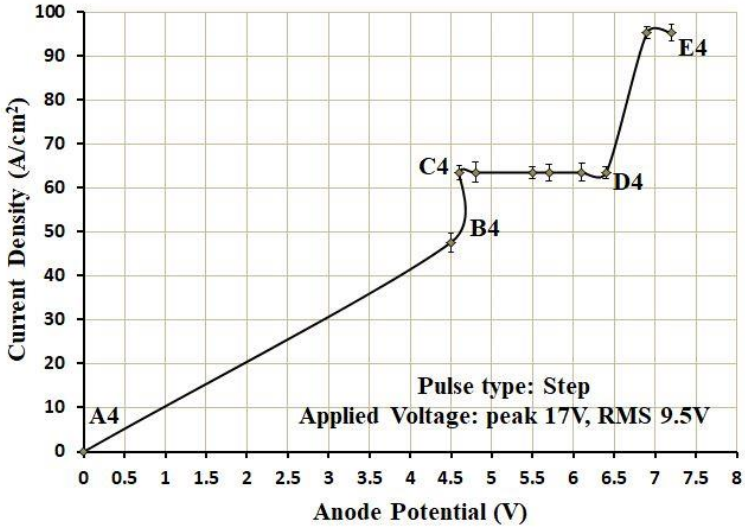

Fig.3.16. Polarization curve at an applied voltage of 17V

3.9.2.3 Transition from active to transpassive dissolution during machining

The transition from active to transpassive state during machining is shown in Figure 3.17. When the applied voltage is increased, the transpassive state becomes more prominent. Thus, it can be clearly understood that at this condition, the oxide layer becomes thinner. The main reason of the appearance of the transpassive state is that the discharging phenomenon of the DL-capacitor during the faradic time, which is occurred due to incorporation of two different peak voltage into the pulse on time of step pulse waveform. Another significant advantage of this discharging effect is that the anode potential oscillates randomly, triggering the current density for acceleration. From the graph (Fig.3.17), it can be observed that at the higher applied voltage, the period of oscillations

increases more. Hence, at a higher applied voltage, the rate of thickness reduction of the oxide layer is greater than the rate of formation. Thus, from the polarization curve, it can be noticed that transpassive state is more prominent and larger. As a result, more anodic dissolution can take place during passive and transpassive states. At the applied voltage of 13V, it can be observed that the period of oscillation is very short and the transition period from active to passive is longer. Hence, the current density can vary in a moderate range during the active state. But at the higher applied voltage, current density increases. As a result, at the applied voltage of 13V, anodic dissolution can be controlled effectively.

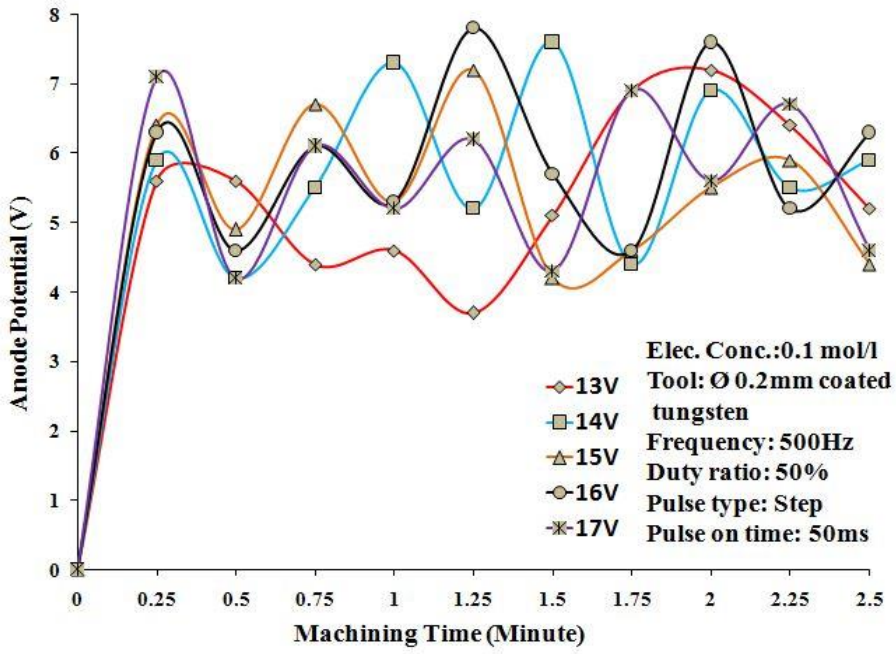

Fig.3.17 Behaviour of anode potential and transpassive mode under step pulse waveform

3.9.2.4 Influence of applied voltages on overcut and tapering

It can be observed from Figure 3.18 that under the application of step pulse waveform overcut also increases with the increase of applied voltage. However, it can also be observed that at the applied voltage of 13V, the overcut is obtained at 20.06µm, which is too small compared to the rectangular pulse waveform (Fig. 3.10). Similarly, at higher voltage, the overcut is always smaller than the conventional rectangular pulse waveform. It has been noticed from the graph that at the applied voltage of 15V to 16V, the overcut varies sharply, otherwise it increases almost linearly. As the step pulse waveform has less energy transfer capacity and discharging phenomena during the faradic time, the rapid formation of the oxide layer has been controlled and thin oxide layer becomes a

conductor. Due to it, current can pass through the thin oxide layer. Alternatively, it has been observed from the polarization curve that the transpassive state appears due to the reduction of the oxide layer. As a consequence, micro-sparks are controlled and transpassive dissolution takes place properly. As a result, for controlled dissolution, the overcut and tapering effect have been minimised significantly. Whereas, at different applied voltages, i.e., 13V, 14V, 15V, 16V, and 17V, the tapering effects of machined microholes have been reduced by 0.17µm, 1.16µm, 3.30µm, 7.49µm, and 8.45µm, respectively. It has also been observed from the polarization curve (Fig. 3.15, 3.16) that at higher applied voltages, current density rises abruptly and more transpassive dissolution takes place. Hence, more tapering effects can be minimised at higher voltages. However, at lower applied voltages, the tapering effect has been reduced significantly under the application of the step pulse waveform.

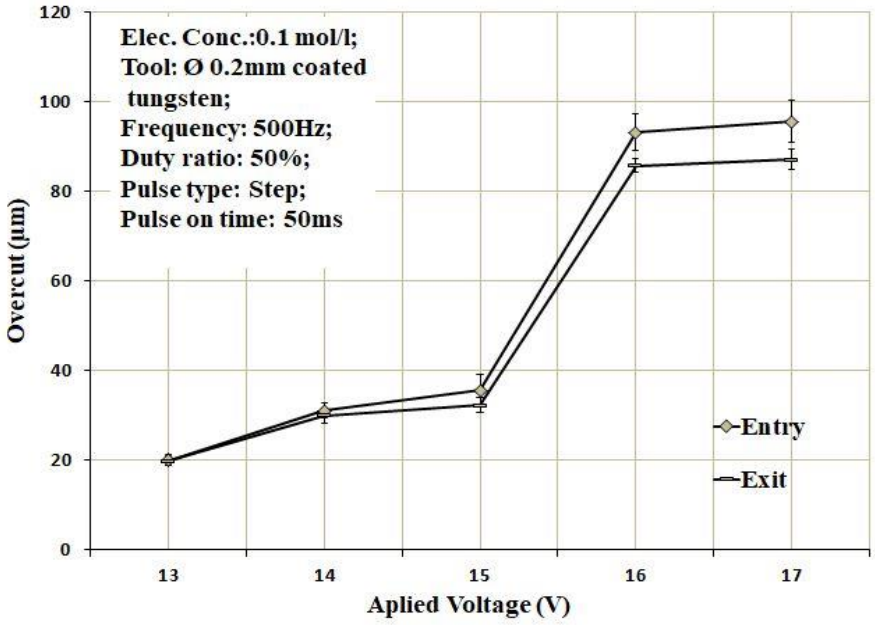

Fig.3.18. Effect of step pulse waveform on overcut and tapering

Under the application of step pulse waveform at 13V, entry side of machined microhole, exit side, and cross-section area have been presented in Figure 3.19 (a, b, c). From the figure, it can be observed that the machined micro-hole wall is more smooth and regular as compared to the rectangular pulse waveform (Fig.3.11). Furthermore, it can also be noticed from the machined microhole that the stray current effect has been minimised. Thus, it can be clearly understood that excessive gas bubble evolution has been controlled by the step pulse waveform. It has also been observed from the polarization curve (Fig.3.12) that the current density varies in a moderate range during the active state and

the transpassive state appears quickly. Due to it, transpassive dissolution takes place properly. As a result, the tapering effect has been reduced significantly. As sludge cannot dissolve completely into the electrolyte, flushing system is essential for the micromachining especially narrow inter-electrode gap when utilising rectangular pulse. However, without flushing arrangement, by using the new pulse pattern technique, i.e., step pulse waveform, the overcut and stray current effects have been reduced significantly by effective sludge removal. Thus, it is a greater success in the improvement of EMM accuracy by utilising step pulse waveform as compared to conventional rectangular pulse waveform.

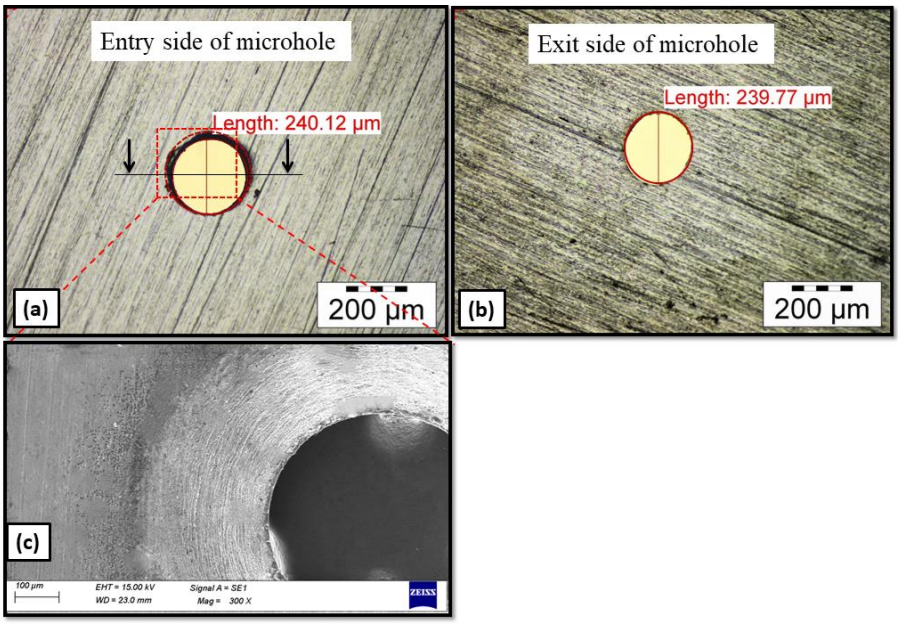

Fig.3.19 Micrograph of a machined microhole under step pulse waveform at 13V, (a) entry side, (b) exit side (c) cross-section area of microhole

3.9.3 Comparison of overcut and tapering for both pulse waveforms

The variation of overcut at different applied voltages has been analysed for both rectangular and step pulse waveform and it has been presented in a comparative bar graph, which is shown in Figure 3.20. The machining accuracy has been investigated under the application of traditional rectangular pulse and step pulse waveforms at the same machining conditions such as voltage of 13V, electrolyte concentration of 0.1 mol/l, frequency of 500Hz, duty ratio of 50%, and 50ms of pulse on time. By employing step pulse waveform, 83.99% of overcut and 98.66% of tapering effects have been reduced when the applied voltage is 13V, which is the best result as compared to other applied voltages. For higher applied voltage of 14V, 15V, 16V, and 17V, the overcut have been

reduced by 76.10%, 76.72%, 39.99%, and 51.39%, and the tapering effects have been minimised by 89.14%, 82.18%, 56.37%, and 44.48%, respectively.

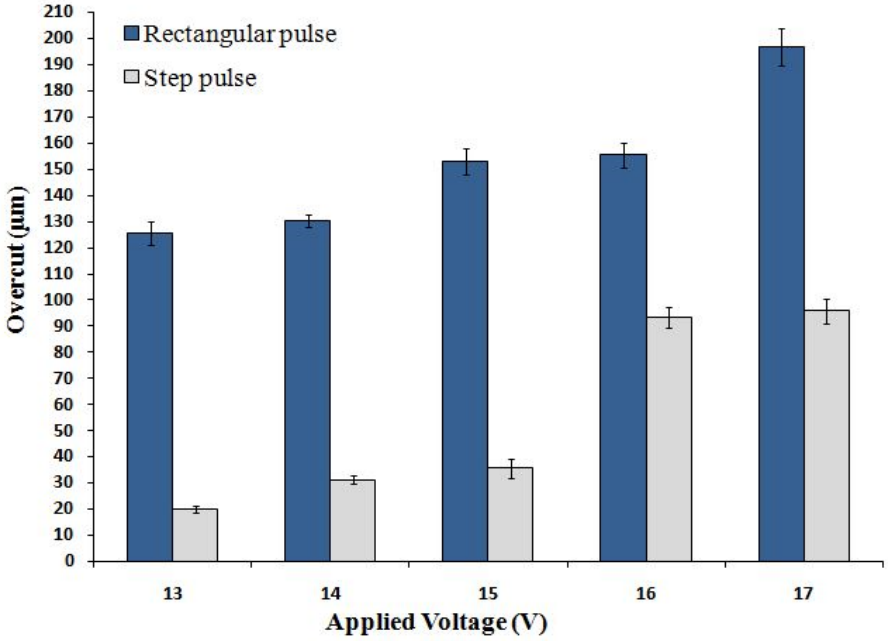

Fig.3.20. Comparison the effect of rectangular and step pulse waveform on overcut at different applied voltages

3.10. Outcomes of experimental investigation

A novel technique has been designed indigenously by modifying the traditional rectangular pulse into a step pulse waveform for the improvement of electrochemical machining (EMM) accuracy in terms of overcut, and tapering. In the present study, the nature of waveforms, the variation of overcut, anode polarization, and transpassive mode have been investigated for both rectangular pulse and step pulse waveforms. As compared to the rectangular pulse waveform, the machining accuracy has been improved significantly by the step pulse waveform.

The traditional rectangular pulse has been modified into a step pulse waveform by selecting two different amplitudes of short pulses and the discharging phenomena of the double layer has been introduced during the faradic time. Thus, at 13V, the current density can be varied in a moderate range, i.e., 0 to 33A/cm^2, resulting in a proper anodic dissolution rate being obtained during the active state. As a result, overcut, tapering effects, and stray current effects, have been reduced significantly as compared to the rectangular pulse waveform. From the polarization curve, it can be observed that the duration of the active state, i.e., 0 to 4V, is always smaller than the rectangular pulse

waveform, i.e., 0 to 5.6V. Therefore, the anodic dissolution rate can be minimised properly for all applied voltages. Thus, the overcut can be reduced significantly more than the rectangular pulse waveform.

At the higher applied voltage, the period of oscillations of anode potential increases, which enlarges the current density abruptly. From the duration of the transpassive state, it can be understood that the thickness of the oxide layer can be reduced more. During the active state, the range of current density increases more, i.e., 0 to 47.62A/cm^2, than the applied voltage of 13V. Therefore, the overcut and tapering effect also increases more at higher applied voltage, but as compared to the traditional rectangular pulse waveform it is very small. In the case of the step pulse waveform, the duration of the passive state is very small, and the transpassive state appears quickly. But in the rectangular pulse waveform, during the passive state, the current density is sustained consistently. At this condition, metal dissolution is controlled by the oxide film.

At the applied voltage of 13V, the least stray current effect has been obtained because the RMS voltage has been reduced by 20.65%. Also, compared to the rectangular pulse waveform, the overcut has been reduced by 83.99%, 76.10%, 76.72%, 39.99%, and 51.39%, at the applied voltages of 13V, 14V, 15V, 16V, and 17V, respectively. Further, the tapering effect has also been reduced by 98.66%, 89.14%, 82.18%, 56.37%, and 44.48% at these applied voltages respectively. Hence, it has been established that step pulse waveform is more effective for better performance of EMM. However, it needs in depth investigation to study other important factors such as variation of pulse on time, frequency and duty cycle of pulse waveform as well as tool feed rate during EMM operation under step pulse waveform application which may further enhance the micromachining performance in EMM.

Chapter 4: Investigation into insulation and micro-tool feed control on machining accuracy under step pulse waveform

4.1 Introduction

Electrochemical micromachining (EMM) technology is expected to play a promising role in the fabrication of micro components for various applications. In EMM, as the tool-tip area is very small compared to the workpiece, the stray current plays a significant role in pitting effects and irregular machining. To reduce the stray current effects, tool and workpiece insulation technique has been employed in EMM. In insulation technique, except machining zone, workpiece is also insulated, which may control the current density and stray current effects during micromachining. Due to it, pitting effects and irregular machining can be minimised. It is crucial to maintain a linear relationship between the microtool feed rate and material removal rate to enhance machine accuracy. Higher feed rates may lead to tool contact with the workpiece, risking tool damage and short circuit. To address this, employing a discontinuous tool movement strategy helps eliminate short circuit effects, enhancing overall machining performance.

From the previous research works, it can be understood that the proper potential transmission during machining is very essential to achieve better accuracy and precision shape of machine products. To fulfil this aim, step pulse waveform (SPW) has been designed as a new pulse pattern technique. As the tool-tip area is very small compared to the workpiece, the potential transmission and current density play a significant role in EMM. To reduce the stray current effects, microtool and workpiece insulation technique has been applied. In insulation technique, except for the machining zone, fully coated workpieces are working as an insulator, which may restrict potential drop during micromachining. Hence, the effects of insulation technique on electrolyte potential and current density have also been investigated through simulation and experimental processes. The effect of insulation technique with step pulse waveform on overcut and precise shape of microhole machining has been investigated for different voltages. Finally, the characteristics of machined microholes have been analysed in depth and compared with non-insulation technique. In the present study, a discontinuous tool feed rate technique is employed for improving the proper localization of anodic dissolution in EMM. In this investigation, overcut, the shape of the machined micro-hole, stray current effect, short circuit effect, and current-voltage characteristics during machining have been investigated. The main objective of this research work is that by employing microtool

feed rate control, short circuit effect eliminates, which improves regular machining and uniformity of profile shape.

4.2 Insulation technique for stagnant electrolyte

The electric field distribution plays a significant role in EMM because the tool-tip area is very small as compared to the workpiece. The behaviour of stray current on machining area for insulated and non-insulated technique has been presented in a schematic diagram, as shown in Fig.4.1. In present experiment, synthetic rubber coating has been used for microtool surface and workpiece insulation. The behaviour of this coating is that except machining area, current cannot pass through coated area. Thus, the current can flow uniformly in the inter-electrode gap. Due to it, potential drop can be restricted during micromachining. As a result, localization of anodic dissolution improves and minimises the stray current effect. When non-insulated microtool and workpiece is utilised for EMM, stray current effect increases significantly. To avoid this problem, researchers have used coated microtool for EMM. But, stray current effect cannot be minimised effectively without workpiece insulation because stray current can flow across the machining area, as shown in Figure 4.1. To overcome this issue, different types of masking have been used in EMM. But, it can be noticed that for complex shape and higher depth micromachining, masking is a very difficult and costly technique. However, for the insulation of microtool and workpiece, synthetic rubber coating is a very simple and cost-effective technique. Another advantage is that during machining synthetic rubber coating is not removed by acidic, bases, and salts type of electrolyte.

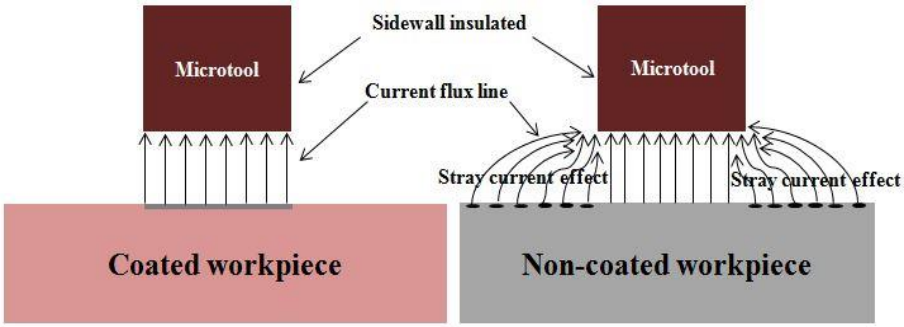

Fig.4.1. Effect of stray current for coated and non-coated workpiece

The design strategy of SPW is that the potential variation can occur during the faradic time. It is caused by discharging effect of the double layer capacitor (DL-capacitor). The pulse on time of SPW has been broken into two parts with different peak voltages such as V_{Smax}, and V_{Shalf} as shown in Figure 4.2.

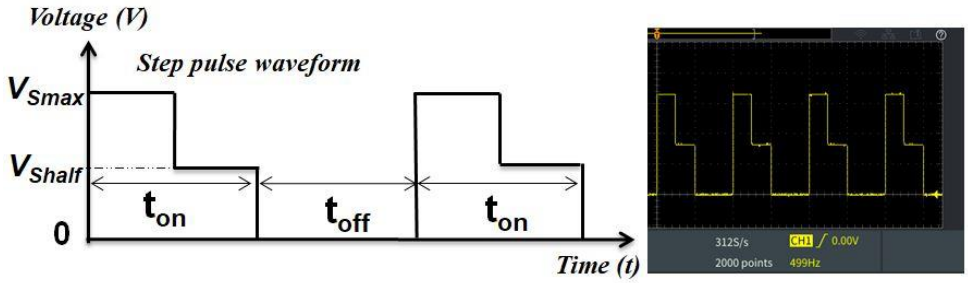

Fig.4.2 Step pulse waveform in schematic and oscilloscopic view

Thus, the discharging of DL-capacitor occurs when the pulse voltage drops down from maximum to the second peak during pulse on time. As a result, the potential transmission can be controlled during micromachining. Due to it, anodic dissolution rate can also be controlled, and improves the accuracy of EMM.

4.3 Simulation of potential transmission and current density under insulation

The electric field distribution plays a significant role in EMM because the tool-tip area is very small compared to the workpiece. When workpiece and microtool surface area have been insulated with synthetic rubber coating, except for the machining area, current cannot pass through the insulated area. Thus, potential drop can be restricted and current flows uniformly during micromachining. Hence, to get a better idea of potential distribution and current density for coated and non-coated workpieces, simulation has been carried out through COMSOL multi-physics software under electrodeposition model. The electrodeposition, deformed geometry branch contains predefined multiphysics interfaces for time-dependent modelling of deformations that occur as a result of dissolution processes in electrochemical cells. The electrodeposition, primary interface describes the current distribution, potential distribution, and geometrical changes in an electrodeposition cell under the assumption that the variations in composition are negligible in the electrolyte, and that the activation overpotentials of the electrode reactions are negligibly small. The simulation process has been conducted with applied voltages ranging from 13V to 16V. Herein, the simulation results are presented for 14V, as this voltage has been observed to be more effective for the fabrication of microfeatures according to simulated observations. For non-coated workpiece, the maximum electrolytes potential is 9.44V as shown in Figure 4.3(a).

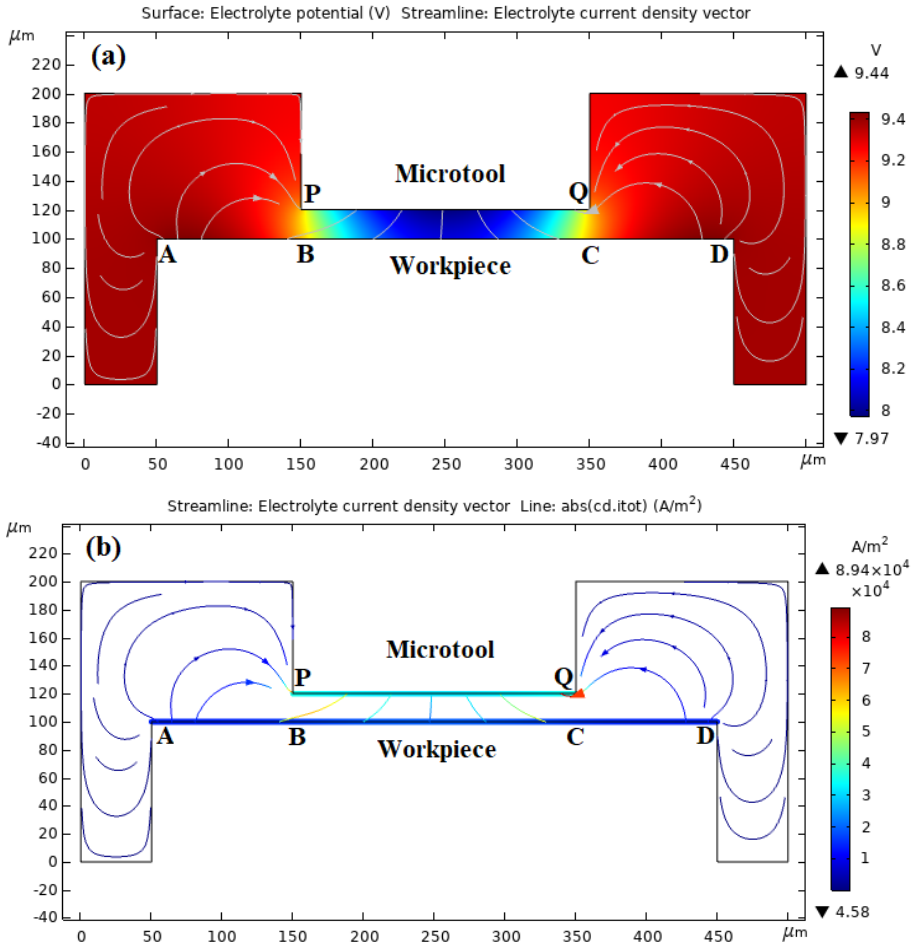

Fig.4.3 Simulation results of non-coated workpiece for (a) electrolyte potential (b) electrolyte current density

Furthermore, it has been noticed that the maximum current density is $8.94 \times 10^4 A/m^2$ as shown in Figure 4.3(b). Streamline or current flux lines exhibit that stray current passes from PQ to AB and CD regions. As a result, pitting and irregular machining affects appears in these regions. But, when workpiece is coated except machining zone, i.e., AB region, the electrolyte potential can be obtained at 6.96V, which is 26.27% less than the non-coated workpiece, as shown in Figure 4.4(a). Similarly, electrolyte current density has been obtained at $3.29 \times 10^4 A/m^2$, which is reduced by 63.19%, as shown in Figure 4.4(b). As a result, by applying insulation technique stray current effects can be minimised significantly.

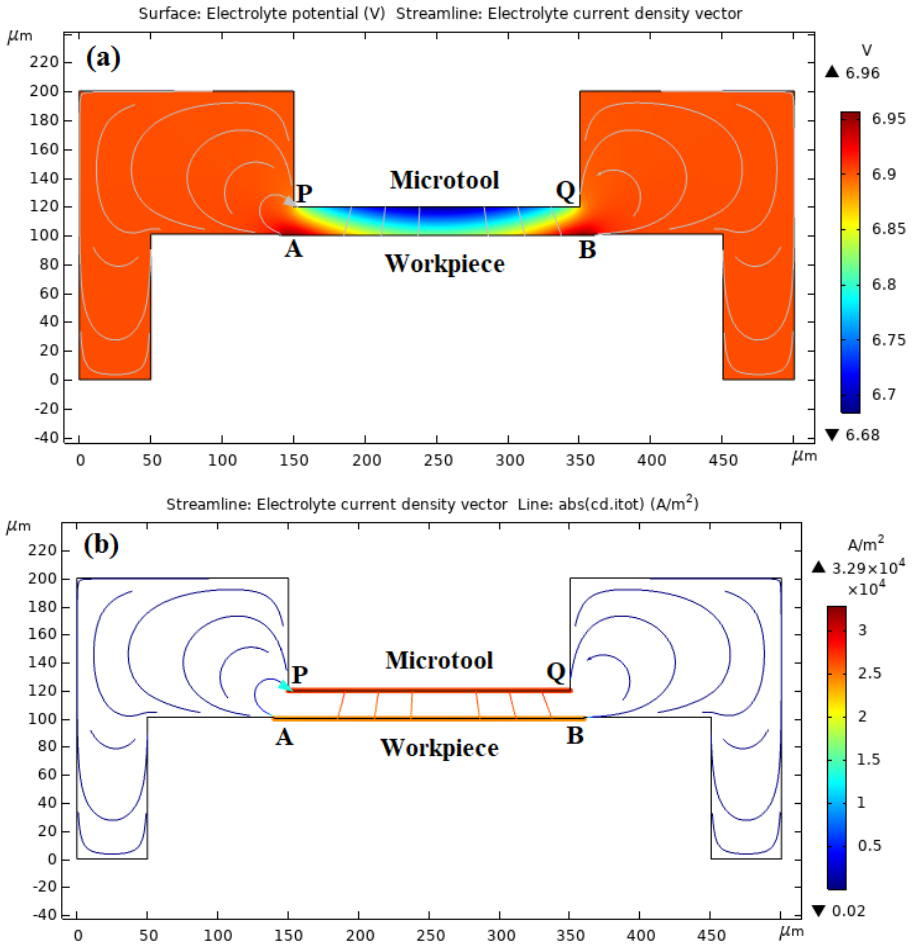

Fig.4.4. Simulation results of coated workpiece for (a) electrolyte potential (b) electrolyte current density

4.4 Experimental planning 1: Insulation technique

Tungsten (W) rod with 200µm diameter and 200µm thickness of stainless steel (SS304) has been chosen as a tool and workpiece for the fabrication of microholes. The sidewalls of microtool and except machining zone total workpiece have been insulated with synthetic rubber coating to minimise the effect of stray current. 0.1 M H_2SO_4 solution has been used as an electrolyte because it can dissolve the sludge during machining from the machining zone, which is most effective for the stagnant electrolyte. The applied voltages 13V to 16V have been selected for a better understanding of the potential distribution in the electrolyte. To avoid the unstable condition of electrolytes at higher voltage, pulse frequency has been selected a lower value, i.e., 500Hz. As the stagnant electrolytes have been used, higher pulse-off time is required to remove the sludge during machining. Thus, 50% of duty cycle has been selected for micromachining. The initial inter-electrode gap and tool feed rate have been selected at 20µm and 0.5µm/s, respectively. These parametric conditions have also been used in earlier experiments under the step pulse

waveform, as mentioned in Chapter 3. Using scanning electronic microscope (SEM) and digital microscope (Leica), the conditions of the machined microholes have been observed and analysed. All machining conditions are listed in Table 4.1.

Table 4.1 Operating conditions for microhole fabrication

Condition	Description
Micro tool (W)	Φ 200μm
Workpiece (SS304)	10 x 15 x 0.2mm
Electrolyte (H_2SO_4)	0.1mol/L
Applied voltage	13V, 14V, 15V, 16V
Pulse frequency	500 Hz
Duty cycle (%)	50 %
Feed rate of micro tool	0.5 μm/sec
Initial IEG	20μm

4.4.1 Results and Discussion

4.4.1.1 Effect of insulation on current density under step pulse waveform

In order to verify the simulation results of insulating, the variation of current density is experimentally investigated under the application of step pulse waveform. It can be noticed that in coated workpiece, current density varied in a moderate range and transpassive state appeared quickly as shown in Figure 4.5. The active state belongs in the region of AB, where the current density accelerated up to 47.62 A/cm^2. In this region, metal surface is etched with a high rate of anodic dissolution. Next, the passive state, i.e., BC region, becomes accompanied by an oxide layer on the anode surface, which interrupts further current flow. Hence, anodic dissolution rate decreases suddenly. But, this passive state does not sustain for a long duration because when anodic potential increases more than 5.2V, the transpassive state of CD appeared with higher current density i.e., 63.49A/cm^2. As a result, the interrupted current can further flow through the oxide layer because during this state oxide layer becomes thinner than the passive state. In consequence, the anodic dissolution rate increases with polishing action which can improve the profile of microholes and reduce pitting effects.

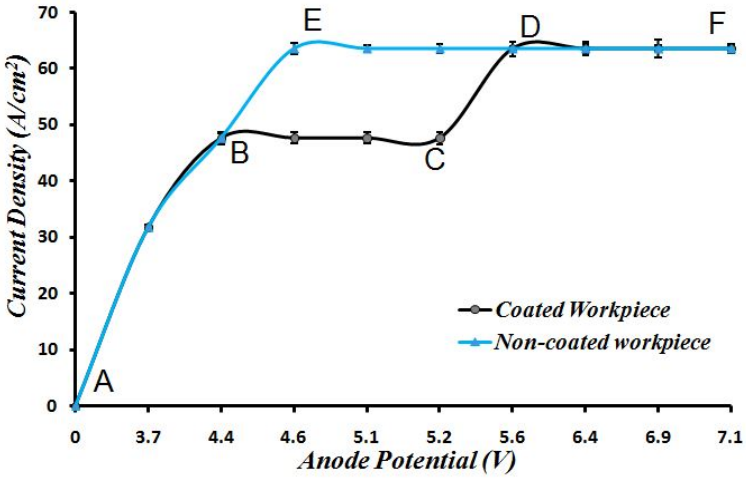

Fig.4.5. Anodic polarization curve for non-coated and coated workpiece at 14V

The reason behind this phenomenon is that for non-coated workpiece, the active state, i.e., AE region, is longer and the current density rises to 63.49A/cm^2. Hence, anodic dissolution rate is greater than coated workpiece during the active state. As an effect, overcut and error of circularity of microhole increases. In addition, another factor is that throughout the total passive state of EF, a larger current density is obtained, resulting in more currents being developed which are engaged to generate the excessive gas bubble. When these gas bubbles are broken, micro-sparks are generated, resulting in unwanted metals removed from the machining zone. Thus, overcut increases and sidewalls become poor surface finish. The minor current can penetrate through the oxide layer and create pitting effects across the entry side of microholes. According to experimental results, it has been noticed that the variation of current density for insulated and non-insulated techniques are similar to simulation results.

4.4.1.2 Effect of insulation on overcut and circularity of machined microhole

Experiments have been carried out at four different pulse voltages, i.e., 13V, 14V, 15V and 16V. In non-coated workpiece, the electrolyte potential and current density are higher as compared to the coated workpiece (Fig.4.5), which is clearly understood from simulation and polarization results (Fig.4.4). Hence, larger overcut of microholes has been obtained than coated workpiece as shown in Figure 4.6. From figure 4.7, it has also been observed that the profile of machined microholes is not circular and edges are not uniform.

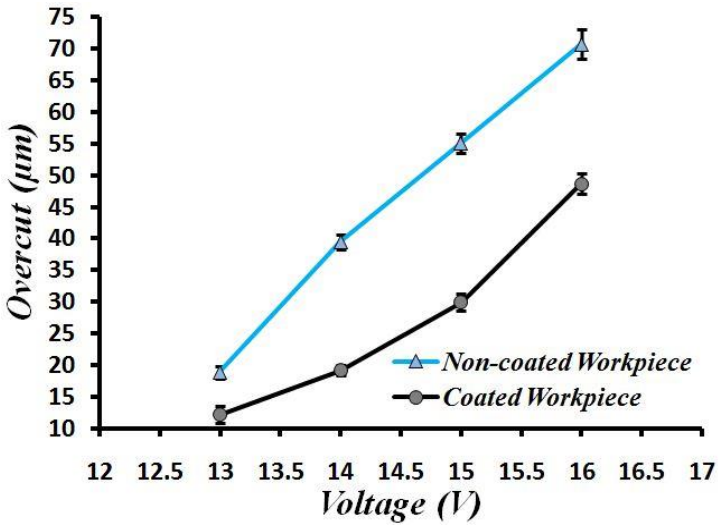

Fig.4.6. Overcut reduction by SPW for coated and non-coated workpiece

But, for coated workpiece, proper circle shape of microhole has been obtained as shown in Figure 4.8. It has also been noticed that minimum overcut has been obtained at 13V, but maximum overcut reduction i.e., 51.49%, and proper circular shape, better uniform edge are obtained at 14V due to proper potential distribution in the machining zone.

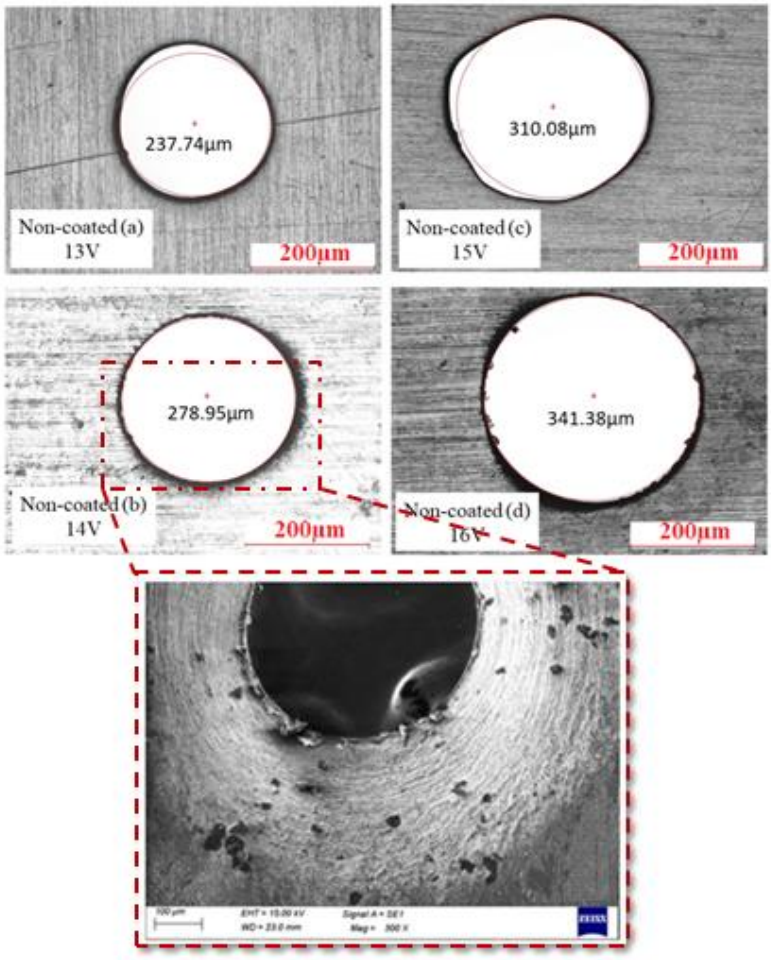

Fig.4.7. Images of machined microholes for non-coated workpiece

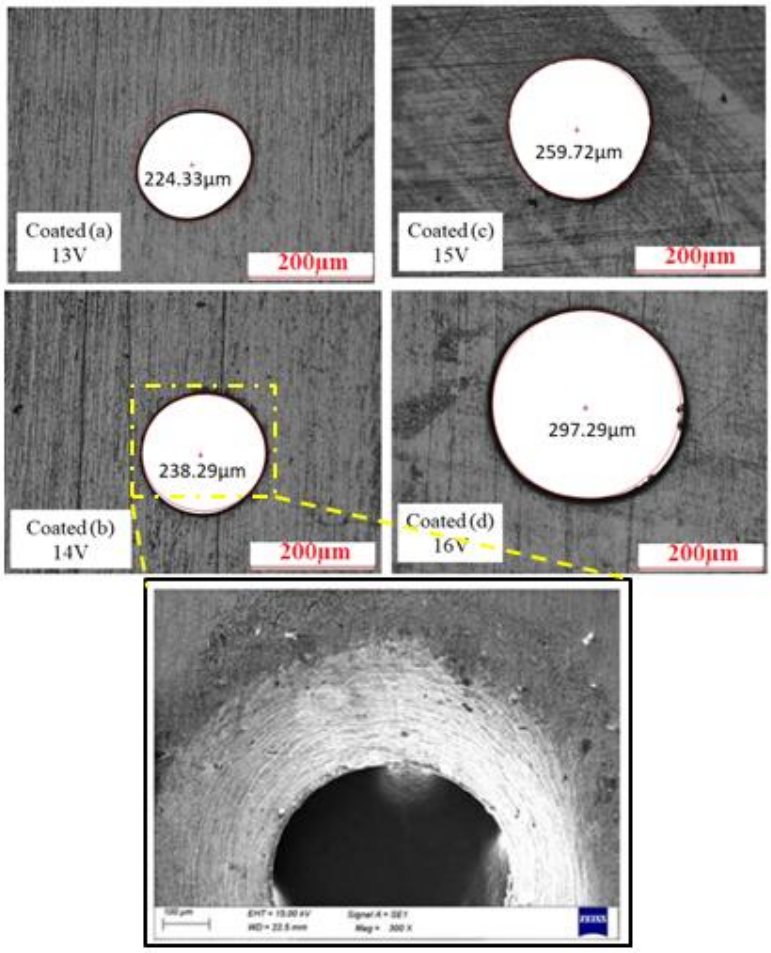

Fig.4.8. Images of machined microholes for coated workpiece

From the image of SEM machined microholes, it has also been noticed that in non-coated workpiece, edges are not uniform; more pitting effects have appeared as shown in Figure 4.7. But, for coated workpiece, edges are uniform, and pitting effects are negligible as shown in Figure 4.8.

4.5 Experimental planning 2: Microtool feed control

4.5.1 Methodology of microtool feed control technique

Machine accuracy can be improved by maintaining a linear relationship between microtool feed rate and material removal rate. If the tool feed rate is greater than the material removal rate, then there is a possibility that the tool will touch the workpiece. It is a dangerous situation for micromachining, which may damage the microtool. Another problem is that short circuit and microspark generates. During machining, microspark plays a significant role in the increment of overcut. This problem can be solved by using discontinue microtool movement, which means that initially, forward movement of microtool is selected with a constant tool feed rate, next tool feed rate is interrupted for a short period, and finally forward movement with a constant feed rate is considered. This process is continued until the tool reaches the absolute target. Employing this strategy, the short circuit effects can be eliminated, which improves machine accuracy because there is a chance to maintain a near about linear relationship between microtool feed rate and metal removal rate.

(a) Control strategy of micro tool feed rate

If microtool movement is selected with a constant feed rate, the above-discussed problem can be noticeable. This problem can be solved by using discontinue tool movements. Throughout machining microtool feed rate has been broken in three different conditions. At first microtool feed rate has been selected as a constant velocity. In second condition, tool feed rate has been interrupted for a certain period, that means no tool feed rate is employed during this time. At third condition, microtool feed rate has been selected with a constant velocity, which is lower than first condition. This process has been continued throughout machining, as presented through flow chart in Figure 4.10. Employing this strategy, elimination of short circuit effects, minimization of microspark generation and uniformity of anodic dissolution can be obtained.

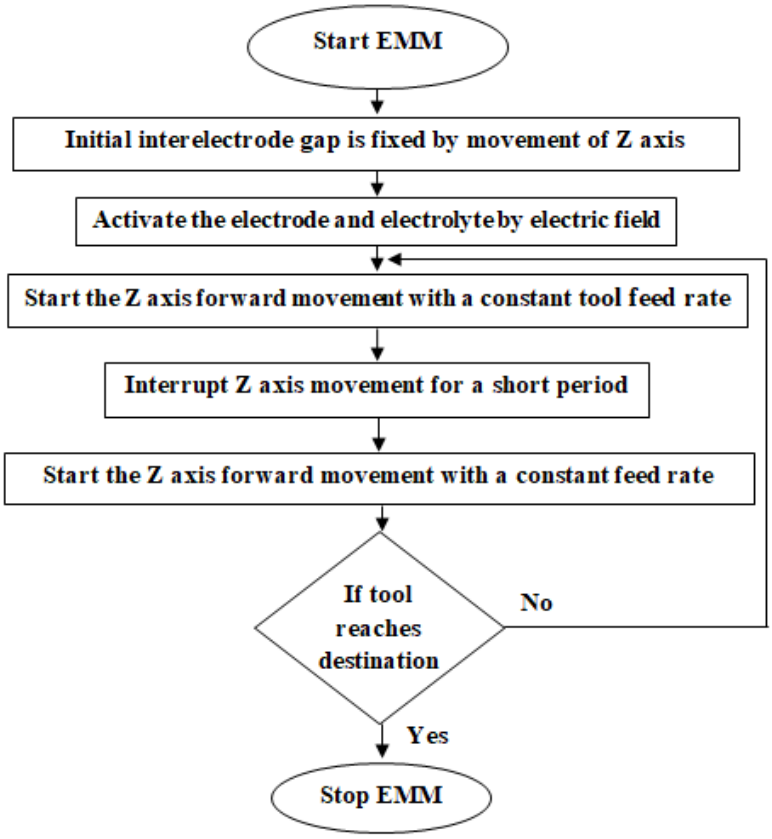

Fig.4.10 Flow diagram of discontinues micro-tool feed control technique

(b) Experimental planning

Utilizing discontinues micro-tool feed control technique under step pulse waveform, microholes can be drilled by the developed EMM setup to analyse performance aspects such as overcut, shape of the hole, stray current effect, machining time, high tool feed rate, short circuit effect, current-voltage characteristics, and compare the machine accuracy with conventional constant microtool feed technique. As copper material has greater electrical conductivity than tungsten material, a copper microtool may be more helpful for facilitating better current flow within the machining area. Hence, microtool with 200µm in diameter made of copper material has been used for experiments. For microhole drilling, stainless steel sheet (SS304) of 200µm thickness has been chosen. In present study, the workpiece has not been coated to allow for detailed identification of the effects of the discontinuous micro-tool feed control technique on the improvement of machining accuracy. As electrolyte flashing is not acceptable for micromachining because it can hamper the machining process so that H_2SO_4 electrolyte has been selected as a stagnant electrolyte. Experimentally, it has been investigated that sludge is dissolved in the electrolyte during micromachining. The low concentration of H_2SO_4 electrolyte can

reduce the side gap and enhance the surface quality. Hence, 0.1mol/L concentrated H_2SO_4 electrolyte was selected for experimentation. The same applied voltage i.e., 14V has been selected for rectangular and step pulse waveform to observe the effect of both waveforms on machining accuracy. The other machining parameters remained fixed for the investigation of the effect of both waveforms, which are a frequency of 500Hz, duty cycle of 50%, micro-tool feed rate of 0.5µm/sec, and an initial inter-electrode gap (IEG) of 20µm. The machining criteria of microhole such as overcut, stray current effect and shape of the hole have been observed and measured by digital microscope (Leica). For the experimental study, other parameters, i.e., RMS voltage, peak voltage duration time, output current, and voltage characteristics were measured by a digital oscilloscope. All machining conditions are listed in Table 4.2.

Table 4.2 Operating conditions for microhole fabrication

Condition	Description
Micro tool (Copper)	Φ 200µm
Workpiece (SS304)	15 x 10 x 0.2mm
Electrolyte (H_2SO_4)	0.1mol/L
Applied voltage	14V
Pulse frequency	500 Hz
Duty cycle (%)	50 %
Feed rate of micro tool	0.5 µm/sec
Initial IEG	20µm

4.5.2 Results and discussion

4.5.2.1 Analysis of current variation in EMM for microtool feed rate control

In order to observe the current variation during EMM under the application of microtool feed control technique, experiments have been carried out at fixed applied voltage of 14V. Without microtool feed control technique or at constant tool feed rate, it can be observed that initially current increases rapidly up to 0.5A, after that current stays at 0.4A throughout machining. Thus, it can be understood that under the application of constant tool feed rate, machining current is higher and sustains throughout machining. As a result, material removal rate increases, resulting in increment of overcut. Another major problem observed in the experiments is that under a constant tool feed rate, short circuits frequently occur, sometimes resulting in damage to the microtool. Figure 4.11 shows that during machining under the constant tool feed rate, the anodic voltage or machining voltage rises from 0V to 11.8V. According to the experimental results of current and anodic voltage, it can be understood that at a constant tool feed rate, the inter-electrode

gap is very small. As a result, under the same applied voltage, a machining current of 0.5A is sustained throughout the machining process, which is greater than that achieved using the discontinuous microtool feed rate technique. Similarly, it can be noticed that the anodic voltage is also higher. Due to it, overcut, and stray current effects and irregular machining can be increased significantly.

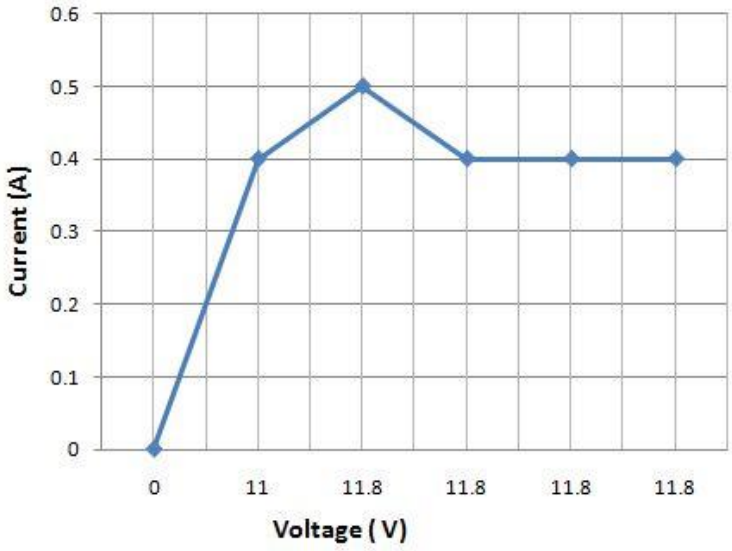

Fig.4.11.Current and anodic voltage characteristics under constant microtool feed rate

Under the application of discontinuous microtool feed as presented earlier in Figure 4.10, it can be noticed that the current initially rises up to 0.4A, and subsequently decreases up to 0.2A, as shown in Figure 4.12. From this observation, it can be understood that during machining, the nature of the current flow is not constant. Initially, machining current increases, but it decreases subsequently.

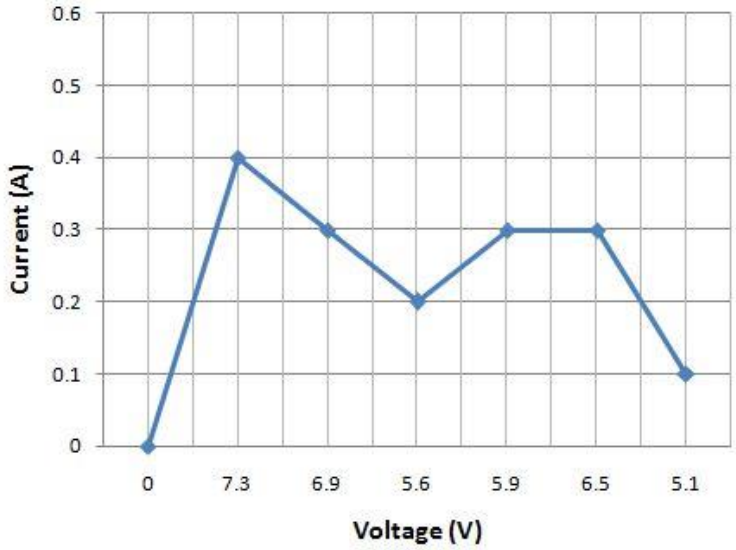

Fig. 4.12.Current and voltage characteristics under discontinuous microtool feed rate

As a result, during the initial stages of machining, the anodic dissolution rate is higher, but it decreases as machining time increases. Hence, it can be said that the current flow rate under the application of discontinuous microtool feed rate is lower than continuous microtool feed rate. As a consequence, extra dissolution from the target area can be minimised. Another advantage can be noticed that during machining short circuit can be eliminated, which protects the microtool from damage.

4.5.2.2 Effect of microtool feed control on machining accuracy

A comparison result of microhole's overcut under the influence of traditionally constant microtool feed rate and discontinuous microtool feed rate has been analysed, as shown in Figure 4.13. From the bar graph, it can be noticed that under constant tool feed rate, overcut of microhole is 95.24µm, which is almost 10 times greater than the innovative discontinuous microtool feed control technique. Utilising this new technique, overcut of microhole has been obtained as 42.96µm.

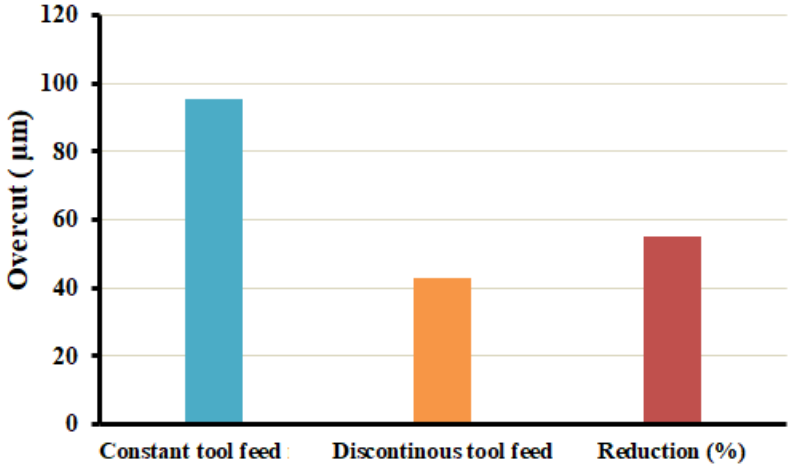

Fig.4.13 Comparison results of overcut for constant tool feed and discontinuous tool feed techniques

SEM images of the machined microholes, as shown in Figure 4.14, exhibit that under the application of traditionally constant tool feed rate, the shape and edge of the machined microhole are not uniform, appears irregular machining and pitting effects, when applied voltage of 14V, frequency of 500Hz, duty cycle of 50%, micro-tool feed rate of 0.5µm/sec. However, under the application of discontinuous microtool feed rate, it can be observed that the smoothness of microhole's side wall is improved, the edge is uniform, no irregular machining sports appear and pitting effects are negligible, as presented in Figure 4.15.

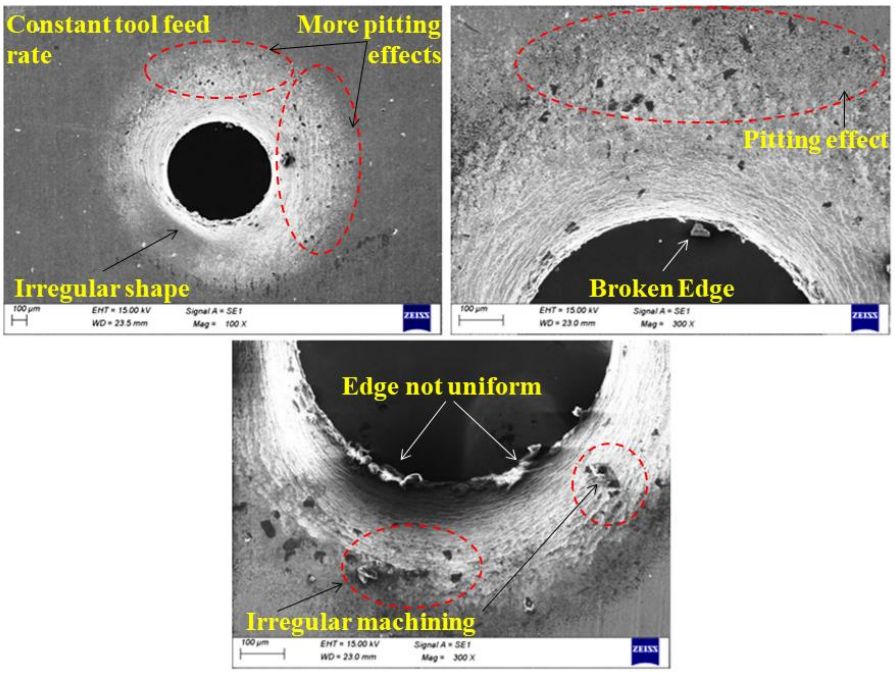

Fig.4.14. SEM images of machined microhole for constant microtool feed

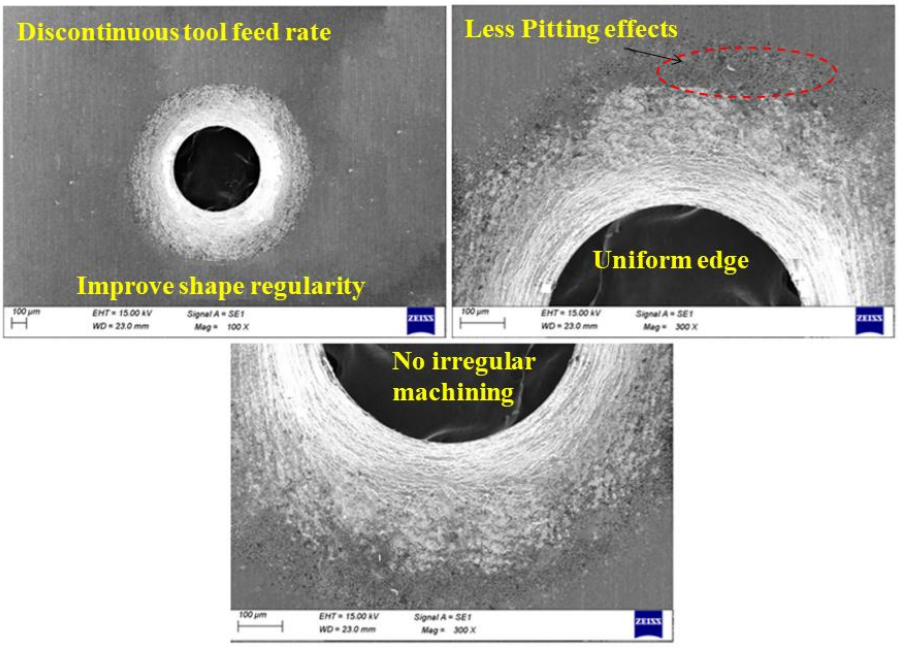

Fig.4.15. SEM images of machined microhole for discontinuous microtool feed

4.6 Outcomes of experimental investigations

By employing the insulation under the step pulse waveform the accuracy of electrochemical micromachining (EMM) has been enhanced significantly and precise microholes have been fabricated. The potential transmission has been controlled significantly by step pulse waveform because the partial discharging effect of double layer capacitor has been incorporated during the faradic time. Thus, anodic dissolution

rate has been controlled. As a result, overcut is minimised significantly. From the simulation results, it can be concluded that by utilising insulated workpiece, current density and potential transmission have been reduced by 63% and 26.37%, respectively. As a result, effect of stray current has been minimised.

The polarization curve reveals that the current density varies within a moderate range, approximately 47.62 A/cm^2 for insulated workpieces. There is a rapid transition of transpassive states from passive state, leading to increased current flow rates. Consequently, the obstructed anodic dissolution rate further increases while the stray current effect decreases. This results in improved sidewall smoothness and circularity profile of microholes. Moreover, compared to non-insulated workpieces, overcut is significantly reduced. Additionally, the profile of microholes in insulated workpieces tends to be almost perfectly circular, with uniform edges and negligible pitting effects. However, in non-insulated workpieces, these effects are more prominent.

Observations under discontinuous microtool feed technique indicates that initially, the current rises linearly up to 0.4A, and subsequently decreases to 0.2A. In contrast, using the traditional constant tool feed method; the current rapidly increases to 0.5A initially, and then remains at 0.4A throughout machining. Notably, the machining current under the discontinuous microtool feed is lower than under continuous feed. Additionally, significant elimination in short circuit has been observed. Consequently, overcut is reduced by 54.89%. Additionally, it is noticed that the smoothness of microhole's side wall is improved, the edge is uniform, no irregular machining sports appear and pitting effects are negligible. Experimental results suggest that the discontinuous microtool feed rate technique can enhance machining accuracy more effectively than the constant feed rate method.

In EMM, when metal dissolution begins, gas bubbles, sludge, and an oxide layer are generated in the narrow inter-electrode gap (IEG), altering the conductivity of the electrolyte and obstructing further current flow. To enhance mass transport, conductivity, and the effective removal of sludge and bubbles from the narrow inter-electrode area, further detailed investigation into the step pulse waveform is required. Modifying the step pulse waveform pattern can be beneficial for reducing the abovementioned drawbacks which may further improve the machining accuracy of EMM.

Chapter 5: Experimentations for improvement of surface finish and machining accuracy utilising multi-step pulse waveforms

5.1. Introduction

In EMM, metal dissolution rate, surface finish, and accuracy depend on electrolyte stoichiometry such as mass transport, current distribution, behaviour of oxide films and bubbles, etc. When metal dissolution starts, gas bubbles, sludge, oxide layer, and heat are generated in the narrow inter-electrode gap (IEG), which changes the conductivity of the electrolyte and hampers further current flow. To improve mass transport and conductivity, high-speed electrolyte flushing is used in conventional electrochemical machining. But, in micromachining, electrolyte flushing creates several problems, such as generating unwanted vibration of the microtool and workpiece, hampering accuracy, and disrupting the proper addressing of electrolytes at the target machining zone. Recently, several new electrical pulse waveforms such as sinusoidal, parabolic, triangular, etc. have been used as an alternative technique to improve the proper localization and for reduction of the extra dissolution from the target area.

In stagnant electrolyte solutions, the improvement of mass transport as well as the conductivity of electrolytes is a challenging task because bubbles and sludge increase the shielding effects. Keeping this in mind, a multi-step pulse waveform (MSPW) has been designed indigenously, where different peak voltages with short duration times are incorporated in each pulse on time. Due to it, voltage drops from maximum peak to minimum peak for each pulse on time, resulting in potential fluctuations occurring during machining. Thus, by utilising this novel MSPW, experimentation is needed to be carried out to study the improvement of the accuracy of EMM and machined surface finish. The effect of the multi-step pulse waveform (MSPW) in EMM has been compared with conventional rectangular pulse waveform (RPW). For better understanding, the power transmission of both pulse waveforms is estimated by mathematical model and compared between the two waveforms. To understand the current density and electric potential distribution, simulation processes have been carried out through COMSOL multi-physics software. In order to verify simulation results, current density has been experimentally analysed for various machining times at different applied frequencies. Finally, depth, diameter, etch factor, surface roughness, micro-sparks affected zone, and pitting effects of microdimples have been investigated. Furthermore, by fabricating microholes, the effects

of MSPW on precision machining have been investigated with the help of a scanning electronic microscope (SEM).

5.2 Multi-step pulse waveform

The schematic view and oscilloscopic image of the rectangular pulse waveform (RPW) and multi-step pulse waveform (MSPW) have been shown in Figure 5.1. To create potential fluctuation during machining, the pulse on time of MSPW has been strategically broken into three pulse duration times with three different peak voltages, i.e., V_{PS1}, V_{PS2}, and V_{PS3}. Due to it, power transmission can be reduced, which minimises the stray current. Alternatively, bubble size and formation rate may also be reduced by MSPW due to lower power transmission. Based on the double layer theory of EMM, it can be identified that during pulse fall time, the bubbles' detachment rate increases effectively [97,98]. As every pulse on time builds with multi pulse fall times, bubbles may detach from the tool rapidly. Thus, more numbers of pulse fall times, short peak voltage duration times, and fluctuations of potential may improve the reduction of bubble size and its detachment rate. As a result, ion transport phenomena improve, sludge may properly remove from the machining zone, and material dissolution rates may also increase. Due to the lower power transmission of MSPW, the stray current effect may also effectively minimise, which plays a significant role in reduction of overcut.

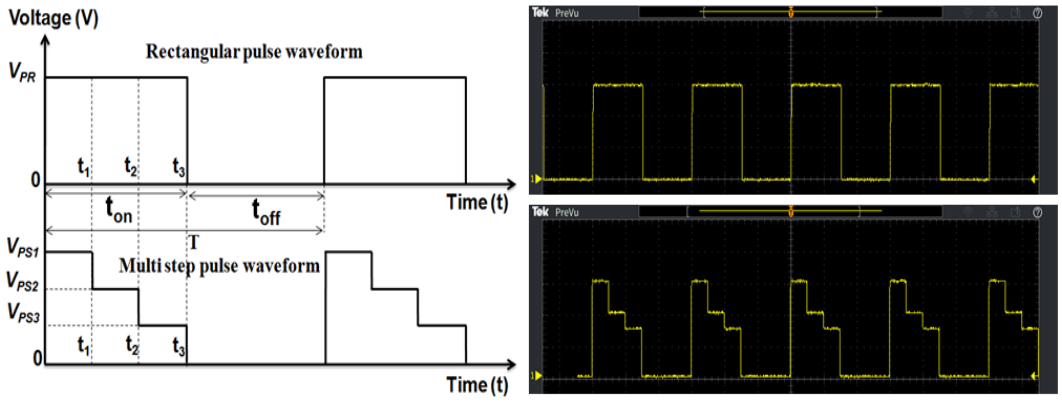

Fig. 5.1 Schematic view and oscilloscopic image of RPW and MSPW

5.3 Mathematical formulation of power transmission for multi-step pulse waveform

In electrochemical micromachining, stray current plays a significant role in the generation of overcuts and surface roughness of microcomponents. By controlling the power of the pulse waveform, the stray current effect can be minimised because stray current depends on power transmission in the electrolyte. Utilising MSPW power transmission can be controlled when the applied voltage, frequency, duty cycle, and pulse period are the same as compared to other pulse waveforms, such as rectangular, sinusoidal, parabolic,

triangular, etc. The reason behind this phenomenon is that MSPW has three different peak voltages during pulse on time and pulse voltage is stepped down from the maximum peak, i.e., V_{PS1}, to the third peak voltage, i.e., V_{PS3}, as shown in Figure 5.1. As a consequence, the applied voltage fluctuates during machining, which is not observed in rectangular pulse waveform (RPW) as well as other pulse waveforms, as mentioned earlier. The resistance R_E of electrolyte in the initial inter-electrode gap can be estimated as:

$$R_{electrolyte} = \frac{\rho_e h}{A} \tag{5.1}$$

Where, initial inter-electrode gap h, resistivity of electrolyte ρ_e, and microtool tip area A. The average power P for each pulse on time of any pulse waveform can be calculated as:

$$P = \frac{1}{Period}\int p(t)dt \tag{5.2}$$

Where, instantaneous power over one period at any time is denoted by p(t). Consider any pulse waveform's applied voltage of V(t) and p(t) can be written as:

$$p(t) = \frac{V^2(t)}{R_E(t)} \tag{5.3}$$

Thus, the average power transmission at electrolyte resistance R_E, can be estimated for each pulse on time of RPW as:

$$P_{RPW} = \frac{1}{t_{on}}\int_0^{t_3} \frac{V_{PR}^2}{R_E} dt \tag{5.4}$$

Similarly, for MSPW, the average power transmission can be determined as:

$$P_{MSPW} = \frac{1}{t_{on}}\left[\int_0^{t_1} \frac{V_{PS1}^2}{R_E} + \int_{t_1}^{t_2} \frac{V_{PS2}^2}{R_E} + \int_{t_2}^{t_3} \frac{V_{PS3}^2}{R_E}\right] dt \tag{5.5}$$

From equations (5.4) and (5.5), the average power transmission can be estimated for RPW and MSPW. Finally, it can be understood that as compared to conventional RPW, the power transmission of MSPW is lower for the same applied voltages. From equations (5.4) and (5.5), the power transmission in the electrolyte for each pulse on time has been theoretically estimated for the rectangular pulse waveform (RPW) and the multi-step pulse waveform (MSPW). It can be noticed from Figure 5.2 that as compared to RPW, MSPW has a lower power transmission capacity for different voltages.

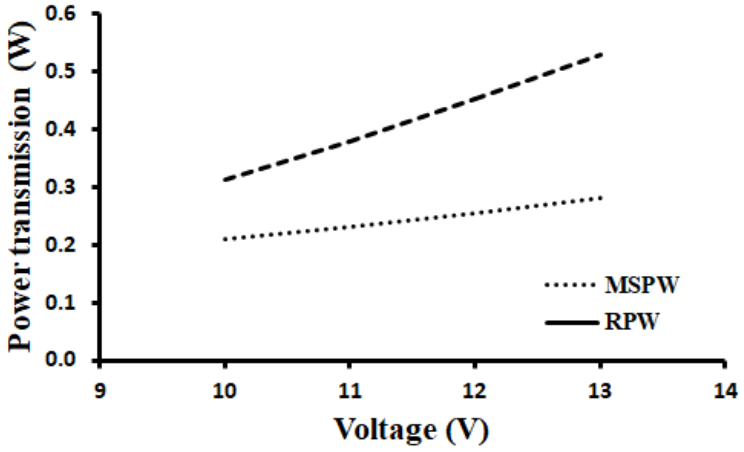

Fig. 5.2 Power transmission with different voltages for RPW and MSPW

It also observed that power transmission increases when applied voltage rise. The lower power transmission is useful for the reduction of stray current effect. Thus, it can be understood that at lower applied voltages, overcut can be minimised due to less stray current. By increasing frequency, pulse duration time can also be minimised, which plays a significant role in anodic dissolution and gas bubble evolution. But, at higher frequencies, pulse duration time reduces more, which decreases faradic time. Due to it, less amount of material is removed from the target area, resulting in the accuracy of machined products may not be achieved as per requirements and longer machining time is required. From the theoretical estimation of power transmission of MSPW, it can be noticed that at 10V power transmission is lower. Hence, in the present study, an applied voltage of 10V has been selected for all experiments. Due to the possibility of improper machining, voltages below 10V have not been considered for micromachining using the MSPW technique.

5.4 Controlling of gas bubble evolution using multi-step pulse waveform

Potential drops are an important factor in EMM because, in a narrow inter-electrode gap, gas bubbles do not conduct the ionic current. Thus, the ionic resistivity increases in the presence of gas bubbles, which is known as shielding effects. Potential drops are considered the combination of active overpotential and ohmic overpotential. The electrolyte concentration depends on the ionic resistivity, which changes the nature of the current flow. Due to difficulties in the measurement of electrolyte concentration in narrow IEG during machining, the estimation of ionic resistivity and concentration is very difficult. Hence, the electrolyte potential and current density have been analysed through the simulation process and polarization curves. The cathode tool surface has only been considered for in-depth analysis of bubble formation and their detachment rate because,

in the electrochemical reaction, at the cathode, hydrogen gas and hydroxide ions are evolved. At the anode workpiece, oxygen gas is evolved which plays a leading role in oxide layer formation. Conventional RPW has a single peak voltage, which is sustained through total pulse on time. Thus, bubble formation is faster than MSPW, and they are accumulated with a gas film as shown in Figure 5.3(a). Due to it, larger bubbles are diffused by buoyant force, few bubbles are broken inside the IEG, and larger shapes of bubbles come out at the electrolyte surface, as presented in Figure 5.3(b). As a consequence, shielding effects increase and ion transport phenomena decrease as compared to MSPW. As a result, the metal dissolution rate can decrease and stray current increases, which enhances pitting effects.

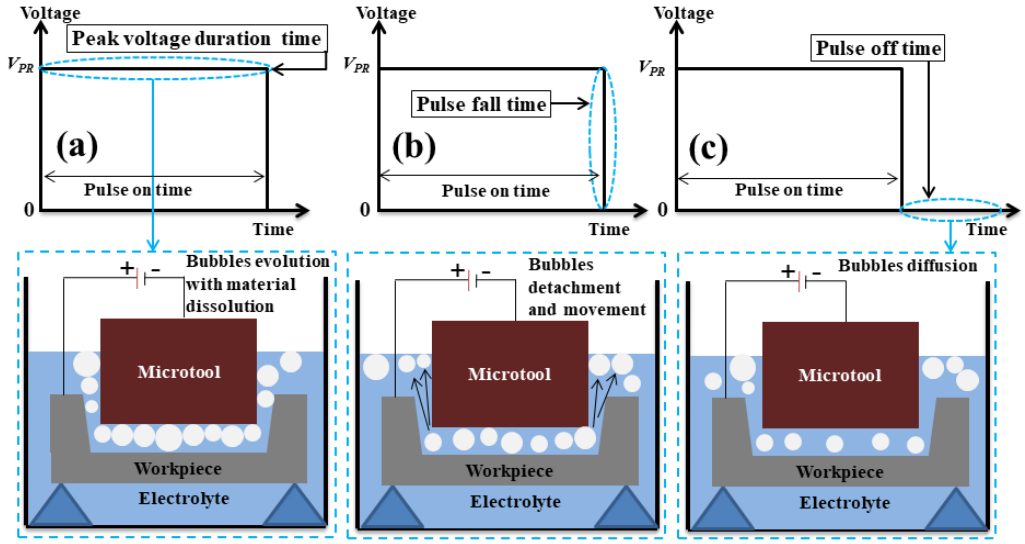

Figure 5.3 Process mechanism of bubbles formation under RPW

The microsparks occur when bubbles are broken inside the IEG during machining. Due to it, the unwanted metal removal rate increases. Therefore, the machining accuracy cannot be achieved as per requirement. During the pulse off time, the applied voltage drops to zero. This change initiates the bubble diffusion process, as illustrated in Figure 5.3(c). The concentration of hydroxide ions at the anode surface can be increased by accelerating ion transport and reducing shielding effects. These phenomena can be achieved by MSPW for the stagnant electrolyte because, during pulse on time, the pulse voltage is stepped down from the maximum peak, i.e., V_{PS1}, to the second peak, i.e., V_{PS2}, and from the second to third peak voltage, i.e., V_{PS3}, as shown in Figure 5.4(a). Due to it, the potential of total pulse on time fluctuates. This potential fluctuation and more numbers of pulse fall times increase the bubbles' detachment rate from the tool i.e., the cathode surface. These released bubbles attempt to flow upward and circulate into the IEG or

attach to the immobile bubbles on the tool surface, as shown in Figure 5.4(b). As a result, ion transport phenomena can improve, and sludge can be removed from the machining zone. Alternatively, shielding effects can also be reduced by minimising the diameters of the bubbles, because, at the tool surface, smaller bubbles attach more closely and enhance the convective ion flux. In pulse off time, the applied voltage drops to zero, initiating the diffusion of bubbles, as illustrated in Figure 5.4(c).The smaller bubbles can be generated by MSPW because the three peak voltage duration times are very small, and more numbers of pulse fall times are incorporated in pulse on time. As a consequence, the voltage does not remain constant throughout the pulse on time. In consequence, excessive bubble evolution can also be minimised.

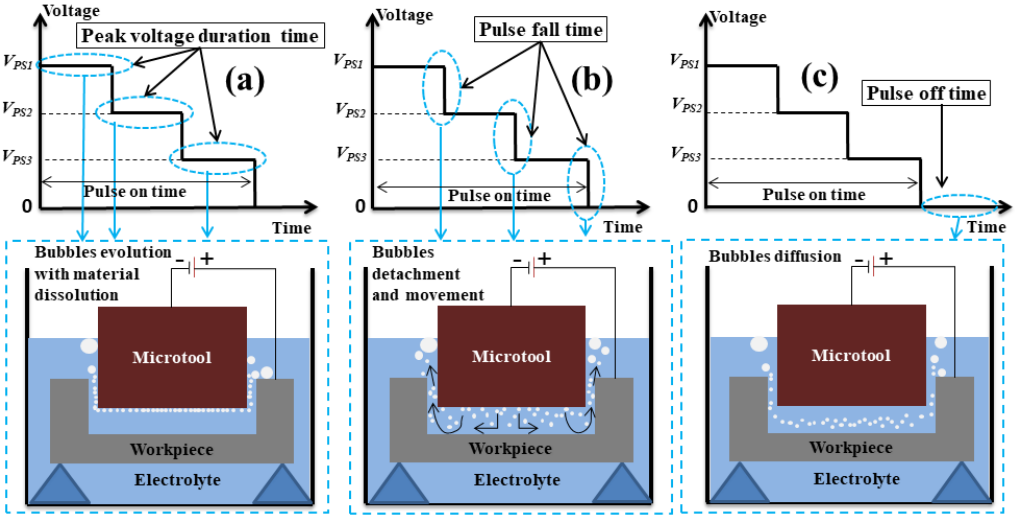

Fig. 5.4 Process mechanism of small size bubbles formation under MSPW

5.5 Simulation of gas bubble's effect on potential transmission and current density

Distributed potential and current density have been simulated using COMSOL multi-physics software (under electrodeposition model) for rectangular pulse waveform (RPW) and multi-step pulse waveform (MSPW) at the applied voltage of 10V. In the simulation process, variations in electrolyte dynamic viscosity, temperature, and workpiece dissolution have not been taken into analysis. For RPW, simulated results exhibit that in the presence of a larger size of bubbles, potential drop and current density increase significantly, as shown in Figure 5.5 (a, b). Thus, it can be understood that when current density increases, gas bubble sizes become larger, resulting in more shielding effects and improper ion transport have occurred. As a result, the gas film is formed, which hampers the anodic dissolution rate. This phenomenon leads to errors in the accuracy of machined products. At the applied voltage of 10V, the maximum electrolyte potential can be obtained at 5.49V and 7.89V for RPW and MSPW, respectively. From the simulation

results, it can be noticed that the current density and potential drop of MSPW are smaller than RPW, as shown in Figure 5.6 (a, b). These simulation results indicate that by utilising MSPW, shielding effects can be significantly minimised and it is effective for improvement of ion transportation. As a consequence, the accuracy of machined microcomponents can be improved.

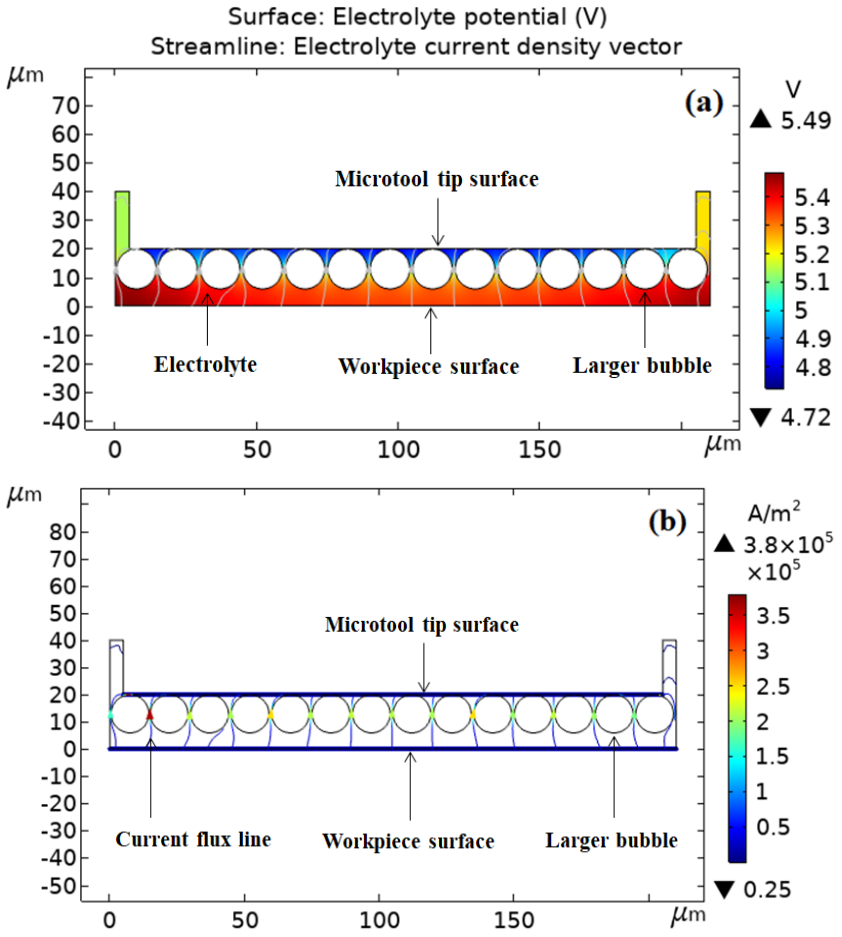

Fig. 5.5 Simulation results of RPW for (a) electrolyte potential (b) current density

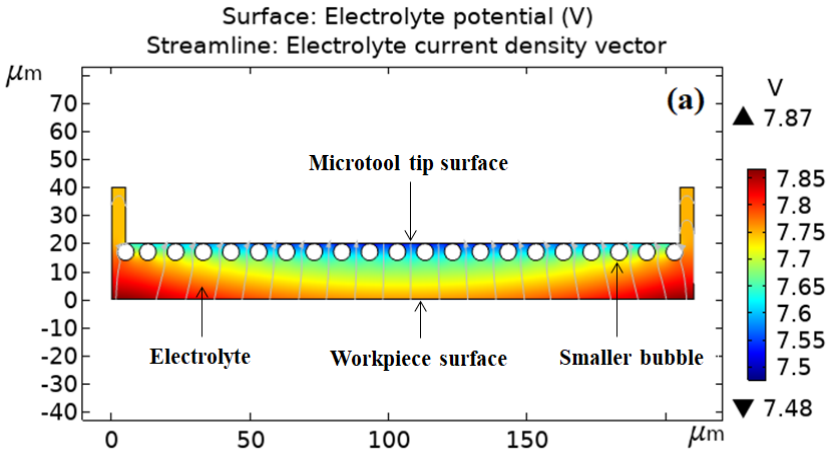

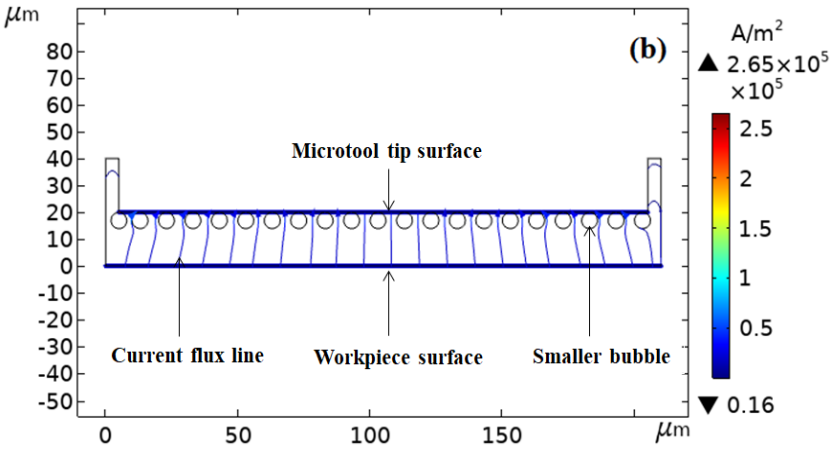

Fig. 5.6 Simulation results of MSPW for (a) electrolyte potential (b) current density

5.6 Experimental planning

Copper (Cu) micro-tool rod with 200µm diameter and 200µm thickness of stainless steel (SS304) has been chosen as the tool and workpiece, respectively. The sidewall of the microtool has been coated with synthetic enamel to reduce stray current effects. 0.1 M H_2SO_4 solution has been used as an electrolyte because it can dissolve the sludge during machining in the machining zone, which is most effective for the stagnant electrolyte. The applied frequencies of 500Hz to 4kHz has been selected for micromachining. The applied voltage of 10V has been selected for experiments because from the theoretical estimation of power transmission of MSPW, it can be noticed that 10V is suitable for lower power transmission. Herein, the second and third peak voltages of MSPW have been selected as 8V and 6V, respectively. As the applied voltage range is higher, a lower range of frequency has been selected to reduce the energy of the waveform. As the stagnant electrolytes have been used, a higher pulse-off time is required to remove the sludge during machining. Thus, 50% duty cycle has been selected for micromachining. As earlier experimental investigation, the same initial inter-electrode gap, i.e., 20µm, and tool feed rate, i.e., 0.5µm/s, have been selected for all experiments. In order to identify the effectiveness of MSPW in EMM, microdimples have been fabricated at different frequencies and compared with rectangular pulse waveform. The surface roughness of microdimples and its sectional profile have been analysed to find out the best operational frequency of MSPW. Additionally, the machining accuracy has been investigated in terms of etch factor (EF), depth and diameter of microdimple. In the electrochemical machining of microdimples, metal is dissolved both in the directions of diameter and depth. This dissolution in the diameter direction often results in undercutting. The etch

factor (EF), which represents the ratio of the material removal rate in depth and diameter, is usually used for evaluate the machining localization of microdimples (Figure 5.7).

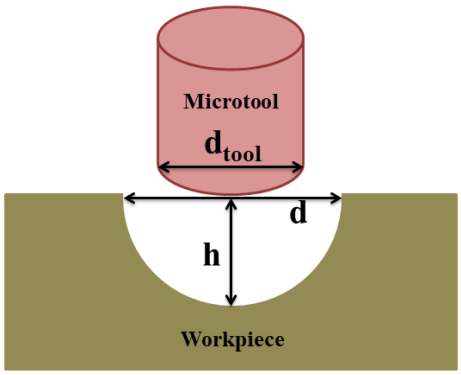

Figure 5.7 Schematic diagram of etch factor (EF).

The etch factor can be estimated as follows:

$$EF=2h/(d-d_{tool}) \quad (5.6)$$

Where, h is the machining depth of micro dimple, d_{tool} is the diameter of microtool, and d is the diameter of microdimple. Furthermore, microholes have been fabricated at the best parametric combination of MSPW. The characteristics of machined microhole has also been investigated from SEM micrographs and compared with those achieved using conventional rectangular pulse waveform.

During micromachining, the image of gas bubbles evolution has been captured by a digital camera, Dino-Lite (AM4815ZTL, Taiwan), whose maximum frame rate is 30fps. Using Talysurf CCI Non-Contact Profilometer (Taylor Hobson), Field Emission Scanning Electronic Microscope (ZEISS), and digital microscope (Leica), the condition of the machined microdimples and microholes have been observed and analysed.

5.7. Results and Discussion

5.7.1 Influence of pulse frequency on gas bubble and current density

Under the application of rectangular pulse waveform (RPW), it can be observed that when the frequency is increased two times, current density rises simultaneously, as presented in Figure 5.8(a). When the machining time reaches almost 60s, it can also be noticed that the current density is nearly constant and sustained to the end of the machining time for all frequencies. According to experimental results, it can be found that by increasing the frequency, current density has been obtained at 57.14A/cm^2, 60.31A/cm^2, 65.07A/cm^2, and 66.67A/cm^2 for 500Hz, 1kHz, 2kHz, and 4kHz, respectively. From the experimental results of current density, it can also be noticed that current density increases with increasing frequency. Conventional RPW has a single peak

voltage, which is sustained through total pulse on time. Hence, under the application of RPW, the larger size of the bubble evolves, increasing the shielding effects and resulting in a decrease in anodic dissolution. When larger size of bubbles is broken, microsparks are generated. As a result, the material dissolution rate is reduced and unwanted material is removed from the machining area which gives negative effects on the machining accuracy and surface finish.

Utilising the multi-step pulse waveform (MSPW), these problems can be overcome. In MSPW, three different peak voltages with short duration time are incorporated into each pulse on time. Thus, the voltage drops from maximum peak to minimum peak during pulse on time, such as 10V to 8V, 8V to 6V, and finally 6V to 0V. Due to it, the potential fluctuates during each pulse on time of MSPW. As each pulse on-time is followed by multiple pulse fall times, bubbles can detach from the tool rapidly. Consequently, increasing the number of pulse fall times, shortening peak voltage duration times, and inducing potential fluctuations may enhance the reduction of bubble size and its detachment rate. As a consequence, bubble movement may increase, which enhances the ion transport phenomena and flow of convective ion flux to the microtool tip surface. Figure 5.8(b) exhibits that current density increases with oscillation at different frequencies due to the fluctuation of potential during pulse on time. From the figure, it can be noticed that at 500Hz, the current density is varied such as 31.75A/cm^2, 45.62A/cm^2, 47.62A/cm^2, 62.49A/cm^2, and 64.49A/cm^2. Similarly, at 1kHz, 2kHz, and 4kHz frequencies, the variation of current density are 44.62A/cm^2 to 63.49A/cm^2, 47.62A/cm^2 to 79.37A/cm^2, 63.49A/cm^2 to 79.37A/cm^2, respectively. When pulse frequency rises, the number of pulse periods per unit time increases. Consequently, pulse duration time, i.e., pulse on time and off time, decreases and enhances the repetition of anodic reactions in unit time. Due to the longer peak voltage duration time at lower frequencies, i.e., 500Hz and 1kHz, the variation of current density and its oscillations are almost the same. At the higher frequency, i.e., 4kHz, the current density is larger, but periodic oscillations are minimised. But, at the applied frequency of 2kHz, it has been observed that more periodic oscillations occur and current density accelerates. Thus, it can be understood that at the frequency of 2kHz, smaller bubbles may be generated with a higher detachment rate due to proper peak voltage duration time. Hence, to obtain better machining accuracy, 2kHz frequency plays a significant role.

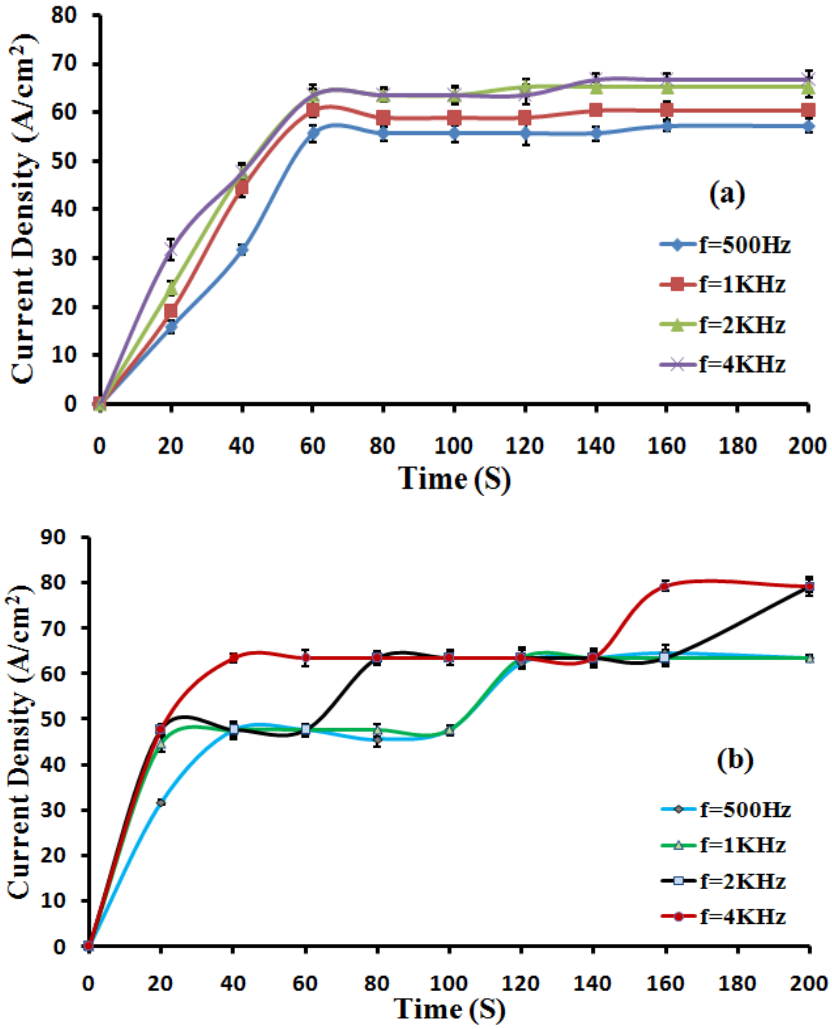

Fig. 5.8 Influence of frequency on current density for (a) RPW (b) MSPW

To verify this phenomenon, at the frequency of 2kHz, gas bubble evolution has also been observed for RPW and MSPW, as shown in Figures 5.9 and 5.10. Figure 5.9 (a) represents the initial condition when time 't' is zero and the power supply is not connected. In the case of RPW, at the times 20s, 40s, and 80s, gas bubble formation has been captured by the camera, and it is noticed that the size of bubbles also increases and attaches to the micro-tool surface as shown in Figure 5.9 (b-e). Similarly, the observation of bubble formation under MSPW has been shown in Figure 5.10 (a-d). It has been found that the bubble sizes are very small as compared to RPW, and maximum bubbles are detached from the microtool. These phenomena occurred continuously throughout machining time.

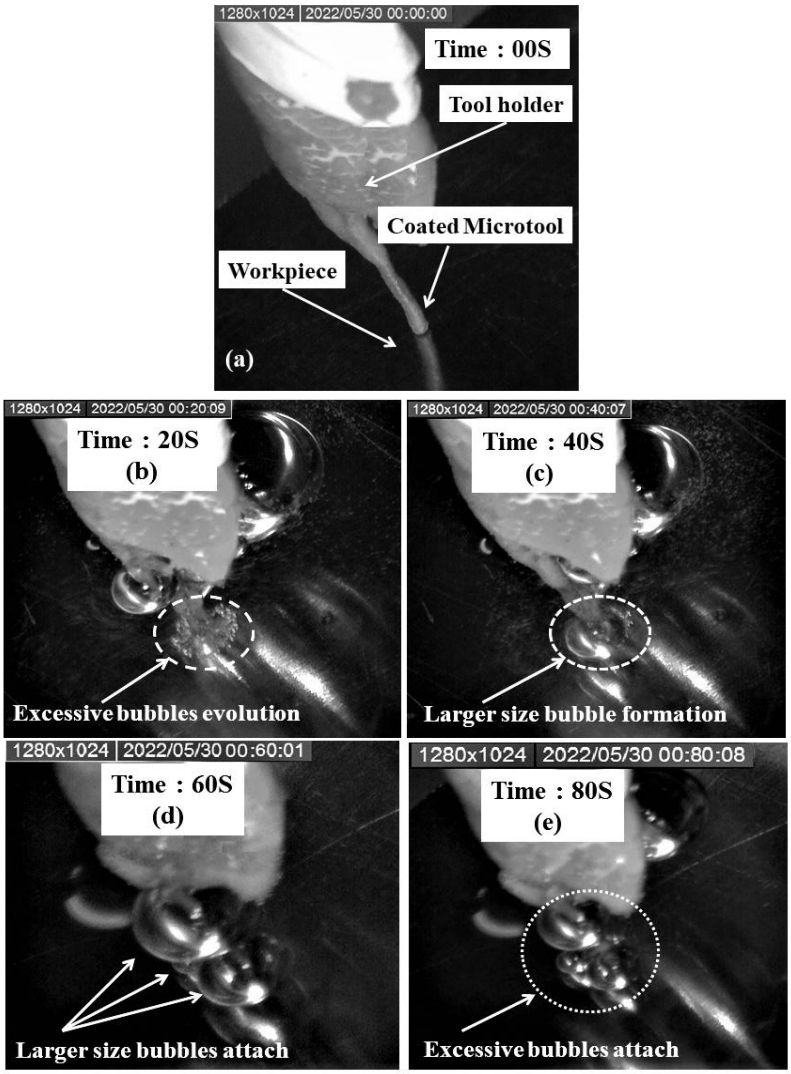

Fig. 5.9 Gas bubbles formation at different time periods under RPW at 2kHz

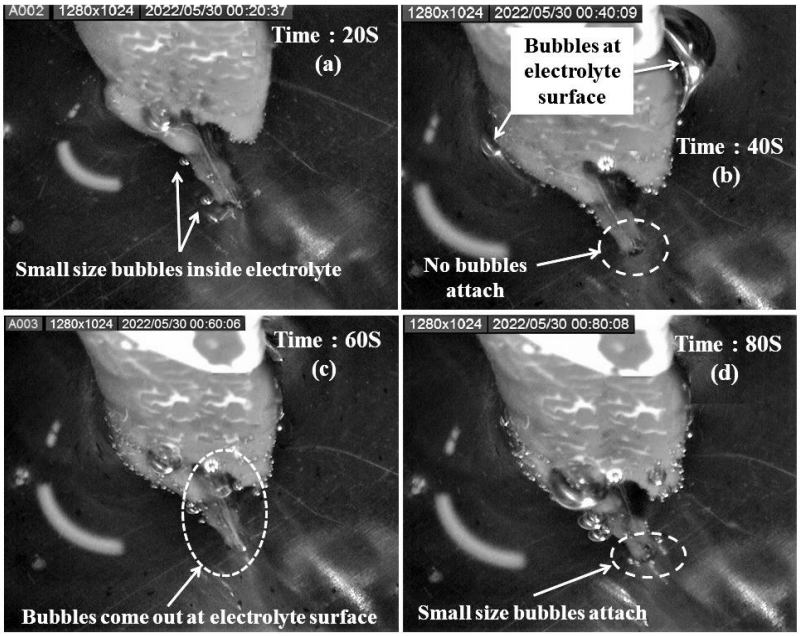

Fig. 5.10 Gas bubbles formation at different time periods under MSPW at 2kHz

5.7.2 Effect of rectangular pulse waveform on machining accuracy and surface roughness for different frequencies

To understand the effect of the rectangular pulse waveform (RPW) and multi-step pulse waveform (MSPW) on surface roughness and machining accuracy, microdimples have been machined at different applied frequencies when the applied voltage is fixed at 10V. The variation of surface roughness has been shown in Figure 5.11. From the figure 5.11, it can be observed that under RPW, the surface roughness of the microdimple decreases at higher frequencies. Thus, at a frequency of 2kHz, a lower surface roughness has been obtained. However, when the frequency increases to 4kHz, it can be noticed that the surface roughness increases due to a very low material removal rate. The inside circumference of microdimples, such as specific surface roughness (Ra), profile error, etch factor, depth, diameter, and 3D optical profilometry image, has been observed and compared between RPW and MSPW. Figure 5.12 (a) exhibits the 3D optical profilometry image of a machined microdimple, which has been fabricated at the frequency of 500Hz under RPW. From the curvature of the profile structure, it can be noticed that the inside bottom surface of microdimple is very rough, which can be understood from the colour contour of the 3D image as shown in Figures 5.12 (a) and (b). The reason behind the generation of pockets with different heights is irregular machining. Due to the longer pulse duration time of 500 Hz frequency, larger size bubbles are evolved and their detachment rate is also decreased. As a result, current flow is obstructed, and heat is generated, causing larger size bubbles to break inside the IEG. In consequence, unwanted microsparks occurred, which removed the extra metal from the machining area. Hence, the poor surface roughness (Ra) of the bottom area of the microdimple is obtained as 1.016µm. When the applied frequency increases twice, i.e., 1kHz, the effect of RPW on machined microdimples is shown in Figure 5.12 (c-d). From the colour contour of the 3D image, it can be observed that no unwanted pockets appeared at the bottom surface of microdimples. But, the shape of the profile becomes poor due to improper metal removal rate. The bubble evolution rate decreases with increasing frequency because the pulse duration time reduces at a higher frequency. Due to it, shielding effects and microsparks are minimised, which helps to improve the surface finish. Thus, at 1kHz, lower surface roughness (Ra) of 0.4118µm is obtained for microdimples. Therefore, by increasing frequency twice, surface roughness can be minimised significantly.

Hence, at the applied frequency of 2kHz, the minimum surface roughness (Ra) of 0.2511µm is obtained, as shown in Figure 5.11. The profile curvature of microdimples is

also improved at 2kHz frequency which also corroborated with microscopic image, as shown in Figure 5.12 (e-f). However, at the applied frequency of 4kHz, surface roughness is obtained as 0.5105µm, which is greater than the frequency of 1kHz and 2kHz, as shown in Figure 5.11. The metal removal rate decreases with increasing frequency due to shorter pulse duration time. Due to it, irregular machining can be occurred. Hence, from the 3D image, it can be noticed that the bottom surface is not uniform, as shown in Figure 5.12 (g-h). From the experimental results, it can be understood that 2kHz frequency is more appropriate for the control of bubble evolution and detachment rate, resulting in improvement in the current flow rate as well as metal removal rates. As a result, at the applied frequency of 2kHz, surface finish and profile accuracy of microdimples are improved by RPW.

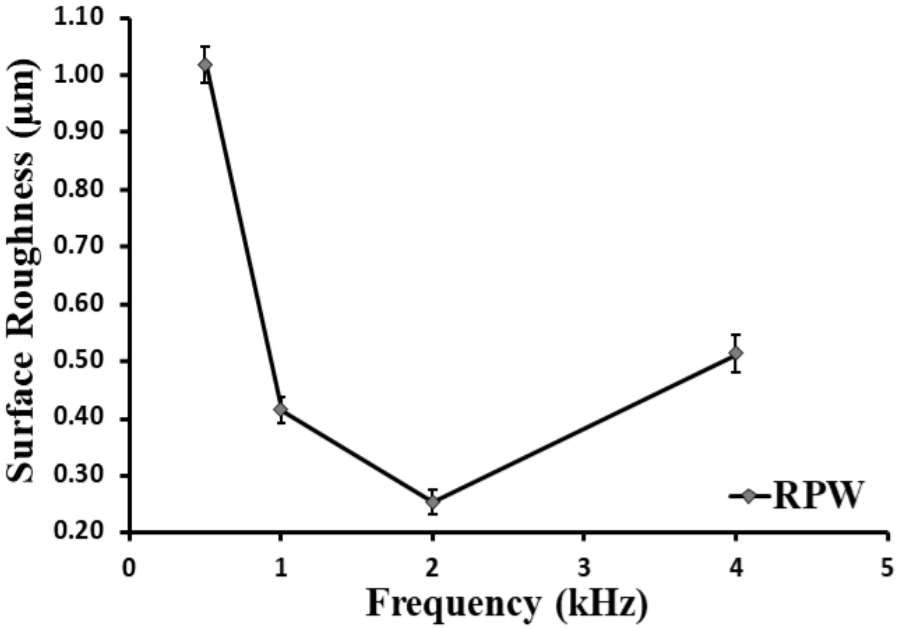

Fig. 5.11 Surface roughness of machined micro-dimple under RPW at different frequencies

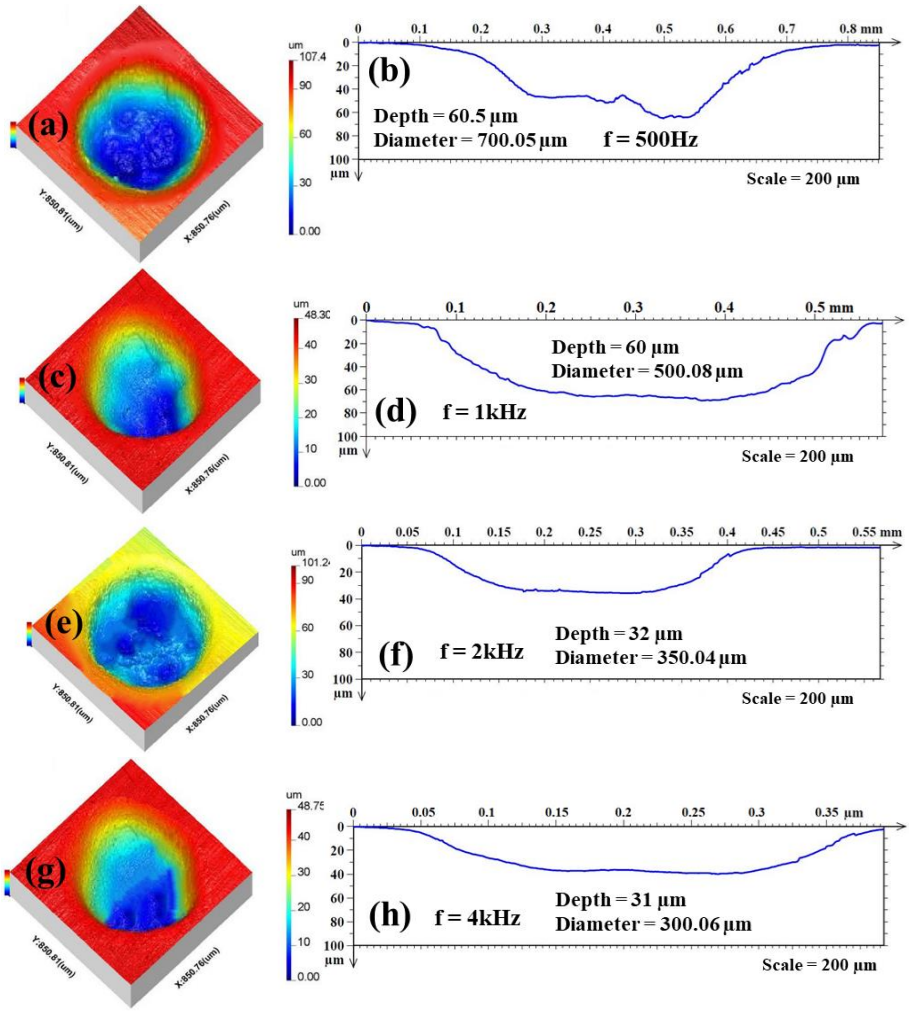

Fig. 5.12 Under RPW, optical images of 3D, and profile structure; 500Hz (a-b), 1kHz (c-d), 2kHz (e-f), 4kHz (g-h)

5.7.3 Effect of multi-step pulse waveform on machining accuracy and surface roughness for different frequencies

By increasing frequency, microdimples have been machined to understand the effect of the multi-step pulse waveform (MSPW) on surface finish and profile accuracy. Furthermore, machining criteria are compared with conventional rectangular pulse waveform (RPW) to justify the application of the MSPW technique. The variation of surface roughness has been shown in Figure 5.13. From the figure 5.13, it can be noticed that at a frequency of 500Hz under MSPW, the surface roughness is greater than at higher frequencies. Due to a higher material removal rate, there is a probability of greater surface roughness at lower frequencies. By increasing the frequency, it can be noticed that the surface roughness is significantly reduced. Hence, at a frequency of 2kHz, lower surface roughness is achieved. However, at frequencies greater than 2kHz, specifically at 4kHz, the surface roughness further increases due to a very low material removal rate. Thus,

under MSPW, 2kHz frequency is suitable for appropriate moderate amount of material removal. At the applied frequency of 500Hz, the characteristics of fabricated machined microholes are shown in Figure 5.14 (a,b). From 3D images, it can be identified that, as compared to RPW, the accuracy of the profile is enhanced, no micro-sparks affected zones appear, and surface roughness, i.e., Ra = 0.05369µm, is also minimised significantly. The reason behind these achievements is that bubble size and its detachment rate have been controlled by MSPW. As the three different peak voltages, i.e., 10V, 8V, and 6V are incorporated during pulse on time of MSPW, voltage drops from the maximum peak to minimum peak voltage. Consequently, potential fluctuates during the pulse on time. Due to potential fluctuation, shorter peak voltage duration time, and more numbers pulse fall times, continuous bubble formations are hampered; bubble detachment rate increases and small-size bubbles can come out quickly from the machining zone. This is helpful for the renewal of electrolytes in the narrow IEG and while promotes better sludge removal. As a consequence, ion transportation improves, shielding effects are minimised, and more sludge can come out due to better flow of electrolyte rotation. From figures 5.14 (a,b), it can be observed that only the centre point of the microdimple's bottom surface is slightly high, which can be removed by increasing frequency. At 1kHz, the accuracy of the profile is improved, and surface roughness, i.e., Ra = 0.04843µm, is reduced, as shown in Figure 5.14 (c,d). When frequency increases twice, i.e., 2kHz, the more accurate profile of microdimple is obtained with minimum surface roughness, i.e., Ra = 0.02413µm, which corroborated with microscopic image, as shown in Figure 5.14(e,f). But, at higher frequencies, i.e., 4kHz, the depth and diameter of microdimple are decreased due to lower pulse duration time as well as lower metal removal rate. Hence, surface roughness (Ra) is obtained at 0.04044µm, which is greater than 2kHz. Additionally, it can be noticed from the figure 5.14 (g,h) that curvature of microdimple is not uniform. According to experimental results, it has been found that by utilising MSPW, better profile accuracy, minimum surface roughness, and precision shape profile can be obtained, which are not observed for conventional RPW (Fig.5.11).

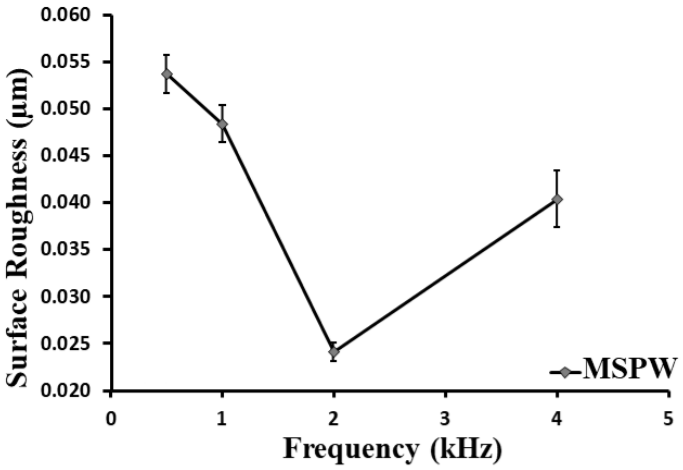

Fig. 5.13 Surface roughness of machined microdimple under MSPW at different frequencies

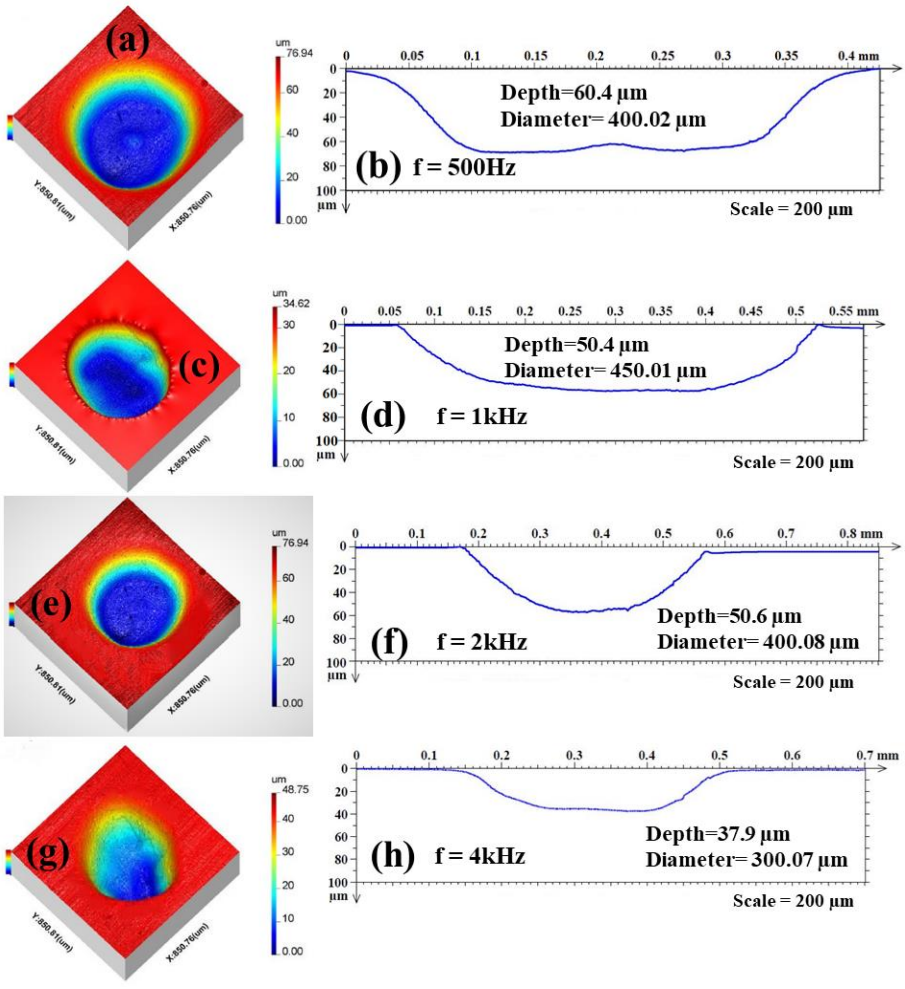

Fig. 5.14 Under MSPW, optical images of 3D, profile structure, and; 500Hz (a,b), 1kHz (c,d), 2kHz (e,f), 4kHz (g,h)

At the frequency of 2kHz, SEM micrographs of machined microdimple of RPW and MSPW are shown separately in Figure 5.15. From the machined image, Figure 5.15 (a),

under the application of RPW, it can be observed that the shape of the microdimple is irregular, the bottom surface finish is poor and irregular machining appears on the bottom surface. But, utilising MSPW, these effects are significantly improved, and it can also be noticed that the surface finish of microdimple also improved, as shown in Figure 5.15(b).

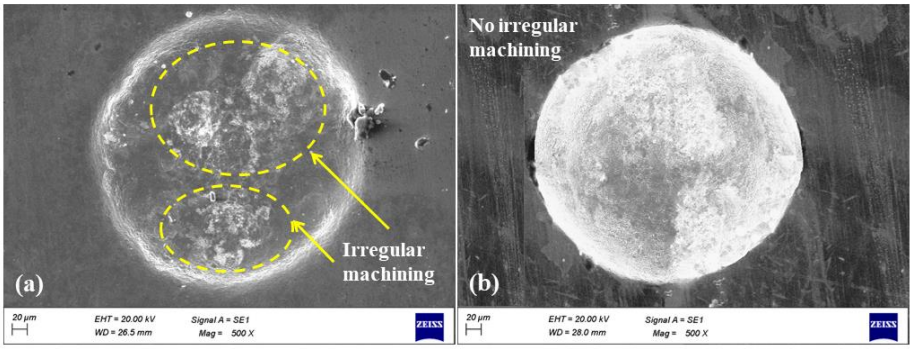

Fig. 5.15 SEM images of microdimple for (a) RPW and (b) MSPW at 2kHz, 10V

5.7.4 Comparison of rectangular pulse waveform and multi-step pulse waveform on diameter, depth, and etch factor of microdimple

The variation of etch factor, diameter, and depth of machined microdimples has been plotted in graphs. The etch factor has been compared between rectangular pulse waveform (RPW) and multi-step pulse waveform (MSPW), as shown in Figure 5.16. From the figure 5.16, it can be observed that etch factor of MSPW is better than RPW for all applied frequencies. For MSPW, it is found that at 1kHz, the depth of microdimple is lower, and at higher frequencies i.e., 2kHz, and 4kHz, it is larger than RPW, as shown in Figure 5.17. It can also be noticed that at 2kHz, the depth difference between RPW and MSPW is maximum. Hence, it is understood that at 2kHz, the ion transportation rate is higher due to the faster detachment rate of smaller bubbles. As a result, ion transportation improves, shielding effects are minimised, and more sludge can come out due to better flow of electrolyte rotation. Thus, the anodic dissolution rate improves more than conventional RPW. It is also found that the diameter of microdimple decreases for all applied frequencies, as shown in Figure 5.17. At the applied frequency of 2kHz, the diameter of microdimple is greater than RPW because of better ion transportation and current flow rate. The reason behind the maximum diameter reduction at 500Hz is that stray current is significantly minimised by MSPW. At higher frequencies, i.e., 4kHz, the diameter of machined microdimples is almost the same due to lower pulse duration time as well as the metal removal rate.

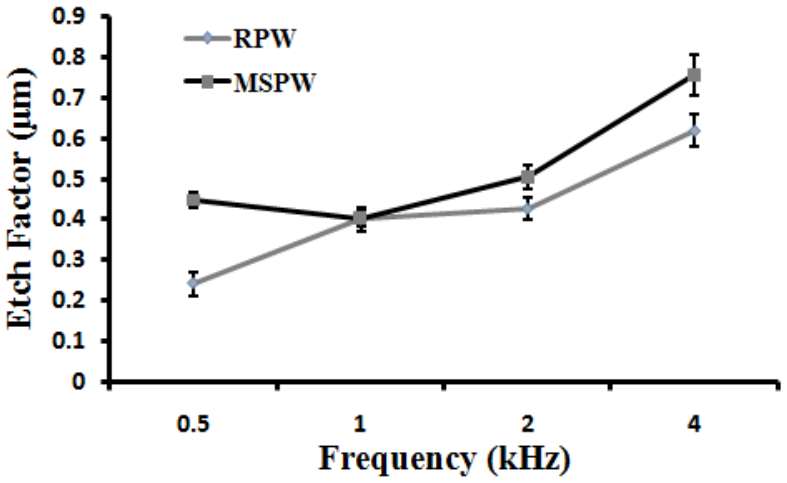

Fig. 5.16 Etch factor of microdimple for RPW and MSPW at different frequencies, 10V

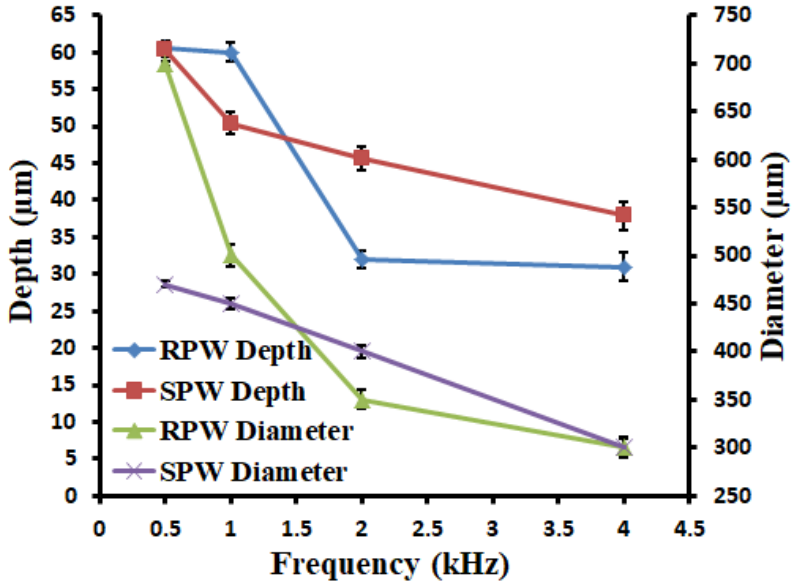

Fig. 5.17 Effect of RPW and MSPW on depth and diameter of microdimple for different frequencies at 10V

In order to identify the better utility of MSPW, microholes have been fabricated at the best parametric combination, such as applied voltage of 10V, frequency of 2kHz, 50% duty cycle, and 0.5µm/s of tool feed rate, which is find out from experimental results initially. Figures 5.18 and 5.19 are SEM micrograph of machined microholes exhibit the condition of microholes which are fabricated under RPW and MSPW when the applied frequency is 2kHz and voltage is 10V. For RPW (Fig. 5.18), it has been observed that the machined microhole have irregularities in their shapes; edges and inside walls are not uniform, the surface quality of inside walls are poor, and more pitting effects appear. The reason behind the generation of these effects is that under the application of RPW, the larger size of bubbles evolution and their lower detachment rate, which increases the stray

current and shielding effects. As a result, the current flow is obstructed and generates heat, resulting in larger size bubbles breaking inside the IEG. In consequence, unwanted microsparks occurred, which removed the extra metal from the machining area. In pulse on time of MSPW, three different peak voltages with shorter duration times are incorporated to drop the voltage from maximum peak to minimum peak. Due to it, potential fluctuation occurs, which interrupts the continuous bubble formations and increases the bubble's detachment rate. As a consequence, the small size of bubbles can come out quickly from the machining zone, which creates a force for the renewal of electrolytes in the IEG. As a result, ion transportation improves, shielding effects are minimised, and more sludge can come out due to better flow of electrolyte rotation. Thus, precise microholes can be machined, as shown in Figure 5.19, accompanied by a better surface quality and less overcut. Overcut has been obtained as 85.71µm and19.88µm for RPW and MSPW, respectively. Thus, by utilising MSPW, 76.8 % of overcut can be reduced. From the SEM images, it can be observed that the edge of the machined microhole is uniform, shape regularity enhances, the surface quality of inside walls improves, and pitting effects are minimised, as exhibits in Figure 5.19.

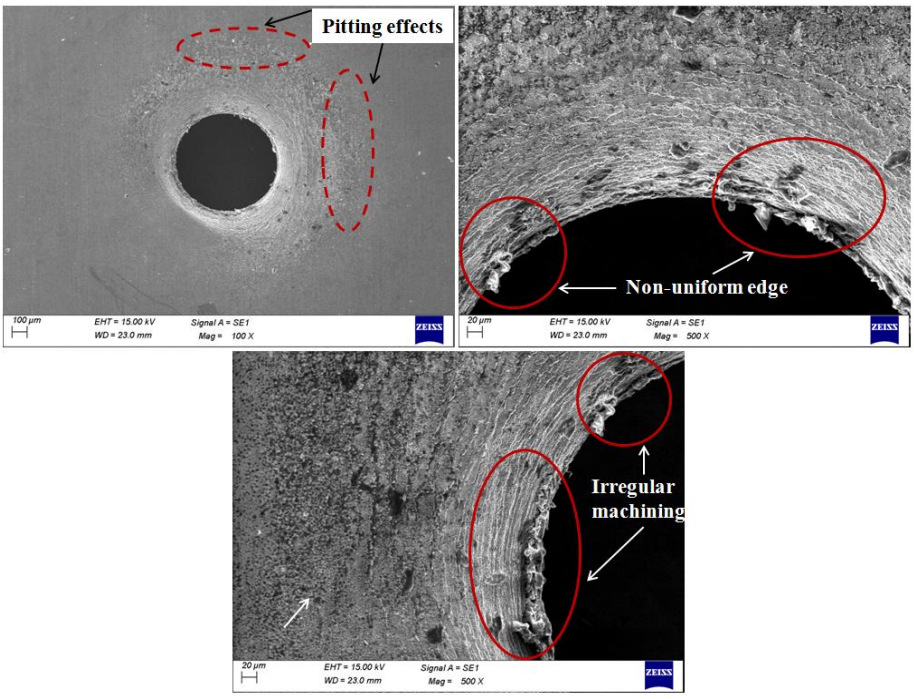

Figure 5.18 SEM images of a machined microhole under RPW at 2kHz frequency, 10V

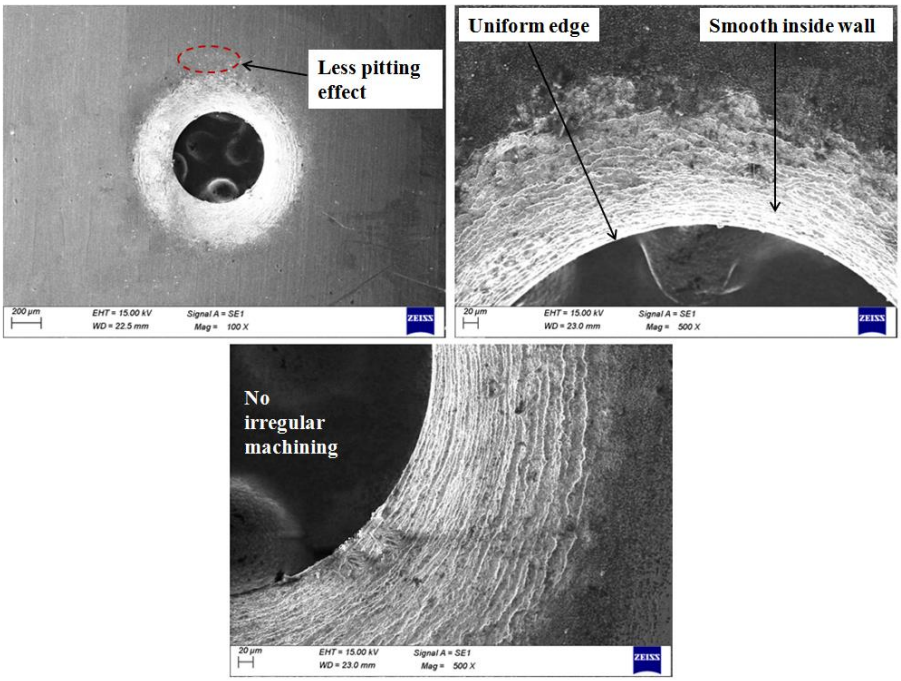

Figure 5.19 SEM images of a machined microhole under MSPW at 2kHz frequency, 10V

5.8. Outcomes of experimental investigation

After a detailed comparison study with conventional rectangular pulse waveform (RPW), it can be concluded that in electrochemical micromachining, the multi-step pulse waveform (MSPW) significantly enhances surface finish, accuracy, and precision structuring. Multi-step pulse waveform (MSPW) also plays a significant role in power transmission because three different peak voltages have been intentionally incorporated during the pulse on time. By theoretical estimating the power transmission for different voltages, it is found that the power transmission of MSPW is lower as compared to conventional RPW. According to the simulation results of MSPW, it can be concluded that due to the formation of smaller size bubbles, the current density is lower and electrolyte potential is greater than RPW. The same trend in current density has been noticed from experimental results. It has also been noticed that in RPW, initially, current density reaches the maximum and remains constant during machining time, but in MSPW, current density oscillates. In between four levels of frequency (500Hz to 4kHz), more oscillation of current density has been obtained at 2kHz. Hence, it can be concluded that at 2kHz, smaller sizes of bubbles are generated with a higher detachment rate. By capturing images of bubble formation, it has also been observed that in MSPW, the sizes of bubbles are very small as compared to RPW.

At the frequency of 500Hz, it has been identified from 3D optical images of machined microdimples that, as compared to RPW, the accuracy of profile structure is enhanced, no

microsparks affected zones appeared, and surface roughness is also reduced significantly, i.e., Ra, 0.05369µm for MSPW and Ra, 1.016µm for RPW. By increasing frequency, the surface finish is further improved as compared to RPW. At 2KHz, more accurate profile structures and minimum surface roughness (Ra) of 0.02413µm have been obtained, whereas Ra is 0.2511µm for RPW. Due to the shorter pulse duration time at higher frequencies, more bubbles evolve, which increases the shielding effects. Hence, at 4kHz, surface roughness (Ra) has been obtained as 0.04044µm, which is greater than 2kHz. It can be noticed that etch factors of MSPW are better than RPW. Hence, it can be concluded that the higher etch factor represents better localization of dissolution. It has also been observed that, as compared to RPW, the diameter of microdimples can be reduced significantly. Due to the faster detachment rate of smaller bubbles, shielding effects can be minimised, resulting in an increment in the depth of microdimples as compared to RPW. From the SEM micrographs, it is found that the edges of machined microholes are uniform and smooth, micro spark affected areas and pitting effects are negligible, but in RPW, these effects are prominent.

The results of this investigation suggest that by utilizing the multi-step pulse waveform, the detachment rate of bubbles from the tool surface, can be improved and reduced the bubble's size as compared to conventional rectangular pulse waveform. As a consequence, the released bubbles attempt to flow upward and circulate into the inter-electrode gap, which is helpful for the renewal of electrolytes in the narrow machining zone and for better sludge removal. Hence, utilizing this technique, the accuracy of EMM, machined surface finish, and shape control can be improved significantly. However, it can be observed from the sectional profile of microdimple that overcut as well as minute tapers are still generated along the sidewalls. Hence, further investigation is needed to study other important factors such as the variation of pulse on time and pulse amplitude of the step pulse waveform, as well as the tool feed rate during EMM. These factors may further reduce the overcut and tapering effect and enhance overall machining performance.

Chapter 6: Investigation of EMM performance by employing pulse width modulation (PWM) and pulse amplitude modulation (PAM)

6.1 Introduction

In EMM, surface finish, and accuracy depends on electrolyte stoichiometry such as mass transport, current distribution, the behaviour of oxide film, bubbles so on. When metal dissolution starts, this electrolyte stoichiometry changes the conductivity of the electrolyte and hampers further current flow. To overcome these problems effectively, a novel pulse width modulation (PWM) technique is proposed. This PWM is applied on step pulse waveform (SPW) which is designed by a function generator. To verify the feasibility of PWM technique, machining accuracy is investigated for different applied voltages, duty cycles, frequencies, and tool feed rates. The machining accuracy is investigated in terms of overcut of microgroove width, maximum depth, taper angle, and surface finish. The machined surface finish is also investigated under best parametric combination utilising different electrolyte concentrations. From these investigations, best parametric combination is identified and furthermore compared with non-PWM method to justify the utility of new PWM technique. As two different peak voltages are incorporated into the pulse on time of SPW, the supply voltage varies from the maximum peak to half of the maximum peak. As a result, the average voltage for each pulse on time reduces significantly. Thus, utilizing SPW, potential transmission into the electrolyte can be controlled. Additionally, when PWM is used, the total pulse period or pulse cycle time remains constant. In this technique, the pulse width of each pulse on time varies from short to long and then returns to the original position. Due to it, when pulse-on time increases from short to long, then pulse-off time decreases, and the opposite effect occurs when pulse-on time decreases. As a result, sludge from the machining area can be removed properly and anodic dissolution can be controlled. As a consequence, machining accuracy and surface quality in terms of performance of EMM can be improved.

In EMM, appropriate voltage choice is crucial for the improvement of material dissolution localization and the control of stray current. A higher voltage increases overcut, taper angle, and surface roughness. Lower voltage minimizes overcut, but due to the lesser amount of material removal, irregular machining and non-uniformity can be observed in EMM. To address these drawbacks, a new pulse amplitude modulation (PAM) of step pulse waveform is designed indigenously with the help of function generator. Herein, each pulse's amplitude during on-time varies from peak to half-peak,

and during off-time, it regulates from zero to half-peak. It is a cost-effective method, because function generator is employed as a power source instead of expensive ultra-high-frequency DC pulse power supply. The effects of applied voltages are investigated by fabricating microdimples and microgrooves. To verify the feasibility of the PAM technique, machining performance in terms of overcut, taper angle and surface roughness is also investigated for different tool feed rates and frequencies. Finally, the PAM technique is compared with a non-PAM method to justify the acceptability of this novel technique.

6.2 Experimental planning 1: Pulse width modulation (PWM)

6.2.1 Working principle of pulse width modulation of step pulse waveform for stagnant electrolyte

In EMM, generally, by changing duty cycle and frequency of the pulse waveform, pulse width can be varied for stable machining. The higher pulse width or pulse on time leads to a larger amount of material dissolution. As a consequence, extra dissolution from the target area increases and it may hamper the precision of micromachining. In addition, more sludge generates due to longer machining time, which also poses negative effects on machining accuracy. Alternatively, in short-pulse width, machining time reduces, resulting in the material removal rate decrease. Hence, by using longer pulse width, the depth of the machining product and uniform machining can be increased accompanied by greater overcut. But, in short-pulse width, it can be noticed that overcut decrease. Hence, an expensive ultra-short pulse power supply is preferable for EMM, as observed in past literature reports. To overcome these disadvantages, a new pulse width modulation (PWM) technique has been used in this research work. In this technique, the pulse width of each pulse on time varies from short to longer duration and comes back to the original position. This movement of pulse width occurs automatically during micromachining. The schematic diagram of PWM is illustrated in Figure 6.1. In this research, step pulse waveform (SPW) has been used in terms of the conventional rectangular pulse waveform. The SPW has significant advantages. Utilizing SPW, potential transmission into the electrolyte can be controlled. As two peak voltages, such as V_{max} and V_{half}, are incorporated into the pulse on time, the supply voltage varies from the maximum peak to half of the maximum peak, as shown in Figure 6.1. As a result, the average voltage for each pulse on time reduces significantly.

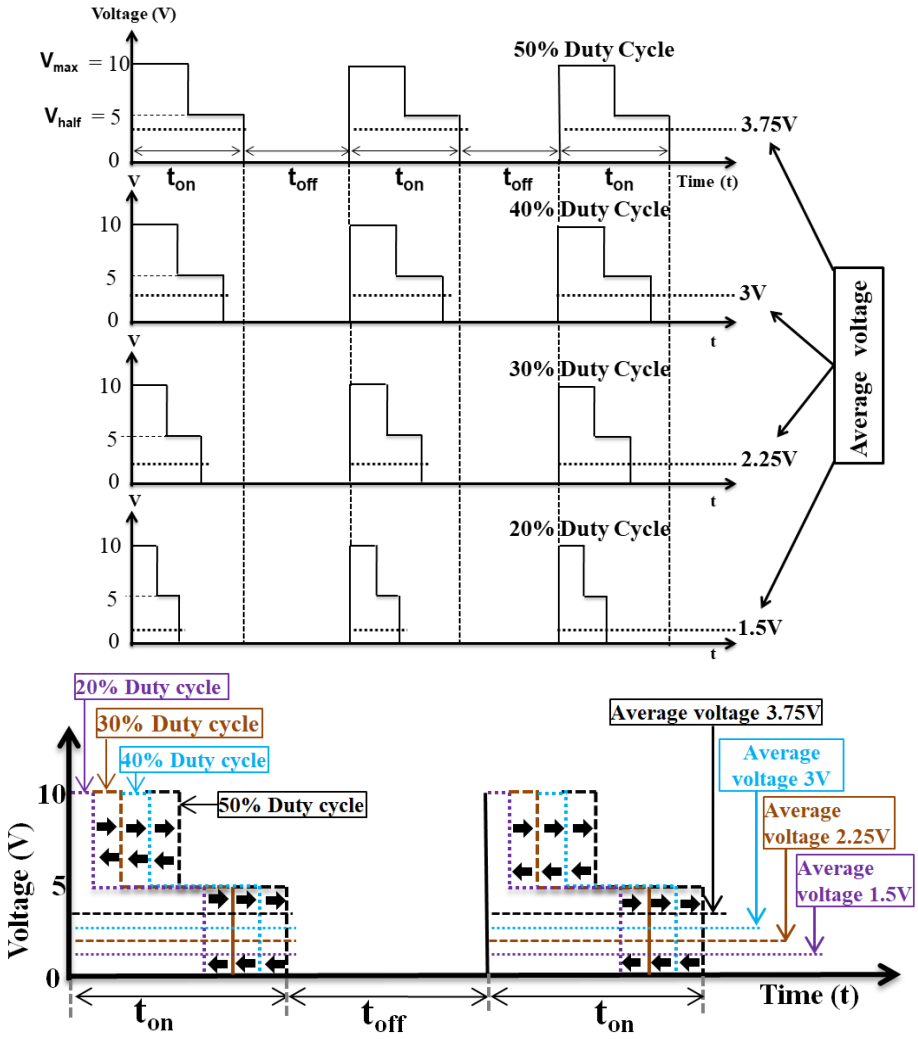

Fig. 6.1 Schematic diagram of Pulse Width Modulation

From the figure (50% duty cycle), it can be noticed that the average voltage is 3.75V when the peak voltages are 10V and 5V. Similarly, for 40%, 30% and 20% of duty cycle, the average voltages are 3V, 2.25V, and 1.5V, respectively as shown in Figure 6.1. But, in rectangular pulse waveform, this average voltage is 5V for the same peak voltage i.e., 10V. Due to incorporating two peak voltages in the pulse on time, a double-layer discharging effect occurs, which can control the anodic dissolution during each pulse on time. This discharging effect occurs when the peak voltage drops from the maximum to half of the maximum peak voltage. Therefore, anodic dissolution is controlled by SPW because during the first peak voltage anodic dissolution is higher than the duration time of the second peak. When PWM is applied to SPW, the total pulse cycle time remains constant. As a consequence, when pulse-on time increases, pulse-off time decreases and the reverse effect occurs during decreasing time of pulse-on time. As a result, sludge can remove properly from the machining area. Due to it, machining accuracy and surface

quality can be improved. The movement of pulse width is illustrated in Figure 6.1 by a schematic diagram, where considered the maximum duty cycle is 50% and the minimum is 20%. When the pulse width moves from 20% to 50% duty cycle, the average voltage increases from 1.5V to 3.75V and comes back to 1.5V. Similarly, for the movement of 30% to 50%, and 40% to 50%, the changes in average voltage are 2.25V to 3.75V and 3V to 3.75V, respectively.

6.2.2 Experimental planning

The stainless steel (SS304) sheets with a dimension of 10mm x 10mm x 0.2mm have been used as a workpiece. The copper (Cu) rod with a 200µm diameter has been employed as a microtool. The sidewall of the micro-tool has been coated with synthetic rubber adhesive to reduce the stray current effects. For all experiments, the initial inter-electrode gap has been selected as 20µm and only y axis movement has been considered for the fabrication of microgrooves. For a better understanding of the effect of PWM on microgroove depth at a constant narrow inter-electrode gap, downward tool movement, i.e., z-axis movement has not been applied. The stagnant electrolyte solution has been used for machining because electrolyte flushing can vibrate the tool and workpiece which may hamper the micromachining. The sulfuric acid solution has been used as an electrolyte because it dissolves the sludge during machining, which is most effective for the stagnant electrolyte. Herein, 0.1M, 0.2M, and 0.3M of H_2SO_4 have been utilised for the investigation of better surface roughness. For a better understanding the influence of major parameters on machining accuracy, the effect of applied voltage, duty cycle, frequency, and tool feed rate on groove width and depth have been investigated under PWM strategy. Standard deviation has been estimated for micro-groove width and depth to evaluate the accuracy of machined microgrooves. The estimation of the standard deviation is based on three distinct microgrooves that have been fabricated using identical parameter settings. In addition, the surface roughness (Ra) has been investigated at different concentrated electrolytes. The surface roughness and profile of micro-grooves have been observed and examined by Talysurf CCI Non-Contact Profilometer (Taylor Hobson). During micromachining, the image of larger gas bubble evolution has been captured by a digital camera, Dino-Lite (AM4815ZTL, Taiwan), whose maximum frame rate is 30fps. The conditions of machined microgrooves have also been observed by a digital microscope (Leica) for further analysis.

6.3. Results and Discussion

6.3.1 Effect of applied voltage on overcut, depth, and tapering effect

In EMM, appropriate voltage choice is crucial for the improvement of material dissolution localization and the control of stray current. Higher voltage improves the precise shape of machining, but it increases overcut, taper angle, and surface roughness. Lower voltage minimizes overcut, but it affects the shape of features due to less amount of material removal. As compared to others parameters such as duty cycle, frequency, horizontal tool feed rate, and electrolyte concentration, applied voltage plays a crucial role in the control of current density. Due to it, initially, the effect of applied voltage in EMM has been investigated under the application of pulse width modulation (PWM) of the step pulse waveform (SPW). The utility of the new PWM technique has been investigated under different applied voltage when other machining conditions, such as 2kHz of frequency, 0.5µm/s tool feed rate, and 0.1M of electrolyte concentration, remain unchanged, which are listed in Table 6.1. From the earlier investigation, it has been found that these are the best parametric combination for multi-step pulse waveform. In the PWM technique, the variation of duty cycle has been selected from 25% to 50%. Within this range of duty cycle, 30% to 50% regulation provides the best condition for EMM, as discussed later in the effect of duty cycle. Compared to other parameters such as duty cycle, frequency, tool feed rate, and electrolyte concentration, applied voltage plays a crucial role in controlling current density. Therefore, the effect of applied voltage in EMM has been initially investigated under the application of pulse width modulation of the step pulse waveform.

Table 6.1: Influence of applied voltage on microgroove formation under the specific machining conditions

Voltage (V)	Duty cycle (%)	Frequency (kHz)	Tool feed (µm/s)	Electrolyte concentration (mol/l)
8 9 10 11 12	30-50	2	0.5	0.1

For the investigation of machining accuracy, voltage changes from 8V to 12V. Experimentally, it is verified that under the machining conditions which are mentioned in table 6.1, below 8V, the machining process is not stable. According to the microgrooves machined, it observes that groove's width overcut, and depth increase by increasing

applied voltage, as shown in Figure 6.2 (a). At the specified applied voltages ranging from 8V to 12V, it can be observed that the minimum taper angle of the side wall is 22.61^0 at voltage of 10V, while the maximum taper angle is 50.19^0 at voltage of 12V, as shown in Figure 6.2 (b,c). From the sectional profile of the microgroove, it can be observed that at 12V, the open face of microgroove is larger and the bottom surface is not uniform, figure 6.2 (b). However, these negative effects can be mitigated by reducing the applied voltage to 10V, Figure 6.2 (c). Therefore, it can be comprehended that when voltage of 10V is applied, moderate quantity of material is removed from the target area. At applied voltages below 10 volts, it can be noticed that the microgroove's width overcut reduces, but the taper angle increases due to non-uniform material removal. In addition, it is noticed that after 10V, the standard deviation increases more, which can be understood from the length of the error bar.

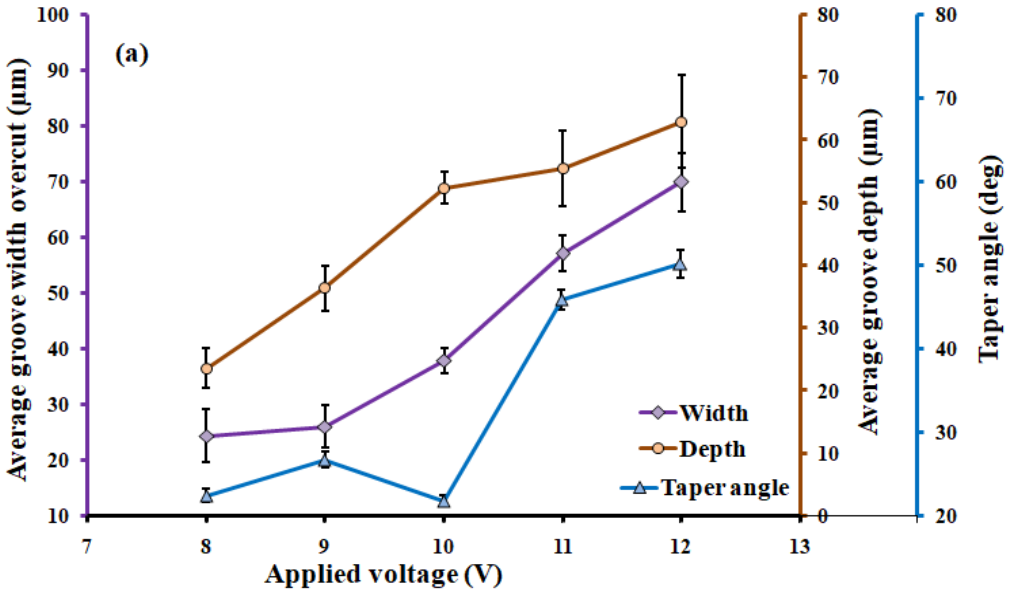

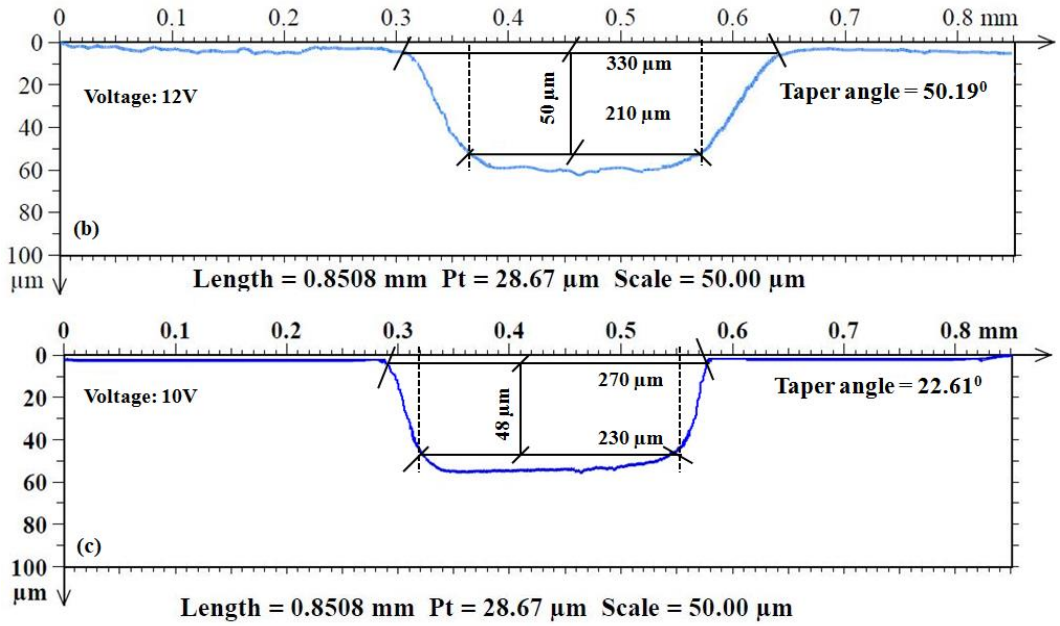

Fig.6.2 Effect of applied voltage on microgroove for average width overcut, depth, taper angle (a) and sectional profile of microgroove (b-c)

At higher voltage, a larger amount of material removes from the target area and deteriorates localization effects, resulting in increment of overcut. Due to it, at higher voltage, the standard deviation increases. But, when the voltage is between 8V to 10V, the localization effect of anodic dissolution improves more and the standard deviation reduces. According to the results as obtained, 10V is most suitable for the fabrication of precise microgrooves.

6.3.2 Effect of duty cycle on overcut, depth, and tapering effect

The duty cycle is used to represent the pulse-on and off time of pulse waveform. The electrochemical dissolution of the anode as workpiece occurs during pulse on-time. The pulse off-time performs two tasks at once; first, because no machining is done during this time, reaction products are not produced; second, it helps in the removal of the dissolution products by flushing the electrolyte. Thus, duty cycle plays a significant role in the control of anodic dissolution during micromachining. Hence, the effect of duty cycle of step pulse waveform on machining accuracy is investigated during machining of microgroove. In PWM technique, the pulse width of SPW is modulated at different duty cycles, where the total pulse period remains unchanged. The machining conditions for investigating the effect of the duty cycle on machining accuracy are listed in Table 6.2. From earlier investigations, it has been noted that 10V is appropriate for improving machining accuracy. Thus, in the investigation of the effect of duty cycle, the applied

voltage is fixed at 10V, while other machining conditions remain the same: 2kHz frequency, 0.5µm/s tool feed rate, and 0.1M electrolyte concentration.

Table 6.2: Influence of duty cycle on microgroove formation under the specific machining conditions

Voltage (V)	Duty cycle (%)	Frequency (kHz)	Tool feed (µm/s)	Electrolyte concentration (mol/l)
10	25-50 30-50 35-50 40-50 45-50	2	0.5	0.1

In these experiments, the duty cycle is increased from 25% to 50% with an increment of 5%, when other machining conditions are unchanged. In Figure 6.3, experimental results are illustrated, where the movement of the duty cycle is represented as a starting point such as 25%, 30%, 35%, 40%, and 45%. In this automatic PWM technique, when the pulse width or pulse-on time of SPW moves from 45% to 50%, it leads to a greater amount of material dissolution because more time is allocated for machining. In addition, the sludge removal decreases, which impacts negative effects on machining accuracy. As a result, there is an increase in the microgroove width overcut, and depth, as well as their respective standard deviations. Additionally, the taper angle exhibits an increment, i.e., 47.72^0, which is shown in Figure 6.3. From the sectional profile of microgroove, Fig.6.3(b), it can also be noticed that open face of microgroove is larger, side wall has larger taper, and bottom surface is not uniform.

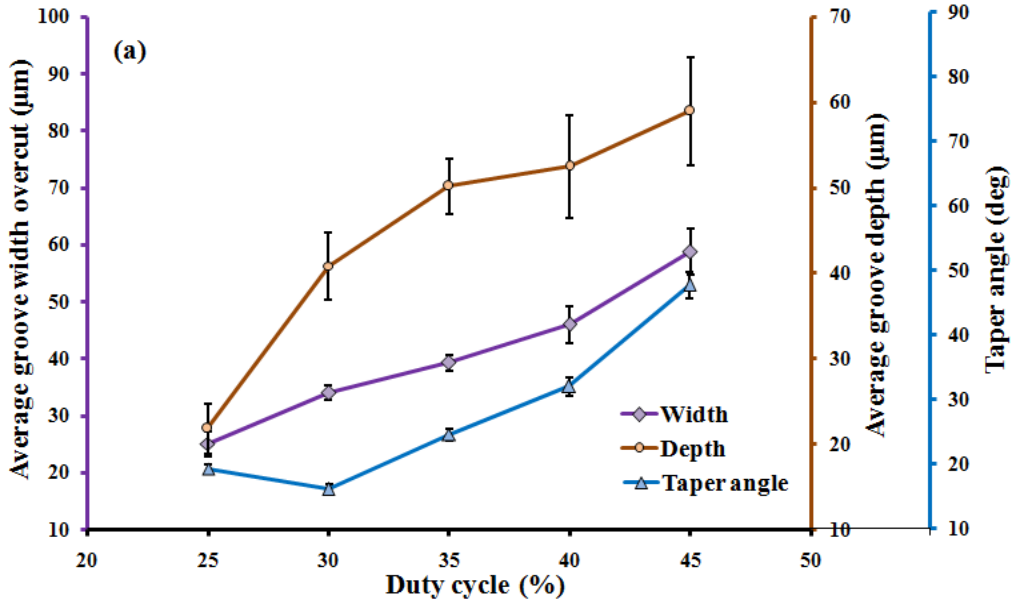

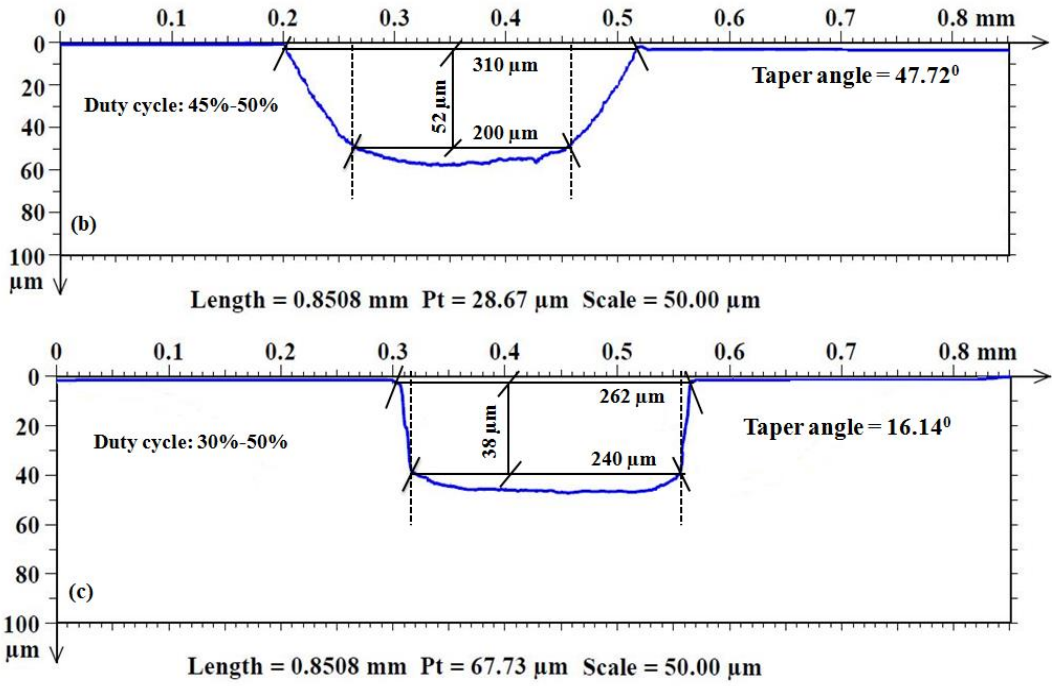

Fig.6.3 Effect of duty cycle on microgroove for average width overcut, depth, taper angle (a) and sectional profile of microgroove (b-c)

However, when operating within the duty cycle range of 30% to 50%, optimal results are achieved with respect to minimum taper angle of 16.14^0 and lower standard deviation of 1.24 µm, as shown in Figure 6.3(a). This is due to appropriate material dissolution; enhance sludge removal, and efficient renewal of the electrolyte within the machining zone. From the sectional profile of microgroove, figure 6.3(c), it can be observed that open face of microgroove reduces, side wall is almost perpendicular, and bottom surface is almost uniform. Therefore, the effective reduction of standard deviation may be observed with an increase in the number of experiment under this specific combination of parameters. Hence, from the obtained results, it is recommended that PWM range of duty cycle i.e., 30% to 50% can be utilised to achieve improved machining accuracy.

6.3.3 Effect of frequency on overcut, maximum depth, and tapering effect

The frequency of SPW is leading a promising role in machining accuracy. When pulse frequency rises, the number of pulse periods in unit time increases. Consequently, pulse duration time, i.e., pulse on time and off time, decreases and enhances the repetition of anodic dissolution in unit time. Due to it, the material removal rate decreases which controls the extra dissolution from the target area. In addition, the standard deviation minimises significantly. In order to verify the machining accuracy under the application of PWM, the frequency of SPW increases from 0.5kHz to 8kHz by an increment of twice.

In this experiment, the machining conditions are listed in Table 6.3. From earlier investigations, it has been noted that applied voltage of 10V and regulated duty cycle of 30% to 50% are appropriate for improving machining accuracy. Thus, in the investigation of the effect of pulse frequency, the applied voltage and duty cycle are fixed at 10V and 30% to 50%, respectively, while other machining conditions remain the same: 0.5µm/s tool feed rate, and 0.1M electrolyte concentration.

Table 6.3: Influence of frequency on microgroove formation under specific machining conditions

Voltage (V)	Duty cycle (%)	Frequency (kHz)	Tool feed (µm/s)	Electrolyte concentration (mol/l)
10	30-50	0.5 1 2 4 8	0.5	0.1

From the experimental results, it can be noticed that when pulse frequency rises, microgroove width overcut, depth decrease simultaneously, as shown in Figure 6.4. At the frequency 8kHz, the depth and width overcut of microgroove are minimum as compared to lower frequency. At higher frequencies, the reduction of pulse duration and the increment of alternative anodic reactions are the reasons for the improper sludge removal from the machining area. Due to it, negative effects develop and reflected on standard deviation in terms of machining accuracy and increases taper of side wall. At a lower frequency of 0.5kHz, the duration of the pulse increases, this promotes the removal of larger amount of material from the target area. From the sectional profile of microgroove, figure 6.4 (b), it can be observed that open face of microgroove is more larger than bottom face, side wall has larger taper. Figure 6.4 shows an increase in the overcut of microgroove width and taper angle. However, at frequency of 2kHz, precise microgroove with a smaller taper angle, i.e., 26.56^0, and minimal standard deviation can be achieved. Additionally, from the sectional profile of microgroove, it can be noticed that open face of microgroove reduces, minimises the tapering effect of side wall, bottom surface is uniform but slightly down at the middle position, as shown in Figure 6.4(c). Pulse duration of 2kHz has been found to be optimal for allowing effective material dissolution and enhancing the removal of sludge. Therefore, it can be understood that frequency of 2kHz may be the best for employing the PWM technique in EMM.

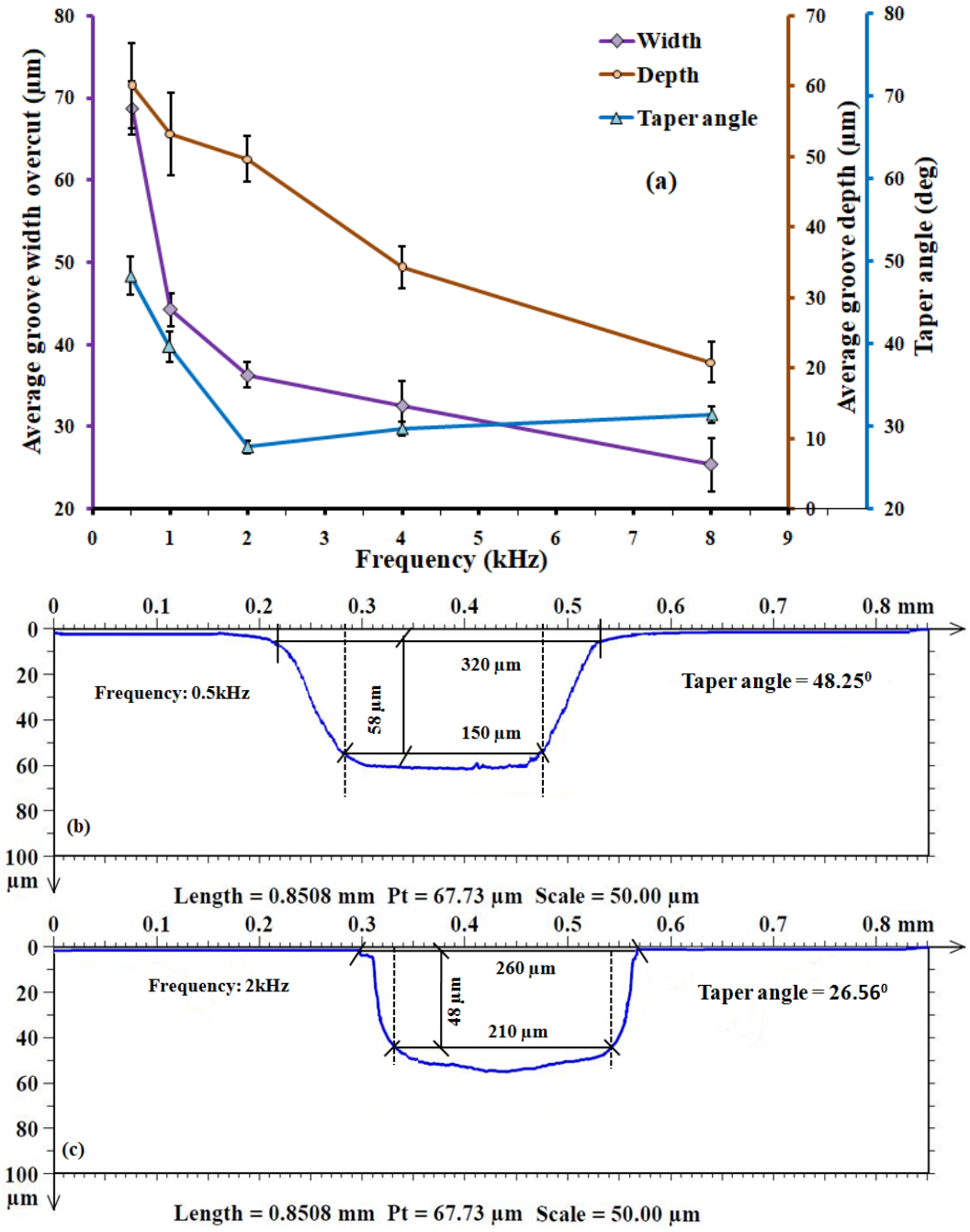

Fig.6.4 Effect of frequency on microgroove for average width overcut, depth, taper angle (a) and sectional profile of microgroove (b-c)

6.3.4 Effect of lateral tool feed rate on overcut, depth, and tapering effect

The lateral tool feed is an important parameter for precise micromachining of microgroove. A slower tool feed indicates that more time is used to remove material at a specific area. As a consequence, a larger amount of material dissolves from the target area, which increases the groove overcut. Therefore, the effect of different lateral tool feeds is investigated for the accuracy of microgroove under the application of PWM.

From earlier investigations, it has been noted that applied voltage of 10V, regulated duty cycle of 30% to 50%, and pulse frequency of 2kHz are appropriate for improving machining accuracy. Thus, in the investigation of the effect of lateral tool feed rate, these machining conditions and 0.1M electrolyte concentration are remain fixed, as listed in Table 6.4.

Table 6.4: Influence of tool feed on microgroove formation under the specific machining conditions

Voltage (V)	Duty cycle (%)	Frequency (kHz)	Tool feed (µm/s)	Electrolyte concentration (mol/l)
10	30-50	2	0.1 0.2 0.3 0.4 0.5	0.1

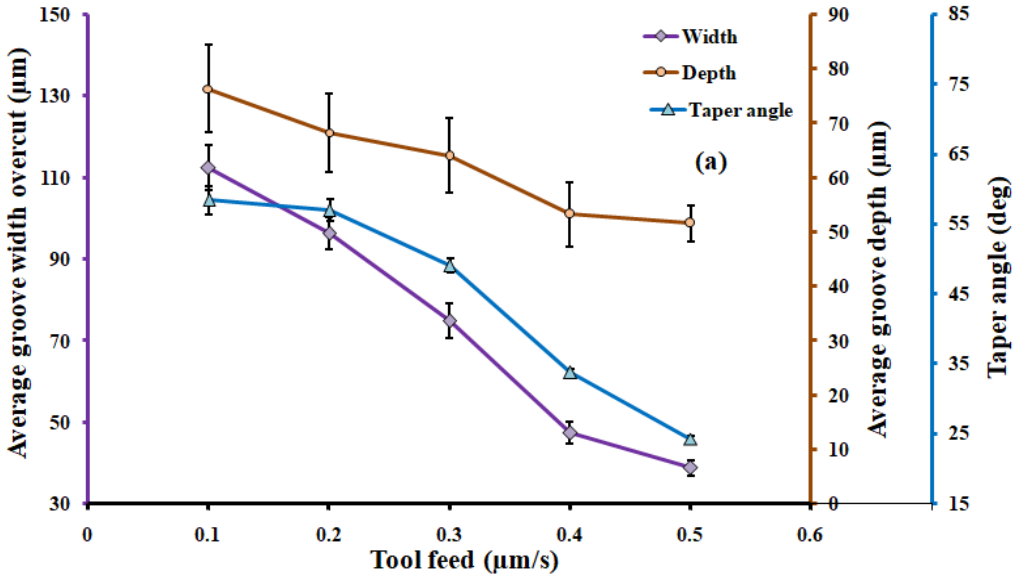

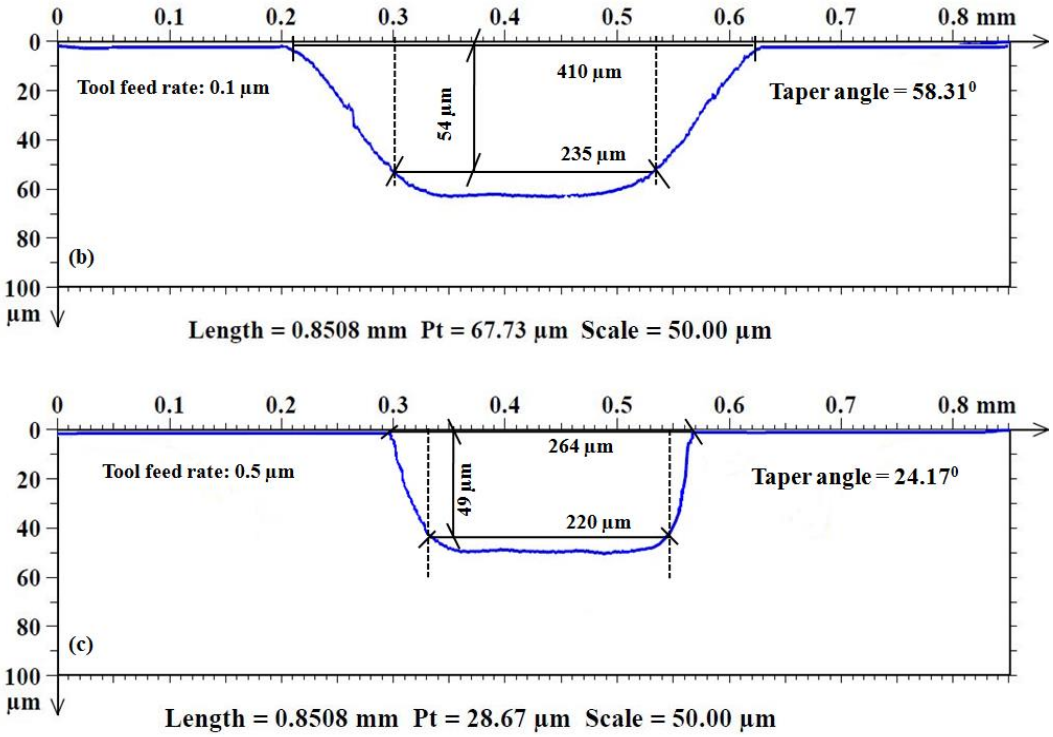

Fig.6.5 Effect of tool feed on microgroove for average width overcut, depth, taper angle (a) and sectional profile of microgroove (b-c)

From the experimental results, it can be noticed that microgroove width overcut, depth, and their standard deviations decrease by increasing the tool feed rate, as presented in Figure 6.5. At slower tool feed rate 0.1µm/s, higher groove width overcut, depth and their standard deviations are observed due to longer machining time per unit area. In addition, it can be noticed that taper angle also rises at 58.31^0 due to greater overcut of microgroove width. However, the width overcut, depth and their standard deviations are minimised at tool feed rate of 0.5µm/s. Due to the fast scanning speed of microtool, machining time reduces, resulting in control of unwanted material dissolution. Due to this phenomenon, the taper angle of the microgroove also reduces, as shown in Figure 6.5. From the sectional profile of the microgroove, figure 6.5 (b), it can be observed that at 0.1µm/s, the open face of microgroove is larger, side wall has larger taper and the bottom surface is not so uniform. However, these negative effects can be mitigated by reducing the lateral tool feed rate to 0.5µm/s, as shown in Figure 6.5 (c). Thus, it can be observed that for the fabrication of precise microgrooves, a tool feed rate of 0.5µm/s is preferable.

6.3.5 Effect of electrolyte concentration on surface roughness

Finally, the effect of 0.1M, 0.2M, and 0.3M concentrated electrolytes on the surface roughness of microgroove is investigated under best parametric combination. Higher electrolyte concentration means more charge-carrying ions are available in the solution. Due to it, a larger current density develops during machining. Alternatively, based on the double layer theory of EMM, it can be identified that higher electrolyte concentration has lower electrolyte resistivity. As a consequence, the charging time of double-layer or non-faradic time is minimised. This means more material dissolution occurs at higher electrolyte concentrations. Therefore, electrolyte concentration plays a leading role in the improvement of surface finish in EMM. In these experiments, 0.1M, 0.2M, and 0.3M H_2SO_4 electrolyte solution are used for the investigation of surface finish, when applied voltage 10V, duty cycle 30%-50%, frequency 2kHz, and tool feed rate 0.5µm/s are selected, as obtained best setting from previous experiment. The advantage of the PWM technique is that pulse duration changes automatically from a lower duty cycle to a higher duty cycle, when the pulse period is unchanged. Due to it, the localization effect of material dissolution, sludge removal rate, and current density improves significantly. As a result, narrow groove width can be achieved accompanied by greater depth, precise profile and better surface finish. The machining results with microscopic plots of machined microgrooves are presented in Figure 6.6. Due to lower conductivity i.e., 0.1M H_2SO_4, the current density minimises. As a result, unwanted material dissolution reduces but irregular machining increases. Thus, when electrolyte concentration of 0.1M is used, the narrow groove width i.e., 262.215µm is obtained as presented in Figure 6.6 (a). The taper angle is obtained as 45.52^0 due to non-uniform material removal as shown in sectional profile of microgroove, Figure 6.6 (a1). Additionally, from the sectional profile, it can be observed that side wall is tapering type and bottom face of groove is narrow. But, it can be noticed that the bottom surface finish is not good as shown in Figure 6.6(b). From the surface roughness profile, Figure 6.6 (b1), it can be observed that the surface roughness (Ra) of the bottom surface is 0.0389µm. However, utilising 0.2M electrolyte solution, it can be found that the less surface roughness (Ra) of microgroove is obtained, which is smaller than 0.1M electrolyte concentration. In addition, the width of microgroove i.e., 275.95µm is obtained by utilising 0.2M of electrolyte concentration which is quite more than 0.1M electrolyte concentration, as presented in Figure 6.6(c). The sectional profile of the microgroove indicates a significant reduction in the tapering

effect on the side wall, while the bottom surface remains uniformly smooth, as illustrated in Figure 6.6 (c1). Due to the increment of electrolyte concentration, conductivity increases, which helps to remove a moderate amount of material from the target area. As a result, irregular machining and protuberances minimise significantly, as shown in Figure 6.6 (d,d1). Due to it, more accurate profile, Figure 6.6 (c1) of microgroove is obtained for 0.2M. This phenomenon contributes to achieving a lower taper angle of 14.03^0 and less surface roughness (Ra) of 0.0244µm. At higher electrolyte concentrations, more charge-carrying ions are available which leads to removing the larger amount of material from the target area. Hence, when the concentration of electrolyte increases to 0.3M, the width of microgroove i.e., 314.408µm also increases simultaneously and surface roughness (Ra) i.e., 0.1567µm rises dramatically, as illustrated in Figure 6.6(e,f). Due to larger amount of material removal and increasing overcut, taper angle also enhances as illustrated in sectional profile of microgroove, Figure 6.6(e1). Additionally, it can be noticed that the tapering effect of the side wall increases further, while the width of the bottom surface reduces, resulting in the sectional profile of the microgroove resembling a parabolic type. The aforementioned experimental results suggest that a concentration of 0.2M of H_2SO_4 is suitable for the fabrication of precise microgrooves under the application of PWM technique.

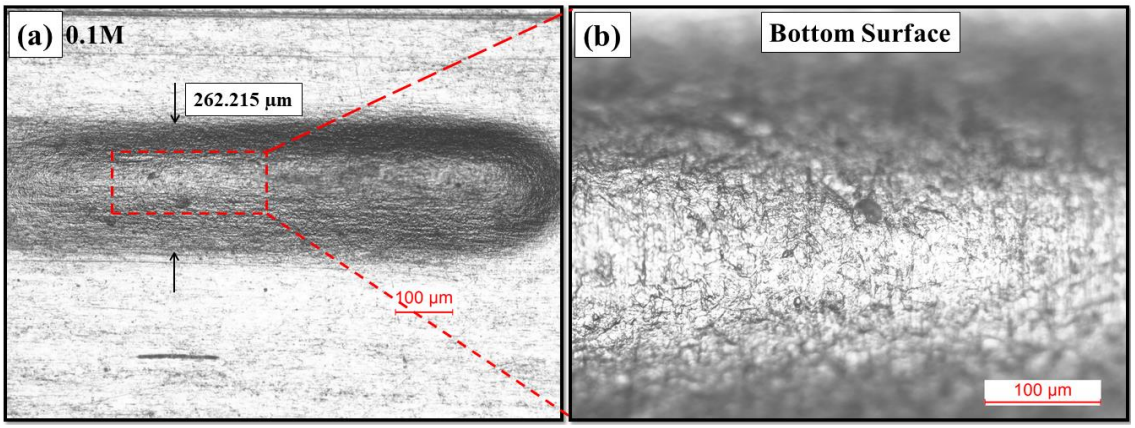

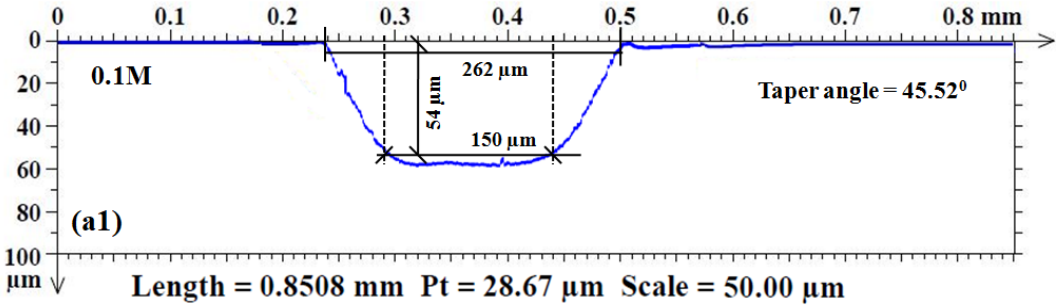
0.1M
262 µm
54 µm
150 µm
Taper angle = 45.52⁰
(a1)
Length = 0.8508 mm Pt = 28.67 µm Scale = 50.00 µm

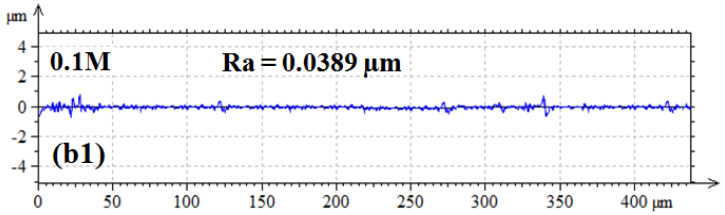
0.1M
Ra = 0.0389 µm
(b1)

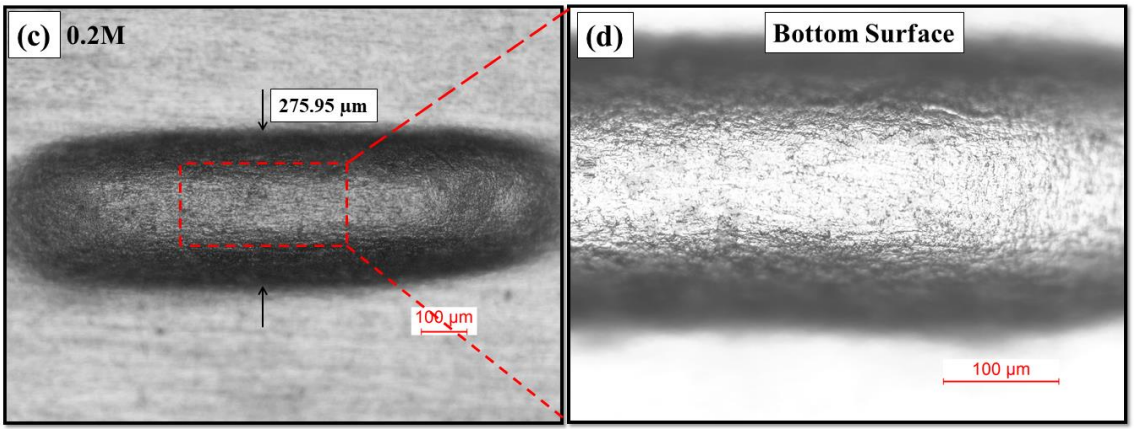
(c) 0.2M
275.95 µm
100 µm
(d)
Bottom Surface
100 µm

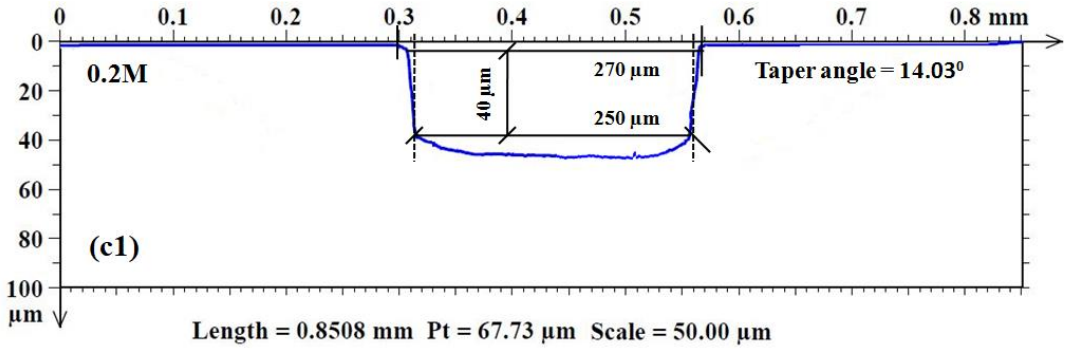
0.2M
270 µm
40 µm
250 µm
Taper angle = 14.03⁰
(c1)
Length = 0.8508 mm Pt = 67.73 µm Scale = 50.00 µm

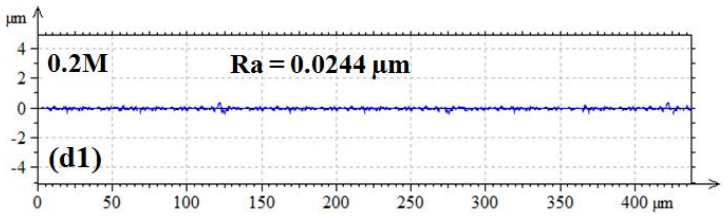
0.2M
Ra = 0.0244 µm
(d1)

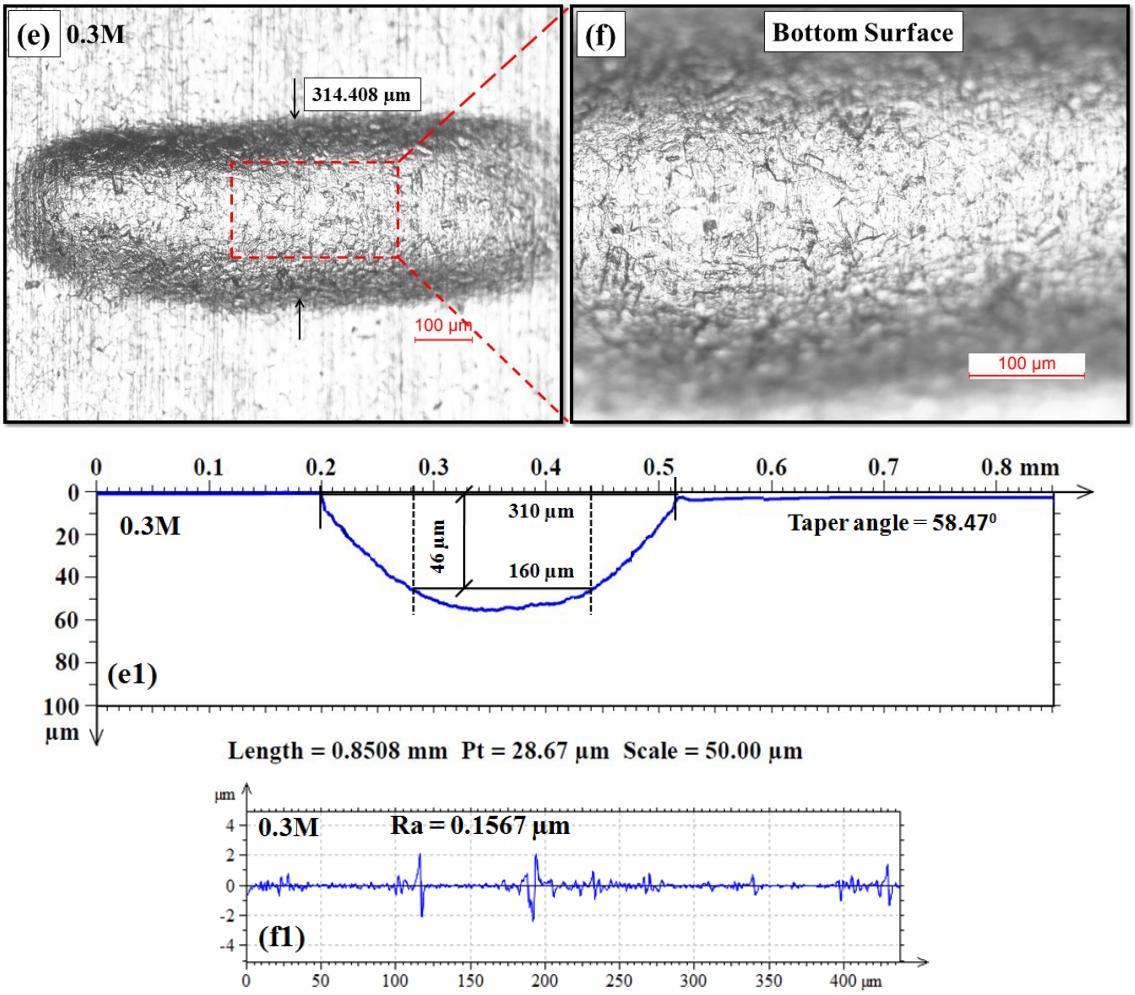

Fig.6.6 Effect of electrolyte concentration on the surface roughness (Ra), taper of side wall of micro-groove for 0.1M (a,b,a1,b1), 0.2M (c,d,c1,d1), 0.3M (e,f,e1,f1)

6.3.6 Comparison between PWM and without PWM

To develop the new pulse width modulation (PWM) of step pulse waveform with best parametric combinations, the effects of different parameters have been investigated initially. Furthermore, for better understanding, the PWM technique is compared with a non-PWM method. When SPW is used without the PWM technique for the fabrication of microgroove, under the machining conditions as selected such as applied voltage 10V, duty cycle 50%, frequency 2kHz, and electrolyte concentration 0.2M. Herein, it is also observed that without PWM condition, sludge cannot flush out properly and gas film appears which is broken inside of machining zone as shown in Figure 6.7(a-b), exhibiting photography of machining zone under without PWM. As a result, microsparks are generated which increases unwanted material removal. However, under the best parametric combination, it can clearly be observed that with PWM technique, sludge

flushes out quickly from the machining zone with the faster movement of bubbles as illustrated in Figure 6.8 (a-b), exhibiting photography of machining zone under with PWM. In addition, it can be noticed that gas film and its broken stage do not appear in machining zone, but gas bubbles come out quickly from the machining zone. As a result, unwanted material removal, and irregular machining are minimised significantly.

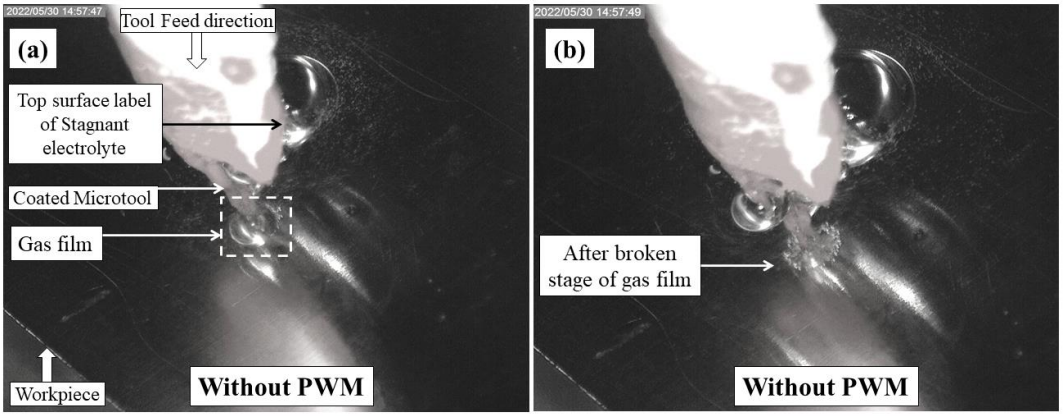

Fig. 6.7 Recorded images for without PWM technique (a) gas film formation time and (b) after gas film broken time

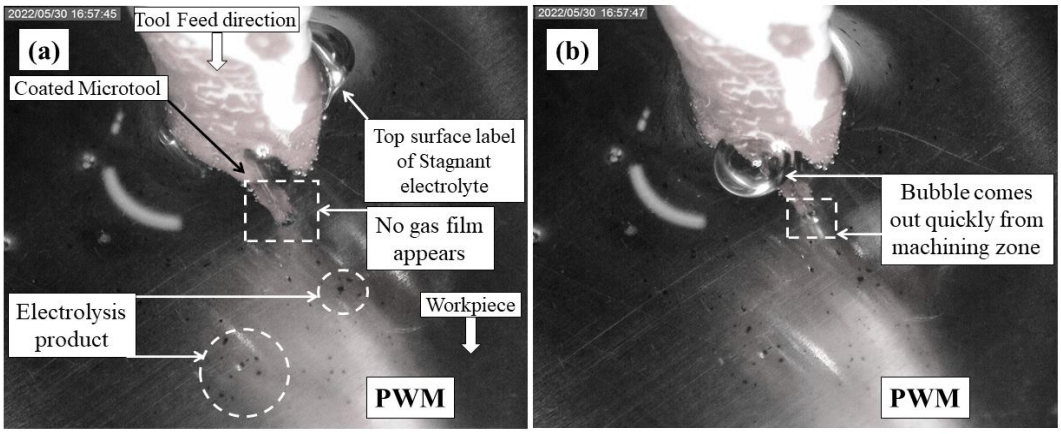

Fig. 6.8 Recorded images for PWM technique (a) no gas film formation time and (b) bubbles emission time

In without PWM condition, it can also be noticed that the microgroove width and depth are wider i.e., 412.227µm and 55.63µm which is presented in Figure 6.9(a). It indicates that more overcut i.e., 106.11µm appears on the microgroove which is occurred due to larger amount of material dissolution. The reason behind this phenomenon is that the duration time of each pulse on time is longer, which means more time is used for material removal. Due to it, more sludge is generated in the machined area which poses negative effects on surface finish. Figure 6.9(b) illustrates that the machined surface of the microgroove is not flat and there have many protuberances. From figure 6.9(c), it seems

that the curvature of the profile is not uniform; irregularity appears on the bottom surface, and open face of microgroove is larger. The surface roughness (Ra) obtained by the without PWM is 0.1609µm as shown in Figure 6.9(d). However, the better surface finish, more profile accuracy, and narrow groove width are obtained by PWM technique as presented in Figure 6.10(a-d). By utilising this technique, the microgroove width and depth are obtained as 268.051µm and 53.26µm which indicates that overcut reduces effectively i.e., overcut 34.026µm, as shown in Figure 6.10(a). In addition, it is also observed that there have no protuberances on the microgroove bottom surface as presented in profile of groove in Figure 6.10(b). Figure 6.10(c) illustrates the curvature of the profile which is uniform and more accurate. From the surface roughness profile, it can be observed that the surface roughness (Ra) of the bottom surface is 0.02903µm, as shown in Figure 6.10(d).

It is apparent that when non-PWM is used in terms of PWM, a larger amount of material dissolves from the target area. As the non-PWM has a longer duration time of each pulse on time, it is leading to removing a larger amount of material resulting in more sludge being generated in the machining zone. As a consequence, more protuberances can be observed in the machining area. But, utilising the PWM technique, material dissolution can be controlled because the pulse duration time of each pulse on time can be varied from lower duty to higher duty cycle. As a result, excessive material dissolution is controlled, sludge is removed properly, and surface roughness is improved significantly.

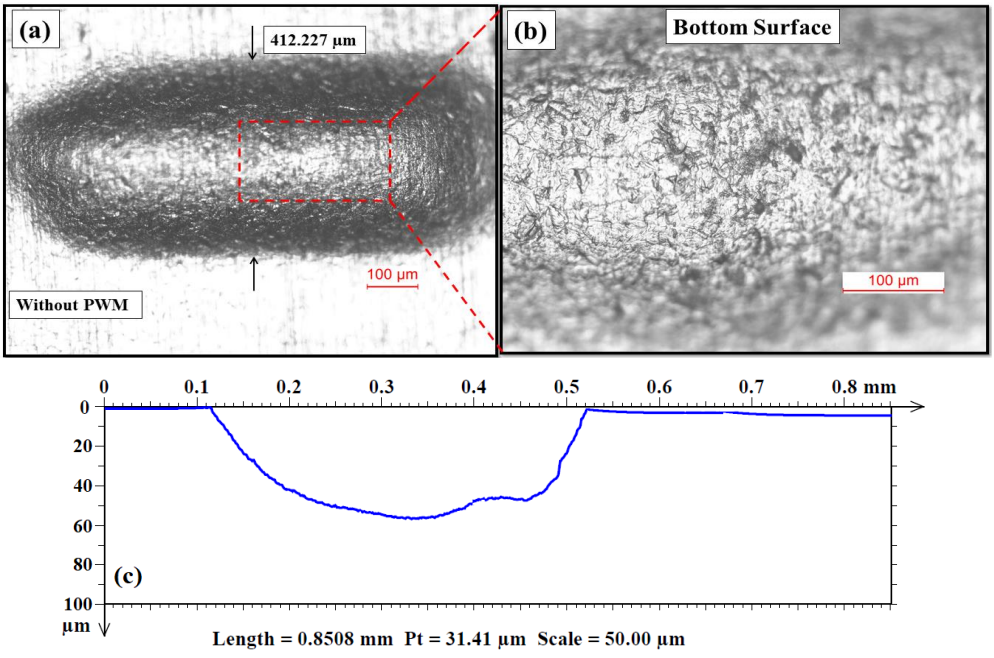

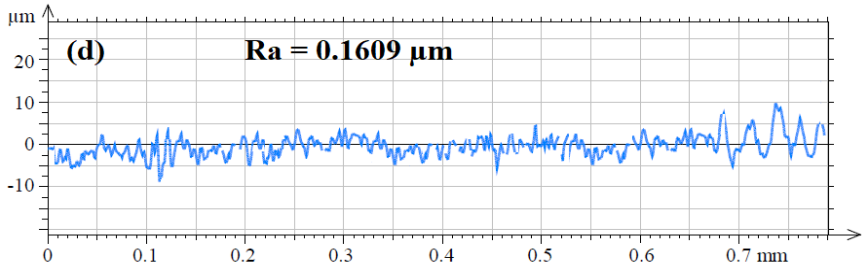

Fig. 6.9 Effect of non-PWM on micro-groove (a) machining results (b) bottom surface (c) curvature of profile (d) surface roughness profile

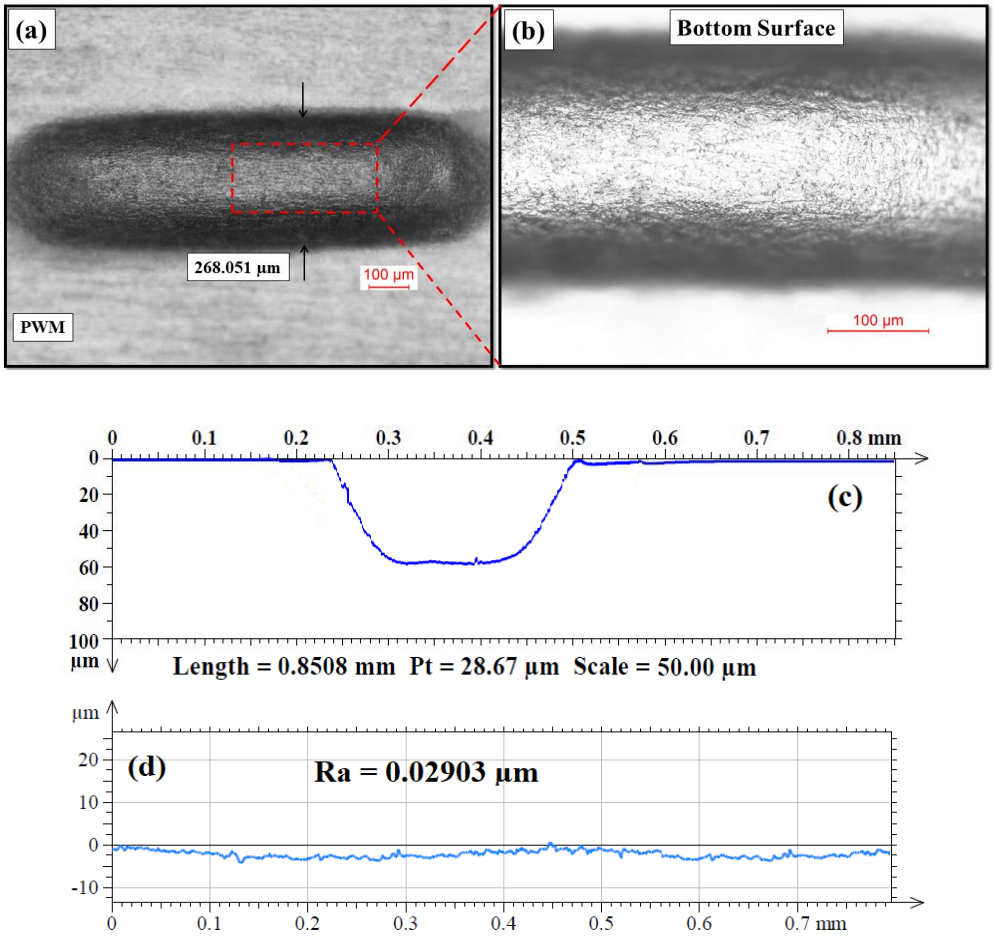

Fig. 6.10 Effect of PWM on micro-groove (a) machining results (b) bottom surface (c) curvature of profile (d) surface roughness profile

6.4 Experimental planning 2: Pulse amplitude modulation (PAM)

6.4.1 Methodology of pulse amplitude modulation of step pulse waveform for stagnant electrolyte

In EMM, appropriate voltage choice is essential for the improvement of material dissolution localization and shape control management of machined products. When the operational voltage is set at a lower level, less amount of material is extracted from the workpiece and also decreases the material dissolution rate. Thus, there have a chance to appear irregular machining and non-uniformity of the profile. By increasing the voltage, more precise and uniform machining can be obtained, but the overcut, taper angle and their standard deviation also increase significantly. At lower voltage levels, the overcut, and its standard deviation are minimized but homogeneity, uniformity and tapering cannot be achieved properly due to less amount of material dissolution. To overcome these disadvantages, a novel pulse amplitude modulation (PAM) technique has been employed in this research. In this technique, the pulse amplitude of each pulse on time regulates from maximum peak to half of the maximum peak and during each pulse off time, voltage increases from zero to half of the maximum peak, as shown in Figure 6.11. This movement of pulse amplitude occurs automatically during micromachining. Due to it, appropriate moderate amount of material can be removed, resulting in reduces the extra dissolution from the target area and improves the localization effects.

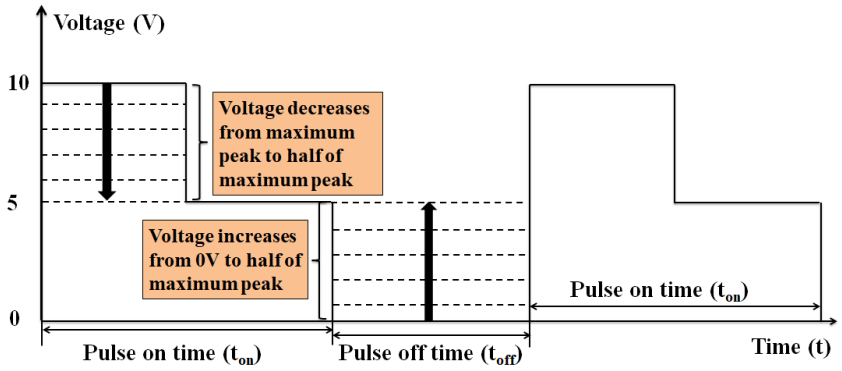

Fig.6.11 Schematic diagram of pulse amplitude modulation

6.4.2 Experimental planning

Copper (Cu) rod with diameter of 200µm and stainless steel (SS304) sheet with thickness of 200µm have been selected for use as the tool and workpiece. From earlier experiments using the PWM technique, it has been observed that a 0.2M H_2SO_4 solution is most effective in reducing surface roughness and tapering effects. Conversely, 0.1 M solution is more suitable for reducing overcut and enhancing the homogeneity of microgrooves.

Consequently, for the PAM technique, 0.1 M electrolyte solution can be selected to further enhance micromachining accuracy. From earlier investigations, it has also been noticed that 10V is appropriate for improving machining accuracy. However, for the PAM technique, voltage regulations ranging from lower than 10V to 5V during the pulse-on time and 0V to 5V variation for pulse-off time can be selected to further enhance machining accuracy. To assess the effectiveness of the PAM technique, experiments have been carried out at pulse frequencies ranging from 0.5 kHz to 4 kHz. For improvement of sludge removal during machining with stagnant electrolytes, it is essential to have a longer pulse-off time. Due to it, duty cycle of 50% has been selected for micromachining. For all experiments, the initial inter-electrode gap has been set as 20µm. Microdimples and microgrooves have been fabricated by moving the microtool downward, specifically 30µm, with a tool feed rate of 0.5µm/s. This choice has been evident from earlier experimental results, which demonstrated that this tool feed rate is best for precise microhole fabrication under a step pulse waveform. To find out the better machining accuracy of microgrooves under new PAM, lower lateral tool feed rate i.e., 0.5µm/s to 0.1µm/s can be selected. Standard deviation has been estimated for microgroove width and depth to evaluate the accuracy of machined products. The surface roughness (Ra) and profile of microgrooves have been observed and examined by Talysurf CCI Non-Contact Profilometer (Taylor Hobson). The conditions of machined microdimples and microgrooves have been also observed by a digital microscope (Leica) for further analysis.

6.5 Results and discussion

6.5.1 Effect of PAM technique on machining performance for different frequencies

Initially, microdimples have been fabricated at different applied frequencies to verify the better utility of PAM of step pulse waveform in improving of machining performance. In this technique, the voltage of pulse on time decreases from 10V to 5V and simultaneously, voltage of pulse off time gradually increases from 0V to 5V, as shown in Figure 6.12(a), capturing image of automatic voltage regulation from oscilloscope. According to figure 6.12(b), it can be noticed that overcut decreases at higher frequencies. At lower frequencies, it can be noticed that overcut increases and bottom surface finish of the microdimple becomes nonuniform, as shown in Figure 6.12(c,d). However, better surface finish and irregularity can be improved at the frequency of 2kHz, as shown in Figure 6.12(e). By increasing the frequency at 4kHz, it has been observed that overcut of

microdimple reduces but bottom surface not improve as compared to 2kHz, as shown in Figure 6.12(f). The reason behind this phenomenon is that when pulse frequency decreases, the number of pulse periods in unit time reduces. Thus, at lower frequency, the duration of pulse on time and off time increases in unit time, resulting in anodic dissolution increasing. Hence, anodic dissolution is not properly controlled by voltage variation of pulse on time and off time at lower frequency. As a result, more sludge is generated in the machined area which poses negative effects on surface finish.

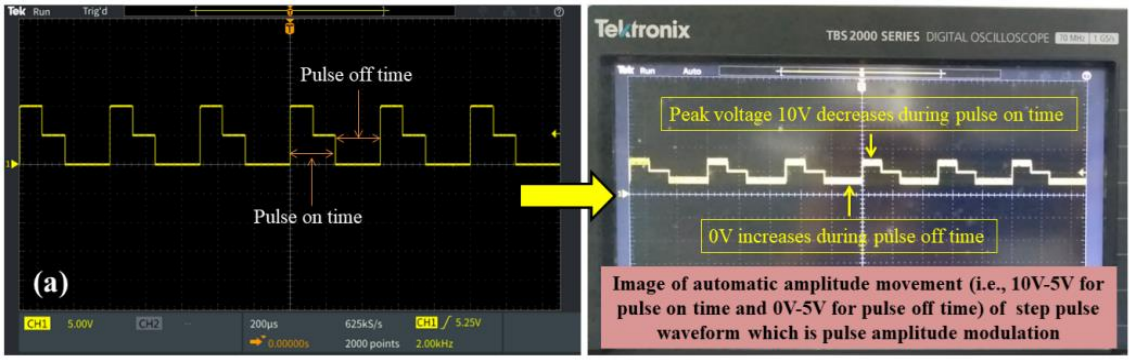

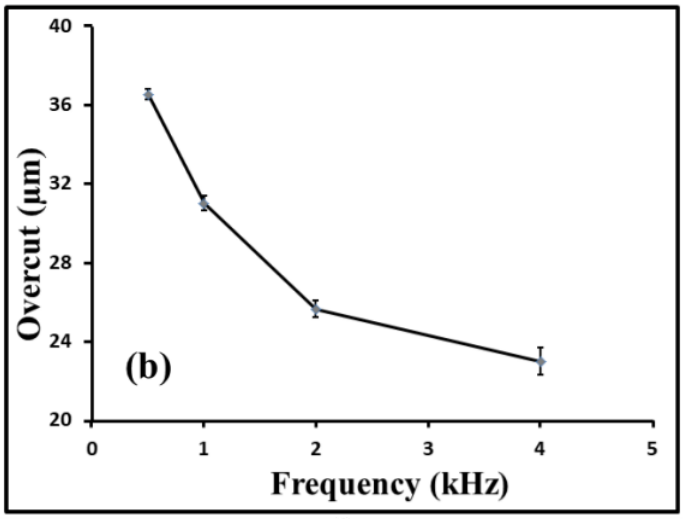

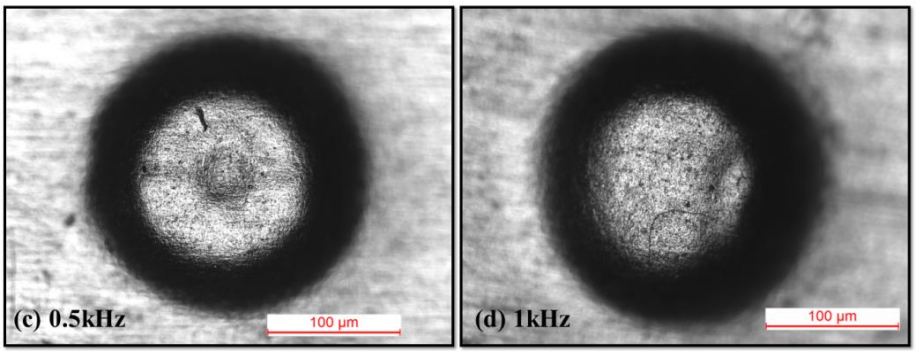

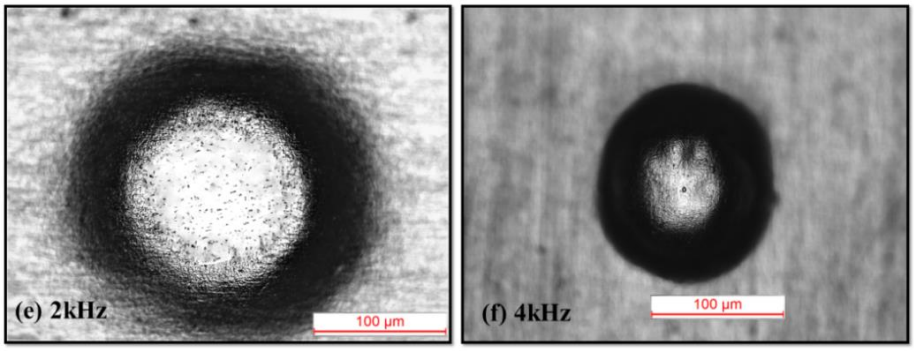

Fig.6.12 Oscilloscopic image of PAM technique (a), variation of overcut (b) and bottom surface of microdimple for different frequencies; (c) 0.5kHz, (d) 1kHz, (e) 2kHz (f) 4kHz

However, at higher frequencies, the number of pulse periods in unit time increases. Due to it, duration pulse on time and off time decreases, and raises the repetition of anodic dissolution in unit time. As a result, the material removal rate decreases, which controls the excessive dissolution from the target area. Furthermore, voltage regulation of pulse on time and off time reduces anodic dissolution simultaneously. Consequently, only minimal amount of material can be removed from the target area, which is not effective for surface finish. However, at 2kHz frequency, the voltage variation of pulse on time and off time is more suitable for moderate amount of material removal. From the experimental results, it can also be observed that at 2kHz frequency, PAM of step pulse waveform is more effective for the fabrication of precise microdimple in EMM.

6.5.3 Effect of PAM technique on microgroove width overcut, depth, taper angle and bottom surface roughness for different lateral tool feed rate

The tool feed is an important parameter for precise micromachining. A slower tool feed indicates that more time is used to remove material at a specific area. As a consequence, a larger amount of material dissolves from the target area, which increases the overcut. Hence, the effects of different lateral tool feeds are investigated for the improvement of microgroove's accuracy under the application of PAM technique and without PAM. From the experimental results, it can be noticed that under without PAM method, microgroove width overcut, depth, and their standard deviations decrease by increasing the tool feed rate, as shown in Figure 6.13(a). At a lateral tool feed rate of 0.5µm/s, it can be observed that there is a maximum reduction in overcut and tapering i.e., 55.107µm and 47.72^0, respectively. However, figure 6.13(b) illustrates the microscopic photograph of the bottom surface of the machined microgroove, which is poor, edge is not uniform, and

irregular machining appears. The tapering effect can also be noticed from the sectional profile of microgroove, as shown in Figure 6.13(c). From the figure, it can also be noticed that the open face of microgroove is larger than bottom width and bottom surface is not uniform. The reason behind this phenomenon is that the average voltage is greater and remains constant during pulse on time, which removes larger amount of material from target area. Due to it, more sludge is generated in the machined area which poses negative effects on surface finish. Thus, greater surface roughness (Ra) is obtained i.e., 0.1567µm, which can be observed from the surface roughness profile, as shown in Figure 6.13(d).

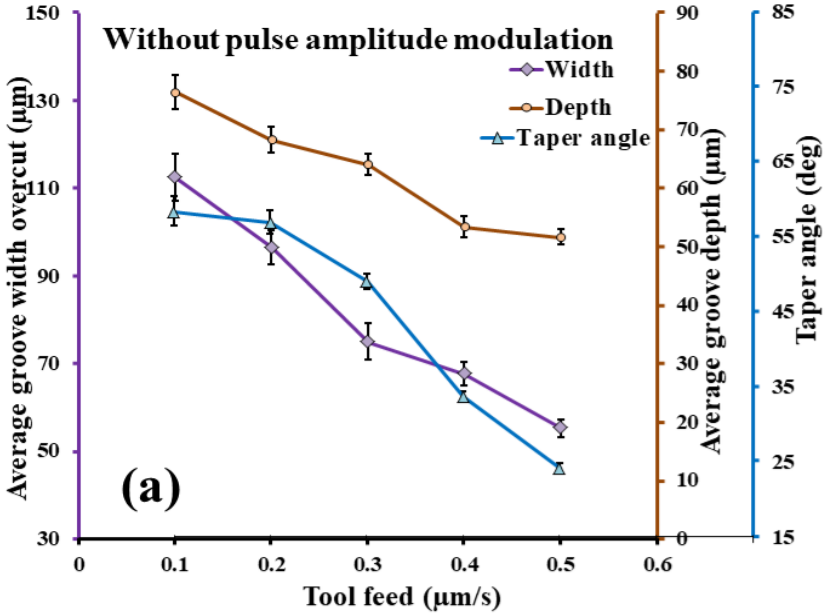

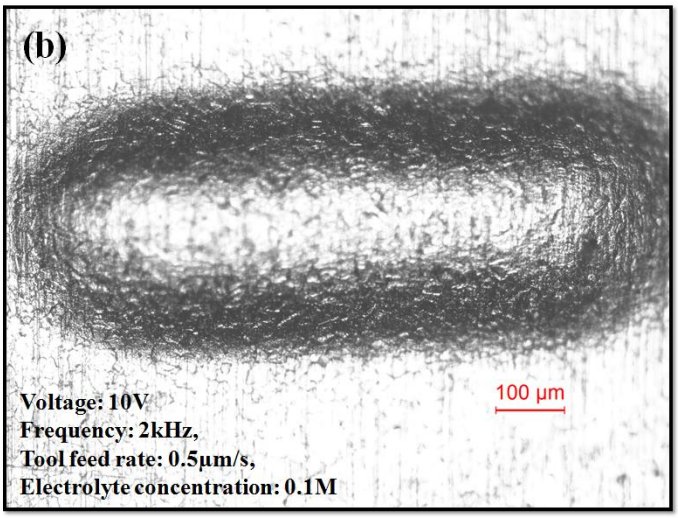

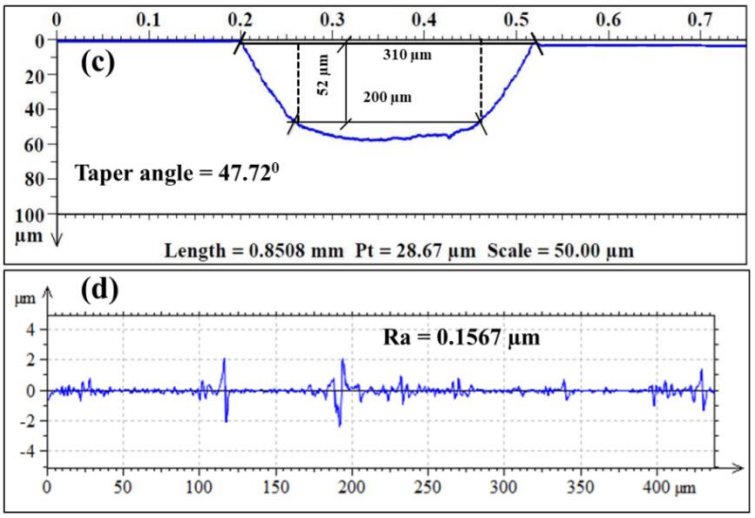

Fig. 6.13 Effect of without PAM technique on microgroove width overcut, depth, taper angle and surface roughness

However, better surface finish, good profile accuracy, and narrow groove width are obtained by the PAM technique. By utilising this technique, at the same lateral tool feed rate of 0.5µm/s, the microgroove width overcut, depth, and taper angle are obtained as 25.055µm, 49.82µm, and 15.37^0 which indicates that machining accuracy improves effectively as compared to without PAM technique, as shown in Figure 6.14(a). It can also be noticed that the edge of microgroove is uniform, homogeneity improves significantly and no irregular machining appears, as shown in Figure 6.14(b). The sectional profile of microgroove indicates that the tapering effect is minimised, bottom surface is uniform, as shown in Figure 6.14(c). From the surface roughness profile, it can be observed that bottom surface roughness (Ra) of the machined microgroove is 0.0744µm, which is lower than without PAM method, as shown in Figure 6.14(d).

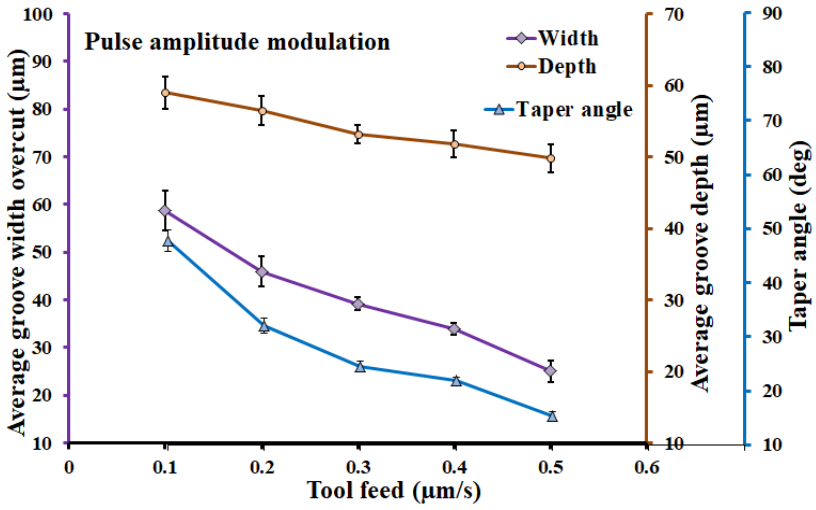

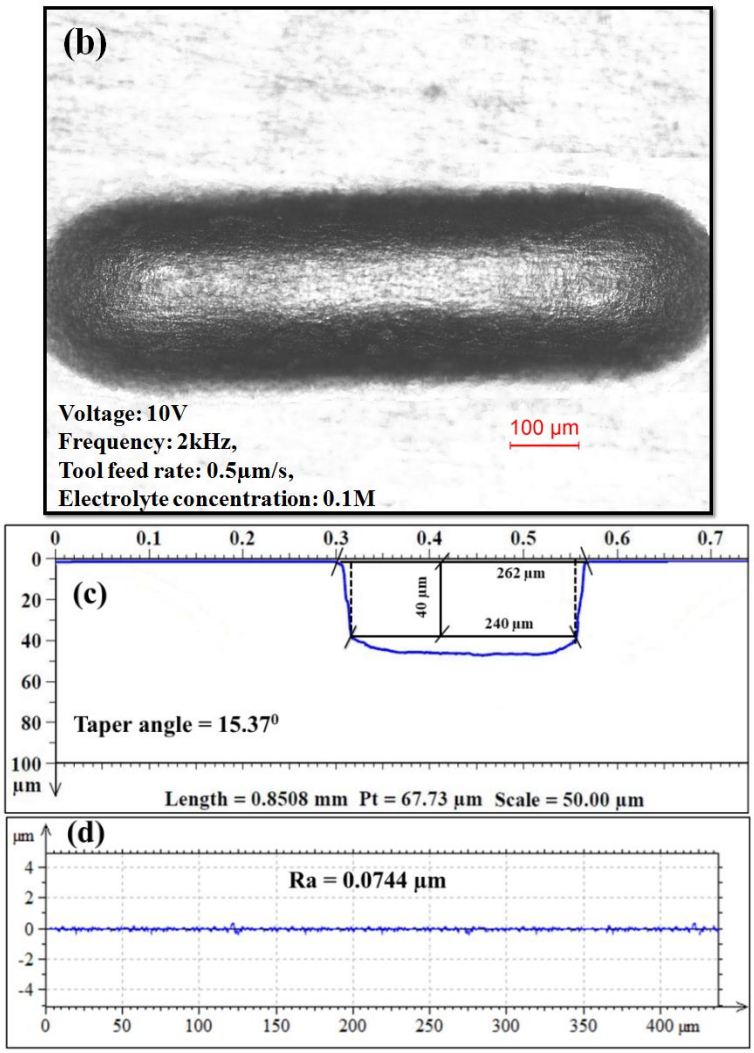

Fig.6.14 Effect of PAM technique on microgroove width overcut, depth, taper angle and surface roughness

6.6. Outcomes of experimental investigation

Based on above mentioned experimental results, it can be concluded that pulse width modulation (PWM) is a novel technique. By utilising this technique, potential transmission into the electrolyte can be controlled which reduces the extra dissolution from the target area and improves the localization effects. In addition, it can facilitate the sludge removal from the machining zone effectively.

The PWM is beneficial to transmit the proper potential into the electrolyte, which leads to a significant role in moderate amount of anodic dissolution. Another advantage of PWM is that it removes the sludge from the machining zone properly. As a result, micro-groove width overcut, depth and their standard deviation decrease. With the most favourable PWM, i.e., movement of duty cycle from 30% to 50%, micro-groove width overcut and

its standard deviation are obtained at 34.026µm and 1.24 µm, accompanied by lower taper angle i.e., 14.03^0. To verify the feasibility of PWM technique, machining accuracy is investigated for different applied voltages, duty cycles, frequencies; tool feed rates and electrolyte concentrations. Based on experimental results, it can be observed that PWM technique is most effective for the improvement of profile accuracy when applied voltage 10V, frequency 2kHz, tool feed rate 0.5µm, and 0.2M of electrolyte concentration are used. By utilising the PWM technique, the surface roughness (Ra) is obtained at 0.0244µm, where Ra is 0.1609µm for the non-PWM method. To obtain precise micromachining, expensive ultra-short voltage pulses are not required in this method. The PWM of step pulse waveform is used in electrochemical micromachining, which can easily be designed by the function generator.

In order to further reduction of overcut and irregular machining pulse amplitude modulation (PAM) technique is employed in EMM. Based on above mentioned experimental results, it can be concluded that pulse amplitude modulation is a novel technique, by which the performance of electrochemical micromachining can be improved. Utilising this new technique pulse voltage can be regulated from higher to lower range. Due to it, material dissolution can be controlled significantly.

The new PAM technique has been investigated for different frequencies and found that 2 kHz frequency is most effective for uniform and regular micromachining. By employing the lower range, i.e., 0.5µm/s to 0.1µm/s, of lateral tool feed rate under the PAM technique, it has also been noticed that precise micro features can be fabricated at a tool feed rate of 0.5µm/s. As a result, lower taper angle 15.37^0, lower groove width overcut i.e., 25.055µm, and better homogeneity are obtained under the application of PAM technique. However, the surface roughness (Ra) is slightly garter i.e., 0.0744µm. In contrast, utilising without PAM method, overcut, taper angle, surface roughness can be obtained as 55.107µm, 47.72^0, and 0.1567µm, respectively. PAM of step pulse waveform is also a cost-effective method because this waveform is designed indigenously with the help of function generator.

The findings from this investigation propose that for the performance improvement of electrochemical micromachining, pulse width modulation is an inexpensive methodology instead of the ultra-short pulse width power supply and ultra-high frequency pulse power supply. The PWM is a promising alternative method which will be more convenient for micromachining applications. While, PAM technique is a promising alternative method

that offers greater accessibility for the fabrication of more precise microgrooves. However, it can be observed from the sectional profile of microgroove that minute tapers are still generated along the sidewalls and edge is slightly irregular. There have a chance to further improvement of homogeneity of the machined profile utilising EMM. Hence, to improve these factors more investigations are needed to study also the frequency modulation of step pulse waveform which may further enhance the machining accuracy of EMM.

Chapter 7: Investigation into EMM performance employing SPW with multi frequency modulation

7.1 Introduction

In the presence of oxide layer, larger gas bubbles, and sludge, improving localization of anodic dissolution poses a challenging task for EMM. Consequently, various arrangements such as tool vibration; electrolyte flushing; electrolyte jet; mixed gas jet etc., have been employed to remove sludge from the machining zone. To address these challenges, a novel multi-frequency modulation technique has been employed in newly designed step pulse waveform. This new technique is introduced in stagnant electrolytes to restrict the appearance of larger gas bubble at microtool tip area and to remove sludge effectively from the narrow interelectrode area.

The objective of this research work is to establish a simple methodology to replace the complex electrolyte flushing arrangements, expensive ultra-high-frequency pulse power supplies, and other mechanical methods for improving the localization of anodic dissolution and the better removal of electrolysis by-products. Step pulse waveform with multi-frequency modulation (MFM) technique has been employed in stagnant electrolytes to flush out the larger gas bubbles and sludge from the machining area. Hence, the investigation into the influence of lower to higher frequencies and multi-frequency have been carried out, with a focus on larger size of gas bubble evolution, accumulation, and attachment on microtool tip area. Additionally, analysis of the overcut, depth, and profile shape of microchannels has been carried out at lower to higher frequency and under the multi-frequency modulation. In order to determine the best parametric conditions for the enhancement of machining performance, in terms of average channel width overcut, maximum depth, taper angle, and corner angle, experiments have also been conducted at different lower and higher frequencies through the machining of linear and complex microchannels. The best pulse cycle time of mixed frequency has been investigated for the improvement of surface finish. Based on the experimental findings, a best parametric combination of MFM has been identified. The effect of different tool feed rates have also been investigated for fabrication of precision microchannels under the best configuration of MFM. Furthermore, the effects of different lower applied voltages have been investigated through the fabrication of complex microchannel to evaluate the utility of MFM. To determine the most effective technique, microchannels have been fabricated using pulse width modulation (PWM), pulse amplitude modulation (PAM), and multi-

frequency modulation (MFM) under the same operating conditions. Finally, the most effective technique has been utilized for fabricating microholes on titanium material to establish its effectiveness over other past research work carried out for machining microholes on titanium.

7.2 Design strategy of Step pulse waveform with multi-frequency modulation

At lower frequencies, the number of pulse cycles in unit time reduces comparatively higher frequency, which means the duration of pulse on time and off time increases per unit time. Thus, at lower frequencies in EMM, larger amount of material can be removed due to longer pulse-on times. Conversely, higher frequencies increase the number of pulse cycles per unit time, resulting in shorter pulse-on and off times. As a consequence, the material removal rate decreases, which helps to prevent excess dissolution in the target area. Keeping in view of this fact, lower and higher frequencies are mixed to design a novel step pulse waveform, as shown in Figure 7.1. Consequently, lower frequency increases the material removal rate, but higher frequency decreases higher material removal rate. Due to it, moderate amount of material can be removed with the help of mixed frequency. Another advantage is that due to the different pulse duration times of two frequencies, larger gas bubble evolution can be controlled significantly and attachment with microtool tip area become restricted. The pulse cycle time of lower and higher frequencies is different, but when two types of frequencies are combined to create a mixed frequency, the pulse cycle time becomes larger and repeated simultaneously throughout the machining.

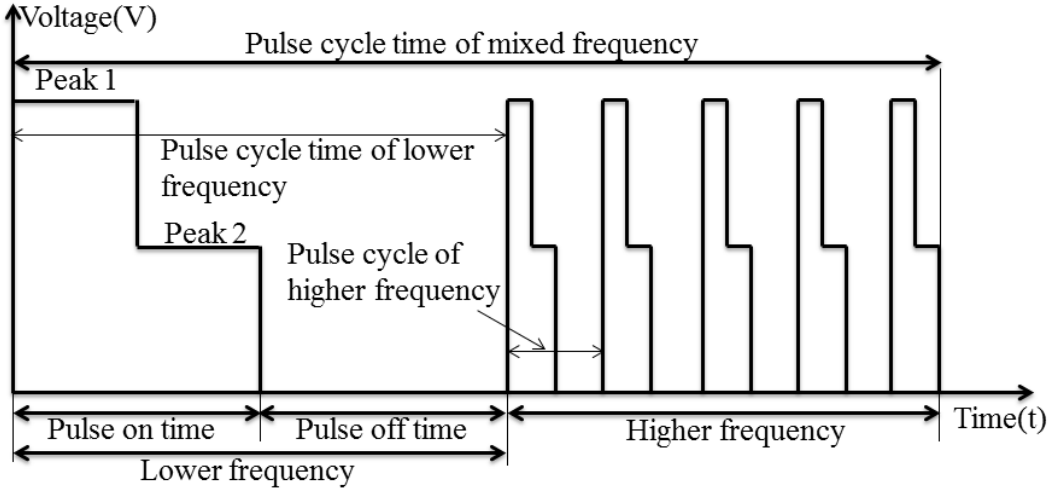

Fig.7.1 Schematic diagram of multi-frequency modulation of step pulse waveform

In this research, the stagnant electrolyte is used to find out the actual behaviour of gas bubbles during machining at different frequencies. In a narrow inter-electrode gap,

hydroxide ions and metal ions generate and form insoluble products i.e., sludge, which accumulate in the machining area and effectively influence the process stability and machining quality. Additionally, hydrogen gas bubbles start to evolve and accumulate on the microtool tip surface, which finally forms a dynamic high-resistance larger gas bubble by collision and combination of bubbles. In the presence of larger gas bubbles and sludge, current flow obstructs and decreases the electrical conductivity of the electrolyte. As a consequence, interelectrode electrolyte resistance increases. Additionally, at machining area, larger gas bubbles obstruct the further bubble flow and sludge removal, resulting in electrolytes not renewing properly into the narrow machining zone. As a result, non-uniform current flow occurs in the machining gap, which leads to irregular micromachining and poor surface finish. Especially when the microtool position is inside of the workpiece, this gas shielding effect increases extremely. As a result, the material dissolution rate decreases rapidly, and in some cases, it can be stopped by gas shielding. The formation of larger gas bubbles and their attachment to the microtool surface can be illustrated through a schematic presentation as shown in Figure 7.2(a).

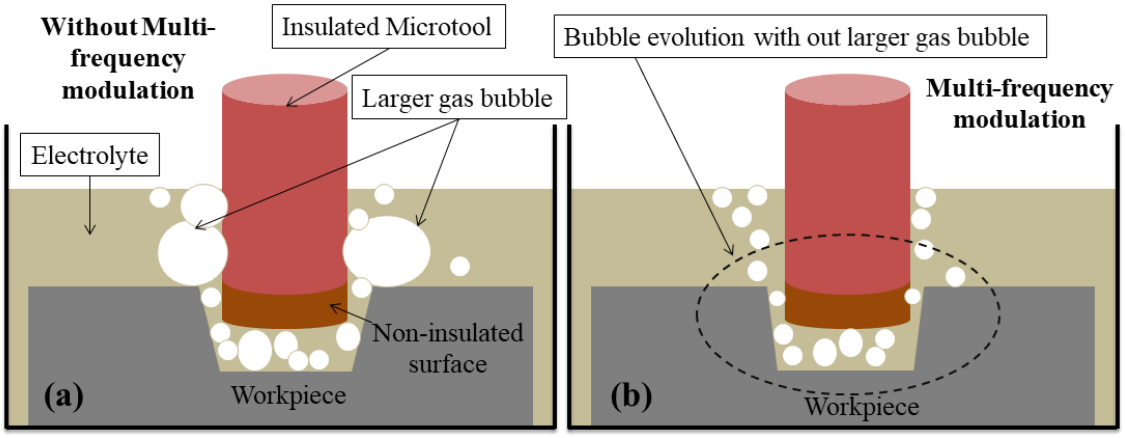

Fig.7.2 Schematic diagram of process mechanism under (a) without multi-frequency modulation technique (b) multi-frequency modulation (MFM)

However, the most effective results can be achieved when multi-frequency modulation technique is used in EMM, as presented in Figure 7.2(b). Excessive bubble formation occurs due to the longer pulse-on time of lower frequencies, whereas higher frequencies, with their shorter pulse duration, effectively control this issue. Hence, the step pulse waveform with the combination of lower and higher frequencies may obstruct bubble accumulation and formation of larger gas bubbles within narrow interelectrode gap. This phenomenon may be helpful for sludge removal effectively and renewal of the fresh electrolyte in the machining zone.

7.3 Experimental planning

A copper (Cu) rod with diameter of 200µm has been chosen as microtool. Stainless steel (SS304) sheet with thickness of 200µm has been chosen for the use of workpiece. As the microtool-tip area is very small compared to the workpiece, the stray current plays a significant role in pitting effects. To reduce the stray current effects, microtool insulation technique has been employed. In electrochemical micromachining, electrolyte flushing may create several problems such as generating unwanted vibration of micro-tool and workpiece, and electrolyte flow disturbs the proper addressing of electrolyte at the target area. To avoid this obstacle and to investigate the behaviour of larger gas bubble evolution, stagnant electrolyte has been considered for micromachining. To evaluate the best operational conditions of the step pulse waveform, experiments have been carried out at different pulse frequencies across a wider range, from 100Hz to 1MHz, with an increment of 10 times. From these investigations, it can be understood that the pulse frequencies at which the step pulse waveform is most suitable for improving machining accuracy. The outcomes of these experiments provide the idea for developing a new step pulse waveform with multi-frequency modulation technique. The multi-frequency consists with both lower and higher frequencies. Furthermore, since the step pulse waveform included both lower and higher frequencies, the best frequency range has been selected as 50Hz to 400Hz for lower frequencies and 8kHz to 14kHz for higher frequencies. To investigate the better surface finish of machined products, pulse cycle time (i.e., pulse period of lower + pulse period of higher frequency) has been selected from 15ms to 30ms. To enhance sludge removal during machining with stagnant electrolytes, it is crucial to have a longer pulse-off time. Consequently, duty cycle of 50% has been chosen for micromachining. In order to determine the best frequency and pulse cycle time of MFM, slightly high voltage of 10V has been considered. After achieving the best combination of lower and high frequency, voltage in the range of 7V to 10V has been employed for further investigation of machining accuracy. L-shape microchannels have been fabricated by downward movement of the Z-axis i.e., 40µm with tool feed rate of 1.5µm/s. To determine the better machining accuracy of L-shape microchannels and complex microchannel, the scanning tool feed rate has been selected from 1µm/s to 4µm/s. The standard deviation has been computed for the width, depth, and taper angle of L-shape microchannels to assess the precision of the machined microchannels. As the sulfuric acid has sludge dissolving ability, 0.1 M H_2SO_4 electrolyte solutions have been

selected for stagnant electrolytes. The machined microchannel's conditions have been observed using a digital microscope (Leica). The surface roughness (Ra) of L-shape microchannels and 3D profiles has been examined using a Talysurf CCI Non-Contact Profilometer by Taylor Hobson. During micromachining, the image of larger gas bubble evolution has been captured by a digital camera, Dino-Lite (AM4815ZTL, Taiwan), whose maximum frame rate is 30fps. The average size of larger gas bubbles has been measured using the Leica Application Suite X (LAS X) software. All machining conditions are listed in Table 7.1.

To establish the effectiveness of the MFM technique of step pulse waveform, microholes have been fabricated on pure commercial grade-1 titanium sheets with thickness of 150µm, in comparison to other past research on machining microholes in titanium. The aqueous solution of sodium nitrate and sodium chloride ($NaNO_3$ + NaCl) has been chosen due to its effectiveness in facilitating the fabrication of microfeatures on a titanium sheet.

Table 7.1. Machining conditions

Condition	Value
Micro tool (Copper)	Φ 0.2 mm
Workpiece (SS304)	15 x 15 x 0.2 mm
Electrolyte (H_2SO_4)	0.1 mol/l
Applied Voltage	7,8,9,10 volt
Pulse frequency	100 Hz to 1MHz
Pulse cycle time of multi-frequency	15ms to 30ms
Duty ratio	50%
Feed rate of micro tool	1 to 4 µm/sec
Initial interelectrode gap	20 µm

7.4 Results and discussion

7.4.1 Influence of different frequencies and multi-frequency on gas bubble formation and attachment at microtool tip area

Experiments have been carried out at different pulse frequencies to find out the behavior of larger gas bubble during micromachining. The oscilloscopic images of step pulse waveform at different frequencies are presented in Figure 7.3. As compared to higher frequencies, the number of pulse periods in a unit of time decreases at lower frequencies, leading to an increase in the duration of pulse-on and pulse-off times per unit of time, as illustrated in Figure 7.3(a to e). Alternatively, it can be stated that the total number of pulse periods increased to10^2, 10^3, 10^4, 10^5, and 10^6 for the frequencies of 100Hz, 1kHz, 10kHz, 100kHz and 1MHz, respectively. Thus, at lower frequencies, the anodic

dissolution still occurs during the pulse-on time, but since there are fewer pulses, this dissolution occurs less frequently within the same unit of time. However, at higher frequencies, the repetition of anodic dissolution increases due to the increment of pulse period in unit time. Figure 7.3(f) exhibits the oscilloscopic image of step pulse waveform with multi-frequency modulation (MFM). In this MFM modulation technique, lower frequency of 100Hz and a higher frequency of 10kHz are combined as a new pulse cycle, which repeats simultaneously throughout the micromachining. In Table 7.2, machining conditions are outlined to investigate the effect of pulse frequency on the evolution of larger gas bubbles. From earlier pulse amplitude modulation (PAM) technique, it can be noticed that 10V applied voltage, 50% duty cycle, and 0.1M electrolyte concentration are suitable for fabrication of precise microgroove. Hence, in the investigation of the effect of pulse frequencies on precision microchannel, the applied voltage has been fixed at 10V, while other machining conditions remain the same: 50% duty cycle, and 0.1M electrolyte concentration. Herein, faster lateral tool feed rate of 2µm/s has been selected for reduction of machining time. The pulse cycle time also selected as 25ms for MFM technique.

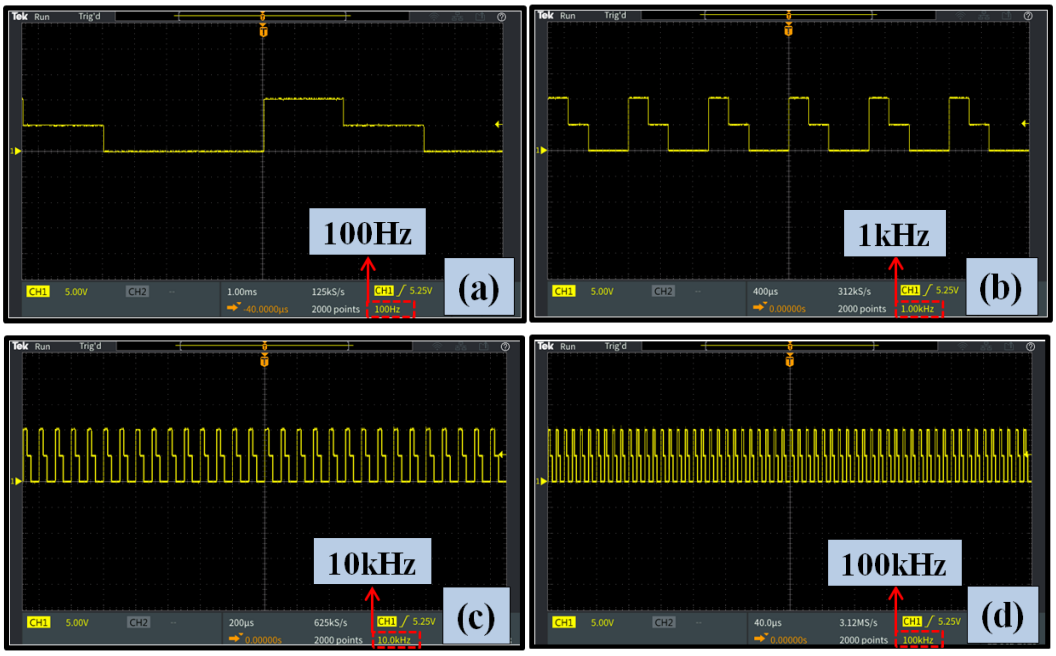

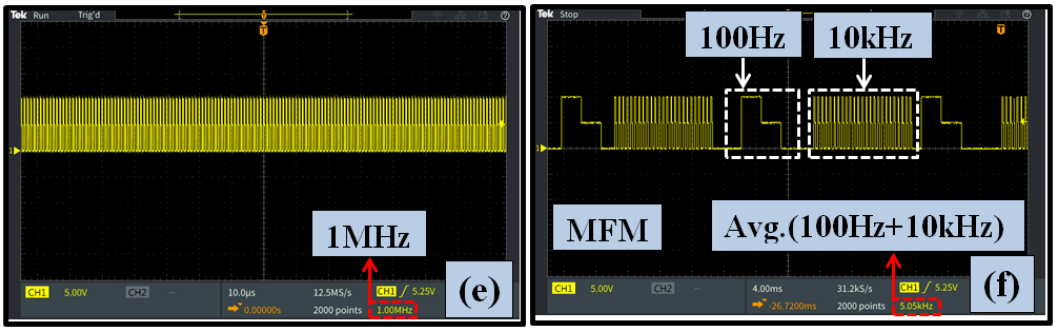

Fig.7.3 Oscilloscopic images of step pulse waveform for different frequencies (a) 100Hz, (b) 1kHz, (c) 10kHz, (d) 100kHz, (e) 1MHz (f) MFM: 100Hz+10kHz

Table 7.2: Machining conditions to investigate the effect of different pulse frequencies on larger gas bubble evolution

Voltage (V)	Duty cycle (%)	Frequency	Tool feed (µm/s)	Electrolyte concentration (mol/l)	Pulse cycle time (ms)
10	50	100Hz 1kHz 10kHz 100kHz 1MHz 100Hz+10kHz	2	0.1	25

At the longer pulse on time, massive gas bubbles generate and create more number of larger gas bubbles, which attach to the microtool surface, as presented in Figure 7.4(a). Consequently, at machining area, larger gas bubbles obstruct the further bubble flow and sludge removal, resulting in electrolytes may not renewing properly into the narrow machining zone. Due to it, non-uniform current density distribution appears in the machining gap, which may lead to irregular machining and poor surface finish of the micro-features. By increasing the frequency 10 times, it can be noticed that the larger shape of gas bubble reduces and the evaluated bubble removes rapidly comparatively lower frequency due to shorter pulse on time, as shown in Figure 7.4(b). It also noticed that at the frequency of 10kHz, larger shape of gas bubble forms, as shown in Figure 7.4(c). But, when pulse frequency increases more i.e., 100kHz, the size of the larger gas bubbles and its attachment with the microtool tip area reduces, as shown in Figure 7.4(d). At the frequency of 1MHz, it can be noticed that very small size gas bubble forms and attached with microtool tip area, as shown in Figure 7.4(e). However, the most effective results can be noticed when multi-frequency modulation technique is used, as presented in Figure 7.4(f). Under the MFM modulation technique, it can be observed that no larger

gas bubble appears, resulting in evaluated bubbles flush out rapidly during machining. This phenomenon effectively flushes out sludge by utilizing the flow of gas bubbles and renewing the supply of fresh electrolyte in the narrow machining zone. The average size of larger gas bubbles has been measured and also listed in Table 7.3, where it is clearly noticeable that when pulse frequency increases the average size of larger gas bubbles reduces significantly. It is observed that from 100Hz to 1MHz, the average size of larger gas bubble reduces from 1062.624µm to 164.399µm, but it is not removed totally. However, when step pulse waveform with multi-frequency (MFM) modulation is employed, larger size of gas bubbles are not generated in machining time.

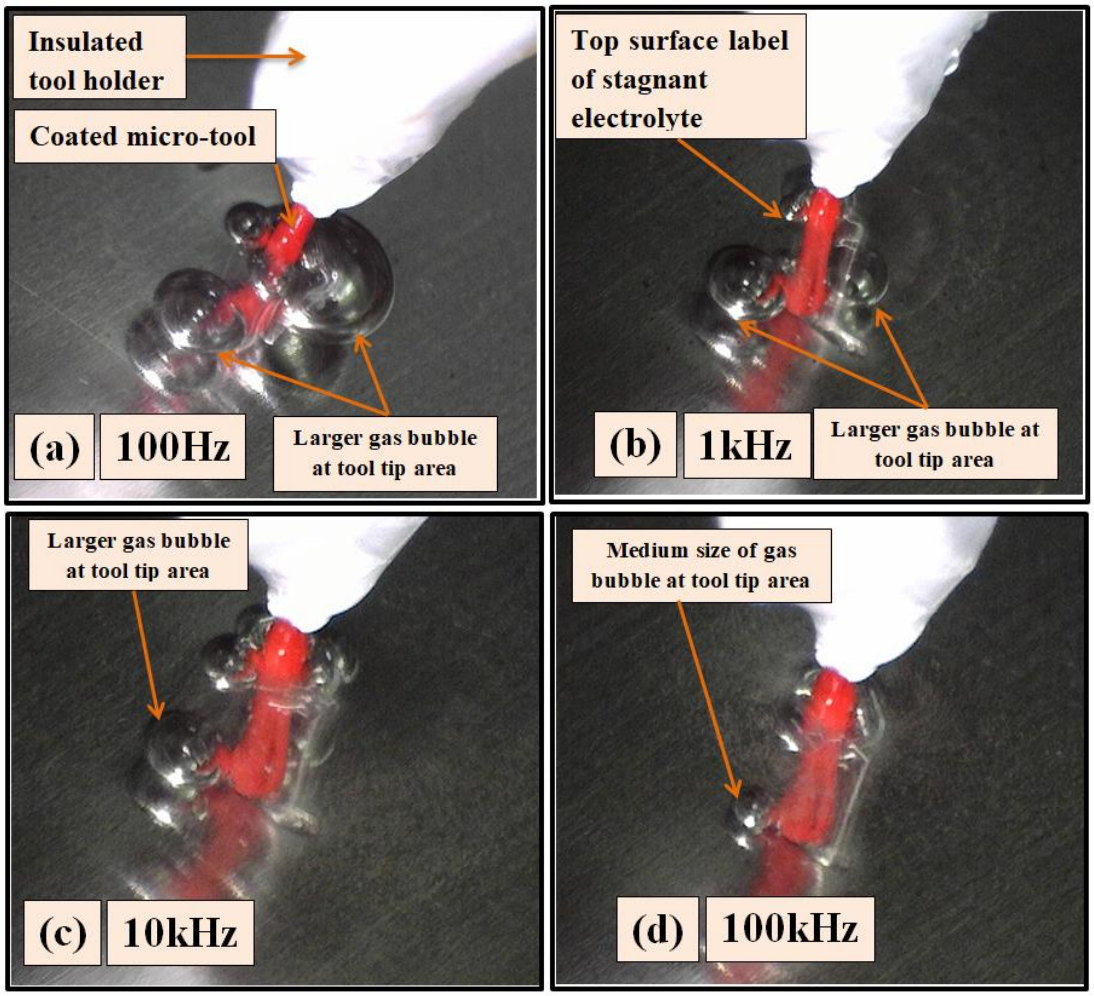

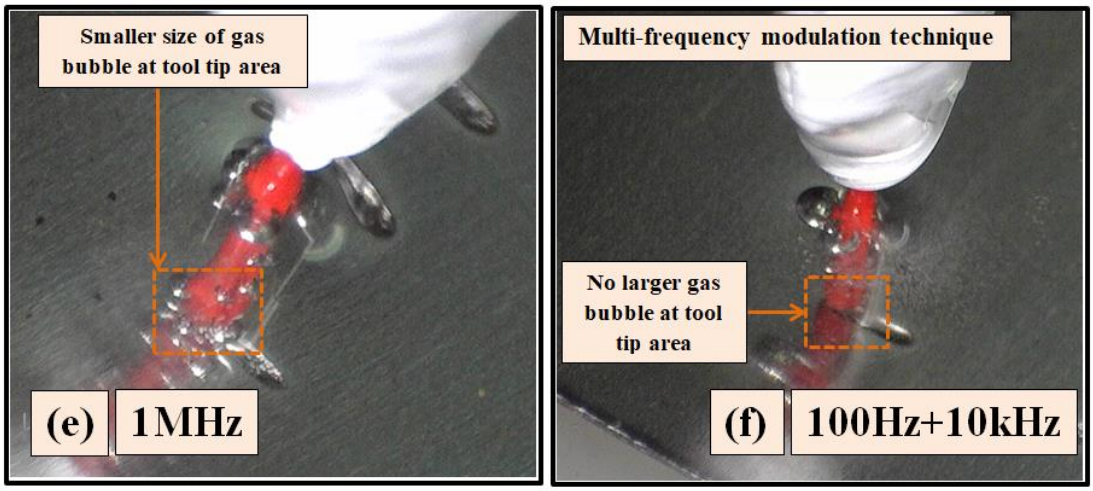

Fig.7.4 Observation of larger size of gas bubble under different frequencies (a) 100Hz, (b) 1kHz, (c) 10kHz, (d) 100kHz, (e) 1MHz (f) MFM: 100Hz+10kHz

Table 7.3: Average size of larger gas bubble during EMM

Frequency of step pulse waveform	Average size of larger gas bubble (μm)
100Hz	1062.624
1kHz	708.736
10kHz	420.980
100kHz	228.977
1MHz	164.399
100Hz+10kHz	No larger gas bubble appears

The effects of pulse frequency on microchannel are presented in a graph as shown in Figure 7.5. From the graph, it can be noticed that the average overcut width, overcut of length and maximum depth of microchannel decrease with increasing frequency when all machining conditions are fixed, as mentioned in Table 7.2. Due to the longer pulse on time at a frequency of 100Hz, more amount of material is removed for every pulse on time during machining. Consequently, the overcut of the linear microchannel's width, length, and maximum depth increases. However, as the applied frequency increases, it can be noticed that the overcut and maximum depth of the linear microchannel decrease significantly. This phenomenon occurs due to the shorter pulse-on time at higher frequencies, resulting in a decrease in the material removal rate.

At lower frequencies, a larger amount of material can be removed during each pulse on time. Another problem that appears for a longer pulse on time is that excessive gas bubbles generate and create more number of larger sizes of gas bubbles, which attach to the microtool surface as observed from Figure 7.4(a to f). Consequently, it obstructs the

further sludge flushing; resulting in, non-uniform distribution of current density, which increases irregular machining with poor homogeneity, and poor bottom surface with numerous protuberances as shown in Figure 7.6(a). For better understanding, the machined microchannels are examined using a Talysurf CCI Non-Contact Profilometer. From the colour contour of the 3D image, the nature of the bottom surface finish can also be observed. It can be noticed from the graph (Figure 7.5) that when pulse frequency is increased at 1kHz, the overcut and depth reduce as compared to the frequency of 100Hz. Additionally, homogeneity and irregularity also improve, but the bottom surface not be improved effectively, as shown in Figure 7.6(b). The cause of this improvement is lower duration of pulse on time and more repetition of anodic reaction. However, at 10kHz frequency, overcut reduces and improves uniformity of profile shape, bottom surface finish, and homogeneity as shown in Figure 7.6(c).

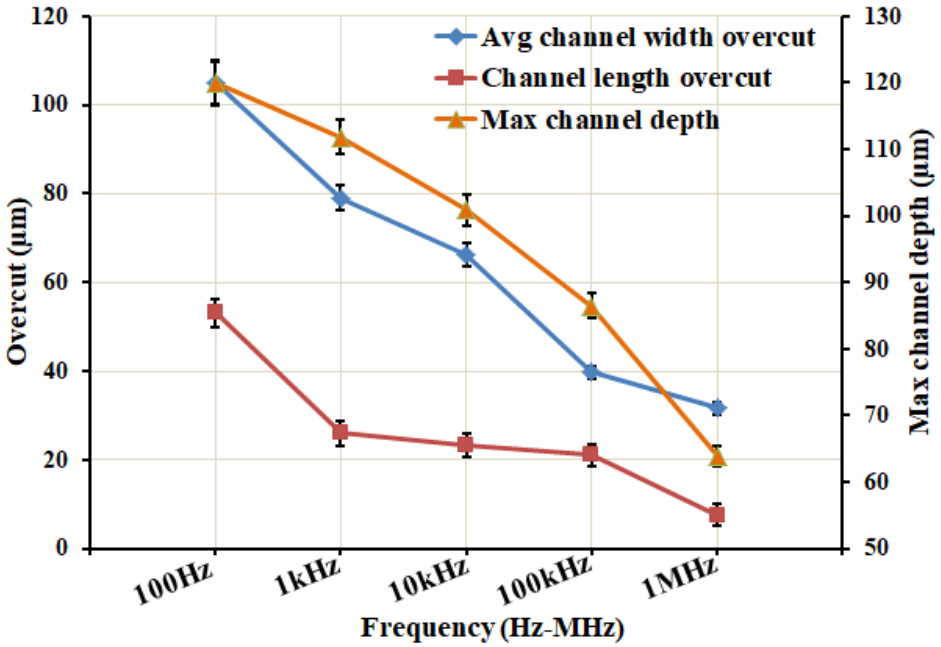

Fig.7.5 Effect of different pulse frequencies on linear microchannel

At this 10kHz frequency, the accuracy of microchannel improves significantly due to the duration of pulse on time and number of repetitions of anodic reaction is appropriate for a moderate amount of material removal. But, due to the presence of larger gas bubble, some protuberances also appear on the bottom surface of microchannel. When frequency increases more i.e., 100kHz, overcut also reduces effectively, but irregular machining appears in the bottom surface and non-uniformity can be observed in the edge of the microchannel, as shown in Figure 7.6(d). At 1MHz frequency, it can be observed that overcut reduces significantly, but irregularity of bottom surface and non-uniformity of

microchannel edge are not minimized, as shown in Figure 7.6(e). Thus, it can be understood that at higher frequencies, the duration of pulse on time is very small and the number of repetitions of anodic reaction is higher, which reduces the material dissolution rate. Thus, higher frequencies are preferable for the reduction of overcut. Hence, to improve irregularity, researchers have used various arrangements to flush out sludge and gas bubbles from the machining zone such as tool vibration, electrolyte flushing, electrolyte jet, mixed gas jet etc., which are discussed in the introduction part in-depth.

However, utilizing a novel step pulse waveform with multi-frequency modulation (MFM) technique in stagnant electrolytes, larger gas bubbles do not appear and sludge is effectively removed from the machining zone. As a result, precise shape of microchannel with better surface finish and homogeneity can be fabricated, as shown in Figure 7.6(f). It can be observed that at 10kHz, there is an improvement in irregular machining, uniformity of profile shape and surface finish, figure 7.6.(c), compared to other frequencies i.e., 100Hz, 1kHz, 100kHz, and 1MHz. It can also be observed that at lower frequency of 100Hz, the depth of microchannel, width and length overcut increases due to a relatively longer pulse duration, figure 7.6.(a), and Figure 7.5. Keeping in view, 100Hz and 10kHz frequencies are mixed in design strategy of novel multi-frequency modulation of step pulse waveform. As a consequence, 100Hz frequency increases the material removal rate for faster micromachining and 10kHz frequency decreases higher material removal rate to improve the accuracy. Due to it, controlled amount of material can be removed with the help of mixed frequency. Another advantage is that due to the different pulse duration times of two frequencies, gas bubble evolution can be controlled significantly and larger size of gas bubble formation becomes restricted. Thus, it can be noticed that at microtool tip area, no large gas bubble appears during machining, which is also discussed earlier and as observed in Figure 7.4(f).

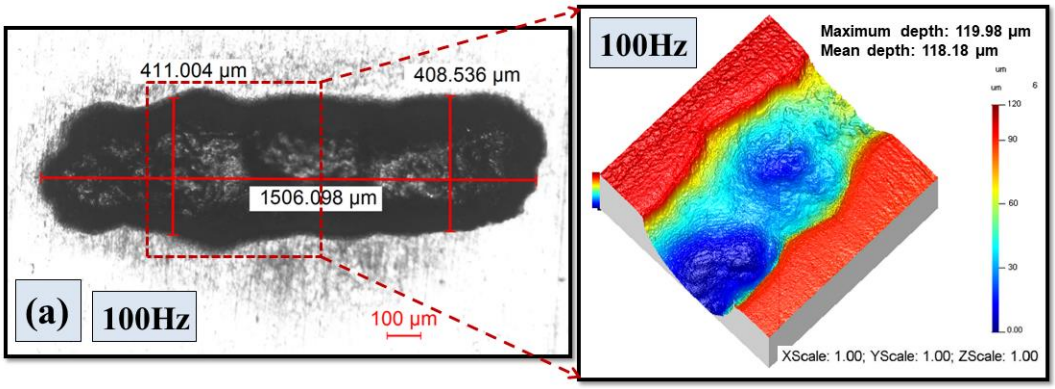

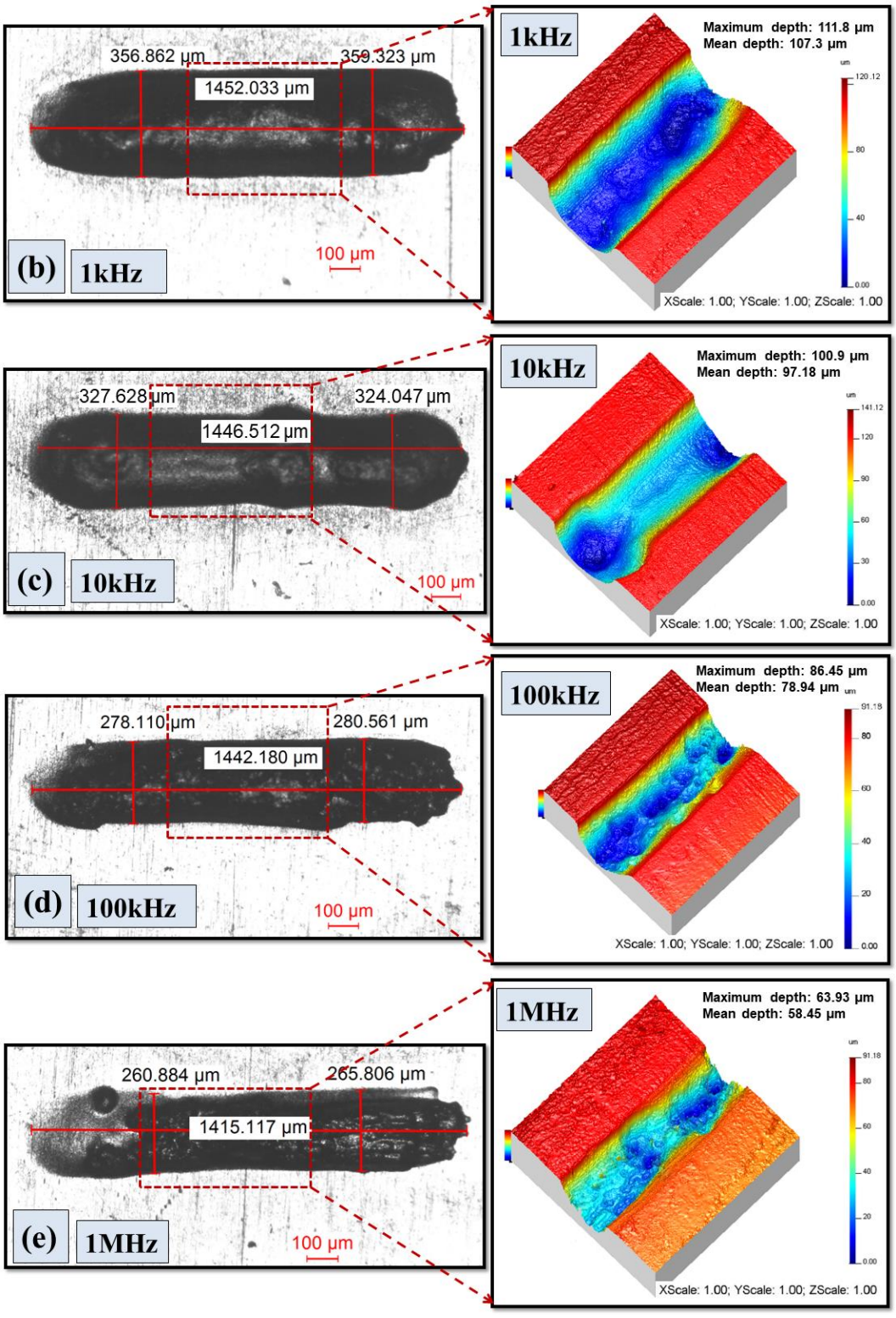
356.862 µm
359.323 µm
1452.033 µm
100 µm
(b)
1kHz
1kHz
Maximum depth: 111.8 µm
Mean depth: 107.3 µm
XScale: 1.00; YScale: 1.00; ZScale: 1.00
327.628 µm
324.047 µm
1446.512 µm
100 µm
(c)
10kHz
10kHz
Maximum depth: 100.9 µm
Mean depth: 97.18 µm
XScale: 1.00; YScale: 1.00; ZScale: 1.00
278.110 µm
280.561 µm
1442.180 µm
100 µm
(d)
100kHz
100kHz
Maximum depth: 86.45 µm
Mean depth: 78.94 µm
XScale: 1.00; YScale: 1.00; ZScale: 1.00
260.884 µm
265.806 µm
1415.117 µm
100 µm
(e)
1MHz
1MHz
Maximum depth: 63.93 µm
Mean depth: 58.45 µm
XScale: 1.00; YScale: 1.00; ZScale: 1.00

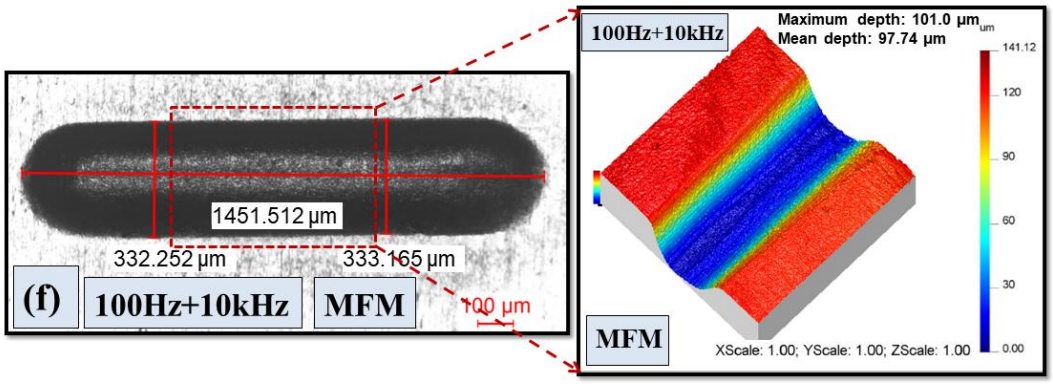

Fig.7.6 Machined microchannels at frequency (a) 100Hz, (b) 1kHz, (c) 10kHz, (d) 100kHz, (e) 1MHz, (f) MFM:100Hz+10kHz

7.4.2 Effect of multi-frequency modulation on output responses of microchannel at the combination of different higher frequencies

At mixed frequencies of 100Hz and 10kHz, microchannels have been fabricated and find out that this mixed frequency is very effective for the fabrication of precise microchannels with better surface finish, as discussed earlier. In order to identify the best combination of higher and lower frequencies and to investigate their effects on precision micromachining, L-shaped microchannels have been fabricated at different higher frequencies combinations. The machining conditions for determine the best combination of multi-frequency at different higher frequencies are listed in Table 7.4. In examining the impact of higher pulse frequencies combined with a lower frequency of 100Hz on precision microchannel, all other machining conditions remain constant: applied voltage of 10V, 50% duty cycle, 0.1M electrolyte concentration, lateral tool feed rate of 2µm/s, and pulse cycle time of 25ms. The graph clearly illustrates a reduction in the overcut of the L-shaped microchannel's width, depth, and taper angle as the frequency increases, as shown in Figure 7.7. The reason for this phenomenon is that as the frequency increases, the material removal rate decreases accordingly. It can be noticed that at the mixed frequency of 100Hz + 8kHz, the edge of machined L-shape microchannel is not smooth, homogeneity is poor, corner angle is 92.292^0 and taper angle is 24.891^0 (Fig.7.7), as shown in Figure 7.8(a). Thus, it can be understood that 8kHz frequency is not suitable for mixing with frequency of 100Hz. By increasing frequency i.e., 10kHz, it can be observed that taper angle and corner angle reduces, homogeneity and bottom surface finish improves, as shown in Figure 7.8(b). However, the edge of L-shape microchannel is not smooth. Consequently, it can be realized that the material removal rate is not appropriate at the mixed frequency of 100Hz + 10kHz. However, the uniformity and smoothness of

edge, homogeneity, and reduction of overcut can be obtained at the mixed frequency of 100Hz + 12kHz, as shown in Figure 7.7 and 7.8(c). At this frequency, corner angle of 91.036^0 can be achieved, which is all most perpendicular, and lower taper angle of 16.119^0 is obtained (Fig.7.7). When, mixed frequency 100Hz + 14kHz is applied, irregularity and poor surface finish can be observed due to smaller pulse on time, as shown in Figure 7.8(d). Accordingly from these results, it can be understood that 12kHz frequency is appropriate for mixing with lower frequency of 100Hz, for MFM.

Table 7.4: Machining conditions to determine the best combination strategy of multi frequency at different higher frequencies

Voltage (V)	Duty cycle (%)	Frequency	Tool feed (µm/s)	Electrolyte concentration (mol/l)	Pulse cycle time of multi-frequency (ms)
10	50	100Hz + 8kHz 100Hz + 10kHz 100Hz + 12kHz 100Hz + 14kHz	2	0.1	25

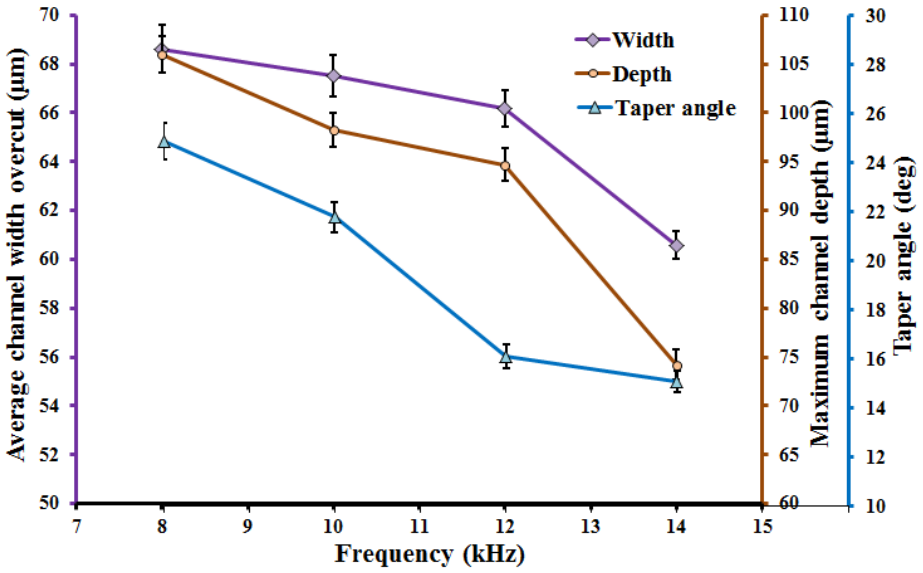

Fig. 7.7 Effect of multi-frequency for fabrication of precision L-shape microchannel at different combination of higher frequencies with 100Hz lower frequency

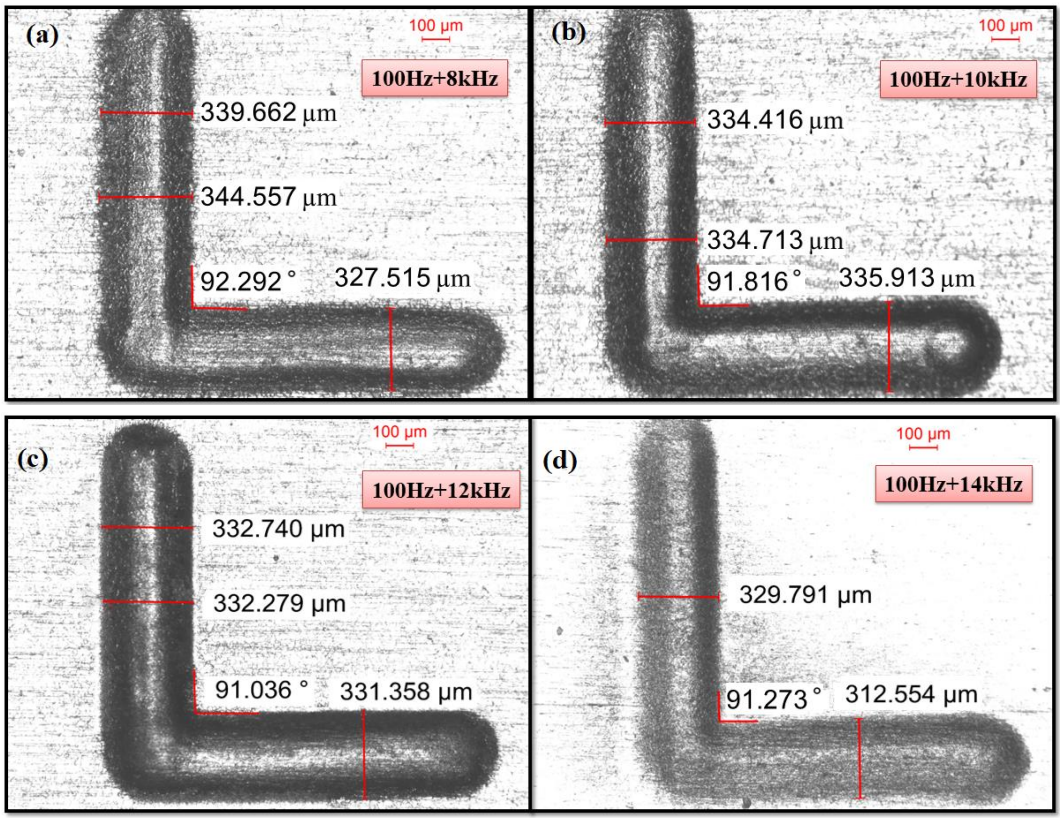

Fig. 7.8 Machined L-shape microchannel at different combination of higher frequencies with 100Hz lower frequency (a) 100Hz+8kHz, (b) 100Hz+10kHz, (c) 100+12kHz, (d) 100+14kHz

7.4.3 Effect of multi-frequency modulation on output responses of microchannel at the combination of different lower frequencies

To identify the best lower frequency for the effective combination of multi-frequency, L-shape microchannels are also fabricated and investigated to performance characteristics of EMM in stagnant electrolyte. From the investigation of different higher frequencies as discussed earlier, it has been observed that 12kHz frequency is appropriate for develop a best combination strategy of lower frequency in MFM. Hence, the lower frequency range of 50Hz to 400Hz is combined separately with a 12kHz frequency to explore the best combination strategy for MFM. The machining conditions are listed in Table 7.5. In examining the effect of lower pulse frequencies combined with a higher frequency of 12kHz on precision microchannel, all other machining conditions remain constant. These conditions include an applied voltage of 10V, 50% duty cycle, 0.1M electrolyte concentration, lateral tool feed rate of 2µm/s, and pulse cycle time of 25ms.

Table 7.5: Machining conditions to determine the best combination strategy of multi frequency at different lower frequencies

Voltage (V)	Duty cycle (%)	Frequency	Tool feed (µm/s)	Electrolyte concentration (mol/l)	Pulse cycle time of multi-frequency (ms)
10	50	50Hz 100Hz + 12kHz 200Hz 400Hz	2	0.1	25

The effects of multi-frequency at the combination of different lower frequencies are presented in a graph, as shown in Figure 7.9. From the graph, it can be noticed that the average overcut L-shape microchannel width, depth and taper angle reduce with the increase of lower frequencies. At the combination of 50Hz + 12kHz frequency, it can be observed that the average overcut of L-shape microchannel width, depth, taper angle and corner angle are larger, figure 7.10(a), than 100Hz frequency, as shown earlier in Figure 7.8(c). It can also be observed that the edge is not uniform, and numerous protuberances and irregularities appear on the bottom surface, as shown in Figure 7.10(a). The cause of this phenomenon is that at 50Hz + 12kHz frequency, the material removal rate is much higher due to a longer pulse on time of lower frequency. When the lower frequency is increased to 100Hz and combined with a higher frequency of 12kHz, overcut, depth, taper angle, and corner angle also decrease. Additionally, it can achieve that homogeneity and irregularity improve, edge is uniform as shown in Figure 7.8(c). From Figure 7.9, it can be observed that overcut, depth and taper angle are reduced at the frequency combination of 200Hz + 12kHz, but uniformity and homoginity of L-shape microchannels can not be obtained as well as 100Hz. Furthermore, by increasing frequency at 400Hz+ 12kHz, it can be noticed that average overcut, depth and taper angle are reduced, but irregularity appears as observed from Figure 7.10 (b).

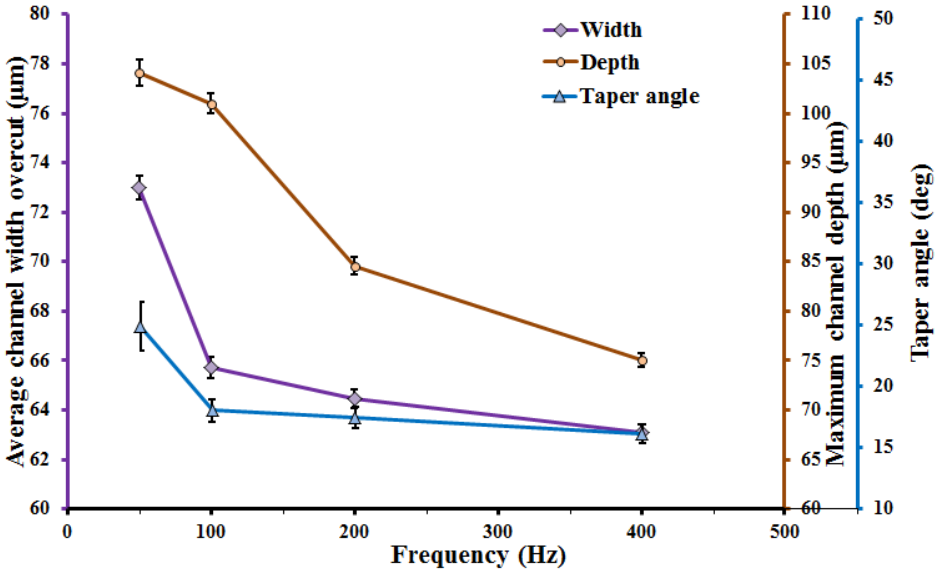

Fig.7.9 Effect of multi-frequency on L-shape microchannel at different combination of lower frequencies with 12kHz higher frequency

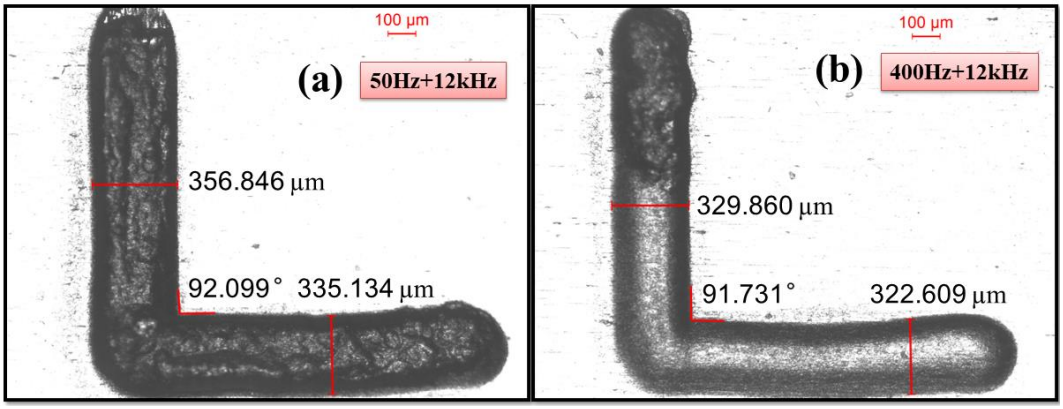

Fig.7.10 Machined L-shape microchannel at different combination of lower frequencies with 12kHz higher frequency (a) 50Hz+12kHz, (b) 400+12kHz

7.4.4 Influence of pulse cycle time of multi-frequency modulation (MFM) on surface finish of microchannel

In multi-frequency modulation technique, pulse cycle time plays an important role in the improvement of bottom surface finish. From the oscilloscopic image as shown in Figure 7.3(f), it can be noticed that at the pulse cycle time of 25ms, the pulse number is 25 for higher frequency. This pulse number depends on pulse cycle time. Thus, when the pulse cycle time rises, the pulse number also increases. The more pulses means more repetitions of anodic reaction. In order to find out better surface finish, the multi-frequency modulation technique is examined for different pulse cycle times. The machining conditions are listed in Table 7.6. Here, in the investigation of the impact of pulse cycle

time on machining surface finish, all other machining conditions remain constant: applied voltage of 10V, 50% duty cycle, best frequency combination of 100Hz +12kHz as obtained, 0.1M electrolyte concentration, and lateral tool feed rate of 2µm/s.

Table 7.6: Machining conditions to determine the best pulse cycle time for effective multi-frequency modulation

Voltage (V)	Duty cycle (%)	Frequency	Tool feed (µm/s)	Electrolyte concentration (mol/l)	Pulse cycle time of multi-frequency (ms)
10	50	100Hz +12kHz	2	0.1	15 20 25 30

From the 2D image (Fig. 7.11) of microchannel which has been measured by Talysurf CCI Non-Contact Profilometer, it can be observed that when pulse cycle time increases bottom surface finish also improves. At the pulse cycle time of 15ms, the colour contour of 2D image exhibits that bottom surface is not smooth, as shown in Figure 7.11(a). This smoothness increases with pulse cycle time. Thus, at 20ms pulse cycle time, colour contour exhibits that the smoothness of the bottom surface is better, but some non-uniformity appears, as shown in Figure 7.11(b). However, at the pulse cycle time of 25ms, surface finish improves comparatively lower pulse cycle time, as shown in Figure 7.11(c). The better smoothness can also be noticed from the colour contour. At this pulse cycle time, pulse number of higher frequency is matched with lower frequency properly. Due to it, the regularity of the material removal is improved throughout machining. But, when pulse cycle time is 30ms, the irregularity and protuberances increase significantly, as shown in Figure 7.11(d). The cause of this fact is that pulse number of higher frequency increases more, which plays a significant role in material removal rate. Due to the small pulse on time, less amount of material is removed, which not help to improve the surface finishes.

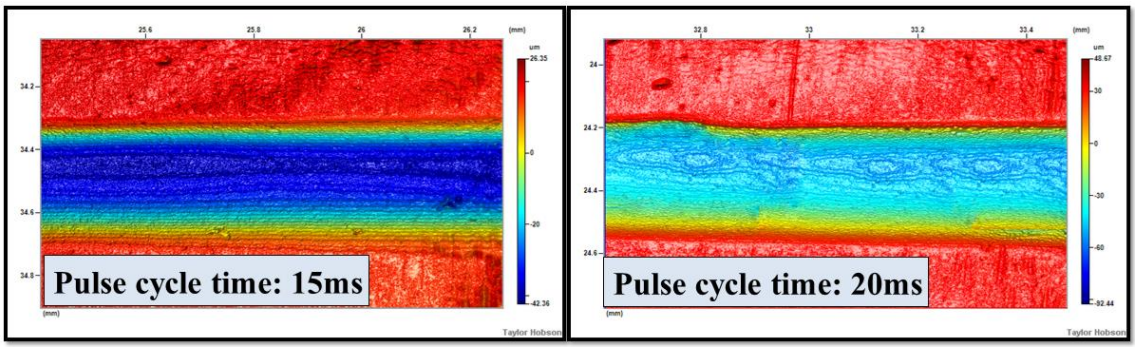

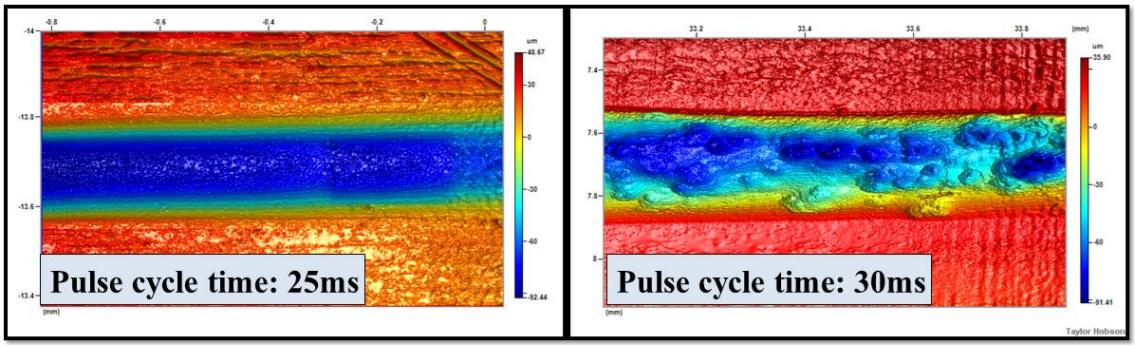

Fig.7.11 2D Images of bottom surface of machined L-shape microchannel for different pulse cycle times; (a)15ms, (b) 20ms, (c) 25ms, (d) 30ms

7.4.5 Influence of tool feed rate on performance characterization of EMM under multi-frequency modulation

The lateral tool feed rate significantly influences on material removal from the target area. Hence, investigating the effect of the lateral tool feed rate on performance characterization of EMM under the application of the multi-frequency modulation technique is essential. The machining conditions are listed in Table 7.7. In this investigation of the impact of lateral tool feed rate on precision microchannel, all other machining conditions remain constant: an applied voltage of 10V, 50% duty cycle, the best frequency combination of 100Hz + 12kHz, 0.1M electrolyte concentration, and pulse cycle time of 25ms. The graph in figure 7.12 clearly shows that increasing the tool feed rate results in a reduction in the average overcut of the microchannel width, depth, and taper angle. A slower tool feed rate means longer machining times resulting in more material removal, which can negatively impact the overcut, and taper angle of the machined microchannel, as shown in Figure 7.12. From the Figure 7.13(a), it can be noticed that the edge is not uniform, and numerous protuberances and irregularities appear on the bottom surface, corner angle is not perpendicular.

Table 7.7: Machining conditions to determine the effect of lateral tool feed rate on performance characterization of EMM

Voltage (V)	Duty cycle (%)	Frequency	Tool feed (µm/s)	Electrolyte concentration (mol/l)	Pulse cycle time of multi-frequency (ms)
10	50	100Hz + 12kHz	1 2 3 4	0.1	25

A higher tool feed rate means faster scanning speed, resulting in machining time reduction. By increasing tool feed rate at 4µm/s, it can also be observed that the overcut and taper angle reduces (Fig.7.12), but irregular machining rises, edge non-uniformity increases, corner angle is not perpendicular, as shown in Figure 7.13(b). However, at 2µm/s tool feed rate, the uniformity and smoothness of edge, homogeneity, better bottom surface finish and reduction of overcut can be obtained, which is presented earlier in Figure 7.8(c). Therefore, it can be understood that 2µm/s lateral tool feed rate is appropriate for proper moderate amount of material removal rate under multi-frequency modulation technique.

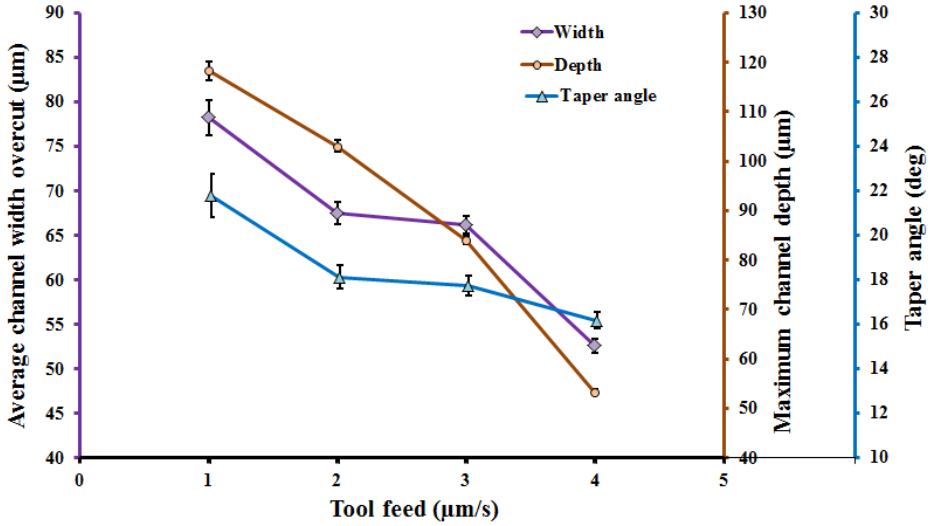

Fig.7.12 Effect of different tool feed rates on precision machining under multi-frequency modulation

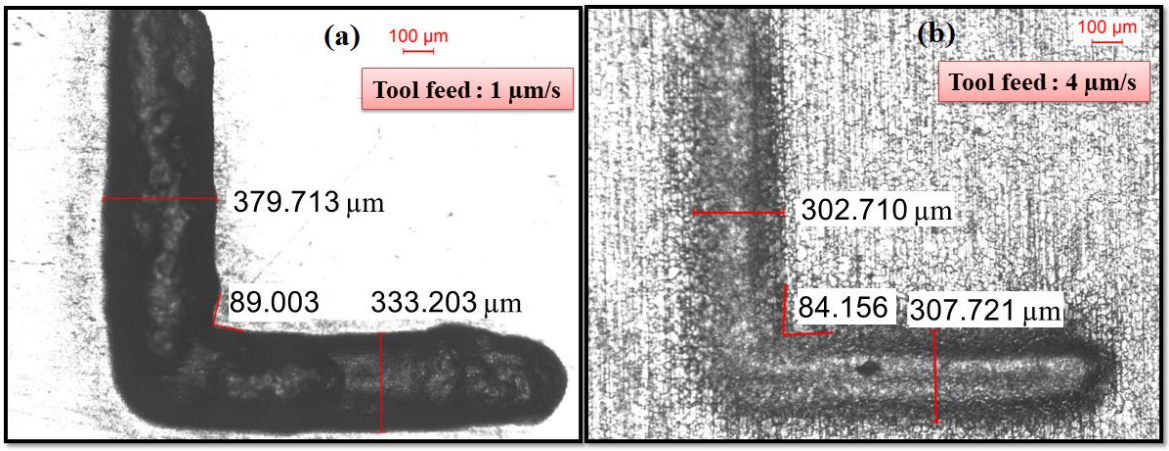

Fig.7.13 L-shape microchannels at lower and higher tool feed rates; (a) 1µm/s, (b) 4µm/s

7.4.6 Influence of applied voltages on performance characterization of EMM under multi-frequency modulation

The aforementioned experimental results reveal that the applied voltage of 10V is suitable for the improvement of precise shape of microchannel with better homogeneity, lower tapering effect and better surface finish. However, to find out further better machining accuracy in terms of overcut, tapering effect, and corner angle, complex and L-shaped microchannels have been fabricated at lower applied voltages using the same best parametric combination as obtained at 10V. These parameters include a frequency of 100Hz + 12kHz, a pulse cycle time of 25ms, a lateral tool feed rate of 2µm/s, and a duty cycle of 50%, as listed in Table 7.8. The effect of different applied voltages on precision electrochemical micromachining of L-shape microchannel is presented in a graph, as shown in Figure 7.14. From the Figure 7.14, it can be noticed that when applied voltage increases, overcut of machined microchannel width, depth, and taper angle also rise due to higher material removal rate. Hence, it can be observed that at 7V, overcut of machined microchannel width, depth, and taper angle is significantly reduced (Fig. 7.14). At the applied voltage of 6V, proper L-shape microchannel cannot be fabricated due to less amount of material removal. Thus, an applied voltage of 6V is not considered for the investigation of better machining accuracy. By fabricating the complex microchannel at 9V as shown in Figure 7.15(a), it can be observed that the overcut of microchannel width and depth decreases compared to 10V. However, at 9V, it can be noticed that homogeneity, uniformity and corner angle remain almost similar to 10V, Figure 7.8 (c). From the SEM image of micrograph, it also observed that bottom surface is smooth and no irregularity appears, as shown in Figure 7.15(b). Thus, the surface roughness profile, illustrated in Figure 7.15 (c), shows that the surface roughness of the complex microchannel is 0.0846µm.

Table 7.8: Machining conditions to determine the effect of different applied voltages on performance characterization of EMM

Voltage (V)	Duty cycle (%)	Frequency	Tool feed (µm/s)	Electrolyte concentration (mol/l)	Pulse cycle time of mixed frequency (ms)
7 8 9 10	50	100Hz + 12kHz	2	0.1	25

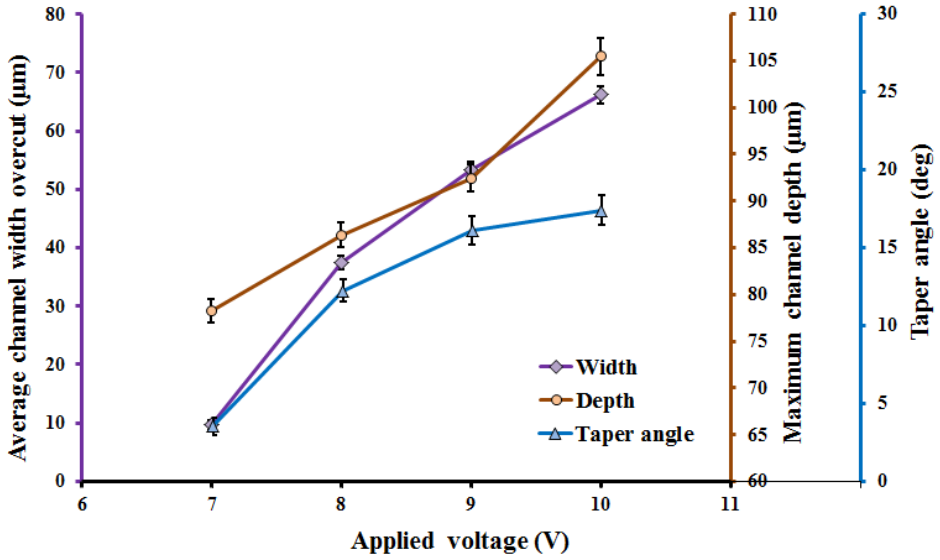

Fig. 7.14 Effect of different applied voltages on L-shape microchannel

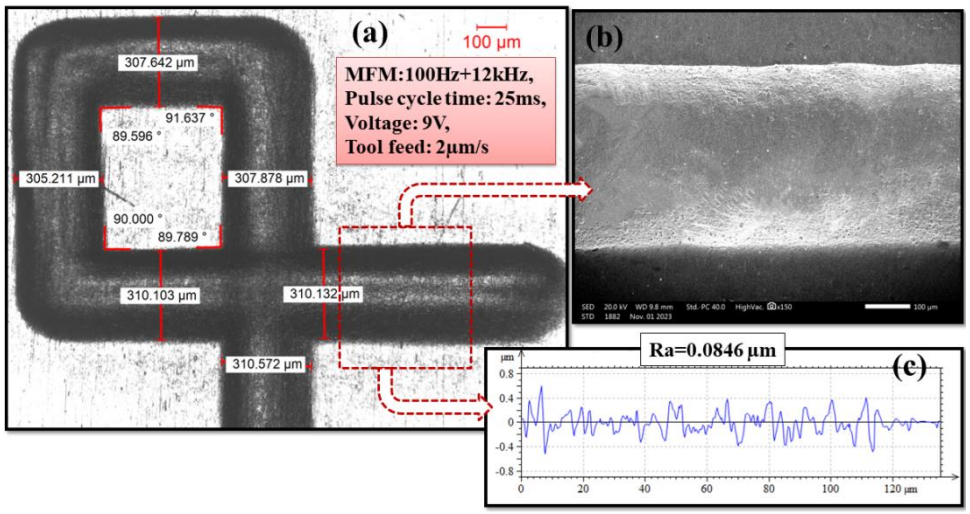

Fig.7.15 Complex microchannel at 9V (a), SEM image of micrograph (b) surface roughness profile (c)

The precision L-shaped microchannels have also been fabricated at an applied voltage of 7V, as shown in microscopic image. From figure 7.16(a), it is noticeable that the edge of the microchannel is uniform and smooth, which improves homogeneity, and the corner angle is almost perpendicular. The measured values for the L-shaped microchannel's average width overcut, taper angle, and corner angle, which are 9.653µm, 3.529^0, and 89.246^0, respectively (figure 7.14), which also corroborated with microscopic image (Figure 7.16). From the SEM image of the micrograph, it is also noticed that the bottom surface is smooth, with no irregularities, as shown in figure 7.16(b). Consequently, the surface roughness profile indicates that the surface roughness of the microchannel is 0.0734µm, as illustrated in Figure 7.16(c). Figure 7.16(d) exhibits the 3D image of L-

shape microchannel whose maximum depth is 78.25µm, as measured by Talysurf CCI Non-Contact Profilometer. It can be understand from the comparison of applied voltages that overcut, depth and taper angle reduce by decreasing applied voltage, but uniformity of edge, homogeneity, and better corner angle are achieved within the range of 7V to 10V.

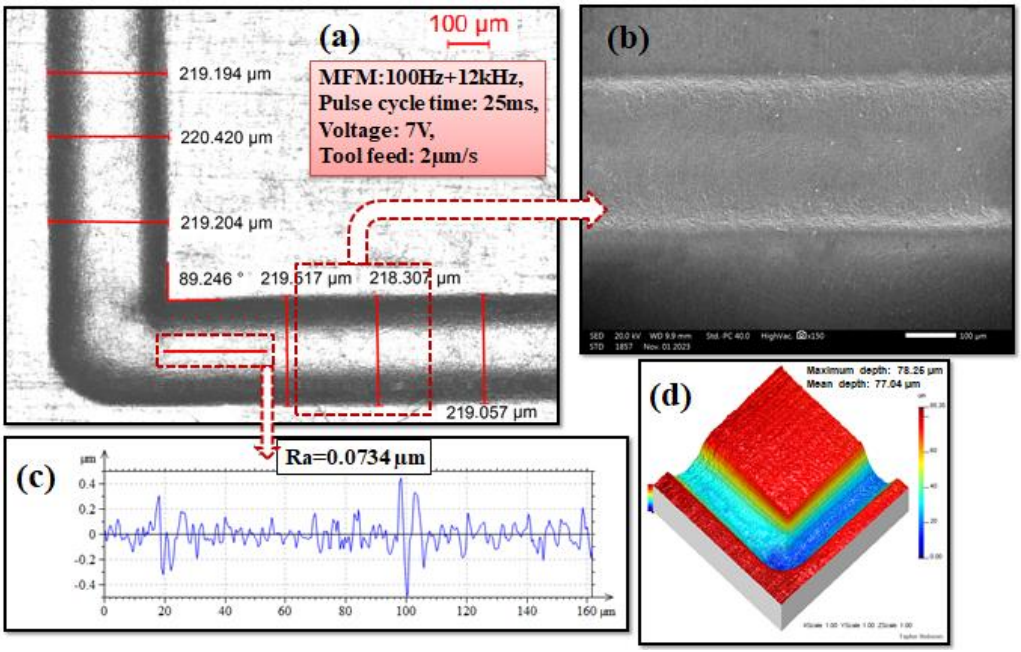

Fig.7.16 Machined L-shape microchannel at 7V(a), SEM image of micrograph (b), surface roughness profile (c), 3D image of microchannel (d)

7.5 Comparison between three developed strategies (PWM, PAM, MFM) under step pulse waveform

Under step pulse waveform (SPW), various strategies have been applied for the improvement of electrochemical micromachining (EMM) performance, which is discussed earlier. In order to identify the best technique, microchannels have been fabricated under the application of pulse width modulation (PWM), pulse amplitude modulation (PAM) and multi-frequencies modulation (MFM). At the best parametric combination of three strategies, microchannels have been fabricated. The best parametric combination of PWM include an applied voltage of 10V, duty cycle regulated from 30% to 50%, frequency of 2kHz, tool feed rate of 0.5µm/s, and 0.1M H_2SO_4, as observed in earlier experiments. For PAM, the best parametric combination has been selected based on earlier experimental results, such as voltage regulated from 10V to 5V, duty cycle of 50%, frequency of 2kHz, tool feed rate of 0.5µm/s, and 0.1M H_2SO_4. Similarly, for the MFM strategy, the best parametric combination has been selected, including an applied

voltage of 10V, duty cycle of 50%, multi-frequency of 100Hz + 12kHz, tool feed rate of 2µm/s, and 0.1M H_2SO_4 as an electrolyte. Herein, faster lateral tool feed rate has been considered compared to PWM and PAM strategies because, from earlier experimental investigations, it has been noticed that 2µm/s lateral tool feed rate is appropriate for the best parametric combination of MFM. The experimental results are presented in a graph, as shown in Figure 7.17. The graph shows that when using the PWM method, the overcut of microchannel width and length, and taper angle are higher compared to the PAM and MFM techniques. This phenomenon arises because when PWM is applied in step pulse waveform, the total pulse cycle time remains constant. But, when pulse-on time increases, pulse-off time decreases and the reverse effect occurs during decreasing time of pulse-on time. As a result, sludge can remove effectively from the narrow machining area. Due to it, localization of anodic dissolution increases significantly, resulting in a higher material removal rate. When PAM technique is employed, it is noticed that overcut of microchannel width and length, and taper angle reduces compared to PWM, but it is greater than that of the MFM method. In this technique, the pulse amplitude of each pulse on time regulates from maximum peak to half of the maximum peak and during each pulse off time, voltage increases from zero to half of the maximum peak. This movement of pulse amplitude occurs automatically during micromachining. Due to it, appropriate average pulse voltage is employed in EMM, which reduces the extra dissolution from the target area and improves the localization effects. As extra dissolution is restricted, overcut of microchannel's width and length and taper angle reduce as compared to PWM technique.

However, the overcut of microchannel can be further reduced by novel step pulse waveform with multi frequencies (MFM) modulation technique, as shown in Figure 7.17. Due to the combination of lower and higher frequencies in MFM method, no larger gas bubble appears, as shown in figure 7.4 (f), and sludge remove rapidly during machining. The reason behind this phenomenon is that two different types of pulse duration control the bubble evolution. At a longer duration of pulse on time, more bubbles are evaluated, which accumulate in a narrow inter-electrode gap, may result in larger gas bubble creation. However, at higher frequencies, due to the smaller duration of pulse on time, bubble evolution can be minimized significantly. Thus, in mixed frequency, during lower frequency, bubble accumulation is obstructed by higher frequency, resulting in no larger gas bubble creating. Additionally, due to a longer pulse on time of lower frequency, the

material removal rate is higher, which can be minimized by higher frequency, because the pulse duration is smaller. Hence, the material removal rate can be effectively controlled by the MFM technique. As the bubble detaches rapidly from the machining zone, as shown in figure 7.4 (f), it creates a force in the electrolyte, resulting in the electrolyte moving upward and circulating more in the machining zone. Due to it, sludge flushes out effectively using the flow of gas bubbles and renewal of the fresh electrolyte in the narrow machining zone.

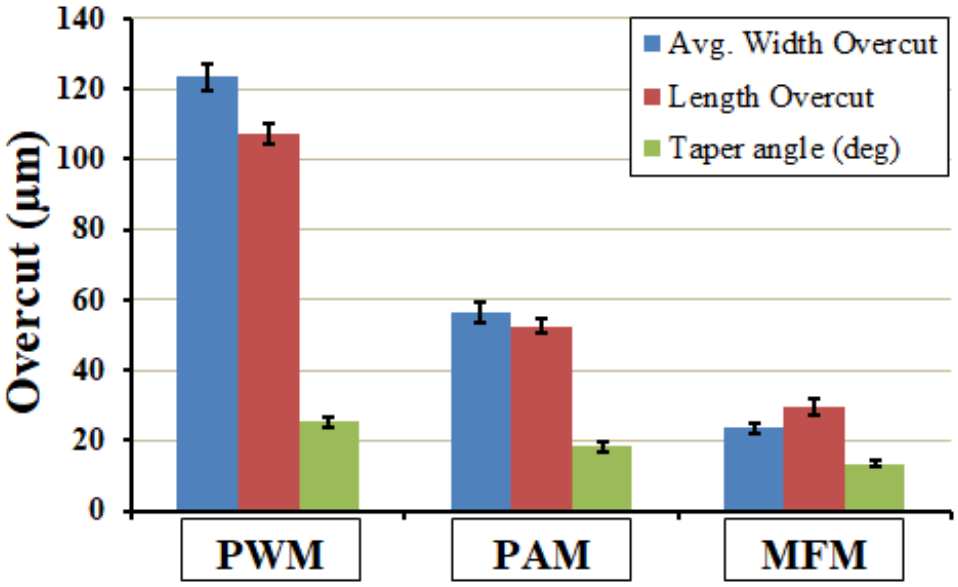

Fig.7.17 Comparison results of overcut and tapering under different techniques

Herein, under the application of three different techniques, the fabricated microchannels are presented in Figure 7.18. From figure 7.18 (a,b), it can be noticed that under the PWM technique, both the entry and exit sides of the microchannel's edge are not uniform, and the channel shape is not precise. However, when the PAM technique is applied, the microchannel shape becomes regular, and better uniformity is also observed, as shown in Figure 7.18 (c,d). Moreover, by utilizing the MFM technique, a more precise microchannel is fabricated compared to the PAM and PWM techniques. Additionally, it can be observed that the edges of the entry and exit sides are uniform and regular, as shown in Figure 7.18 (e,f). According to the experimental results which corroborated with microscopic image, it can be understood that MFM is the best strategy for characterization performance improvement in EMM.

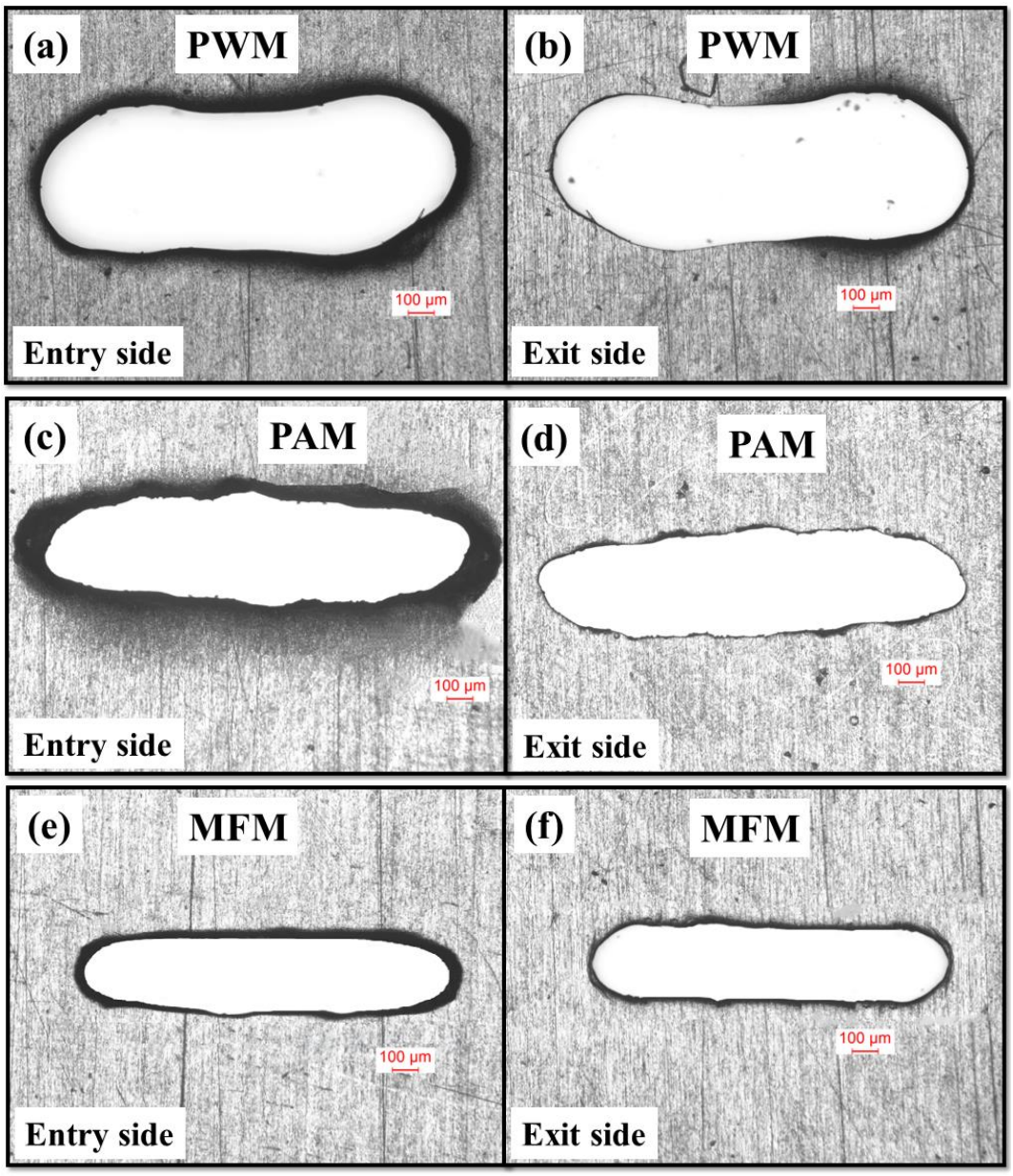

Fig.7.18 Microchannel under three different techniques PWM (a,b) PAM (c,d) MFM (e,f)

7.6 Effectiveness of multi-frequency modulation technique for titanium micromachining

In order to find out the effectiveness of new step pulse waveform with multi-frequency (MFM) modulation technique, comparison in made with results as obtained by other research employing tool vibration technique during machining of titanium by EMM. Herein, pure commercial titanium of grade-1 sheet has been utilised for microhole fabrication. Titanium is renowned for its outstanding physical and mechanical attributes, including a high strength-to-weight ratio, impressive compressive and tensile strength, low density, and excellent fatigue resistance in both air and seawater. Additionally, it

boasts exceptional corrosion resistance. Consequently, titanium stands out as an ideal material for micro engineering and related applications.

However, micromachining of titanium remains a challenging task, whether using conventional or non-conventional methods. The process of anodic dissolution of titanium through electrochemical micromachining is relatively different from that of commonly used metals due to the tendency of titanium to form a passive oxide layer. Titanium is recognized as a metal whose surface is consistently coated with a natural oxide film when exposed to air, water, or other oxygen-containing media. To overcome the passive nature of the oxide layer and facilitate the anodic dissolution of titanium in electrochemical micromachining (EMM), the choice of electrolytes becomes crucial. Previously, researchers preferred to use non aqueous base electrolytes such as ethylene glycol (EG) and sodium bromide (EG+NaBr), ethylene glycol (EG), sodium bromide and sodium chloride (EG+NaBr+NaCl), etc. [98]. However, aqueous solution of sodium nitrate and sodium chloride ($NaNO_3$ +NaCl) has also been utilised in EMM for fabrication of micro features on titanium sheet. Tool vibration technique is useful for electrochemical micromachining of titanium [98]. In other research work, this tool vibration technique was employed for fabrication of microhole on titanium at the applied voltage of 12V. By utilising this technique, sludge and bubbles as well as passive oxide layer can be removed effectively from narrow machining area.

However, the step pulse waveform with multi-frequency modulation is a new innovative technique that can restrict the formation of larger gas bubbles and improve the removal of sludge and bubbles. By fabricating the microholes at the same applied voltage of 12V under the MFM modulation technique, overcut has been investigated and compared with tool vibration technique. From the figure 7.19, it is noticed that MFM modulation technique is more effective for reduction of overcut as compared to tool vibration, with reduction of 62.9% for EG+NaBr, and 42.5% for EG+NaBr+NaCl. The tapering effect also investigated for both tool vibration and MFM techniques. From the experimental results, it can be noticed that tapering angle also reduces as compared to tool vibration, with reduction of 50% reduction for EG+NaBr and 35.41% for EG+NaBr+NaCl, as shown in Figure 7.20.

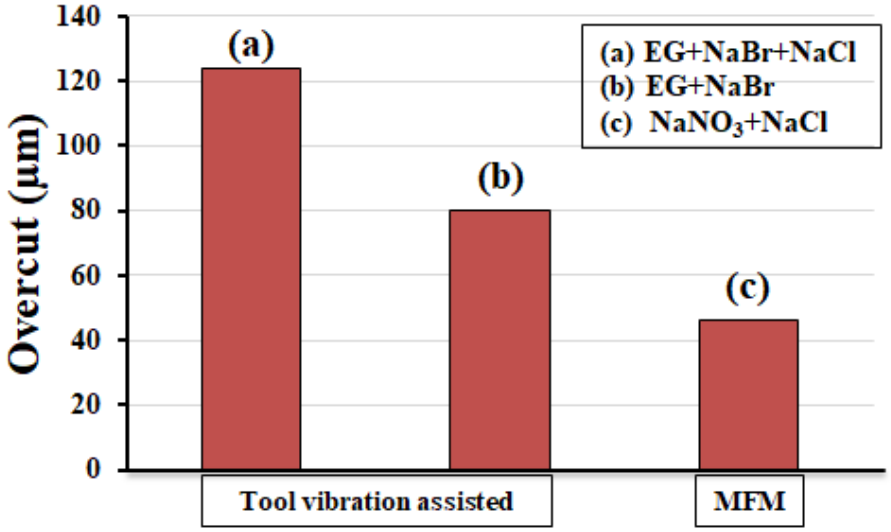

Fig.7.19 Overcut of microhole under tool vibration assisted and MFM techniques at 12V

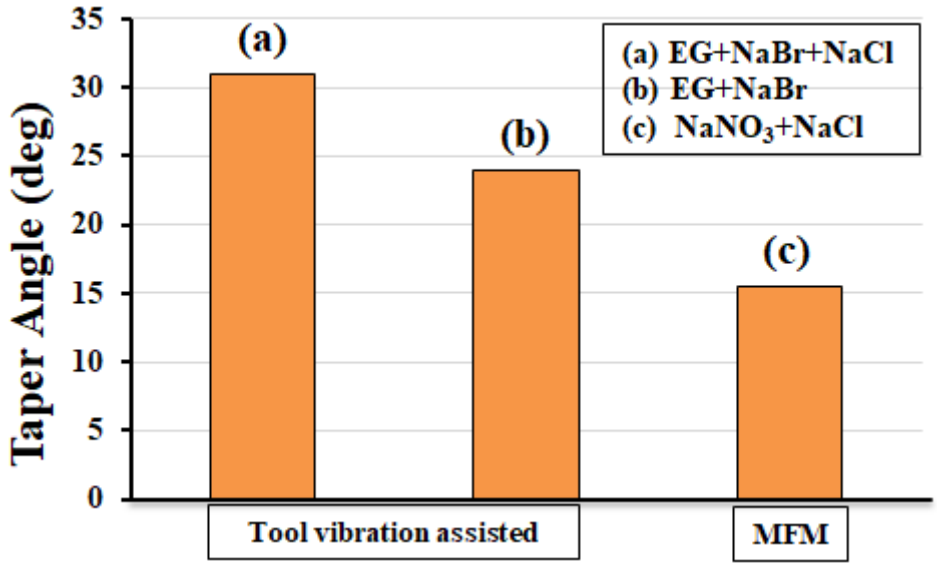

Fig.7.20 Taper angle of microhole under tool vibration assisted and MFM techniques at 12V

From the SEM images of machined microholes, it can be noticed that shiny ring is formed across the area of entry hole with local pitting marks, as shown in Figure 7.21(a). Additionally, Figure 7.21(b) indicates that a smoother surface has been achieved when titanium is electrochemically dissolved in sodium chloride with low or no water content. Consequently, an electrolyte containing a combination of NaCl and NaBr in ethylene glycol has been utilized in further investigations. The addition of NaCl with NaBr in ethylene glycol has been observed to decrease the occurrence of pitting at the entry point of the hole. This combination exhibit reduced stray current effects on the entry side compared to those machined in electrolytes containing NaBr with ethylene glycol, as

shown in Figure 7.21(a). However, when step pulse waveform with multi-frequency modulation technique has been employed for fabrication of microhole, it is noticed that formation of shiny ring across the entry side of microhole fully restricted and pitting effect minimises significantly. Additionally, it is also observed that entry edge of microhole is more uniform. Experimental results reveal that the MFM modulation technique is a novel innovative method for fabrication of precise microhole, utilizing EMM.

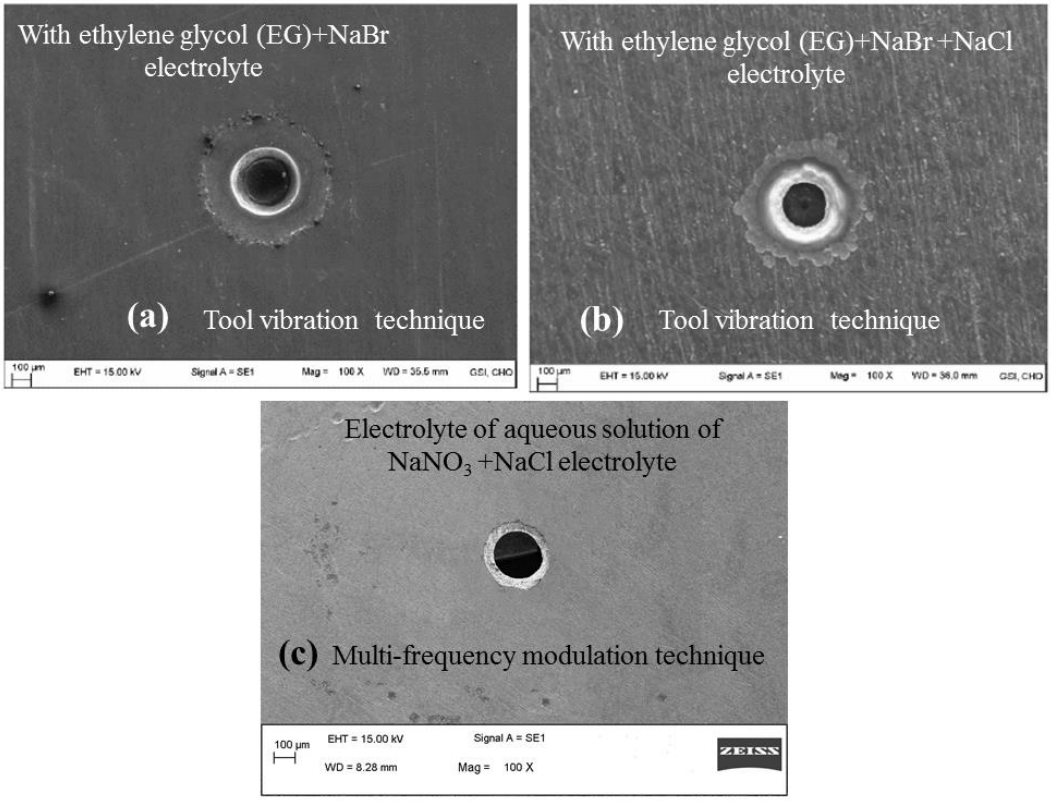

Fig.7.21 Machined microhole under tool vibration assisted (a,b) [98] and SPWMF modulation (c) techniques at 12V

7.7 Outcomes of experimental investigation

A novel step pulse waveform with multi-frequency modulation (MFM) technique has been developed for fabrication of microchannel in electrochemical micromachining (EMM). This new technique has been employed innovatively in stagnant electrolytes to prevent larger gas bubble formation at microtool tip area and remove sludge effectively from the narrow interelectrode gap without complex electrolyte flushing and tool vibration arrangements. The best parametric combinations of multi-frequency pulse

waveforms are determined experimentally for improvement of micromachining performance characterisation.

From the bubble evaluation phenomenon, it can be noticed that due to longer pulse on time at lower frequencies, bubble generation is excessive and larger gas bubbles create which attaches at microtool tip area. By increasing frequency from 100Hz to 1MHz, it is observed that the average size of larger gas bubble reduces from 1062.624µm to 164.399µm, but they are not completely removed.

The negative effects can be overcome and the localization of material dissolution with better surface finish can be improved by multi-frequency modulation of step pulse waveform. To determine the optimal combination of multi-frequency modulation, meticulous experiments have been conducted, varying both lower and higher frequencies. The combination of 100Hz and 12kHz is suitable for the improvement of precise shape of microchannel with better homogeneity, lower tapering effect and better surface finish when optimal pulse cycle time is 25ms and lateral tool feed rate is 2µm/s.

In order to verify the acceptability of the novel multi frequency modulation technique, precise microchannel is fabricated at lower applied voltage of 10V. It can be concluded from the comparison of applied voltages that overcut, depth and taper angle reduces by decreasing applied voltage, but uniformity of edge, homogeneity, and better corner angle are achieved within 7V to 10V. By fabricating precise complex microchannel at 9V with better surface finish i.e., 0.0846µm, it can also be noticed that edges are uniform, corner angles are almost perpendicular, and no irregularity appears on the bottom surface. Utilizing the best parametric combination of multi-frequency modulation, it is found that the precision L-shape of microchannels can be fabricated at the applied voltage of 7V. It also noticeable that the overcut of L-shape average microchannel width, maximum depth, taper angle, corner angle, and surface roughness (Ra) of bottom surface are 9.653µm, 78.25µm, 3.529^0, 89.246^0, and 0.0734µm, respectively.

The experimental results reveal that precision microchannels can be fabricated in stagnant electrolytes using the multi-frequency modulation technique which shows promise as an alternative to replacing complex electrolyte flushing arrangements, expensive ultra-high-frequency pulse power supplies, and other mechanical methods. Multi-frequency modulation technique facilitates the fabrication of precise microholes on titanium material without complex electrolyte flushing and tool vibration arrangements. As compared to tool vibration technique, it is observed that overcut and tapering effect of microhole are

reduced by 42.5% and 35.41%, respectively. Additionally, it is noticed that formation of shiny ring across the entry side of microhole fully restricted, pitting effect minimises, and edge uniformity improves significantly.

Comparison of experimental results reveal that the MFM technique is a novel innovative method as compared to PWM and PAM techniques by which larger gas bubble, accumulated bubbles, and sludge can be flush out from the machining zone. Additionally, this technique plays an important role for improvement of anodic dissolution localization and better control of material removal rate. As function generator is used instead of ultra-high frequency pulse power supply for developing and employing the MFM in EMM, it is an inexpensive methodology for the improvement of machining performance. Furthermore, this novel technique has ability for precision micromachining of titanium material also.

Chapter 8: General conclusions

8.1 General conclusions

As industrial and scientific technologies continue to advance, there is a growing focus on micro components, which are increasingly finding extensive applications in fields such as optoelectronics, biomedical system, robotic systems and microfluidic systems, etc. In response to the growing need for miniaturization, electrochemical micromachining (EMM) has emerged as a key technique for shaping and surface finishing of advance and exotic metals. At the presence of oxide layer, gas film, bubbles, and sludge, the improvement of anodic dissolution is a challenging task for EMM. Researchers have been used various arrangements to remove sludge and gas bubbles from the narrow machining zone such as tool vibration, electrolyte flushing, electrolyte jet, mixed gas jet, etc. Extensive researches have been carried out under different process parameter combination, to improve the localization effects and reduce the extra dissolution from the target area. In EMM, electrolyte flushing creates several problems such as generating unwanted vibration of micro-tool and workpiece, hampers accuracy, and electrolyte flow disturbs the proper addressing of electrolyte at the target machining zone. To achieve the proper localization of anodic dissolution for precision machining, the control of potential transmission and current density are very essential.

The aim of this research work is determined to be the invention of a simple methodology for improving the flushing efficiency and confining the current distribution within the machining gap. In order to achieve this, novel step pulse waveform (SPW) has been designed indigenously by a function generator and utilized as an inexpensive technique to improve the electrochemical micromachining performance. This new step pulse waveform with various techniques i.e., tool and workpiece insulation, microtool feed control, multi-step pulse, automatic pulse width modulation, automatic pulse amplitude modulation, multi frequency modulation have been employed innovatively in stagnant electrolyte to flush out the larger gas bubble, bubbles and sludge from the narrow machining area. In order to verify the feasibility of new techniques, various micro-features i.e., microholes, microdimples, microgrooves, L-shape microchannels, complex microchannels, have been successfully fabricated. In the context of enhancing electrochemical micromachining performance, the machining criteria i.e., overcut, maximum depth, tapering effects, homogeneity, uniformity, profile shape, corner angle, and surface finish have been investigated in depth. To get an idea about the performance

of step pulse waveform, volumetric material removal (VMR) and power transmission for each pulse on time has been estimated and compared with conventional rectangular pulse waveform. For better understanding, the operational mechanism of the step pulse waveform has also been investigated through simulation procedures. To execute the comprehensive research, a simple EMM setup has been developed within the limitations of available resources. Based on experimental results, the point-wise conclusions are as follows:

(i) An experimental setup has been developed to effectively analyze the impacts of the newly developed step pulse waveform on the performance improvement of electrochemical micromachining. This indigenously developed setup consists of several key subcomponents, including mechanical machining unit, motion controller unit, machining chamber, high-frequency pulse power supply system, function generator, process monitoring system, and other accessories. The developed setup is employed successfully for machining stainless steel and difficult-to-cut titanium microfeatures to justify the uniqueness of the investigation with different pulse waveforms approaches for effective analysis of the influences of various process parameters of the power supply and exploration of significant electrochemical phenomena. This setup facilitates the fabrication of precise machining for various microfeatures, fulfilling the micromachining requirements at different stages of experimentation.

(ii) The traditional rectangular pulse has been modified into a step pulse waveform by selecting two different amplitudes of short pulses and the discharging phenomena of the double layer (DL) capacitor has been introduced during the faradic time. Consequently, at 13V, the current density can be varied in a moderate range, i.e., 0 to 33A/cm^2, resulting in a proper anodic dissolution rate being obtained during the active state. From the polarization curve, it can also be observed that the duration of the active state, i.e., 0 to 4V, is always smaller than the rectangular pulse waveform, i.e., 0 to 5.6V. It can also be observed that under the step pulse waveform, the duration of the passive state is very small and the transpassive state appears quickly as compared to rectangular pulse waveform. Consequently, metal dissolution can be effectively controlled by step pulse waveform. Furthermore, the least stray current effect can be noticed at the applied voltage of 13V because the root mean square (RMS) voltage of the step pulse waveform reduces by 20.65% compared to the rectangular pulse waveform. As a result, compared to the

rectangular pulse waveform, the overcut of machined microhole on SS304 has been reduced by 83.99%, 76.10%, 76.72%, 39.99%, and 51.39%, at the applied voltages of 13V, 14V, 15V, 16V, and 17V, respectively. Moreover, the tapering effect has also been reduced by 98.66%, 89.14%, 82.18%, 56.37%, and 44.48% at these applied voltages.

(iii) The insulation technique under the step pulse waveform (SPW) has been employed in EMM to further improve machining accuracy, reduce stray current effects, and fabricate more precise microholes. From simulation results, it can be concluded that by utilising step pulse waveform in insulated workpiece (SS304), current density and potential transmission have been reduced by 63% and 26.37%, respectively. As a result, the effect of stray current can be minimised. Polarization curve exhibits that current density obtained in a moderate amount i.e., 47.62A/cm^2 for insulated workpieces and during the active state and transpassive state appears quickly which can increase further current flow rate. In consequence, the obstructed anodic dissolution rate further increases and stray current effect decreases. As a result, the overcut has been significantly reduced compared to non-insulated workpiece. Additionally, from SEM micrographs, it can be observed that the smoothness of sidewall and the circularity profile of microhole improve. Furthermore, it has been noticed that the profile of microholes is almost circular, edges are uniform, and pitting effects are negligible. But in non-insulated workpiece, these effects are prominent.

(iv) A new discontinuous microtool feed rate technique has been employed successfully in EMM to further improve of machining accuracy i.e., overcut and shape of the machined microhole. Under discontinuous microtool feed rate technique, it has been observed that initially current raises linearly up to 0.4A, and subsequently decreases up to 0.2A. However, utilising traditional constant tool feed rate method, it has been observed that initially current increases rapidly up to 0.5A, after that current stays at 0.4A throughout machining. The machining current under the application of discontinuous microtool feed rate is lower than continuous microtool feed rate. Other advantages can be noticed that short circuit effect also removes significantly. As a result, the overcut has been reduced by 54.89%. Additionally, it is noticed from SEM micrographs that the smoothness of microhole's side wall is improved, the edge is uniform, no irregular machining sports appear and pitting effects are negligible. According the experimental

results, it can be concluded that discontinous microtool feed control can improve machine accuracy significantly than the constant feed rate.

(v) Multi-step pulse waveform (MSPW) has been designed and employed successfully in EMM to control the bubble evolution. This new technique plays a significant role in power transmission because three different peak voltages have been intentionally incorporated during the pulse on time. By estimating the power transmission at different voltages, it is found that the power transmission of MSPW is lower as compared to conventional rectangular pulse waveform (RPW). As a result, stray current effects are minimised. According to the simulation results of MSPW, it can be concluded that due to the formation of smaller size bubbles, the current density is lower than RPW. From experimental results, it can be noticed that in RPW, initially, current density reaches the maximum and remains constant during machining time, but in MSPW, current density oscillates. At 2kHz, greater oscillation of current density can be observed. Hence, 2kHz frequency is responsible for faster removal of bubbles from the machining zone. This findings can be considered as one of the significant contributions of the present research.

(vi) Utilising MSPW technique, more precise microdimple structures and minimum surface roughness (Ra) of 0.02413µm have been obtained at 2KHz, whereas Ra is 0.2511µm for RPW. Additionally, it has been noticed that at 2kHz, the etch factors of microdimple are better than RPW. Hence, it is understood that at 2kHz, the ion transportation rate is higher due to the faster removal of bubbles. As a result, ion transportation improves, shielding effects are minimised, and more sludge can come out due to better flow of electrolyte rotation. Thus, the localization of anodic dissolution improves more than conventional RPW. By fabricating microholes at 2kHz, it has been observed from the SEM micrographs that the edges of machined microholes are uniform and smooth, micro spark affected areas and pitting effects are negligible, but in RPW, these effects are prominent. Using MSPW, overcut of machined microholes has also been reduced significantly.

(vii) The pulse width modulation (PWM) of step pulse waveform has been developed to further control the potential transmission into the electrolyte, which leads to a significant control in moderate amount of anodic dissolution. Due to the movement of pulse width from shorter to longer, PWM technique has capability to

remove the sludge from the machining zone effectively. Utilising this new technique, it has been noticed that microgroove width overcut, depth and their standard deviation decrease. It can be observed that PWM technique is most effective for the improvement of profile accuracy when applied voltage 10V, movement of duty cycle from 30% to 50%, frequency 2kHz, tool feed rate 0.5µm, and 0.2M of electrolyte concentration have been used. At best parametric combination of PWM, microgroove width overcut and its standard deviation, and taper angle have been obtained as 34.026µm, 1.24µm, and 14.03^0, respectively. Additionally, surface roughness (Ra) can be minimised at 0.0244µm, where Ra is 0.1609µm for the non-PWM method.

(viii) A pulse amplitude modulation (PAM) of step pulse waveform has been developed for further reduction of overcut of precise microfeatures, as applied voltage plays a crucial role in control of anodic dissolution,. Utilising this new technique pulse voltage can be automatically regulated from higher to lower amplitude. Due to it, potential transmission into the electrolyte can be controlled which reduces the extra dissolution from the target area and improves the localization effects. It has been observed that proper potential can be transmitted when pulse on time voltage regulates from 10V to 5V and pulse off time voltage rises from 0V to 5V. This new technique has been investigated at different frequencies and found that 2kHz frequency is most effective for uniform and regular micromachining. As a result, better surface roughness (Ra) i.e., 0.0744µm, lower taper angle 15.37^0, and lower groove width overcut i.e., 25.055µm are obtained under the application of PAM technique. Whereas, utilising without PAM method, overcut, taper angle, surface roughness can be obtained as 55.107µm, 47.72^0, and 0.1567µm, respectively.

(ix) A novel step pulse waveform with multi-frequency modulation (MFM) technique has been developed for fabrication of precision microchannel through EMM. This new technique has been employed innovatively in stagnant electrolytes to prevent larger gas bubble formation at microtool tip area and remove sludge effectively from the narrow interelectrode gap without complex electrolyte flushing and tool vibration arrangements. By increasing frequency from 100Hz to 1MHz, it is observed that the average size of larger gas bubble reduces from 1062.624µm to 164.399µm, but they are not completely removed. To determine the optimal combination of multi-frequency modulation, meticulous experiments have been conducted, varying both lower and higher frequencies. The combination of 100Hz

and 12kHz is most effective for the improvement of precise shape of microchannel with better homogeneity, lower tapering effect and better surface finish when optimal pulse cycle time is 25ms and lateral tool feed rate is 2µm/s.

(x) One of the major contributions of the present research is that by utilizing the best parametric combination of multi-frequency modulation of step pulse waveform, precision L-shape of microchannels on SS 304 can be successfully fabricated at the applied voltage of 7V. It also noticeable that the overcut of L-shape average microchannel width, maximum depth, taper angle, corner angle, and surface roughness (Ra) of bottom surface are 9.653µm, 78.25µm, 3.529^0, 89.246^0, and 0.0734µm, respectively. In order to verify the acceptability of the novel multi frequency modulation technique, precise complex microchannel is also fabricated at the applied voltage of 10V. It can be concluded from the comparison of applied voltages that overcut, depth and taper angle reduces by decreasing applied voltage, but uniformity of edge, homogeneity, and better corner angle are achieved within 7V to 10V.

Furthermore, another significant contribution is that the MFM technique of step pulse waveform enables to successfully fabrication of precise microholes on titanium material without the need for complex electrolyte flushing and tool vibration arrangements which is most difficult to machining by EMM. A comparison with past research utilizing tool vibration techniques reveals a significant reduction in overcut i.e., 42.5% and tapering i.e., 35.41% effects of the microholes. Furthermore, from the SEM micrographs, the formation of a shiny ring across the entry side of the microhole is completely restricted, the pitting effect is minimized, and edge uniformity improves significantly.

In summary, abovementioned experimental results reveal that multi frequency modulation (MFM) of step pulse waveform is best technique as compared to others methods, which is also employed in EMM to improve machining performance. Furthermore, this novel technique has ability for precision micromachining of titanium material which is difficult to machine by EMM. By applying MFM, larger gas bubble, accumulated bubbles, and sludge can be flush out from the machining zone significantly. As a consequence, the released bubbles attempt to flow upward and circulate into the inter-electrode gap, which is helpful for the renewal of electrolytes in the narrow machining zone and for better sludge removal. Additionally, this technique plays an important role for improvement of anodic dissolution localization and better control of material removal rate. As function

generator is used instead of ultra-high frequency pulse power supply for developing and employing the MFM in EMM, it is an inexpensive methodology for the improvement of machining performance of EMM.

Finally, the present research in the area of electrochemical micromachining under step pulse waveform with different techniques will be an important substitution and will fulfil various urgent needs of fabrication of microcomponents for the modern microengineering applications like biomedical diagnostics applications, aviation, cooling channels for electronic circuits, automobile, mechanical and related precision industries especially in the area of micro fabrication and micro manufacturing. According the experimental results obtained, the best parametric combinations of different waveform techniques in EMM under step pulse waveform are listed in Table 8.1 can be considered as a technological guidelines for fabrication of microfeatures.

Table 8.1: Technological guidelines of step pulse waveform (SPW) techniques in EMM

SL No	**Type of Methodology**	**Machining conditions**						**Type of microfeatures**
		Applied voltage (V)	**Pulse freq.**	**Duty cycle (%)**	**Tool feed rate (µm/s)**	**Elec. Conc. (H_2SO_4)**	**IEG (µm)**	
I	Multi-step pulse waveform (MSPW)	10V	2kHz	50%	0.5 µm/s	0.1M	20 µm	Microholes, Microdimples
II	Pulse width modulation (PWM)	10V	2kHz	Pulse on time: (30-50)%	0.5 µm/s	0.1M (less overcut) 0.2M (better surface finish)	20 µm	Microdimples, Microholes, Microgrooves
III	Pulse amplitude modulation (PAM)	Pulse on time: 10V-5V Pulse off time: 0V-5V	2kHz	50%	0.5 µm/s	0.1M	20 µm	Microholes, Microgrooves
IV	Multi-frequency modulation (MFM)	7V	100Hz + 12kHz	50%	2 µm/s	0.1M	20 µm	Microchannels Complex microchannels, Complex microgrooves

8.2 Future scope of the work

To fulfil the demand for miniaturisation, electrochemical micromachining (EMM) has been utilised in the shaping and surface finishing of advance metals. As EMM has some unique advantages over other competing micro-fabrication process technologies, various remarkable researches have been carried out on EMM at various research centres, universities, and industries. In the presence of an oxide layer, larger gas bubble, accumulated bubbles, and sludge, the improvement of material removal from the workpiece is a challenging task for EMM. However, without the help of electrolyte flushing arrangements, expensive ultra-high-frequency pulse power supplies, and other mechanical applications, author developed various new innovative pulse waveform techniques for the improvement of EMM performance. Thus, the complexity of the EMM setup arrangement can be eliminated. However, the author feels that more development of the EMM setup is needed for further investigation in EMM to meet the demanding applications in various micro-engineering fields. Hence, further scopes of researches are as follows:

(i) Development of EMM setup with sensor technology, by which very narrow inter-electrode gap can be identified through a real-time monitoring system. Further research is necessary on the step pulse waveform and its ideal combination with process parameters to reduce micromachining time when machining diverse micro components.

(ii) Implementation of a close loop feedback control system and a current monitoring system, by which microtool feed can be controlled automatically. This system can help to maintain almost constant inter-electrode gap during EMM.

(iii) Development of EMM stage with robot arm is very essential for fabrication of complex structure of hard material. In comparison to a conventional 3-axis stage, a single-axis robot arm holds a distinct advantage due to its ability to execute a 360^0 movement with a single command.

(iv) Industry 4.0 influences digital technologies like IoT, AI, big data, and automation to enable smart manufacturing. EMM involves complex electrical, chemical, and mechanical parameters. The complexity of EMM can be mitigated using AI or machine learning, even without extensive data and expertise. Thus, EMM can be transformed into a fully automated system, making it highly effective for Industry 4.0.

(v) Industry 4.0 emphasizes data-driven optimization to enhance productivity. In EMM, capturing and analyzing large datasets (e.g., real-time sensor data such as voltage, current, electrolyte flow rate, and pH) for optimization poses significant challenges. Additionally, electrochemical processes are highly nonlinear, and high-fidelity models are often lacking. These difficulties can be addressed by applying AI and machine learning to improve the process.

Still, the author believes that this research will provide useful insights to researchers, scientists, and engineers working on EMM processes. Additionally, it can guide the development of EMM systems, including new step pulse waveform technological guidelines as developed, and their practical use in industries for both simple and complex microfeatures machining. This is particularly important in the context of the growing demand for miniaturization.

BIBLIOGRAPHY

1. M. Datta, D. Landolt, Fundamental aspects and applications electrochemical micro fabrication, Electrochim Acta 45 (2000) 2535–2558.
2. A.J. Bard, L.R. Faulkner, Electrochemical Methods, second ed., John Wiley & Sons, 2001.
3. A.K.M. De Silva, H.S.J. Altena, J.A. Mc Geough, Precision ECM by process characteristic modeling, Ann. CIRP 49 (1) (2000) 151–156.
4. J. Pattavanitch, S. Hinduja, J. Atkinson, Modelling of the electrochemical machining process by the boundary element method, CIRP Ann. Manuf. Technol. 59 (2010) 243–246.
5. J. Kozak, Computer simulation system for electrochemical shaping, J. Mater. Process. Technol. 109 (2001) 354–359.
6. B. Bhattacharyya (2015) Electrochemical Micromachining for Nanofabrication, MEMS and Nanotechnology. William Andrew Applied Science Publishers/Elsevier, USA
7. K. B. Oldham (2008) A Gouy–Chapman–Stern, model of the double layer at a metal/ionic liquid interface. Journal of Electroanalytical Chemistry 613: 131-138.
8. J. kozak, K.P. Rajurkar, Y. Makkar, Selected problems of micro-electrochemical machining, Int. J. Mater. Process. Technol. 149 (2004) 426–431.
9. J. Munda, B. Bhattacharyya, Investigation into electrochemical micromachining (EMM) through response surface methodology based approach, Int. J. Adv. Manuf. Technol. 35 (2008) 821–832.
10. B. Bhattacharyya, S. K. Sorkhel, Investigation for controlled electrochemical machining through response surface methodology-based approach, Int. J. Mater. Process. Technol. 86 (1999) 200–207.
11. B. Bhattacharyya, J. Munda, M. Malapati, Advancement in electrochemical micro-machining, Int. J. Mach. Tools Manufacture 44 (2004) 1577–1589.
12. C. Kasper, Trans. Electrochem. Soc. 82.1 (1942); 153.
13. J. A. V. Butler (1940) Electrocapillarity, Methuen, London.
14. C. W. Tobias, R. Wijsman, Theory of the effect of electrode resistance on current density distribution in electrolytic cells. Journal of the electrochemical society, 100.10 (1953): 459.
15. J. R. Selman, C. W. Tobias, Mass-transfer measurements by the limiting-current technique, Advances in chemical engineering, Vol. 10. Academic Press, (1978) 211-318.
16. R. H. Muller, Studies of natural convection at vertical electrodes. Journal of the electrochemical society 105.6 (1958): 346.
17. O. Kardos, D.O. Foulke, P. Delahay, C.W. Tobias, (1962) Advances in Electrochemistry and Electrochemical Engineering, vol. 2, John Wiley, New York, p. 146.

18. J. Newman, (1973) Electrochemical Systems, Prentice Hall, Englewood Cliffs, NJ, p. 431.
19. R. Selman, C.W. Tobias, T.A. Drew, (1978) Advances in Chemical Engineering, vol. 10, Academic Press, New York, p. 211.
20. V. K. Jain, K. P. Rajurkar, An integrated approach for tool design in ECM, Precision Engineering 13 (2) (1991) 111–124.
21. K.P. Rajurkar, B. Wei, J. Kozak, Modeling and monitoring inter electrode gap in pulse electrochemical machining, Annals of the CIRP 44 (1) (1995) 177–180.
22. K. Chikamori, Possibilities of electrochemical micromachining, International Journal of the Japan Society for Precision Engineering 32 (1) (1998) 37–38.
23. B. Bhattacharyya, S.K. Sorkhel, Investigation for controlled electrochemical machining through response surface methodology-based approach, International Journal of Materials Processing Technology 86 (1999) 200–207.
24. D. Landolt, P. F. Chauvy, O. Zinger, Electrochemical micromachining, polishing and surface structuring of metals: fundamental aspects and new developments, Electrochimica Acta 48 (2003) 3185–3201.
25. M. Kock, V. Kirchner, R. Schuster, Electrochemical micromachining with ultra-short voltage pulses—a versatile method with lithographical precision, Electrochimica Acta 48 (1) (2003) 3213–3219.
26. M. A. H. Mithu, G. Fantoni, J. Ciampi, The effect of high frequency and duty cycle in electrochemical microdrilling. Int J Adv Manuf Technol (2011); 55: 921–933.
27. M Datta, L. T. Romankiw, Applications of chemical and electrochemical micromachining in the electronic industry, Journal of the Electrochemical Society, 136 (6) (1989) 2850–2857.
28. M. Datta and D. Harris, Electrochemical micromachining: An environmentally friendly, high speed processing technology, Electrochimica Acta, 42.20-22 (1997): 3007-3013.
29. K. P. Rajurkar, D. Zhu, J. A. Mc Geough, J. Kozak, A. De Silva, New Developments in Electro-Chemical Machining, Annals of the ClRP, 48.2 (1999): 567-579.
30. T. Masuzawa (2000) State of the art of micromachining, Annals of the CIRP, 49 (2): 473-488.
31. M. Datta, D. Landolt, Fundamental aspects and applications of electrochemical, Electrochimica Acta, 45 (2000) 2535–2558.
32. R. Schuster, V. Kirchner, P. Allongue, G. Ertl, Electrochemical micromachining, Science, 289.5476 (2000): 98-101.
33. B. Bhattacharyya, B. Doloi, P.S. Shridhar, Electrochemical micromachining: New possibilities

for micro manufacturing, Journal of Materials Processing Technology, 113 (2001) 301–305.

34. V. Kirchner, L. Cagnon, R. Schuster, G. Ertl, Electrochemical machining of stainless steel microelements with ultra-short voltage pulses, Applied Physics Letters, 79 (2001) 1721–1723.
35. J. Kozak, K. P. Rajurkar, Y. Makkar, Study of Pulse Electrochemical Micromachining, Journal of Manufacturing Processes Vol. 6/No. 1 2004.
36. R. Fosrster, A. Schoth, W. Menz, Micro-ECM for production of microsystems with a high aspect ratio, Microsystem Technologies 11 (2005) 246–249 Springer-Verlag 2005.
37. L. Cagnon , V. Kirchner , M. Kock , R. Schuster, G. Ertl, W. Thomas Gmelin, H. Kuck, Electrochemical Micromachining of Stainless Steel by Ultra-short Voltage Pulses, Z. Phys. Chem. 217 (2003) 299–313.
38. J. Kozak, K. P. Rajurkar, Y. Makkar, Selected problems of micro- electrochemical machining, Journal of Materials Processing Technology 149 (2004) 426–431.
39. K.P. Rajurkar, G. Levy, A. Malshe, M.M. Sundaram, J. Mc Gough, X. Hu, R. Resnick, A. De Silva, Micro and nano machining by electro-physicaland chemical processes, Annals of the CIRP, 55 (2) (2006) 643–666.
40. M. Kock, V. Kirchner, R. Schuster, Electrochemical micromachining with ultra-short voltage pulses_a versatile method with lithographical precision, Electrochimica Acta 48 (2003) 3213/3219.
41. S. H. Ryu, Micro fabrication by electrochemical process in citric acid electrolyte, Journal of Materials Processing Technology 209.6 (2009): 2831-2837.
42. B. Bhattacharyya, S. Mitra, A. K. Boro, Electrochemical machining: new possibility for micromachining Int. Journal of Robotics and Computer Integrated Manufacturing, 18 (2002) 283 – 289.
43. W. Zhao, X. Li, Z. Wang, Zhao, Study on micro electrochemical machining at micro to meso-scale. 2006 1st IEEE International Conference on Nano/Micro Engineered and Molecular Systems. IEEE, 2006.
44. L. Yong, Z. Yunfei, Y. Guang, P. Liangqiang, Localized electrochemical micromachining with gap control, Sensors and Actuators, A 108(2003) 144–148.
45. T. Kurita, K. Chikamori, S. Kubota, M. Hattori, A study of three-dimensional shape machining with an ECμM system, International Journal of Machine Tools and Manufacture, 46 (2006) 1311–1318.
46. Y.J. Zhang, Y.J. Tang, X.K. Liu, Z.N. Guo, F. Li, Development of Ultra-Short Pulse Power Supply Applicable to Micro-ECM, Materials Science Forum Vols. 626-627 (2009) pp 369-374.
47. B. Huaiqian, X. Jiawen, L. Ying, Aviation oriented micromachining technology- Micro-ECM

in Pure Water, Chinese Journal of Aeronautics, 21(5) (2008) 455–461.

48. Z. Zhang, D. Zhu, Experimental Research on the Localized Electrochemical Micro-machining, Russian Journal of Electrochemistry, (2008) Vol. 44, No. 8, pp. 926–930.
49. Z. Zhangz, Y. Wang, F. Chen, W. Mao, A micromachining system based on electrochemical dissolution of material, Russian Journal of Electrochemistry, 47 (7) (2011) 819–824.
50. M. A. H. Mithu, G. Fantoni, J. Ciampi, A step towards the in-process monitoring for electrochemical micro-drilling, International Journal of Advance Manufacturing Technology, 57 (2011) 969–982.
51. R. Thanigaivelan, R M. Arunachalam, Experimental Study on the Influence of Tool Electrode Tip Shape on Electrochemical Micromachining of 304 Stainless Steel, Materials and Manufacturing Processes, 25: 1181–1185, 2010.
52. J. Munda, B. Bhattacharyya, Investigation into electrochemical micromachining (EMM) through response surface methodology based approach, Int J Adv Manuf Technol (2008) 35:821–832.
53. D. Zhu , Y.B. Zeng, Z.Y. Xu, X.Y. Zhang, Precision machining of small holes by the hybrid process of electrochemical removal and grinding, CIRP Annals - Manufacturing Technology 60 (2011) 247–250.
54. A. Spieser, A. Ivanov, Recent developments and research challenges in electrochemical micromachining (μECM). The International Journal of Advanced Manufacturing Technology 69 (2013): 563-581.
55. B. Bhattacharyya, J. Munda, Experimental investigation into electrochemical micromachining (EMM) process, Journal of Materials Processing Technology 140 (2003) 287–291.
56. B. Bhattacharyya, M. Malapati, J. Munda, Experimental study on electrochemical micromachining, Journal of Materials Processing Technology 169 (2005) 485–492.
57. Z. Li, G. Yuan, Experimental investigation of micro-holes in electrochemical machining using pulse current. 2008 3rd IEEE International Conference on Nano/Micro Engineered and Molecular Systems. IEEE, 2008.
58. E. S. Lee. S. Y. Baek. C. R. Cho, A study of the characteristics for electrochemical micromachining with ultrashort voltage pulses, Int J Adv Manuf Technol (2007) 31: 762–769.
59. B. Bhattacharyya, J. Munda, Experimental investigation on the influence of electrochemical machining parameters on machining rate and accuracy in micromachining domain, International Journal of Machine Tools & Manufacture 43 (2003) 1301–1310.
60. L. Yong, Z. Di, Z. Yongbin, H. Shaofu, Y. Hongbing, Experimental Investigation on Complex Structures Machining by Electrochemical Micromachining Technology, Chinese Journal of

Aeronautics 23(2010) 578-584.

61. L. Yong, Z. Yunfei, Y. Guanga, P. Liangqiang, Localized electrochemical micromachining with gap control. Sensors and Actuators A: Physical 108.1-3 (2003): 144-148.
62. Z. Zhang, D. Zhu, N. Qu, M. Wang, Theoretical and experimental investigation on electrochemical micromachining, Microsystems Technol (2007) 13:607–612.
63. C. H. Jo, B. H. Kim, C. N. Chu, Micro electrochemical machining for complex internal micro features, CIRP Annals - Manufacturing Technology 58 (2009) 181–184.
64. M. Malapati, A. Sarkar, B. Bhattacharyya, Frequency pulse period and duty factor effects on electrochemical micromachining (EMM). Advanced Materials Research 264 (2011): 1334-1339.
65. V. K. Jain, S. Kalia, A. Sidpara, V. N. Kulkarni, Fabrication of micro-features and micro-tools using electrochemical micromachining. The International Journal of Advanced Manufacturing Technology 61 (2012): 1175-1183.
66. B. H. Kim, S. H. Ryu, D. K. Choi, C. N. Chu, Micro electrochemical milling, Journal of Micromechanics and Micro engineering, 15 (2005) 124–129.
67. B. Ghoshal, B. Bhattacharyya, Generation of microfeatures on stainless steel by electrochemical micromachining. The International Journal of Advanced Manufacturing Technology 76 (2015): 39-50.
68. F.M. Ozkeskin, S.S. Sundarram, S. Allison, N.P. Hung, M. Powers, G. Strohm, L.A. Godinez, and J.R. Mariquez, Feedback controlled high frequency electrochemical micromachining, Diss. Texas A&M University, 2008.
69. S. H. Ahna, S. H. Ryua, D. K. Choi, C. N. Chu, Electro- chemical micro drilling using ultra short pulses, Precision Engineering 28 (2004) 129–134.
70. M. Sen, H. S. Shan, A review of electrochemical macro- to micro-hole drilling processes, International Journal of Machine Tools & Manufacture 45 (2005) 137–152.
71. M. A. H. Mithu, G. Fantoni, J. Ciampi, The effect of high frequency and duty cycle in electrochemical microdrilling, Int J Adv Manuf Technol (2011) 55:921–933.
72. Z. W. Fan, L. W. Hourng, Electrochemical micro-drilling of deep holes by rotational cathode tools, Int J Adv Manuf Technol 52: (2011) 555–563.
73. H. P. Tsui , J. C. Hung , J. C. You, B. H. Yan, Improvement of electrochemical microdrilling accuracy using helical tool, Materials and Manufacturing Processes, 23:5(2008) 499-505.
74. I. Yang, M. S. Park, C. N. Chu, Micro ECM with ultrasonic vibrations using a semi-cylindrical tool. International Journal of Precision Engineering and Manufacturing 10 (2009): 5-10.
75. T. Koyano, M. Kunieda, Micro electrochemical machining using electrostatic induction

feeding method, CIRP Annals - Manufacturing Technology 62 (2013) 175–178.

76. B. J. Park, B. H. Kim, C. N. Chu, The Effects of Tool Electrode Size on Characteristics of Micro Electrochemical Machining, *CIRP annals* 55.1 (2006): 197-200.
77. R. Thanigaivelan, R. M. Arunachalam, P. Drukpa, Drilling of micro-holes on copper using electrochemical micromachining, Int J AdvManufTechnol 61: (2012) 1185–1190.
78. S. Ryu, Micro electrochemical machining of stainless steel using citric acid. Journal of the Korean Society for Precision Engineering 25.3 (2008): 134-140.
79. A. K. Das, P. Saha, Machining of circular micro holes by electrochemical micro-machining process, Adv. Manuf. 1: (2013) 314–319.
80. M. Malapati, B. Bhattacharyya, Investigation into Electrochemical Micromachining Process during Micro-Channel Generation, Materials and Manufacturing Processes, 26: (2011) 1019–1027.
81. B. Ghoshal, B. Bhattacharyya, Micro electrochemical sinking and milling method for generation of micro features. Proceedings of the Institution of Mechanical Engineers, Part B: Journal of Engineering Manufacture 227.11 (2013): 1651-1663.
82. V. Rathod, B. Doloi, B. Bhattacharyya, Influence of electrochemical micromachining parameters during generation of microgrooves. The International Journal of Advanced Manufacturing Technology 76 (2015): 51-60.
83. V. Rathod, B. Doloi, B. Bhattacharyya, Experimental investigations into machining accuracy and surface roughness of microgrooves fabricated by electrochemical micromachining. Proceedings of the Institution of Mechanical Engineers, Part B: Journal of Engineering Manufacture 229.10 (2015): 1781-1802.
84. Y. Liu, D. Zhu, L. Zhu, Micro electrochemical milling of complex structures by using in situ fabricated cylindrical electrode, Int J Adv Manuf Technol 60 (2012): 977-984.
85. Y. Yuan, L. Han, D. Huang, J.J. Su, Z.Q. Tian, Z.W. Tian, D. Zhan, Electrochemical Micromachining under Mechanical Motion Mode, Electrochimica Acta 183 (2015) 3–7.
86. B. Ghoshal, B. Bhattacharyya, Electrochemical micromachining of microchannel using optimum scan feed rate, Journal of Manufacturing Processes 23 (2016): 258-268.
87. L. Xu, X. Wang, C. Zhao, Electrochemical Micromachining with Sinusoidal Signals. Journal of The Electrochemical Society 166.10 (2019): E275.
88. L. Xu, J. Ning, C. Zhao, Electrochemical micromachining based on time constant control. Mechanical Systems and Signal Processing 145: (2020) 106920.
89. D. S. Patel, V. Sharma, V. K. Jain, J. Ramkumar, Reducing overcut in electrochemical micromachining process by altering the energy of voltage pulse using sinusoidal and triangular

waveform. International Journal of Machine Tools & Manufacture 151: (2020) 103526.

90. L.Xu, J. Wang, C. Zhao, Electrochemical Micromachining Using Real Pulse Signals. Journal of The Electrochemical Society 168: (2021) 083504.
91. V. Sharma, M. D. Gyanprakash, P. Gupta, J. Ramkumar, Analysis of circuit current in electrochemical micromachining process under the application of different waveforms of pulsed voltage. Journal of Manufacturing Processes 75: (2022) 110–124.
92. C. Zhao, T. Huang, J. Wang, L. Xu, Improve the precision of electrochemical micromachining with parabolic pulse current. The International Journal of Advanced Manufacturing Technolog 121: (2022) 3067–3078.
93. A. Tyagi, V. Sharma, V. K. Jain, J. Ramkumar, Investigations into side gap in wire electrochemical micromachining (wire-ECMM), The International Journal of Advanced Manufacturing Technology 94 (2018): 4469-4478.
94. V. Sharma, D. S. Patel, V. K. Jain, J. Ramkumar, Wire electrochemical micromachining: An overview. International Journal of Machine Tools & Manufacture 155: (2020) 103579.
95. J.A. Mc Geough, (1974) Principles of Electrochemical Machining, Chapman and Hall, London.
96. A.J. Bard, L.R. Faulkner, (2001) Electrochemical methods: fundamentals and applications, 2nd ed., John Wiley & Sons, New York.
97. C. Gabrielli, F. Huet, M. Keddam, A. Macias, A . Sahar, Potential drops due to an attached bubble on a gas-evolving electrode. Journal of applied electrochemistry 19(5): (1989) 617–629.
98. S. S. Anasane, B. Bhattacharyya, Experimental investigation on suitability of electrolytes for electrochemical micromachining of titanium. The International Journal of Advanced Manufacturing Technology 86: (2016) 2147-2160.

Journal of The Electrochemical Society, 2022 **169** 053504
1945-7111/2022/169(5)/053504/14/$40.00 © 2022 The Electrochemical Society ("ECS"). Published on behalf of ECS by IOP Publishing Limited

Anodic Polarization Study of Step Pulse Waveform for Machining Accuracy in Electrochemical Micromachining

Himadri Sekhar Panda,[1,z] Koushik Mishra,[2] and B. Bhattacharyya[1]

[1] *Production Engineering Department, Jadavpur University, Kolkata-700032, India*
[2] *Mechanical Engineering Department, Swami Vivekananda Institute of Science and Technology, Dakshin Gobindapur, Sonarpur, Kolkata 700145, India*

Electrochemical micromachining (EMM) shows promise as a versatile process for machining chemically resistant metallic materials in microsystems applications. A traditional rectangular pulse pattern has been modified into a step pulse waveform with a series of short rectangular pulses with different amplitudes. By establishing the experimental setup, anodic polarization behavior has been investigated throughout the dissolution process with 0.1 M H_2SO_4 electrolyte solution at different applied voltages under the application of rectangular and step pulse waveforms. Utilizing the step pulse waveform, oscillation of the anode potential and transpassive state have been obtained during machining. Thus, from polarization studies, it has been observed that at 13 V, the current density is accelerated in a moderate range, i.e., 0 to 33 A cm^{-2}, which can reduce the anodic dissolution rate during the active state. Alternatively, the stray current effects and micro-sparks can be controlled because the duration of the passive state is very small and the RMS voltage can be reduced by 20.65% as compared to the rectangular pulse waveform. Further, overcut and tapering effects have been reduced by 83.99% to 51.39% and by 98.66% to 44.48% at the applied voltage of 13 to 17 V, respectively.
 [DOI: 10.1149/1945-7111/ac6e8e]

Manuscript submitted January 10, 2022; revised manuscript received April 18, 2022. Published May 18, 2022.

Electrochemical micromachining (EMM) has several advantages, such as better precision, and control, as well as different fields of micro-component design applications in aerospace, biomedical, automobile, micro-electromechanical systems (MEMS), electronics, etc. Due to this, EMM has become a promising micro-machining technique for ultra-precision components design. In EMM, the rate of anodic dissolution and hydrogen bubble generation must be controlled to enhance the machining accuracy. Therefore, meaningful investigations on the polarization are necessary to obtain a better understanding of the influence of various pulse power supplies on machining characteristics in the micromachining domain.

Utilizing a galvanostatic-pulse method, anode potentials under prevailing conditions of the high-rate dissolution of copper have been studied in electrochemical machining (ECM).[1] Overvoltage has been measured by the electrical circuit influence of ohmic voltage drops in the solution. Tafel behavior is observed up to the highest current densities, from 0.01 to 100 A cm^{-2} during dissolution in the active mode for short electrolysis times. Using a current interruption technique, the anode potentials of mild steel in NaC1 solutions have been studied at current densities of 5 to 100 A cm^{-2} in ECM.[2] It has been observed that in the presence of an anodic film, the dissolution process is affected by the influence of electrolyte flow rate, NaCl concentration, and current density during machining. But at the turbulent region, i.e., Re $>$ 4700, the anodic film is minor affected by the electrolyte flow. The anodic polarization has been elaborately described by anodic potential against current density, which represents a better idea of machining characteristics.[3] The machining rate and accuracy of EMM have been investigated under the influence of machining parameters such as machining voltage of 6 to 10 V, electrolyte concentration of 15–20 g l^{-1}, pulse on-time of 10–15 ms, and 50 Hz of pulse frequency.[4] The results revealed that overcut can be reduced by controlling the material removal rate (MRR). The behavior of the oxide layer, current distribution, mass transport, and the critical electrochemical parameters has been illustrated for shape control and surface finishing of material under the application of EMM.[5] Utilizing the rectangular pulse waveform, the polarization behavior has been studied with an electronic model system in EMM and it has been found out that the passive electrode can be treated like an actively dissolving electrode at the transpassive potential region.[6] Furthermore, the feasibility of different pre-polarization strategies of Fe-based bulk metallic glasses with low Cr content has been evaluated in the micromachining domain.[7] The breakdown time of oxide film has been determined using a cylindrical electrode with different rotational speeds in $NaNO_3$ solution at different applied potentials.[8] Microstructures have been fabricated using the sinusoidal signal, resulting in good machining resolution.[9] In this study, by developing the relationship between machining accuracy and the frequency of the sinusoidal signals, machining resolution has been enhanced. Recently, the overcut has been investigated by utilizing different voltage pulse waveforms such as rectangular, triangular, and sinusoidal. In this investigation, the overcut has been reduced by the triangular voltage pulse compared to the sinusoidal and rectangular voltage pulses. In comparison to the rectangular voltage pulse, the energy of the triangle and sinusoidal voltage pulses have been reduced by 33% and 50%, respectively.

Due to industrial interest, different aspects of the EMM process have been researched, such as machining accuracy, high MRR, smooth surface finish, stress-free surfaces, and machining ability of complex shapes with environmentally acceptable limits. However, after a literature review, it is understood that the investigation of anodic polarization for machining accuracy under the application of various pulse waveforms is inadequate. Thus, the present study has been focused on machining accuracy by modifying the traditional rectangular pulse waveform into a step pulse waveform. Meticulous research and experiments have been carried out indigenously by developing the EMM setup to investigate the different machining characteristics such as overcut, tapering effect, anode potential, anode polarization, etc.

Design methodology and working principle of step pulse waveform.—The traditional rectangular pulse waveform has long been used to improve the machining accuracy of EMM. In narrow interelectrode gap (IEG), anode potential, overpotential, ohmic (IR) drop, and electrolyte resistance are more prominent and have much more impact on anodic dissolution. In the case of a DC power supply for narrow IEG, an adequate amount of sludge is deposited on the tool surface, which acts as an electrical insulator that interrupts the anodic dissolution and creates the short-circuit effect. Due to this, the anodic dissolution can not be continued uniformly during micromachining.[4] However, by applying pulsed DC instead of a constant DC power supply, the maximum amount of sludge can be flushed away from the machine zone during the pulse off-time.[4,10] During pulse off time, machining cannot be possible because, at that time, the applied voltage is zero. Thus, at that time, the formation of new sludge is much less than during pulse on time. Therefore, after

[z] E-mail: himadrispanda26@gmail.com

Sādhanā (2023)48:134
https://doi.org/10.1007/s12046-023-02212-1

Improvement of surface finish and accuracy utilising multi-step pulse waveforms in electrochemical micromachining

HIMADRI SEKHAR PANDA* and B BHATTACHARYYA

Production Engineering Department, Jadavpur University, Kolkata 700032, India
e-mail: himadrispanda26@gmail.com

MS received 24 January 2023; revised 30 April 2023; accepted 12 June 2023

Abstract. To improve the localization of material dissolution and fabrication of microstructures with better surface finish, high process complexity, such as different tool shapes, electrolyte flow, and tool insulation, has been utilised in electrochemical micromachining (EMM). Improvement of mass transport, sludge removal, and continuous dissolution are challenging tasks for EMM because bubbles and sludge increase the shielding effects. To solve the problems and achieve precision machining with a better surface finish, a new multi-step pulse waveform (MSPW) is designed indigenously. By incorporating three different peak voltages with a short duration time in the pulse on time of MSPW, potential fluctuation is intentionally induced during machining. Thus, more pulse fall times, short peak voltage duration times, and fluctuations of potential can improve the reduction of bubble size and its detachment rate. Due to it, ion transport phenomena improve, sludge is properly removed from the machining zone, and material dissolution rates increase. The effects of MSPW in EMM are compared with conventional rectangular pulse waveform (RPW). From mathematical estimation, it is found that the power transmission of MSPW is less than RPW, which plays a significant role in stray current minimization. The proposed method is verified by simulation, where it can be observed that current density decreases with increasing bubble size. By capturing images, it is also noticed that the size of gas bubbles decreases, accompanied by a higher detachment rate. Utilising MSPW, precise microdimples are fabricated with minimum surface roughness (Ra), i.e., 0.0241μm, whereas Ra is 0.251μm for RPW. Further, it is identified from the machined microdimples that etch factor improves, diameter minimises, depth increases, no irregular machining appears on the bottom surface, and surface finish also improves as compared to RPW. These improvements are also observed in machined microholes.

Keywords. Electrochemical micromachining; multi-step pulse waveform; bubble size control; power transmission; surface finish; machining accuracy.

1. Introduction

Electrochemical micromachining (EMM) technology is expected to play a promising role in shape control and surface smoothing for various fields of miniaturised applications. Recently, EMM has been engaged in machining hard metal into an ultra-precision complex shape without thermal and stress effects. The mechanism of metal removal is that in the presence of electrolyte, anodic dissolution takes place in the form of ionic levels by applying an electrical voltage pulse waveform between tool and workpiece. In EMM, metal dissolution rate, surface finish, and accuracy depend on electrolyte stoichiometry such as mass transport, current distribution, behaviour of oxide films and bubbles, etc. When metal dissolution starts, gas bubbles, sludge, oxide layer, and heat are generated in the narrow inter-electrode gap (IEG), which changes the conductivity of the electrolyte and hampers further current flow. To improve mass transport and conductivity, high-speed electrolyte flushing is used in conventional electrochemical machining. But, in micromachining, electrolyte flushing creates several problems, such as generating unwanted vibration of the microtool and workpiece, hampering accuracy, and disrupting the proper addressing of electrolytes at the target machining zone. Recently, several new electrical pulse waveforms such as sinusoidal, parabolic, triangular, etc. have been used as an alternative technique to improve the proper localization and reduce the extra dissolution from the target area. Recent studies on EMM for machining and surface structuring of chemically resistant hard metals for microsystem applications are reviewed and found to improve machining performance [1]. From the review of experimental investigations, a new prospect of electrochemical machining for the processes of shape control and surface smoothing in the micro-machining domain can be achieved [2]. It is concluded from

*For correspondence
Published online: 12 July 2023

Journal of Manufacturing Processes 112 (2024) 187–201

Contents lists available at ScienceDirect

Journal of Manufacturing Processes

journal homepage: www.elsevier.com/locate/manpro

Full length article

Performance improvement of electrochemical micromachining employing pulse width modulation

Himadri Sekhar Panda *, B. Bhattacharyya

Production Engineering Department, Jadavpur University, Kolkata 700032, India

ARTICLE INFO

Keywords:
Electrochemical micromachining
Pulse width modulation
Step pulse waveform
Machining performance

ABSTRACT

Electrochemical micromachining (EMM) is leading a promising role in the fabrication of microcomponents which are used in different fields of micro-engineering applications. By reducing the energy of pulse waveform, machining accuracy can be improved, but in stagnant electrolytes, generated sludge during machining which creates an obstacle to further improvement of machining performance. To overcome this problem, pulse width modulation (PWM) technique is employed in EMM, where pulse width moves from shortest to longer duration without changing pulse period. Due to it, sludge can remove quickly from the narrow machining zone when the duration of pulse off time is longer and anodic dissolution can be controlled. This PWM is applied on step pulse waveform which is designed indigenously. In this waveform, two different peak voltages are incorporated into the pulse on time, resulting in potential transmission during each pulse on time is controlled. As a consequence, during each pulse on time, larger amount of material dissolution can be controlled precisely. To verify the feasibility of PWM technique, machining accuracy is investigated for different applied voltages, duty cycles, frequencies, and tool feed rates. In addition, the machined surface finish is also investigated under best parametric combination utilising different electrolyte concentrations. This PWM makes an effective contribution to profile accuracy, where at the movement of duty cycle from 30 % to 50 %, micro-groove width overcut is obtained as 34.026 μm accompanied by less standard deviation of 1.24 μm and taper angle of 14.03^0. By using this novel method, the machined surface roughness (Ra) is achieved as 0.0244 μm, whereas Ra is 0.1609 μm for the non-PWM method.

1. Introduction

Due to the advancement of technology in the industry, precise micro-component fabrication is essential for different fields of micro-engineering applications such as biomedical, electronics, aviation, micro-mechanics, and so on. To fulfil the demand for miniaturization, electrochemical micromachining (EMM) has been engaged in shaping and surface finishing of hard metal. The mechanism of EMM is that material removes in the form of ionic levels by applying an electrical voltage between the tool and workpiece, where electrolyte solution is used as a conducting medium. The machining accuracy and surface finish can be improved by EMM because it has several advantages such as no tool wear, absence of thermal and stress effects, higher metal removal rate, and localization effect of anodic dissolution which can be controlled. As per design requirements, different advanced variants have been developed, such as wire electrochemical micromachining (WECM) [1], pulse electrochemical micromachining (PECM) [2], jet electrochemical micromachining (Jet-ECM) [3], and through-mask electrochemical micromachining (TMECM) [4], etc. From a fundamental point of view, i.e., mass transport, current distribution, and passive layer formation, there have many similarities in these techniques [5]. Recently, different pulse waveforms i.e., sinusoidal, parabolic, triangular, etc. have been employed for the investigation of machining accuracy. It is found that intermittent pulse power supply leads a crucial role in the flushing of sludge and bubbles from the machining zone. As a consequence, localization effects improve and reduce the extra dissolution from the target area.

In recent decades, research has been carried out on pulse duration, which is reducing from the short to the ultra-short range to improve precision micromachining. Kozak et al. analysed electrode potential, current density, and electrical charge by developing a mathematical model, to improve the localization effects and performance of EMM under the application of ultra-short voltage pulses [6]. Spieser et al. studied the effect of ultra-short voltage pulse for the fabrication of deep

* Corresponding author.
E-mail address: himadrispanda26@gmail.com (H.S. Panda).

https://doi.org/10.1016/j.jmapro.2024.01.033
Received 7 April 2023; Received in revised form 6 January 2024; Accepted 10 January 2024
Available online 20 January 2024

Himadri Sekhar Panda
08/04/2024